DIPARTIMENTO DI SCIENZE
DOTTORATO IN SCIENZE DELLA TERRA (SDT)
CURRICULUM GEODINAMICA E VULCANOLOGIA

Experimental determination of impact parameters of the most recent eruptions of Ischia Island

Tutor:
Prof. Guido Giordano

Co-Tutor:
Dott. Sandro de Vita
Prof. Alessandro Vona

Ph.D. candidate:
Dott. Paolo Primerano

XXXII Cycle

Index

Introduction

This research project owes his birth from the needs which comes out from the Tavolo di Lavoro – Ischia 2016 which led to the publication of the Selva et al., (2019) paper. The knowledge about the hazard in the island is mostly qualitative and exist a lack in eruptions characterization in terms of eruption dynamics and about the associated impacts.
Starting with this kind of considerations in mind, it has been decided to focus the attention on a set of eruptions, which could represent a set of relevant and applicable scenarios which can be used by the Department of Civil Protection to reduce the risk connected to a renewal of activity.
The object of this study is the investigation of the mechanisms of emplacement of both effusive and explosive eruption in order to determine the impact parameters of the most recent eruption of Ischia Island.

Ischia island is a densely inhabited active volcano at the northwestern corner of the Gulf of Naples. After the Greek and the Roman establishments on the island (Buchner, 1986; Civetta et al., 1999), the ‘‘re-discovery’’ of Ischia as a destination occurred from the mid sixteenth century with the publication of *De’ rimedi naturali che sono nell’isola di Pithecusa, hoggi detta Ischia* (On the natural remedies on the island of Pithecusa, today called Ischia) (Jasolino 1763). Since the end of Second World War a lack of land-use planning regulation has generated an undisciplined boom in construction (Carlino et al., 2010). Nowadays, Ischia hosts a permanent population of about 65’000 people which increases during summer because of the presence of tourist resorts, commercial enterprises and farms. Nonetheless, the volcanic risk in case of renewal of activity is relatively understudied.

The island of Ischia is an active volcanic field and its geological history is characterized by an interplay among tectonism, volcanism, volcano-tectonism, erosion, and sedimentation (Capaldi 1976; Buchner 1986; Vezzoli 1988; Orsi et al. 1991, 1996; de Vita et al. 2006; Brown et al. 2008; de Vita et al., 2010; Sbrana et al. 2011, 2018).
The oldest outcrops date back to about 150 kyrs BP, while the most recent eruption occurred in 1302 A.D. in the eastern sector of the island (Vezzoli 1988; Civetta et al. 1991). During this period, five phases of activity (Fig. 1) have been distinguished (Poli 1989; Civetta et al., 1991; Casalini et al., 2017).

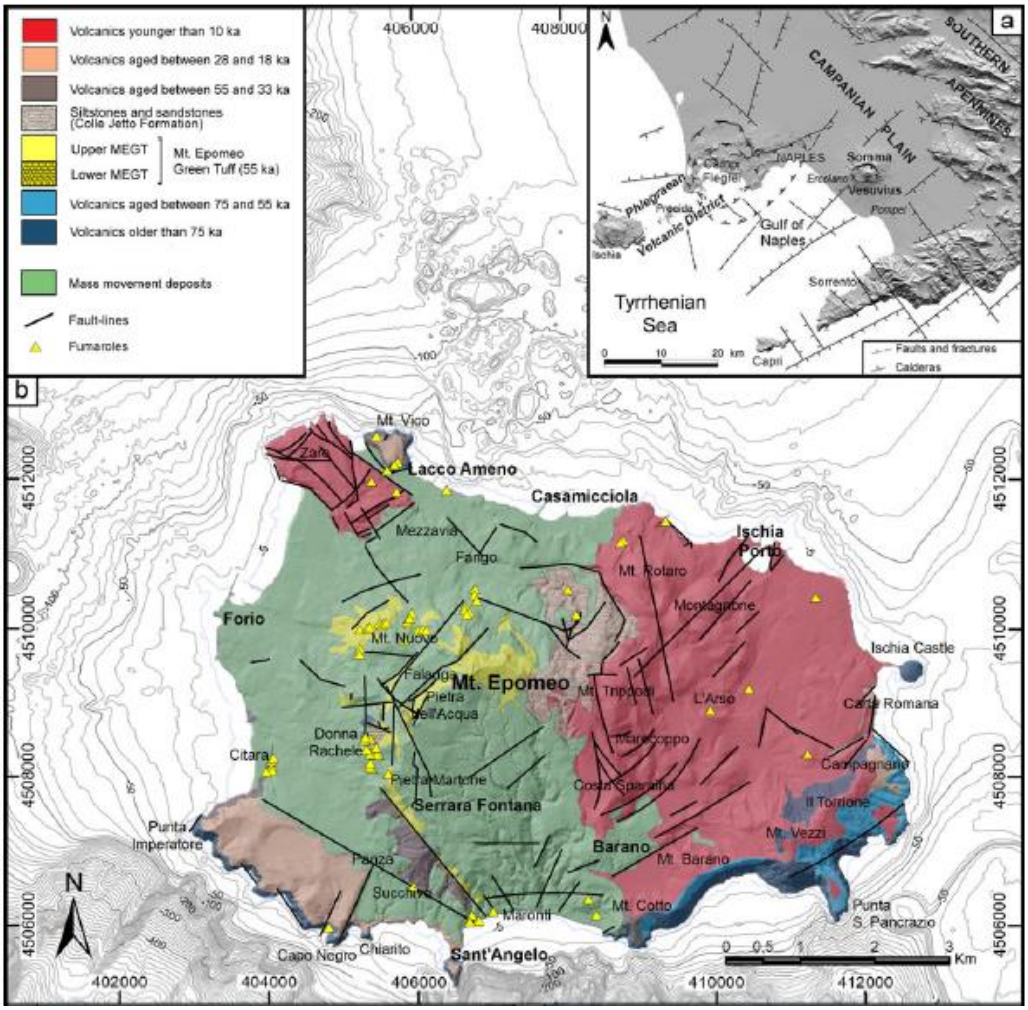

Fig.1 - Simplified geological map of Ischia island showing the volcanic products of the five eruptive phases (Della Seta et al., 2012).

The I Phase is the oldest outcropping phase of subaerial volcanic activity and occurred between 150 and 75 kyrs with eruption of mainly trachytic and trachyphonolitic lava flows and domes, with minor pyroclastic rocks (Vezzoli 1988; Brown et al. 2014; Melluso et al. 2014).

The II Phase occurred between 75 and 55 kyrs, and was marked by a change of the eruptive style from mainly effusive to highly explosive eruptions with emplacement of complex successions of trachytic pumice falls interlayered with pyroclastic density currents and breccias (Orsi et al. 1991; Brown et al. 2008).

The III Phase occurred between 55 and 33 kyrs, and started with the paroxysmal Mt. Epomeo Green Tuff eruption, forming a ~10 × 7 km caldera and erupting some 40 km^3 of volcanic products (Vezzoli 1988; Tibaldi and Vezzoli 1998; Tomlinson et al. 2014). The Mt. Epomeo Green Tuff consists of trachytic ignimbrites partially filling a submerged depression, which now makes up the central part of the island. Minor trachytic hydromagmatic to magmatic eruptions from small vents along the southwestern and northwestern sectors of the island prolonged this phase up to 33 kyrs (de Vita et al. 2010).

The IV Phase occurred at 28 kyrs, after 5 kyrs of quiescence, with the arrival of shoshonitic magma into the main reservoir, which triggered the Mt. Epomeo caldera resurgence of some 900 m (Poli et al. 1989; Civetta et al. 1991; Orsi et al. 1991; de Vita et al. 2006). This phase continued sporadically

with explosive and effusive eruptions until 18 kyrs, and its products are scattered along the peripheral sector of the island, at Mt. Vico, between Punta Imperatore and Mt. St. Angelo, and south of Castello.

The V Phase is the last phase of activity and commenced at about 10 kyrs and is still active with the last historic lava flow eruption recorded at Mt. Arso in 1302 A.D. (Chiesa et al., 1986). This phase is characterized by mainly latitic to trachytic monogenetic volcanic activity and ongoing Mt. Epomeo caldera resurgence (Orsi et al. 1991, 1996; de Vita et al. 2006, 2010). Caldera resurgence restricted eruptions to the eastern sector of the island with only a few vents located outside this sector, along regional fault systems. The volcanic activity was characterized by lava domes and high aspect ratio lava flows, together with magmatic and phreatomagmatic explosive eruptions that generated tuff-cones, tuff-rings, and variably dispersed pyroclastic fall and pyroclastic current deposits (de Vita et al. 2010).

Considering the temporal variation of erupted magmas over the past 150 kyr of volcanic activity at Ischia, the recurrence of more- and less-evolved products is indicative of alternating periods of replenishment, differentiation, eruption, and quiescence in a dynamic volcanic system (Poli et al. 1989; Civetta et al. 1991; de Vita et al. 2010; D'Antonio et al. 2013; Brown et al. 2014).
More-evolved compositions (i.e., trachytes) are more common in the volcanic products preceding the Mt. Epomeo eruption at 55 kyrs (Sbrana & Toccaceli 2011; Casalini et al., 2017). In particular volcanism on Ischia during the time span 75–50 kyrs BP was affected by variable magma differentiation processes at deep and shallow depths, such as replenishment, fractional crystallization, mixing and assimilation. The Sr- and Nd- isotopic and geochemical variations through time suggest that the pre-MEGT volcanic activity was characterized by extrusion of magma batches poorly enriched in radiogenic Sr that mostly differentiated at shallow depth, where they attained a TiO_2–Fe_2O_3-rich phonolitic composition through assimilation of a feldspar-rich mush. Prior the MEGT eruption, the magmatic system was recharged by a more enriched in radiogenic Sr magma, potentially contaminated by both Hercynian crust at 8–12 km depth and by assimilation of feldspar mush at ca. 5 km depth. After the MEGT eruption, influx of poorly evolved magma fed the later eruptions (Casalini et al., 2017).
The magmatism in the last 55 kyrs is divided into three phases of activity, each characterized by a distinct trend in Sr-isotope composition.

The 55-30 kyrs phase is characterized by a narrow range of Sr-isotope compositions and by constant Nd-isotope composition, is dominated by explosive eruptions, with the rocks showing an increasing degree of differentiation with decreasing age. The range in chemical composition displayed by coeval rocks suggests the existence of an evolving, chemically zoned magma chamber, tapped at different levels during each eruption.
The beginning of the 28-18 kyrs phase is marked by an abrupt change in Sr- and Nd-isotope compositions. In fact, at 28 kyrs, trachybasaltic magma with Sr-isotope composition ranging from 0.70608 to 0.70617 and Nd isotope composition of 0.51259 was erupted in the southern part of the island. This suggests the arrival in the system of magma with a lower Sr-isotope ratio and a higher Nd-isotope ratio. The age of this arrival has been assumed to correspond to the beginning of the uplift of the Mt. Epomeo block. The triggering mechanism for the resurgence was probably the increase of pressure in the magma chamber due to the addition of new magma (Civetta et al., 1991).

The last phase of activity (10 kyrs-1302 A.D.) is characterized by complex geochemical and isotopic trends. At 10 kyrs, alkalitrachyte with less radiogenic Sr composition in comparison with the 18-kyrs-old alkalitrachyte was erupted. This probably indicates the arrival of a geochemically distinct magma into the system. During the last 10 kyrs mostly alkali-trachytic lavas and pyroclastics were erupted, suggesting a periodic tapping from the capping low-density layer of a zoned magma chamber. Subordinately latitic magmas were also erupted. The latites are characterized by more radiogenic Sr composition in comparison with the trachytes and alkali-trachytes. The inverse correlation between degree of differentiation and Sr-isotope ratio is also shown by samples collected at different stratigraphic heights from the Arso (1302 A.D.) lavas, which show a range of variation in Sr-isotope ratio from 0.70626 (last-erupted trachyte) to 0.70658 (first-erupted latite) (Civetta et al., 1991).

Different primary mafic magmas, coming from large depths and carrying distinct isotopic features generated mafic to felsic magmas with variable O-Sr–Nd isotope ratios. These magmas interacted in shallower reservoirs of the Ischia plumbing system. This has occurred many times during Ischia's volcanic history. Mingling/mixing processes among magmas characterized by different chemical and isotopic composition are shared by other volcanoes of the Phlegraean Volcanic District located along the N60°E trending, regional fault system, passing through Ischia and Procida islands and possibly the Campi Flegrei caldera (D'Antonio et al., 2013). This prominent tectonic structure must play a significant role in giving mafic magmas coming from large depth the opportunity to meet felsic magmas stagnating in shallower reservoirs, eventually triggering explosive eruptions (Orsi et al., 1991, 1996; Acocella and Funiciello, 2006; Vezzoli et al., 2009; de Vita et al., 2010; Moretti et al., 2013).
At Ischia some magmatic bodies have been recognized by Orsi et al., (1999) beneath the north-eastern side and only one below the north-western side of the island. The shallower body is 2.5 km deep, 1.5 km thick and oriented in a NW–SE direction. The location of this body, its depth and orientation seem to coincide with a seismic discontinuity (unpublished data of the Vesuvian Observatory, Naples). Furthermore, the gravity map by Nunziata and Rapolla (1987), shows a NW–SE alignment of the Bouguer anomaly isolines in this zone. Thus, this body could be considered as evidence of a fault, the magnetization of which is due to a cooled magma filling. Moreover, the depth of the top of this body together with the absence of structural evidence on the surface suggest that this fault is buried below the less than 10 kyrs (Orsi et al., 1996) volcanics and thus it is older than 10 kyrs. Directly below this, at 4 km of depth, another body is located. It is located directly beneath the area characterized by less than 10 kyrs volcanic activity (Vezzoli, 1988; Orsi et al., 1991). Thus, it could represent a large zone intensively fractured through which the magmas ascended to the surface. Finally, the deepest is located at 7 km depth. Since geological and petrological data suggest the existence of a deep magma chamber at Ischia (Orsi et al., 1991; Piochi et al., 1999) we suppose that could represent a magma batch totally solidified, or otherwise, tentatively, a magma chamber, as the geothermal flux (Della Vedova et al., 1991) suggests that at this depth the temperature could reach the solidus temperature value about 1000°C. In the latter hypothesis, the chamber can be a very anisotropic, magnetized igneous body being constituted by two likely interconnected parts: a part with temperature below the Curie point and magnetization higher than the average body such as a solidified magma portion, and a nonmagnetic partly liquid part (Orsi et al., 1999).

We decided to choose as a reference period for our analysis, in accord with Selva et al., (2019), the last 10 kyrs, which can be considered as a distinct period of activity respect to the preceding eruptive history of Ischia because occurred a significant change in average eruption rate and in geochemical composition of magmas after an 8 kyrs period of relative quiescence. The total number of eruptions occurred in the last 10 kyrs is 49, with 34 eruptions in the last 3 kyrs.

Before starting to analyze a set of specific eruptions, there is the need to describe the distribution of the events in time, in order to characterize the volcanic history in the reference period and to understand the role of the current period of pause in the eruption activity. Eruptions in the last 10 kyrs has been characterized in terms of volume, and a volume-time distributions diagram has been produced.

Products of both effusive and explosive eruptions have been considered for the scenarios. For the explosive activity we have chosen Cretaio Tephra that is the highest magnitude event in the last 10 kyrs in Ischia, which covered almost all the eastern sector of the island. This eruption started with a phreatomagmatic phase that produced base surges, and was followed by the formation of a pulsating sub-Plinian to Plinian eruption column. In order to produce a new scenario of explosive eruptions, a reconstructing total grain-size distribution, fallout dispersal and fallout hazard maps through field data analysis and numerical modelling have been performed.

For the effusive activity we have chosen Arso Lava and Zaro Lava Domes and Flows.
Arso Lava is the product of the last eruption at Ischia, which occurred in 1302 A.D. The eruption duration is known and this information make possible to set constraints to a rheological model that can be extended to estimate duration and behavior of other lava flows in the island, with similar physical properties and chemical composition.
Zaro Lava Domes and Flows is a lava field located in the north-western corner of the island, it is composed of lavas that is characterized by a very high degree of porphiricity and, therefore, it has been selected as a second case study for this investigation.
In order to reconstruct the syneruptive rheology of the lava flows, textural and rheological studies have been performed.

References

Acocella, V. and R. Funiciello (1999). The interaction between regional and local tectonics during resurgent doming: the case of the island of Ischia, Italy. Journal of Volcanology and Geothermal Research 88(1): 109-123.

Brown, R. J., G. Orsi, et al. (2008). "New insights into Late Pleistocene explosive volcanic activity and caldera formation on Ischia (southern Italy)." Bulletin of Volcanology 70(5): 583-603.

Brown, R., L. Civetta, et al. (2014). "Geochemical and isotopic insights into the assembly, evolution and disruption of a magmatic plumbing system before and after a cataclysmic caldera-collapse eruption at Ischia volcano (Italy)." Contributions to Mineralogy and Petrology 168(3): 1035.

Buchner, G. (1986). Eruzioni vulcaniche e fenomeni vulcanotettonici di età preistorica e storica nell'isola d'Ischia. *Tremblements de terre, eruptions volcaniques et vie des hommes dans la Campanie antique*, *7*, 145-188.

Capaldi, G., Civetta, L., & Gasparini, P. (1976). Volcanic history of the island of Ischia (South Italy). Bulletin Volcanologique, 40(1), 11-22.

Casalini, M., R. Avanzinelli, et al. (2017). "Geochemical and radiogenic isotope probes of Ischia volcano, Southern Italy: Constraints on magma chamber dynamics and residence time." American Mineralogist 102(2): 262-274.

Chiesa, S., Poli, S., & Vezzoli, L. (1986). Studio dell'ultima eruzione storica dell'isola di Ischia. Bollettino GNV, 1, 153-166.

Civetta, L., G. Gallo, et al. (1991). "Sr-and Nd-isotope and trace-element constraints on the chemical evolution of the magmatic system of Ischia (Italy) in the last 55 ka." Journal of Volcanology and Geothermal Research 46(3-4): 213-230.

Civetta, L., A. De Vivo, et al. (1999). "Il vulcanismo a Ischia in età greco-romana secondo le evidenze geologiche e le testimonianze storico-letterarie." Vichiana, Loffredo Editore. Napoli 15732.

D'Antonio, M., Tonarini, S., Arienzo, I., Civetta, L., Dallai, L., Moretti, R., ... & Trecalli, A. (2013). Mantle and crustal processes in the magmatism of the Campania region: inferences from mineralogy, geochemistry, and Sr–Nd–O isotopes of young hybrid volcanics of the Ischia island (South Italy). *Contributions to Mineralogy and Petrology*, *165*(6), 1173-1194.

Della Vedova, B., Mongelli, F., Pellis, G., Squarci, P., Taffi, L., & Zito, G. (1991). Heat flow map of Italy.

de Vita, S., Sansivero, F., Orsi, G., & Marotta, E. (2006). Cyclical slope instability and volcanism related to volcano-tectonism in resurgent calderas: the Ischia island (Italy) case study. *Engineering Geology*, *86*(2-3), 148-165.

de Vita, S., Sansivero, F., Orsi, G., Marotta, E., & Piochi, M. (2010). Volcanological and structural evolution of the Ischia resurgent caldera (Italy) over the past 10 ky. *Geol. Soc. Am. Spec. Pap*, *464*, 193-239.

Jasolino, G. da Pistoja, (1763). *De' rimedi naturali che sono nell'isola di Pithecusa, hoggi detta Ischia*.

Melluso, L., V. Morra, et al. (2014). "The crystallization of shoshonitic to peralkaline trachyphonolitic magmas in a H2O–Cl–F-rich environment at Ischia (Italy), with implications for the feeder system of the Campania Plain volcanoes." Lithos 210: 242-259.

Moretti, R., I. Arienzo, et al. (2013). "The deep plumbing system of Ischia: A physico-chemical window on the fluid-saturated and CO2-sustained Neapolitan Volcanism (Southern Italy)." Journal of Petrology 54(5): 951-984.

Nunziata, C. and A. Rapolla (1987). "A gravity and magnetic study of the volcanic island of Ischia, Naples (Italy)." Journal of Volcanology and Geothermal Research 31(3-4): 333-344.

Orsi, G., Gallo, G., & Zanchi, A. (1991). Simple-shearing block resurgence in caldera depressions. A model from Pantelleria and Ischia. *Journal of Volcanology and Geothermal Research*, *47*(1-2), 1-11.

Orsi, G., Piochi, M., Campajola, L., D'Onofrio, A., Gialanella, L., & Terrasi, F. (1996). 14C geochronological constraints for the volcanic history of the island of Ischia (Italy) over the last 5000 years. *Journal of Volcanology and Geothermal Research*, *71*(2-4), 249-257.

Orsi, G., D. Patella, et al. (1999). "Magnetic modeling of the Phlegraean Volcanic District with extension to the Ponza archipelago, Italy." Journal of Volcanology and Geothermal Research 91(2-4): 345-360.

Piochi, M., L. Civetta, et al. (1999). "Mingling in the magmatic system of Ischia (Italy) in the past 5 ka." Mineralogy and Petrology 66(4): 227-258.

Poli, S., S. Chiesa, et al. (1989). "Time dimension in the geochemical approach and hazard estimates of a volcanic area: The isle of Ischia case (Italy)." Journal of Volcanology and Geothermal Research 36(4): 327-335.

Sbrana, A., R. Toccaceli, et al. (2011). "Carta Geologica della Regione Campania, Note Illustrative della Carta Geologica alla scala 1: 10.000, Foglio 464 Isola di Ischia, Regione Campania-Assessorato Difesa del Suolo."

Sbrana, A., P. Marianelli, et al. (2018). "Volcanology of Ischia (Italy)." Journal of Maps 14(2): 494-503.

Selva, J. et al., (2019) Multiple natural hazards at volcanic islands: a review for the Ischia volcano (Italy). Journal of Applied Volcanology.

Tibaldi, A. and L. Vezzoli (1998). "The space problem of caldera resurgence: an example from Ischia Island, Italy." Geologische Rundschau 87(1): 53-66.

Tomlinson, E. L., P. G. Albert, et al. (2014). "Age and geochemistry of tephra layers from Ischia, Italy: constraints from proximal-distal correlations with Lago Grande di Monticchio." Journal of Volcanology and Geothermal Research 287: 22-39.

Vezzoli, L., & Barberi, F. (1988). Progetto finalizzato geodinamica: monografie finali. X: Island of Ischia. *Quaderni de La ricerca scientifica*, (114).

Vezzoli, L., C. Principe, et al. (2009). Modes and times of caldera resurgence: the< 10 ka evolution of Ischia Caldera, Italy, from high-precision archaeomagnetic dating. Journal of Volcanology and Geothermal Research 186(3-4): 305-319.

Chapter 1: Volume-time distribution of Ischia island eruption units of the last 10 kyrs

Paolo Primerano[1], Guido Giordano[1], Jacopo Selva[2], Sandro de Vita[3]

[1]Dipartimento di Scienze, Università degli Studi Roma Tre, L.go San Leonardo Murialdo 1, 00146 Roma, Italy.
[2]Istituto Nazionale di Geofisica e Vulcanologia - Via Donato Creti, 12, 40126 Bologna, Italy.
[3]Istituto Nazionale di Geofisica e Vulcanologia - Osservatorio Vesuviano, Via Diocleziano 328, 80124 Napoli, Italy.

Abstract

The need to assess the localization and the timing for next eruptions, their typology and their duration are essential questions that the scientific community has to answer. Deterministic forecasting is not possible, so the first step is the characterization of the history of a volcanic system. In the existing literature about Ischia island, a high-risk volcanic environment, works which combined dataset in order to produce hazard maps, are relatively poor and the analysis are only qualitative and the use of the existent data debatable.

In this work, a volume-time distribution in the last 10 kyrs has been performed, by the volume calculation of each eruption.

Different methodology has been applied for effusive and explosive eruptions. Lava domes and flows volumes have been calculated above the base of the lava by reconstructing the TIN of the vectorialized base, on the basis of the extent identified by de Vita et al., (2010) and according to evidence in the field, DEM and aerial photos. Explosive eruptions volumes have been calculated by a dispersal-based methodology.

Eruptions have been firstly classified in domes and lava flows for the effusive and magmatic, phreatomagmatic, and mixed for the explosive eruptions. The total number of eruptions occurred in the last 10 kyrs is 49, with 34 eruptions in the last 3 kyrs.

The preferred size of eruptive volume has been identified and the role of the last period of quiescence, since 1302 A.D. has been characterized in respect to other periods of quiescence in the past.

Introduction

Ischia island is a densely inhabited active volcano located in the north-western part of the Gulf of Naples, which hosts a permanent population of about 65'000 people which increases during summer.
Ischia is located in one of the most densely populated area of the world, so the impact of a new eruption in the island could potentially not only affect Ischia itself, but directly and indirectly all the population living in Neapolis and in the Campanian region.
The expected impact is proper of a populated volcanic Islands close to densely urbanized district in the mainland. This configuration can be recognised in several part of the world such as in Indonesia, Japan and Philippines (Shimozuru, 1996; Thouret, 1999; Chester et al., 2000).

The need to assess when and where eruptions will occur, as well as their typology and how long them will last are essential questions that administrators and public opinion urge the scientific community to answer, but volcanoes are complex systems and a deterministic forecasting is not possible (Sparks, 2003). Long-term eruption forecasting represents a fundamental goal in volcanology. Long-term probabilistic eruption forecasting (Newhall & Hoblitt, 2002) is the basic component for hazard quantifications (Marzocchi et al., 2008) land use and emergency planning, and depends on the quality and quantity of the available past eruption data (Marzocchi & Bebbington, 2012).
In the existing literature about Ischia volcano, only few works focus on the forecast of potential vent positions (Selva et al., 2019 for a review). Among them, Sbrana & Toccaceli, (2011) combines the existent data about localization of earthquake epicentres (from Alessio et al., 1996), fumaroles, vents and geological and tectonic data (Cubellis et al., 2004) to produce a boolean probability map on the opening of new eruptive vents. As it regards the possible size of the eruptions, Sbrana & Toccaceli (2011) present a list of five possible eruptive scenarios based on the different typology of eruption present in the island in the Holocene period. This kind of analyses is only qualitative and the used eruption trigger data is debatable.

More recently Selva et al. (2019) have reappraised the assessment of the multi-hazard at Ischia based on the existent knowledge, reviewing the existing data and hazard approaches. The authors have identified the last 10 kyrs as the reference period for the long-term assessment of the frequency and style of eruptions.
Our work has the aim to extend the study of Selva et al. (2019) focussing on the statistical distribution of past eruptive activity and the calculation of the associated erupted volumes to better frame the present state of quiescence of the volcano, which lasts since its last effusive eruption occurred in 1302 A.D. known as the Arso lava.

Here we review the existing database of Ischia eruptions to provide a more robust statistics of eruption size and frequency at Ischia in the last 10 kyrs, constraining also relative uncertainty. The understanding of the eruptive history of the island is indeed crucial for hazard quantifications, allowing also the potential identification of the more likely eruptive scenarios for both explosive and effusive eruption styles.

This may also allow interpreting the significance of the current period of quiescence since the last event in 1302 A.D. (Capaldi et al., 1976; Chiesa et al., 1986; Vezzoli 1988). Understanding the relationship between the current period of quiescence and the time to the next eruption is indeed one of the most important part for hazard assessment (Bebbington, 2015). For example, the new data may allow testing a "time predictable" behaviour model (relationship between the time to the next eruption and the size of the previous event), or a "size predictable" model (relationship between the size of an event and the previous repose time) (Marzocchi & Zaccarelli, 2006), established that a homogenous Poisson distribution could not be sufficient to describe the temporal distribution of eruptions at Ischia (Zaccarelli et al., 2018) and therefore the Arso eruption may have ended a long-lasting cluster of eruptions (Selva et al., 2019).

Results such as eruptive frequencies, periods of quiescence and volcanic activity acceleration have been compared with the surrounding volcanic systems as Vesuvius and with similar activity as Campi Flegrei. Vesuvius, for example, was characterized by an average rate of eruption of 0.3 per year in the time period 1631–1944 (Marzocchi & Zaccarelli, 2006), showing frequent eruptions of smaller size and intensity (Sandri et al., 2009), after a quiescence period of centuries. The information about the number and the volume of eruptions can be used to produce probability hazard map for future vent opening (Selva et al., 2012).

Moreover, the understanding of the eruptive history of the island is crucial for the identification of the eruptions that can be taken as the likely scenarios for both explosive and effusive eruption styles.

1. Geological background

The volcanic activity of Ischia can be subdivided in several phases (Poli et al., 1989; Civetta et al., 1991; Casalini et al., 2017). The most important event occurred at 55 kyrs and consisted in the caldera-forming eruption of Monte Epomeo Green Tuff. The resurgence of the caldera floor started after 33 kyrs forming progressively the Monte Epomeo dome, which is now more than 1000m a.s.l.

The last period of activity in the island began at about 10 kyrs (Selva et al., 2019 and reference therein) and is still active with the last historic lava flow eruption recorded at Mt. Arso in 1302 A.D. (Chiesa et al., 1986). This phase is characterized by mainly latitic to trachytic monogenetic volcanic activity and ongoing Mt. Epomeo caldera resurgence (Orsi et al. 1991, 1996; de Vita et al., 2006, 2010). The volcanic activity was characterized by lava domes and high aspect ratio lava flows, with magmatic and phreatomagmatic explosive eruptions that generated variably dispersed pyroclastic fall and PDC deposits (de Vita et al., 2010).

According to Selva et al., 2019 (and references therein), the last 10 kyrs of volcanic activity at Ischia can be differentiated with respect to the previous period for a series of distinct characteristics, such as the significantly larger total number of recorded eruptions (de Vita et al., 2010), the change in the magma chemistry and a change in the isotopic signatures (Civetta et al., 1991; Casalini et al., 2017), and the localization of the eruptive centres at the border of the most resurgent block (Fig. 1).

We also take the last 10 kyrs of volcanic activity as the reference of the current state of the volcano and its associated hazards and therefore the time frame where to perform our analysis.
The state of preservation of the eruptive deposits, belonging to this time interval, may not be the same for all units. The oldest and smallest deposits, especially in a volcanic sporadic activity, may be subject to erosion and this means an under-recording in the eruptive catalogue (Brown et al., 2014).
However, most of the eruptions of the last 10 kyrs at Ischia issued from vents scattered across the eastern side of the caldera, at the base of the Monte Epomeo uplifted block, defining an intracaldera monogenetic field. For this reason, we are confident that the deposits mappable by surface geology (de Vita et al., 2010; Sbrana et al., 2011) reflect accurately the number of eruptions occurred in the last 10 kyrs, with little chance to have deposits completely buried or deposits totally eroded away. This is particularly true for the effusive units, which at Ischia are mostly lava domes and thick flows, which mostly preserve very pristine morphologies and are very resistant to erosion.

For these reasons, last 10 kyrs is therefore chosen as the reference period for our analysis.

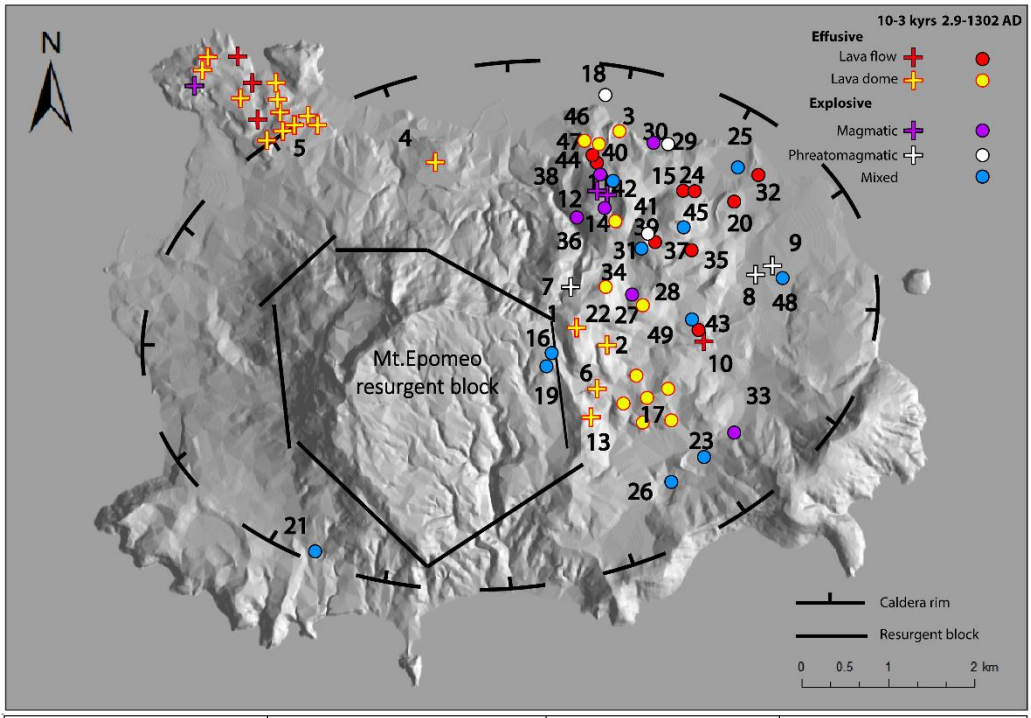

1	Trippodi Lavas	14	Cava del Puzzillo III Tephra	27	Cava Bianca Tephra	40	Villammare Tephra
2	Selva del Napolitano Lavas	15	Sant'Alessandro Lavas	28	Posta Lubrano Lavas	41	Fondo d'Oglio Tephra
3	Castiglione and Bagnetielli Lavas	16	Cannavale Tephra	29	Cafieri Tephra	42	Bosco della Maddalena Tephra
4	Fundera Lavas	17	Cantariello Lavas	30	Cafieri Lavas	43	Fiaiano Tephra
5	Zaro Lava domes and flows	18	Punta La Scrofa Tephra	31	Posta Lubrano Tephra	44	Rotaro Lavas
6	Cannavale Lavas	19	Marecoppo Tephra	32	San Pietro Lavas	45	Montagnone-Maschiata Lavas
7	Maisto Tephra	20	San Ciro Lavas	33	Cava Nocelle Tephra	46	Punta La Scrofa Lavas
8	Catavola Tephra	21	Punta Chiarito Tephra	34	Cretaio Tephra	47	Pietra Vono Lavas
9	Piano Liguori Tephra	22	Mt. Toppo Lavas	35	Arcamone-Sacchetta Lavas	48	Fondo Bosso Tephra
10	Rio Corbore Lavas	23	Molara Tephra	36	Cava Buceto Tephra	49	Arso Lavas and Tephra
11	Cava del Puzzillo I Tephra	24	Montagnone I and La Quercia Lavas	37	Bosco dei Conti Tephra		
12	Cava del Puzzillo II Tephra	25	Ischia Porto Tephra	38	Mt. Tabor Lavas		
13	Costa Sparaina Lavas	26	Vateliero Tephra	39	Bosco della Maddalena Lavas		

Fig.1 – DEM of ischia island. With different colour, the volcanic vents with their typology of activity have been reported. Plus and dots indicate different times of activity (modified from Selva et al., 2019).

Nowadays Ischia Island is in a period of quiescence in terms of eruptive activity. The last event in the island was in 1302 A.D. with the eruption of Arso Lavas. A lava flow of about 0.03 km^3 (Chiesa et al., 1986), a scoria fallout and a pyroclastic deposit are the products of this eruption. The flow, from Faiano vent to Punta Molina, lasted 2 months and the historical chronicles describe this event as a pestilence which involved most of the districts in the Gulf of Naples (Chiesa et al., 1986).

Since 1302 A.D., the permanent population in the island is highly increased, which means a relative increase of the volcanic risk. The main critical point is a gap of knowledge about magnitude and intensity assessment of the past explosive eruptions (Selva et al., 2019).

On the island thermal springs are widely diffused, especially in the western flank of Mt. Epomeo with the Donna Rachele fumarolic area. Thermal springs, with T up to 90°C and fumaroles with T at about 100°C (Pecoraino et al., 2005) are the surface expression of an active geothermal system. The geothermal gradient reaches values of about 200°C/km (Castaldo et al., 2017) according to the rheology of the crustal local structure (De Novellis et al., 2018).
Regarding the soil deformation, the Geometric High Precision Levelling survey performed by Del Gaudio et al., (2010), produced a dataset which shows a deflation of Mt. Epomeo of about 8mm/yr, which is consistent with the current period of quiescence. However, volcano-tectonic activity has produced strong and shallow destructive earthquakes in the northern part of the island (Casamicciola), in 1883 (Carlino et al., 2010) and in 2017 (De Novellis et al., 2018).

2. Material and methods

The eruptive record of the last 10 kyrs of Ischia is made of lava units and pyroclastic units; the latter are both magmatic and phreatomagmatic in origin and made by fall and pyroclastic density current deposits (de Vita et al., 2010; Sbrana and Toccaceli, 2011). In the eruptive catalogue of the last 10 kyrs the total number of recognised eruptions is 49 of which 24 effusive and 25 explosive (Selva et al., 2019 and references therein).
In order to reconstruct the time-volume distribution we describe now the methods for the computation of the volumes of both lavas and pyroclastic units, which so far has never been calculated.
No new age determinations have been performed for this work, because all investigated units are well constrained, based on available stratigraphic (Vezzoli et al., 1988; de Vita et al., 2010; Sbrana et al., 2011) historical documents (Buchner, 1986; Iacono, 1996) and geochronological data (Orsi et al., 1996; Selva et al., 2019; Speranza personal communication).

2.1 Calculation of the volume of lava units

For lava domes, coulees and thick lava flows, the volumes have been calculated by masking a DEM, with a resolution of 10m, with the lava extent identified by de Vita et al., (2010), according to evidence in the field and morphology cross-checked by both DEM and aerial photos (1955, 1990, 2003 surveys). The lava volumes have been calculated above the base of the lava by reconstructing the Triangular Irregular Networks (TIN) of the vectorialized base. The products of the effusive

activity are characterized by reduced erosional processes because of their recent emplacement and hard lithology. Since the intracaldera activity consisted mainly of a monogenetic volcanic field, the products of the effusive eruptions are not, in general, overlapping. For these reasons the main sources of uncertainty are the resolution of the DEM and the unknown shape of the paleotopography onto which the lavas emplaced; however, at first order, a 10 m resolution DEM can be considered accurate enough when compared with the areal extents of the lavas which are all in the order of 0.1/1 km^2 to provide fully reliable shapes. Furthermore, the considered lavas are emplaced on the Ischia caldera floor, where the paleotopography can be considered sufficiently flat, so that we exclude that a significant volume is buried in a paleo-valley or replaced by paleo-ridges. Younger pyroclastics cover has been instead estimated and removed from calculation of the volume, when appropriate. This kind of correction has been applied only in a few cases, when the thickness of the coverage represents a real source of error. Field work has been performed to check and validate all choices regarding the location of the base of lava units, the paleotopography and the presence of covers.

2.2 Calculation of the volume of pyroclastic units

The calculation of the volume of pyroclastic units on Ischia island is much more problematic respect to lava units. This is because: I) the preservation potential of the deposits is low and erosion can be extensive even for recent units; II) the deposits generally mantle the topography on wide areas making low aspect ratio deposits respect to the high aspect ratio lavas; III) a large part of the deposits is deposited off-shore so that the medial and distal deposits are not observable (cf. next Chapter 2), making it very problematic the assessment of the volume both for fall deposits, for which well constrained methods are available (Morton et al., 1956; Carey & Sigurdsson 1982; Carey & Sparks 1986; Pyle 1989; Bonadonna & Houghton 2005; Sulpizio 2005; Macedonio et al., 2008; Taddeucci et al., 2011; Bonadonna et al., 2011; Bonadonna et al., 2015, Costa et al., 2016) and for pyroclastic density current deposit.

One empirical way to approach the problem is by comparing the on-land areal extent, taken by de Vita et al. (2010) and reviewed in Selva et al. (2019) (Fig. 2), assuming the area included in the 10 cm isopach (A_{10cm}) as total area, and thicknesses of the various pyroclastic units with those of the largest among the recent explosive eruptions at Ischia (Selva et al., 2019) that is the Cretaio Tephra (Orsi et al 1992). Assuming that the areal extent of a deposit can be used as a proxy for the eruption size estimation (Scott et al., 1996).

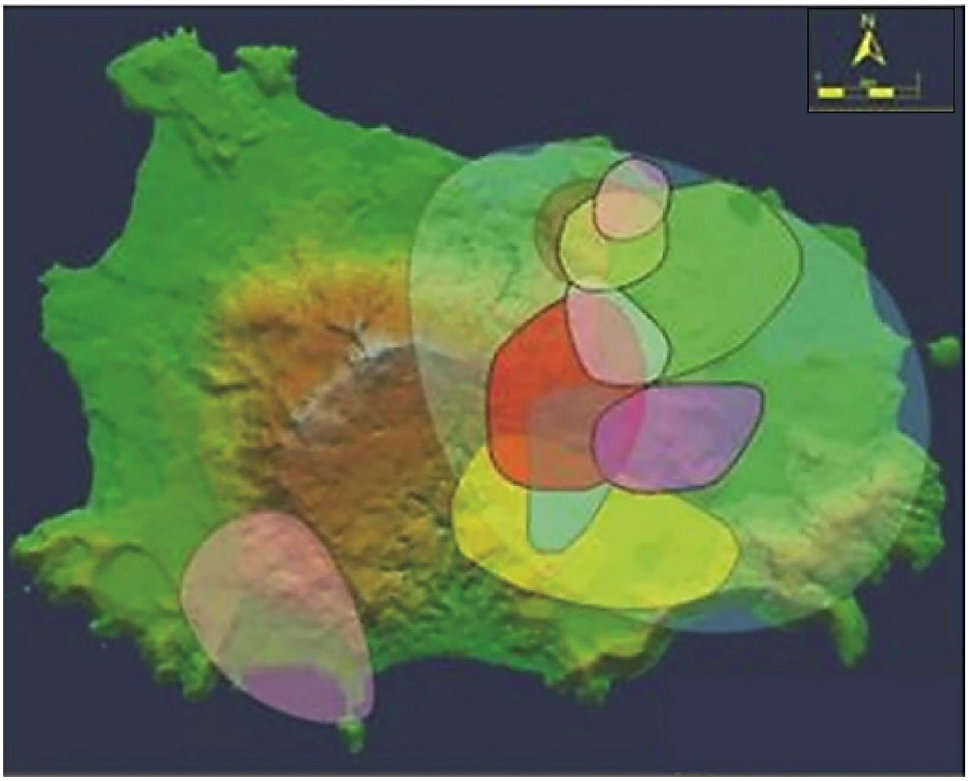

Fig.2 – Distribution of pyroclastic fall deposits in the past 10 kyrs. With different colours are reported the largest among the recent explosive eruptions (modified from Selva et al., 2019).

Given the lack of appropriate data for Ischia, we seek for a similarity between the eruption styles of the pyroclastic deposits of Ischia of the last 10 kyrs and those erupted from the nearby Campi Flegrei caldera in the same period (Orsi et al., 2009). In the Campi Flegrei system, the deposits can be followed on land until their distal reaches and therefore the relationship between areal extent, thickness and volume is well constrained (Fig. 3). Campi Flegrei eruptions described from Orsi et al., (2009), have been used for the comparison because of the many similarities between Campi Flegrei and Ischia volcanic systems. Into the caldera, affected by an ongoing resurgence, volcanism has been very intense in the past 15 kyrs (Orsi et al., 1996; Di Vito et al., 1999). Small-volume lava flows and lava domes have been emplaced and the explosive activity has emplaced an alternation of magmatic and phreatomagmatic deposits from direct fallout and dilute and turbulent density currents (Di Vito et al., 1999, Orsi et al., 2009). Furthermore, the most common erupted compositions are trachyte and alkali-trachyte (D'Antonio et al., 2007).

In this analysis we have taken into account the updated information about Agnano-Monte Spina eruption, which has been subdivided in two eruptive phases which emplaced units B1 and D1 respectively, with a DRE volume of 0.11 and 0.1 km^3 corresponding to a A_{10cm} of 427 and 701 km^2, respectively (Costa et al., 2009).

Eruption	Age (kyrs	Area 10cm (km^2)	Volume DRE (km^3)
Agnano 1	4.80	56	0.018
Averno 1	4.70	103	0.053
Agnano 2	4.60	19	0.014
Agnano 3	4.55	414	0.186
Cigliano	4.50	54	0.052
Pignatiello 2	4.45	18	0.016
Monte S. Angelo	4.40	121	0.070
Paleo Astroni 1	4.30	82	0.050
Paleo Astroni 2	4.20	218	0.100
Agnano–Monte Spina (B1)	4.10	427	0.110
Agnano–Monte Spina (D1)	4.10	701	0.100
Paleo Astroni 3	3.95	29	0.018
Solfatara	3.90	31	0.026
Astroni 1	3.88	127	0.060
Astroni 2	3.87	46	0.020
Astroni 3	3.86	274	0.157
Astroni 4	3.85	226	0.135
Astroni 5	3.84	427	0.103
Astroni 6	3.83	365	0.121
Astroni 7	3.82	50	0.065
Averno 2	3.80	45	0.067
Fossa Lupara	3.75	11	0.016
Monte Nuovo	0.50	17	0.029

Fig. 3 – Dispersal area and volumes for the explosive eruptions of the past 5 kyrs at Campi Flegrei caldera. (Modified from Orsi et al., 2009). Agnano-Monte Spina has been subdivided in two eruptive phases (Costa et al., 2009).

As it is possible to see in Fig 4, the Campi Flegrei units show an approximately linear relationship between areal extent at 10 cm of thickness and DRE volume;

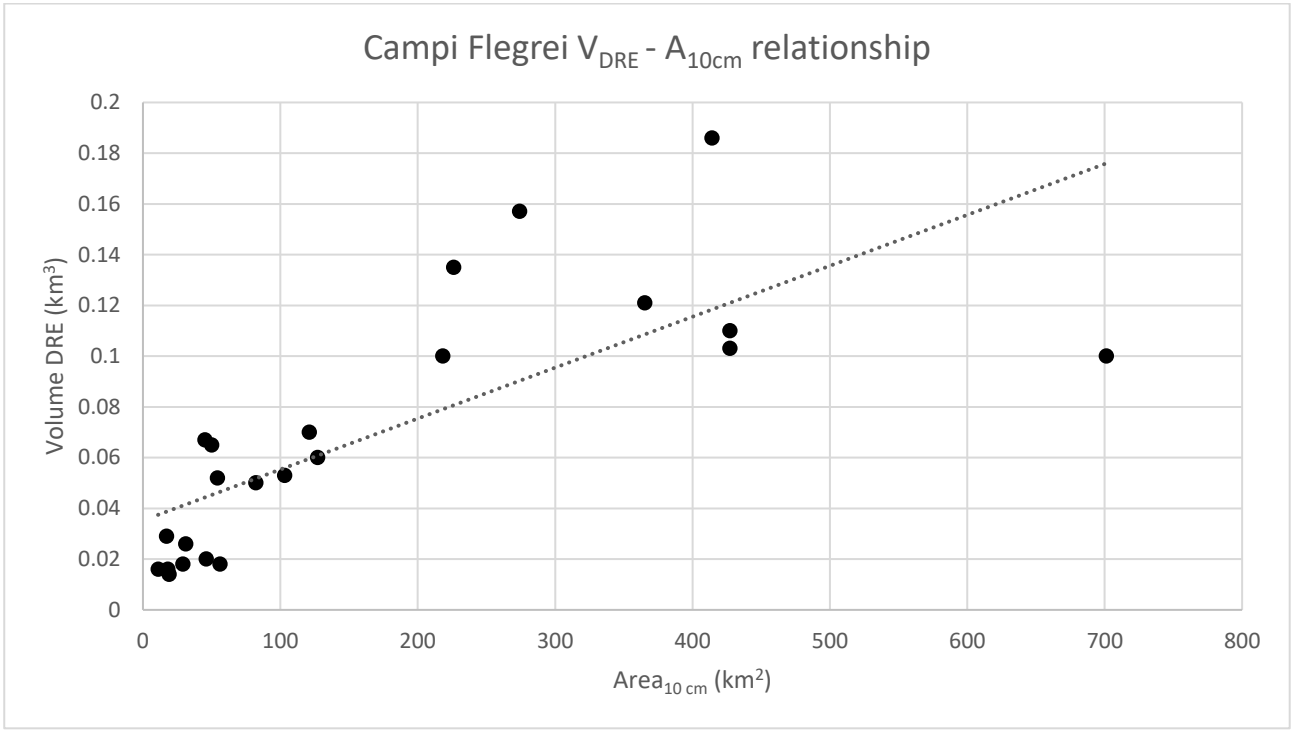

Fig. 4 – Linear relationship between areal extent and DRE volumes for the explosive eruptions of the past 5 kyrs at Campi Flegrei caldera (data from Orsi et al., 2009 and Costa et al, 2009). The relationship has been used for Ischia deposits.

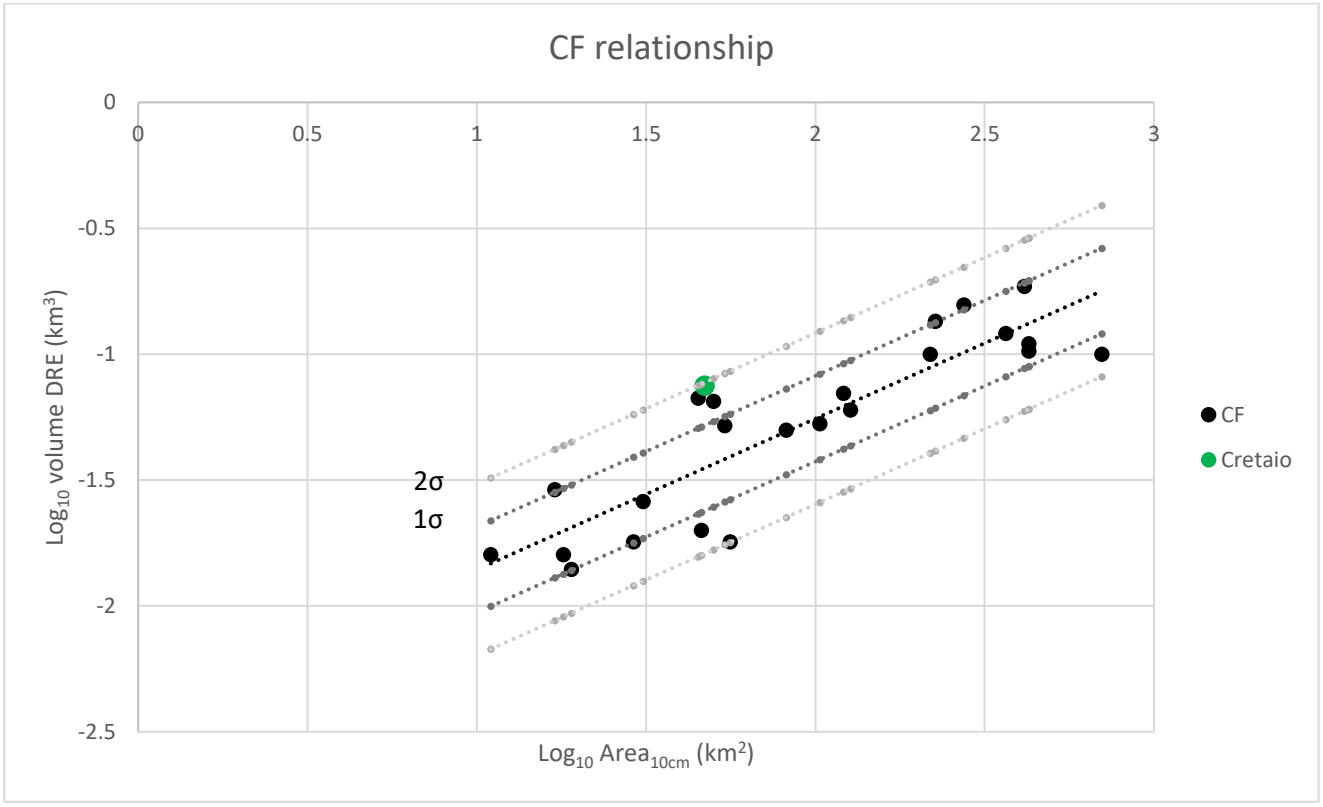

Fig. 5 – Log-Log distribution of CF (Campi Flegrei) linear relationship with 1σ and 2σ. Cretaio Tephra is included within the 2σ in the CF relationship.

The volume of the Cretaio Tephra was reported as < 0.02 km^3 DRE in the literature (Orsi et al., 1992) and it is revised in this PhD thesis at Chapter 2, computed at 0.075 km^3 DRE. From the simulations, the aerial extension of the 10 cm isopach is approximately 47 km^2. With these data, in the same Log-Log distribution diagram (Fig.5) the obtained data for Cretaio Tephra (Chapter 2 of this PhD thesis) results within the relationship in the 2σ (σ=0.17). Given the large uncertainty on the Cretaio and Campi Flegrei data, this may be considered acceptable at the very first order.

Even though we are well aware of the many limitations and large uncertainties of the proposed empirical method for correlating the volume with the reconstructed areal extent by comparing CF data and Ischia data, we believe that we can have a first order evaluation of the relative volume among the Ischia units by applying the proportionality shown by the Campi Flegrei units.

The first empirical proportionally based method on the calculus of A_{10cm} can be maintained only for explosive eruptions in which are verified both of these conditions: the deposit extent (from de Vita et al., 2010) is entirely or largely on the island and it includes the vent. For the others, a correction is needed, given that it is likely that the available areal data is severely underestimated.

To make this correction, we rely on Crataio Tephra data. The comparison of the areal extent on-land and thicknesses indeed may allow to have a first order idea of the magnitude of the selected eruption respect to Cretaio, so even if a quantitative assessment is not possible, we can assess whether the selected unit is of the same order of magnitude, or lower. The dispersal area of Cretaio Tephra on the island is 15 km^2. On the basis of this value, other volumes of other explosive units have been proportionally obtained, after the calculation of their dispersal area on the island.
In this way, with the CF relationship about Volume DRE and A_{10cm} it has been possible to calculate the volumes relative to the explosive eruption of Ischia Island.

The volume values have been calculated as DRE, in order to make it possible the comparison between the volumes of the lavas and the volumes of the pyroclastic units. The dataset about these explosive volumes has therefore to be considered valid only on the order of magnitude, and in the final results, which take into account the entire eruptive record, it can still be useful to have an overview in the volcanic history of the island.

2.3 Uncertainties

The uncertainty on the dating of the eruption is modelled as a uniform distribution, limited by the error of the dating and constrained by stratigraphic positions (Buchner, 1986; Vezzoli et al., 1988; Orsi et al., 1996; Iacono, 1996; de Vita et al., 2010; Sbrana et al., 2011; Selva et al., 2019; Speranza personal communication)

For the volumes, a log normal distribution is adopted (Garcia-Aristizabal et al., 2012). The parameters are set through the method of moments, where the average is set as the best-guess available estimation (from the previous Section) and the variance has been evaluated case by case depending on the strength of the calculation process.
Five cases have been individuated and treated in the analysis of the uncertainty:

1) Effusive eruptions: the uncertainty about volume values has origin from the GIS applied method limitations discussed above and has been estimated at 30% (Coltelli et al., 2007).
2) Explosive eruptions with deposit entirely on Ischia Island: estimated A_{10cm} with the empirical method have an uncertainty at 50% (Bonadonna et al., 2015). To this value is added the uncertainty about the CF relationship in the calculus of volumes between 0σ and 2σ.
3) Explosive eruptions with deposit partially in the sea: estimated A_{10cm} with the empirical method have an uncertainty at 50% (Bonadonna et al., 2015). To this value is added the uncertainty about the dispersal area in the sea with a factor between 1 and 3, and the uncertainty about CF relationship in the calculus of volumes, between 0σ and 2σ.
4) Explosive eruptions with deposit largely in the sea: estimated A_{10cm} with the empirical method have an uncertainty at 50% (Bonadonna et al., 2015). To this value is added the uncertainty about the dispersal area in the sea with a factor between 1 and 6 (greater than the previous case) and the uncertainty about CF relationship in the calculus of volumes, between 0σ and 2σ.
5) Explosive eruption with volume calculation external to this Chapter 1 (as Cretaio Tephra calculated with numerical modelling in the Chapter 2 of this PhD thesis). The uncertainty of the volume calculation is associated to the numerical modelling and according to Bonadonna et al. (2015) could be up to 70%, depending on the deposit exposure, distribution of the sampling points and eruption magnitude.

3. Results

During the analysis, eruptions have been classified in the following simple categories (Fig. 6), in agreement with Selva et al. (2019): domes and lava flows for the effusive and magmatic, phreatomagmatic, and mixed for the explosive eruptions.
The total number of eruptions occurred in the last 10 kyrs is 49, with 34 eruptions in the last 3 kyrs (Fig.5). The volume values of each unit with the relative uncertainty model is reported in the Appendix A.

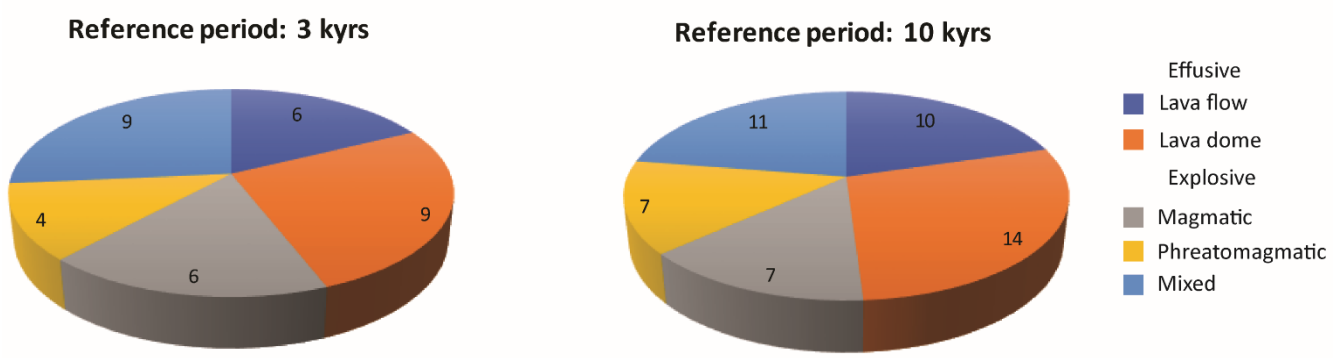

Fig.6 - Number of eruptions for different typologies, in the last 10 kyrs and the last 3 kyrs.

Best guess volume values of effusive eruption have been reported with the estimation of uncertainty in Table 1**.** With the green colour have been highlighted the largest volumes for each typology. In Appendix A, we report the uncertainty distribution for each individual eruption.

Unit	volume DRE (km^3) ± 30%
Trippodi Lavas	0.0100
Selva del Napolitano Lavas	0.0200
Castiglione and Bagnetielli Lavas	0.0002
Fundera Lavas	0.0100
Zaro Lava domes and flows	0.0300
Cannavale Lavas	0.0010
Rio Corbore Lavas	0.0020
Costa Sparaina Lavas	0.0200
Sant'Alessandro Lavas	0.0001
Cantariello Lavas	0.0040
San Ciro Lavas	0.0002
Mt. Toppo Lavas	0.0090
Montagnone I and La Quercia Lavas	0.0008
Posta Lubrano Lavas	0.0040
Cafieri Lavas	0.0010
San Pietro Lavas	0.0002
Arcamone-Sacchetta Lavas	0.0010
Mt. Tabor Lavas	0.0004
Bosco della Maddalena Lavas	0.0560
Rotaro Lavas	0.0040
Montagnone-Maschiata Lavas	0.0200
Punta La Scrofa Lavas	0.0017
Pietra Vono Lavas	0.0003
Arso Lavas	0.0050

Table 1 – Volume values of effusive eruptions in the last 10kyrs. In green: largest volume eruptions.

Best guess volume values of explosive eruption have been reported with the estimation of uncertainty in Table 2. With the green colour, have been highlighted the largest volume eruptions for each typology. In Appendix A, we report the uncertainty distribution for each individual eruption.

Unit	volume DRE (km^3)
Maisto Tephra	0.0042
Catavola Tephra	0.0236
Piano Liguori Tephra	0.0237
Cava del Puzzillo I Tephra	0.0016
Cava del Puzzillo II Tephra	0.0016
Cava del Puzzillo III Tephra	0.0016
Cannavale Tephra	0.0096
Punta La Scrofa Tephra	0.0057
Punta Chiarito Tephra	0.0127
Marecoppo Tephra	0.0051
Molara Tephra	0.0034
Vateliero Tephra	0.0071
Ischia Porto Tephra	0.0043
Cava Bianca Tephra	0.0056
Cafieri Tephra	0.0027
Cava Nocelle Tephra	0.0016
Posta Lubrano Tephra	0.0053
Cretaio Tephra	0.0750
Cava Buceto	0.0001
Bosco dei Conti Tephra	0.0067
Villammare Tephra	0.0007
Fondo d'Oglio Tephra	0.0028
Bosco della Maddalena Tephra	0.0026
Fiaiano Tephra	0.0047
Fondo Bosso Tephra	0.0073

Table 2 – Volume values of explosive eruptions in the last 10kyrs. In green: largest volume eruptions.

Based on our volumes estimations, we evaluate that volumes involved in explosive and effusive eruptions are of similar order of magnitude, in the range of 10^{-4} - 10^{-2} km^3 DRE, and have been erupted through time in the percentage shows in the Fig. 7. It is possible to see that in the last 3 kyrs the number of high magnitude events is relatively decreased.

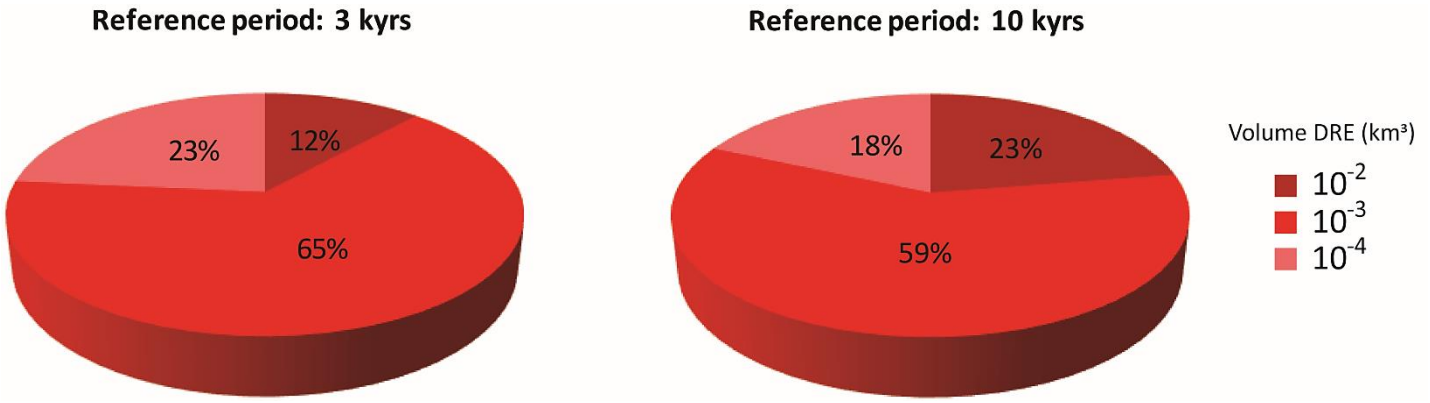

Fig.7 - Percentage of eruption for each order of magnitude of emitted volume DRE (km^3) for different reference periods.

In the following map (Figure 8) the calculated order of magnitude of emitted DRE volumes (km^3) have been reported with the related vent positions that have been active in the last 10 kyrs.

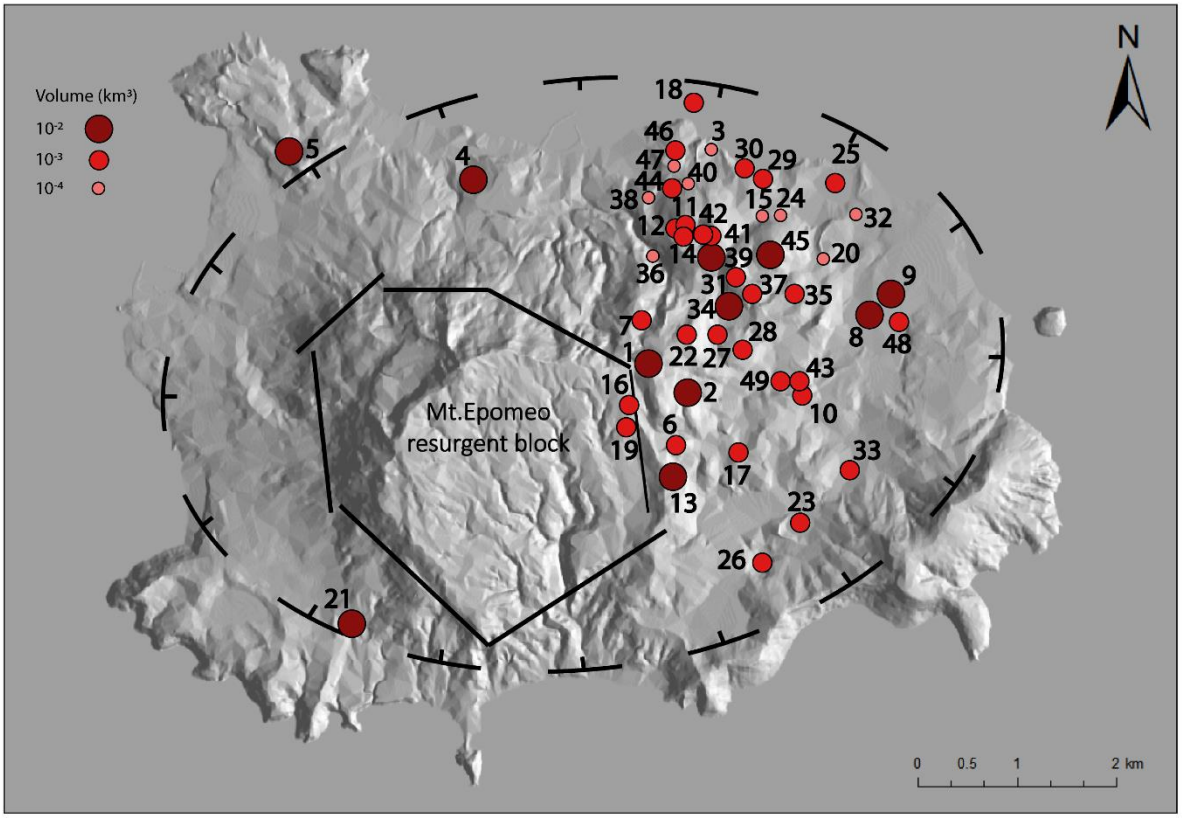

1	Trippodi Lavas	14	Cava del Puzzillo III Tephra	27	Cava Bianca Tephra	40	Villammare Tephra
2	Selva del Napolitano Lavas	15	Sant'Alessandro Lavas	28	Posta Lubrano Lavas	41	Fondo d'Oglio Tephra
3	Castiglione and Bagnetielli Lavas	16	Cannavale Tephra	29	Cafieri Tephra	42	Bosco della Maddalena Tephra
4	Fundera Lavas	17	Cantariello Lavas	30	Cafieri Lavas	43	Fiaiano Tephra
5	Zaro Lava domes and flows	18	Punta La Scrofa Tephra	31	Posta Lubrano Tephra	44	Rotaro Lavas
6	Cannavale Lavas	19	Marecoppo Tephra	32	San Pietro Lavas	45	Montagnone-Maschiata Lavas
7	Maisto Tephra	20	San Ciro Lavas	33	Cava Nocelle Tephra	46	Punta La Scrofa Lavas
8	Catavola Tephra	21	Punta Chiarito Tephra	34	Cretaio Tephra	47	Pietra Vono Lavas
9	Piano Liguori Tephra	22	Mt. Toppo Lavas	35	Arcamone-Sacchetta Lavas	48	Fondo Bosso Tephra
10	Rio Corbore Lavas	23	Molara Tephra	36	Cava Buceto Tephra	49	Arso Lavas and Tephra
11	Cava del Puzzillo I Tephra	24	Montagnone I and La Quercia Lavas	37	Bosco dei Conti Tephra		
12	Cava del Puzzillo II Tephra	25	Ischia Porto Tephra	38	Mt. Tabor Lavas		
13	Costa Sparaina Lavas	26	Vateliero Tephra	39	Bosco della Maddalena Lavas		

Fig. 8 – Emitted DRE volumes and relative vents in the last 10 kyrs. Larger and darker points indicate larger erupted volumes.

The time distribution of cumulative eruptive volume within the last 10 kyrs period is plotted in Fig. 9, accounting for all the involved uncertainty in time and volume of the eruptions, as well as for the constrains set by the stratigraphic sequences. The total erupted volume is 0.5 km^3 DRE of magma from the intra-caldera monogenetic field.

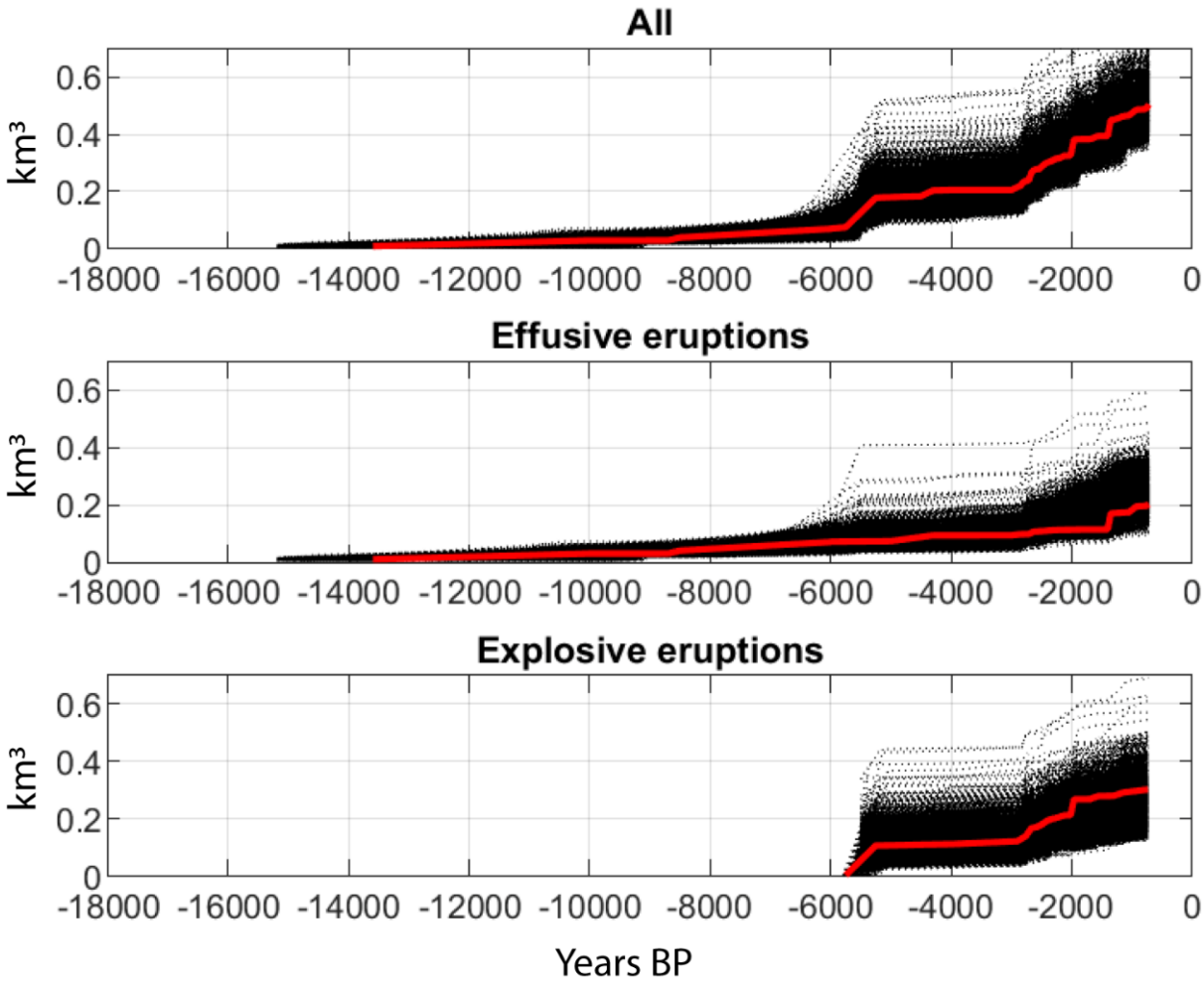

Fig. 9 –Cumulative volume – time distribution of eruptions (divided also for typology) in Ischia island in the reference period.

4. Discussion

Ischia island is an active volcano which hosts a large permanent and seasonal populations. It is located in a very densely populated area; the assessment of the current state of quiescence in respect to the recent eruptive behaviour of the volcano is essential for hazard and risk studies. Works which treat this problem are only few. Only few studies which focus on a qualitative probability maps for the opening of vents are available (Alberico et al., 2008; Sbrana and Toccaceli, 2011; Zaccarelli et al., 2018; Selva et al. 2019). Zaccarelli et al., (2018) tried to make a long–term eruption forecasting estimating the probability of next eruption localization in a given time interval, suggesting a classification of the possible eruptive types and using a general frequency–size relationship without knowing the magnitude of erupted units.
Here we present the analysis of the distribution of volumes of lava and explosive units during the last 10 kyrs, accompanied by an explicit quantification of the involved uncertainty.

Even if this quantification is in many cases (e.g., for explosive eruptions) at the very first order, thus accompanied by large uncertainty, several important considerations have been drawn.

The cumulative volume through time distribution shows at least 3 changes in the slope with a relative decrease of high magnitude eruptions in the last 3 kyrs.
Changes in the slope in the cumulative diagram (Fig.9) may be due to an under-recording especially in the oldest and smallest deposits in the eruptive catalogue (Brown et al., 2014). Moreover, the estimation of the incompleteness of an eruptive catalogue is much more questionable than a seismic one. In seismology, the well-known power law distribution for the magnitude of events (the Gutenberg-Richter law), and the time evolution of the rate of main shocks events, allow to reveal the incompleteness of a seismic catalogue.

From the cumulative diagrams derived from this analysis, it can be noticed that the current period of quiescence, started after the last eruption of Arso in 1302 A.D., resulting apparently anomalous in comparison with the other periods of quiescence occurred within the last 10 kyrs. Moreover, in the last 3 kyrs, there was an acceleration in the eruptive activity, which resumes with sharp ramps about every 500 years. The major contribution in terms of activity ramps is given by the explosive activity, since 6 kyrs, which present almost 3 first order sharp ramps. The effusive activity shows a substantial continuous degree of activity, with only a singular event in the last 3 kyrs which represent a change to this pattern. Effusive activity seems to be an always present background on which explosive activity occur sporadically, roughly every 1000 yrs. Assumed that in the present past the effusion activity has stopped for volcano-tectonic reasons and assumed that the explosive activity works separately to this, the present period of quiescence represents the period between two ramps of explosive activity, if the volcanic system could be considered unchanged.
Taking in consideration the whole activity, in the last 3 kyrs, the average eruption frequency is 1 every 88 years, and the time passed from the last eruption in 1302 A.D. is nowadays greater than 8 times. Nevertheless, it is important to consider the fact that Ischia is currently in a quiescence period and signs of deflation of the Monte Epomeo (Del Gaudio et al., 2010) does not seem to indicate a resumption of magmatic activity.

Generally, after a relatively long period of quiescence the activity resume with a marked and progressive increase in seismic activity and degassing. Before the activity resume at Turrialba Volcano after a long period of quiescence, a drastic compositional change of the fumarolic fluids has been measured together with several peaks in the seismic activity (Martini et al., 2010).

Confident with the fact that the used eruptive catalogue reflects sufficiently accurately the number of eruptions occurred in the last 10 kyrs, we can assert that the changes in the slope in the cumulative plot (Fig. 9) reflect a real evolution of the Ischia volcanic system, although the configuration of the monogenetic intracaldera volcanism concentrated in the eastern part of the Monte Epomeo, seems to be quite stable with only a few exceptions in the area of Monte Rotaro, with his complex morphology (Rittmann & Gottini, 1980), and the case of Cantariello Lavas (de Vita et al., 2010).
In a volcanic system, changes in the slope in the cumulative diagrams could be explained by changes in the eruptive regime in a determined period (Marzocchi & Zaccarelli, 2006). For example, the activity acceleration seen at Vesuvius in the time period 1631–1944 (Scandone et al., 1993) was due to the passage, after centuries, from a closed conduit regime to an open one (Marzocchi & Zaccarelli, 2006).

The power law distribution for the magnitude of events for the refence period analysed cannot be applied as in the cases of Campi Flegrei (Orsi et al. 2009), Vesuvius (Marzocchi et al. 2004) or Mt. Taranaki (Bebbington et al. 2008), where past activities seem to fit well a power law distribution. In Miyakejima Volcano, for example, the volume distribution is characterized by a preferred size (Garcia-Aristizabal et al., 2012), and this seems the case of Ischia Island, where the preferred DRE erupted volume has been largely of 10^{-3} km^3 (Fig. 7). For this, it is reasonable to think that there is a high probability that in the future, an eruption that could happen, will erupt a volume of about this order of magnitude. The largest eruptions in the past (e.g., the Cretaio Tephra eruption) result indeed in the tail of the distribution.

Following the work done by Orsi et al., (2009) for Campi Flegrei volcanic system, it may be also useful to do a work enabling a size classification of the past eruption onto which base the construction for future reference scenarios (Selva et al., 2018). The present work allows to individuate the reference eruption and the range of variability within each typology of used classification scheme. Here, we tried to identify the largest eruptions in each class, so to provide quantitative upper limits to each eruptive class.
For effusive activity the maximum size eruptions are Montagnone-Maschiata Lavas/Rotaro Complex and Selva del Napolitano Lavas for the dome-producing eruptions and Zaro Lava Domes and Flows for the lava flows. For explosive activity the maximum size eruptions are Cava Bianca Tephra for magmatic fragmentation, Piano Liguori Tephra for phreatomagmatic typology and Cretaio Tephra and Punta Chiarito Tephra for the mixed one. The way in which each typology of eruption works in the Ischia volcanic system needs to be better understood. Impact parameters have to be considered by the authorities.

5. Conclusions

This work represents a first attempt to a description of the volcanic history of Ischia island and it is clear that in the future it will be continually subject to changes and updates. Especially in the estimation of the explosive eruptions volume. Through a detailed fieldwork dedicated to each eruption is possible to calculate the volumes by a dispersal model applied with different mechanism from quite purely ballistic depositions (as strombolian eruption such as Fondo d'Oglio Tephra) to fallout or PDC/surge deposits (like Piano Liguori Tephra).
From the present reconstruction is evident the acceleration in the erupted volumes in the last 3 kyrs, with a relatively decreasing in the number of high magnitude events.
The eruptions on which base the construction of most likely scenarios, will have to be searched in this period, in which the Island was subjected to a complex evolution with about a 1/3 of eruption with a DRE volume of 10^{-3} km^3.

In this thesis will be treated in details both effusive and explosive eruptive scenarios.
Cretaio Tephra has been characterized and treated for the production of the explosive scenario, and Zaro Lava Domes and Flows and Arso Lava have been investigated in order to produce a rheology model to produce an effusive scenario.
A useful scenario for the phreatomagmatic events could be Piano Liguori Tephra, not analysed in this PhD thesis because older than 3 kyrs.

Appendix A

The Probability Density Function (PDF) distribution on volume values of each eruption unit quantified as discussed in Uncertainty and Results Sections are here reported:

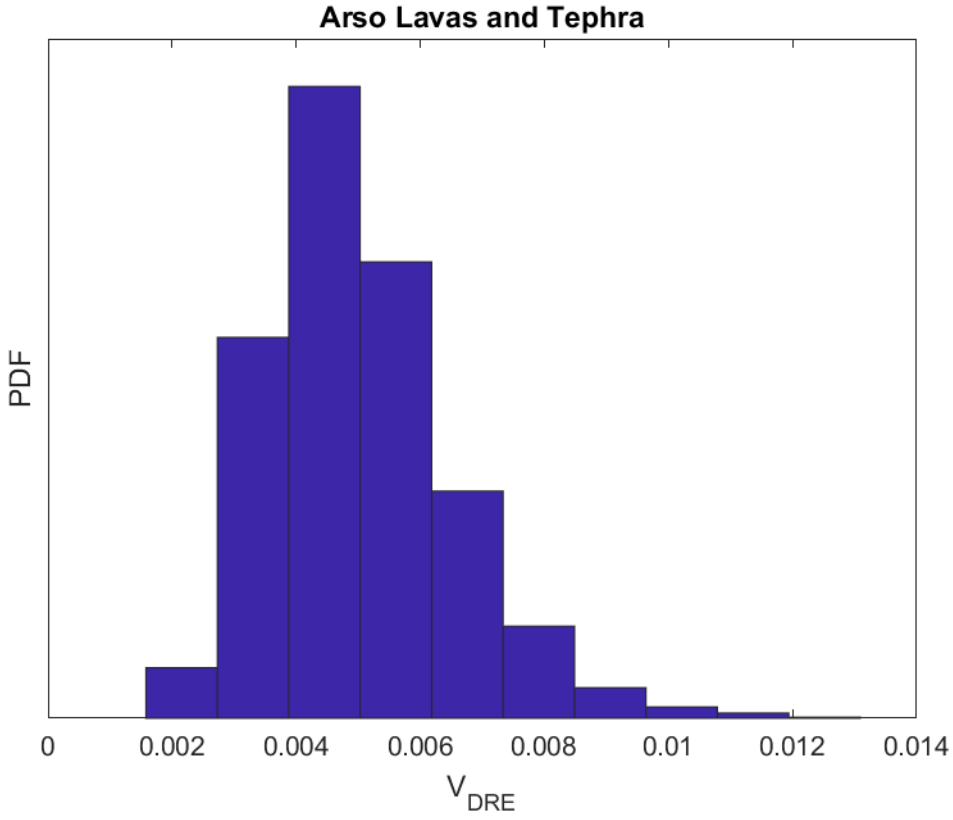

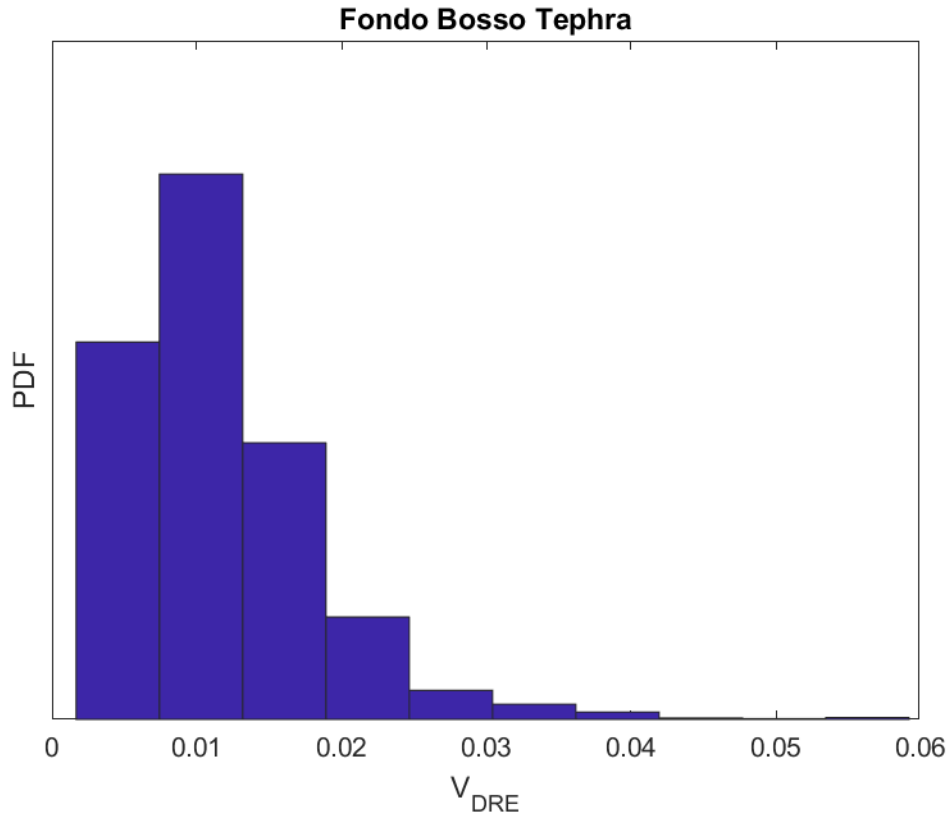
Fondo Bosso Tephra
PDF
0
0.01
0.02
0.03
0.04
0.05
0.06
V DRE

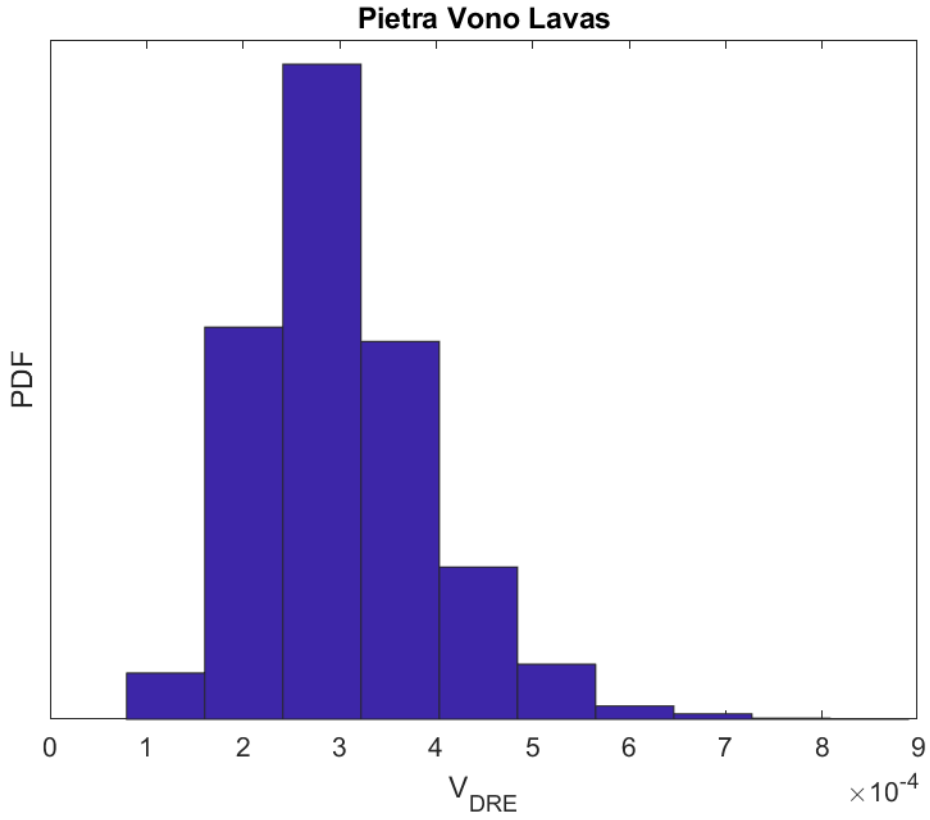
Pietra Vono Lavas
PDF
0
1
2
3
4
5
6
7
8
9
V DRE
×10-4

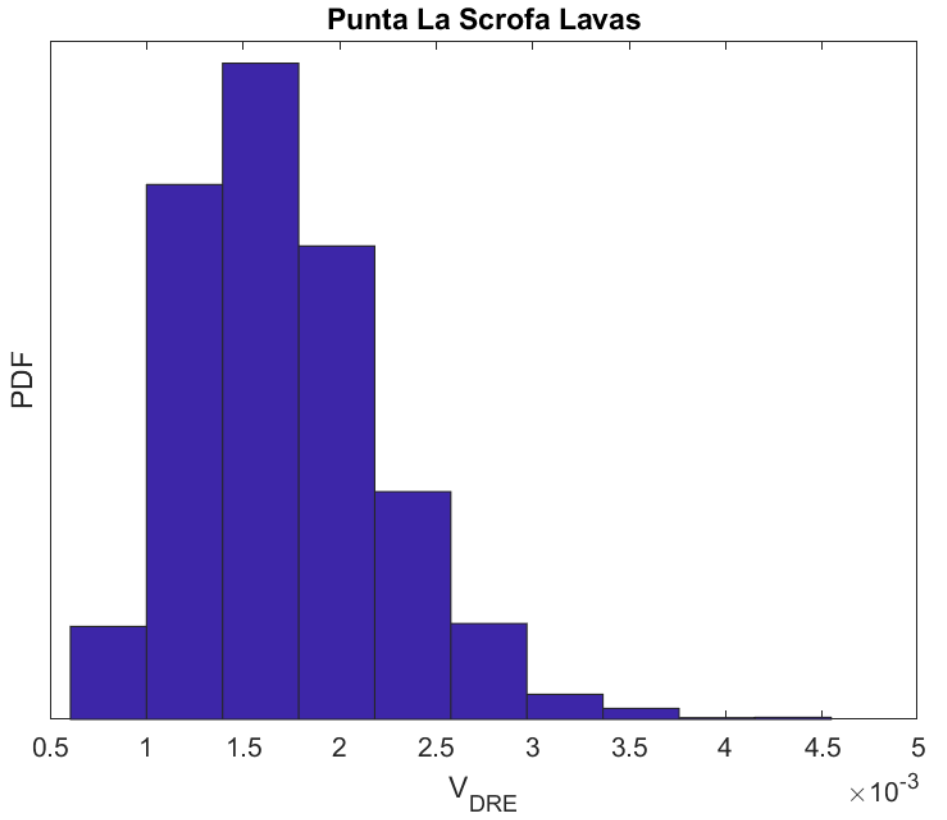
Punta La Scrofa Lavas
PDF
0.5
1
1.5
2
2.5
3
3.5
4
4.5
5
V DRE
×10-3

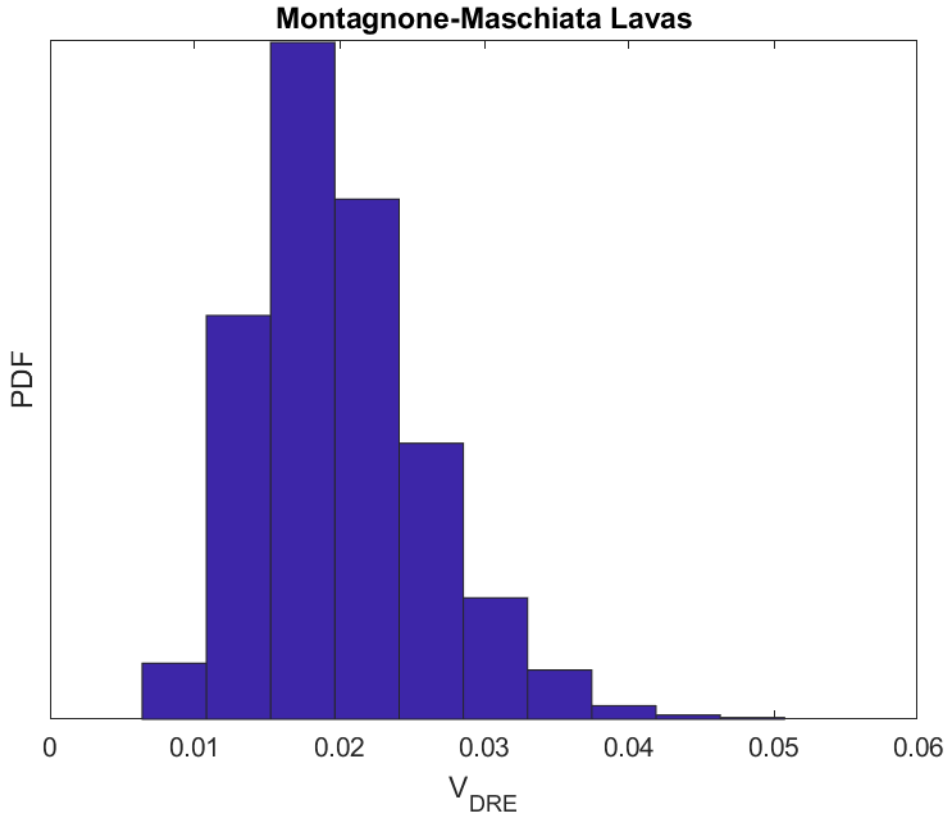
Montagnone-Maschiata Lavas
PDF
0
0.01
0.02
0.03
0.04
0.05
0.06
V DRE

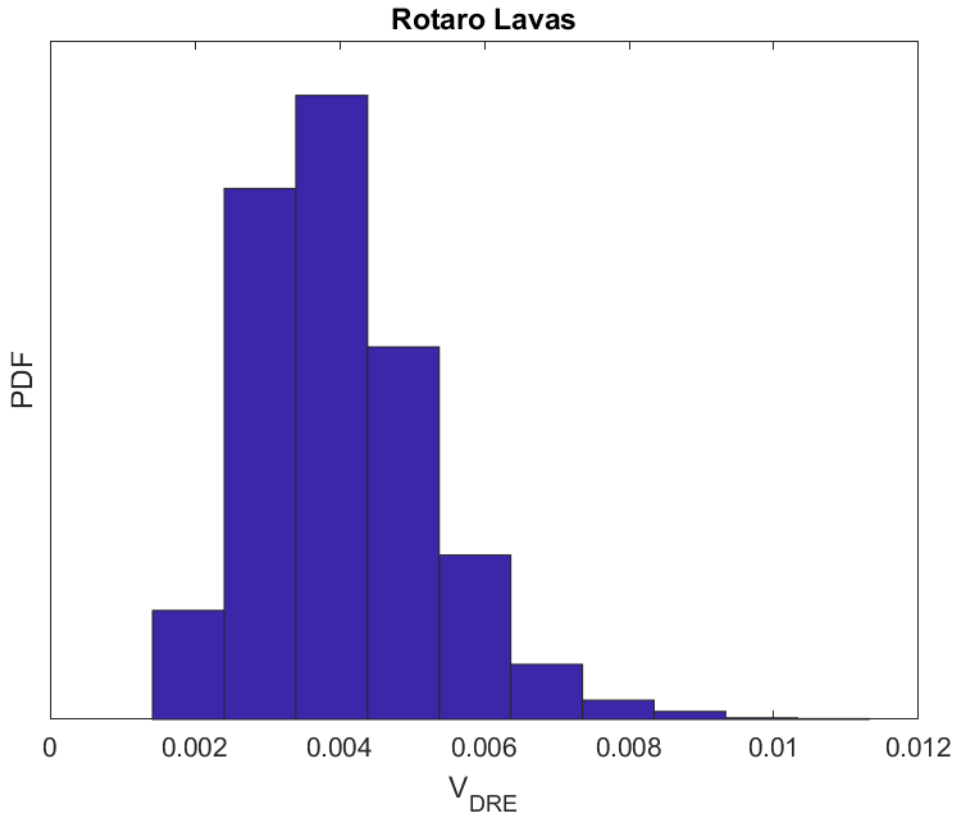
Rotaro Lavas
PDF
0
0.002
0.004
0.006
0.008
0.01
0.012
V DRE

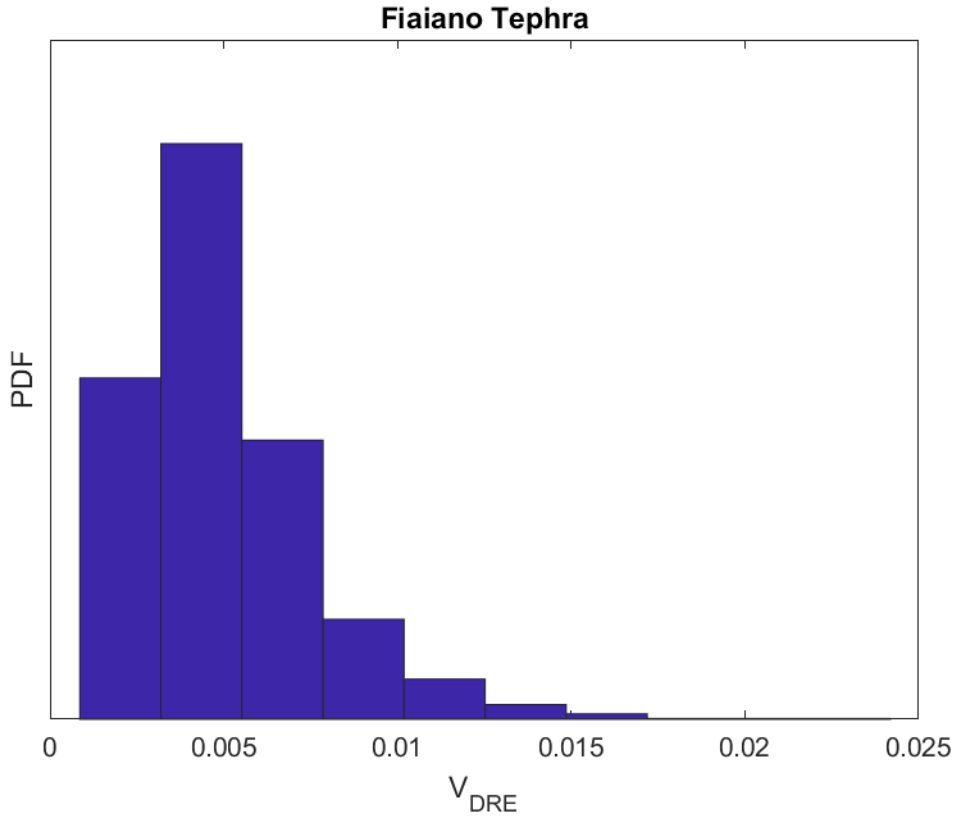
Fiaiano Tephra
PDF
0
0.005
0.01
0.015
0.02
0.025
V DRE

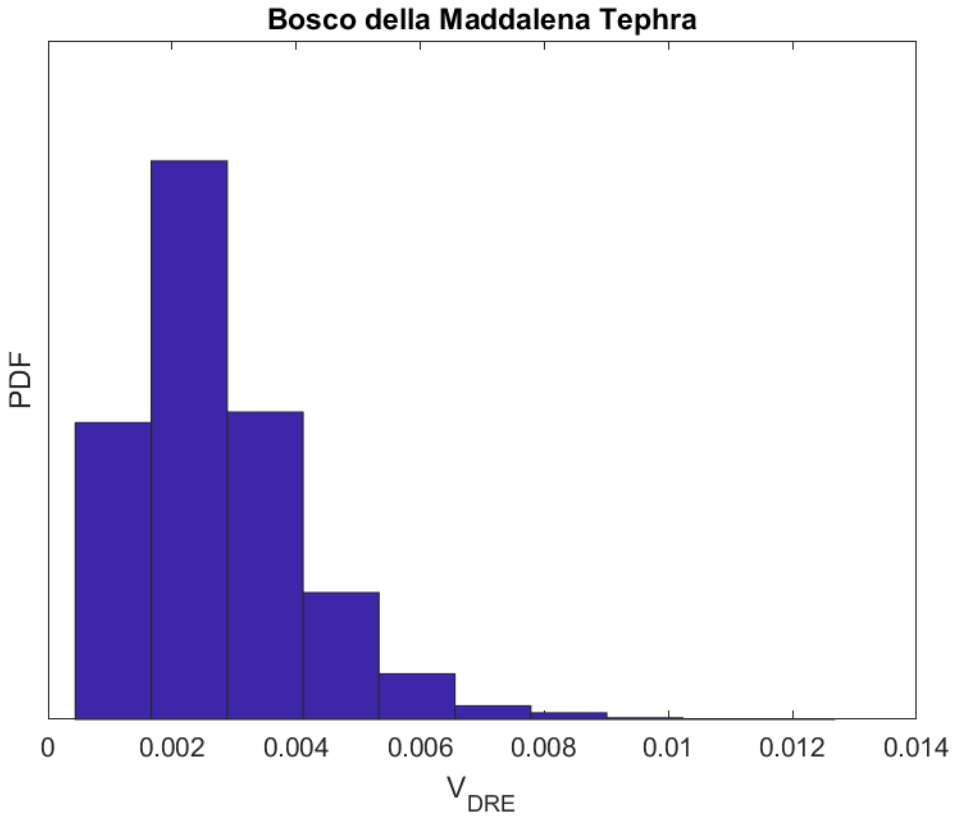
Bosco della Maddalena Tephra
PDF
0
0.002
0.004
0.006
0.008
0.01
0.012
0.014
V_{DRE}

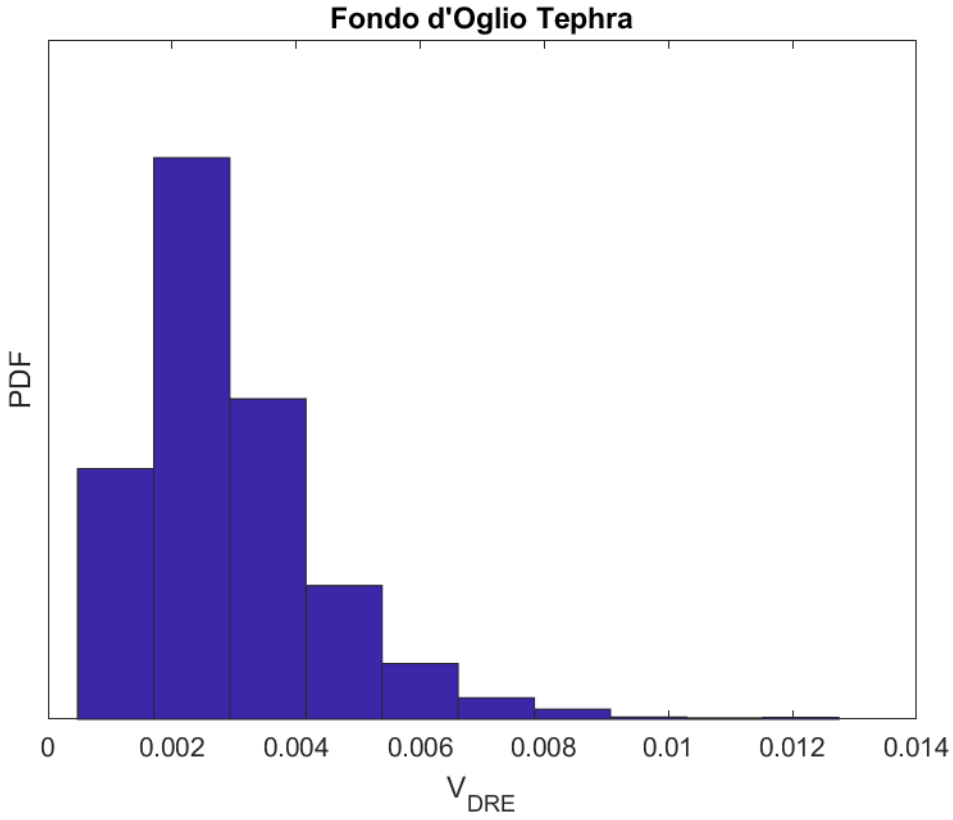
Fondo d'Oglio Tephra
PDF
0
0.002
0.004
0.006
0.008
0.01
0.012
0.014
V_{DRE}

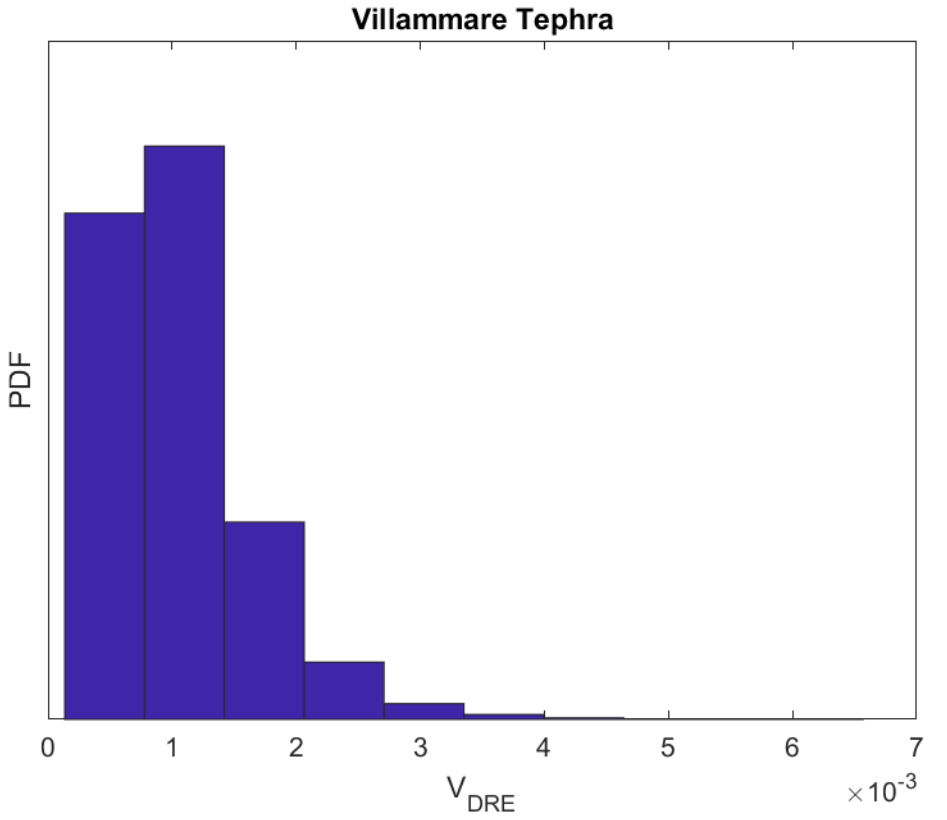
Villammare Tephra
PDF
0
1
2
3
4
5
6
7
V_{DRE}
$\times 10^{-3}$

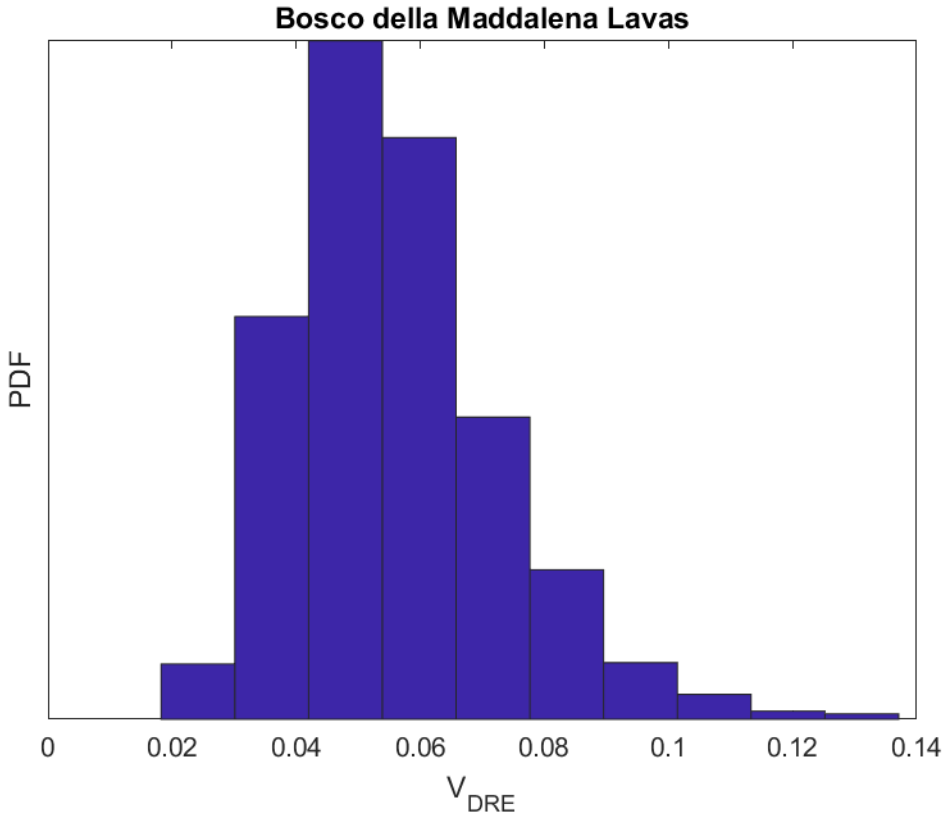
Bosco della Maddalena Lavas
PDF
0
0.02
0.04
0.06
0.08
0.1
0.12
0.14
V_{DRE}

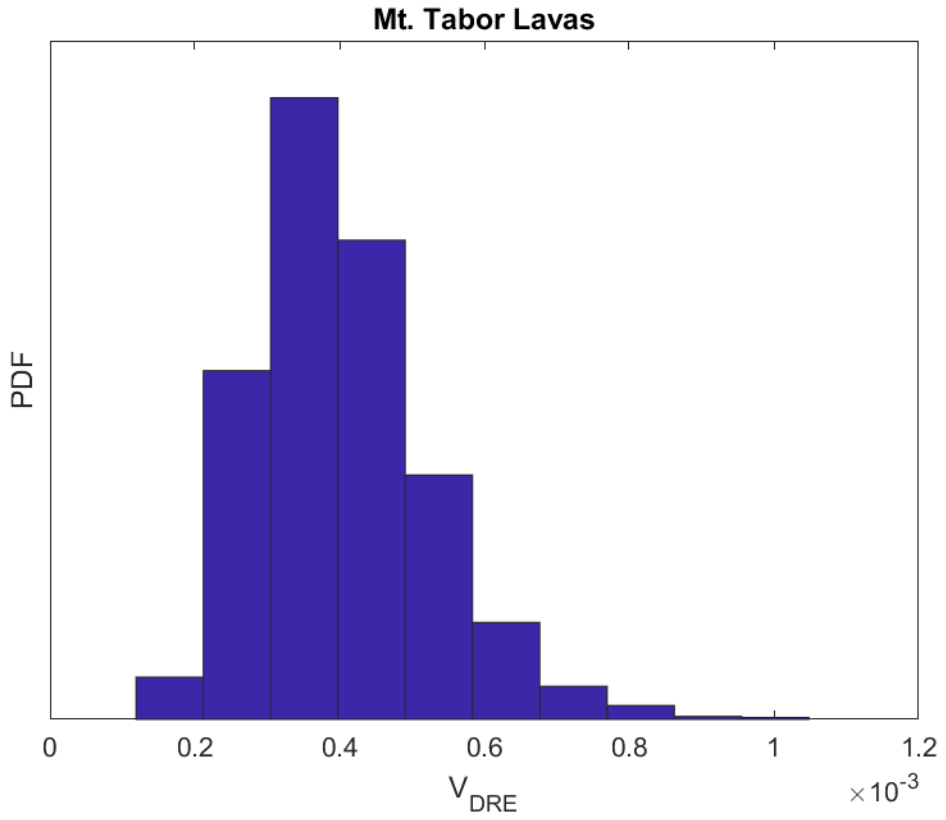
Mt. Tabor Lavas
PDF
0
0.2
0.4
0.6
0.8
1
1.2
V_{DRE}
$\times 10^{-3}$

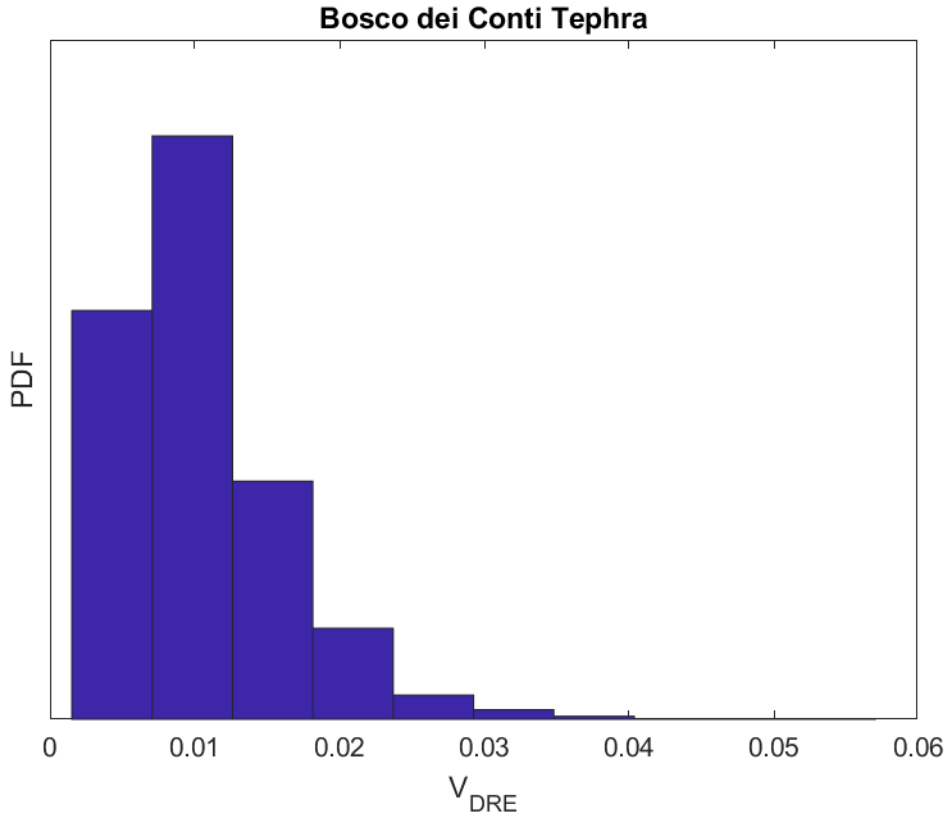
Bosco dei Conti Tephra
PDF
0
0.01
0.02
0.03
0.04
0.05
0.06
V_{DRE}

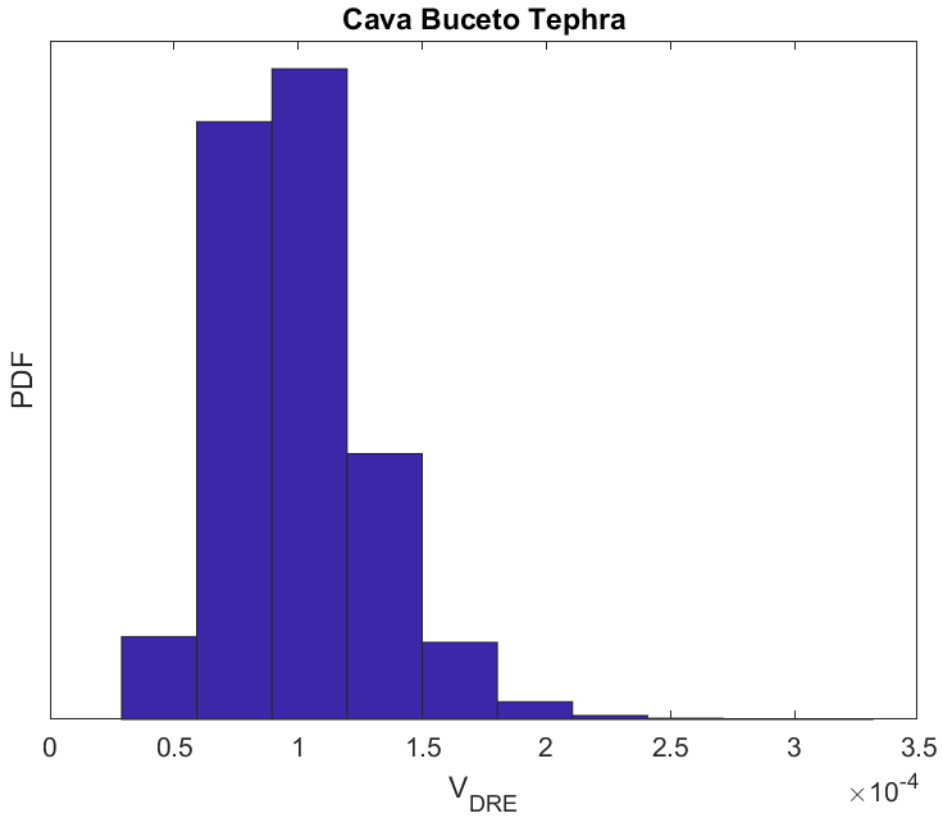
Cava Buceto Tephra
PDF
0
0.5
1
1.5
2
2.5
3
3.5
V_{DRE}
$\times 10^{-4}$

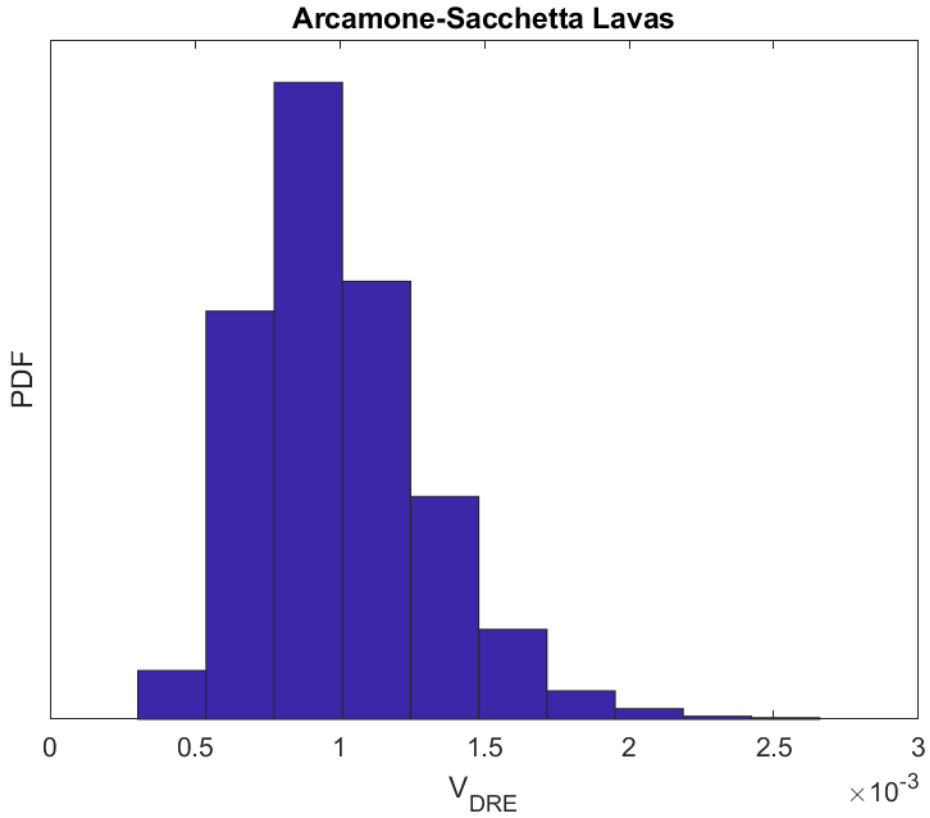
Arcamone-Sacchetta Lavas
PDF
0
0.5
1
1.5
2
2.5
3
V_{DRE}
$\times 10^{-3}$

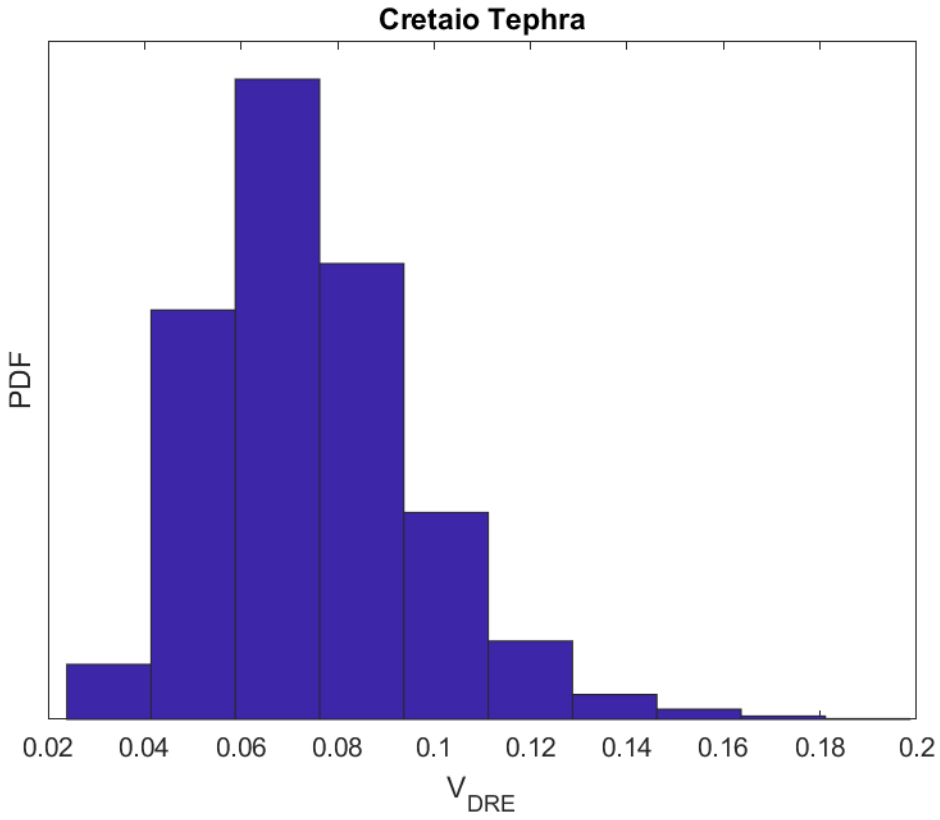
Cretaio Tephra
PDF
0.02
0.04
0.06
0.08
0.1
0.12
0.14
0.16
0.18
0.2
V DRE

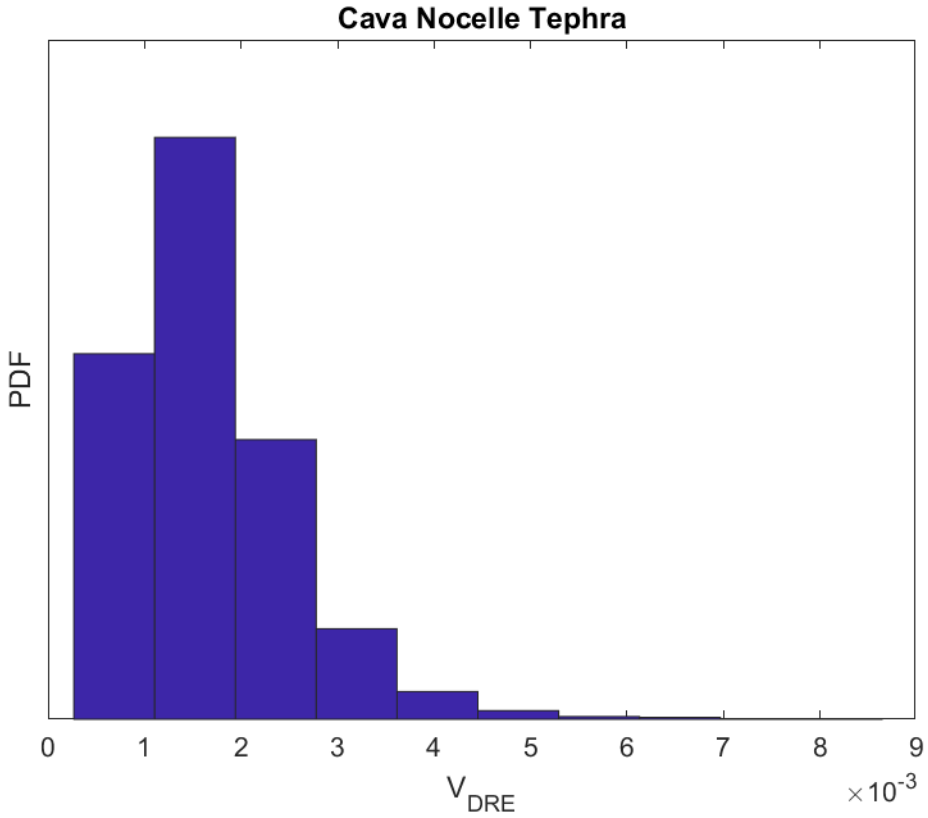
Cava Nocelle Tephra
PDF
0
1
2
3
4
5
6
7
8
9
V DRE
×10-3

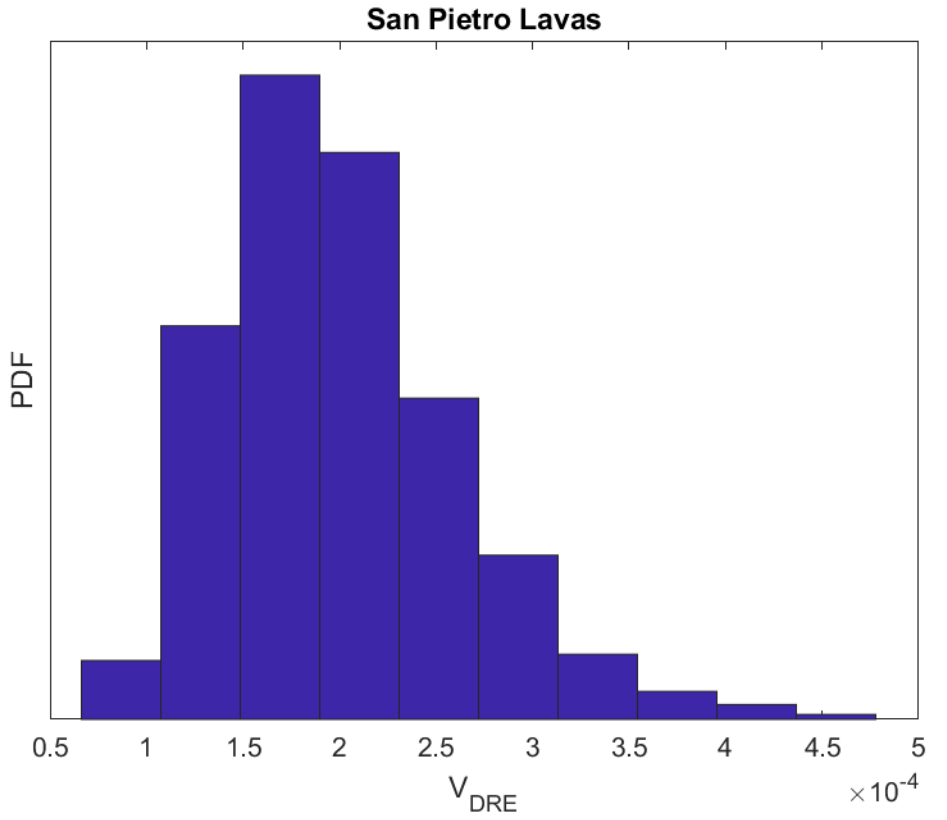
San Pietro Lavas
PDF
0.5
1
1.5
2
2.5
3
3.5
4
4.5
5
V_{DRE}
$\times 10^{-4}$

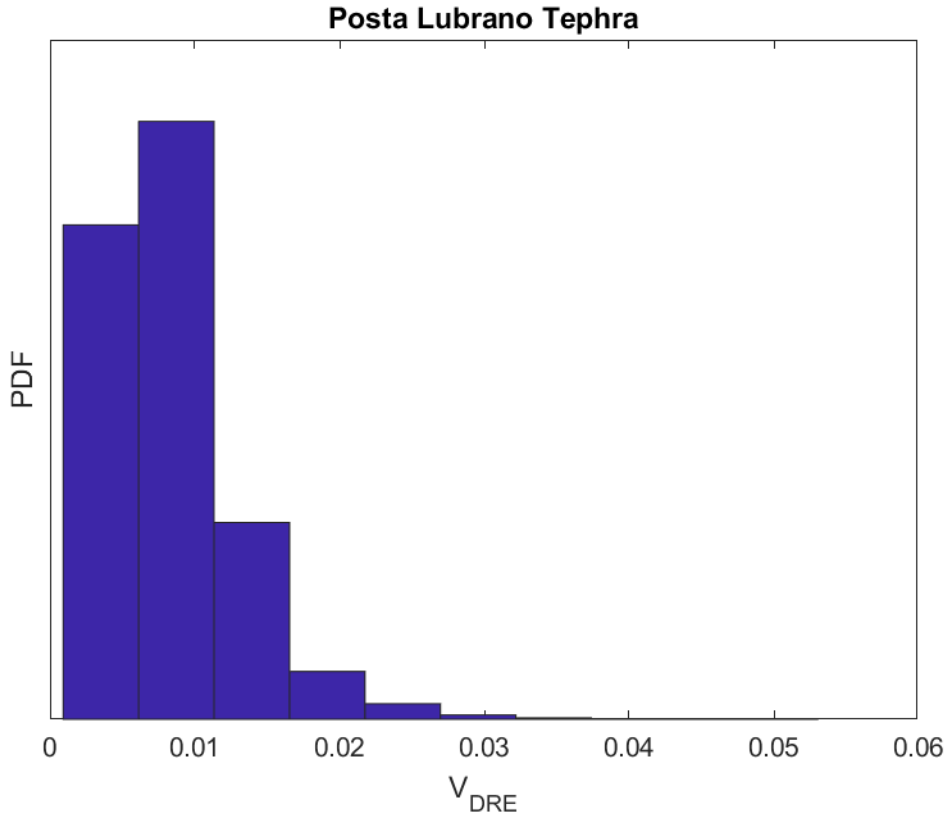
Posta Lubrano Tephra
PDF
0
0.01
0.02
0.03
0.04
0.05
0.06
V_{DRE}

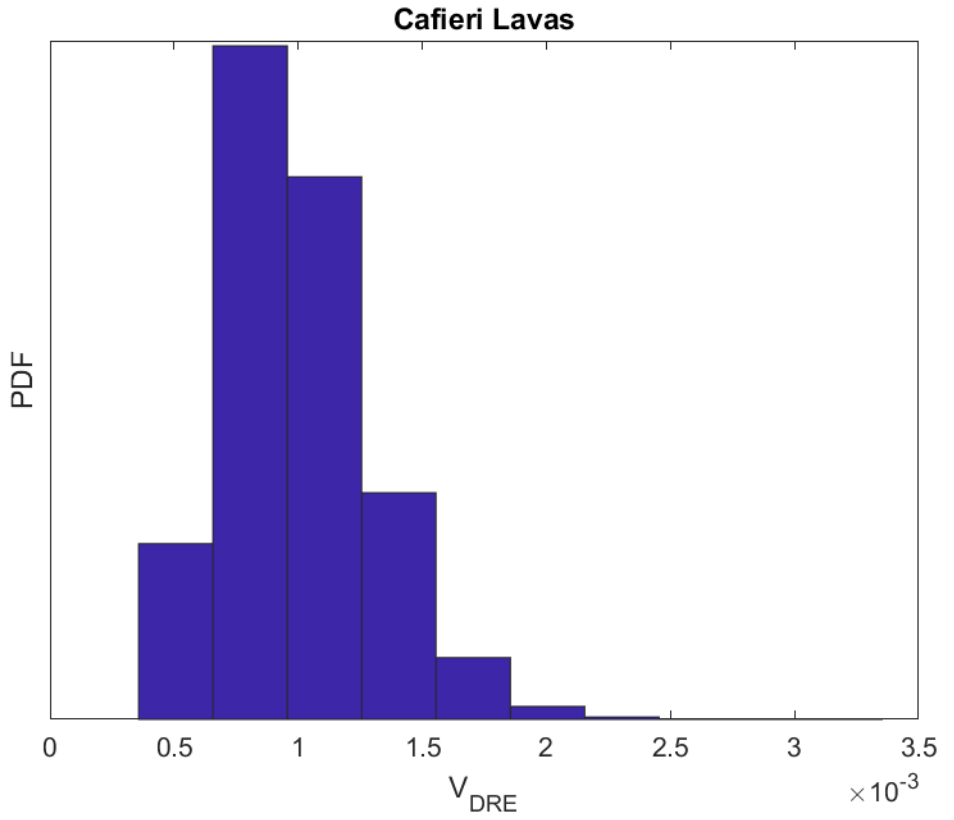
Cafieri Lavas
PDF
0
0.5
1
1.5
2
2.5
3
3.5
V_{DRE}
$\times 10^{-3}$

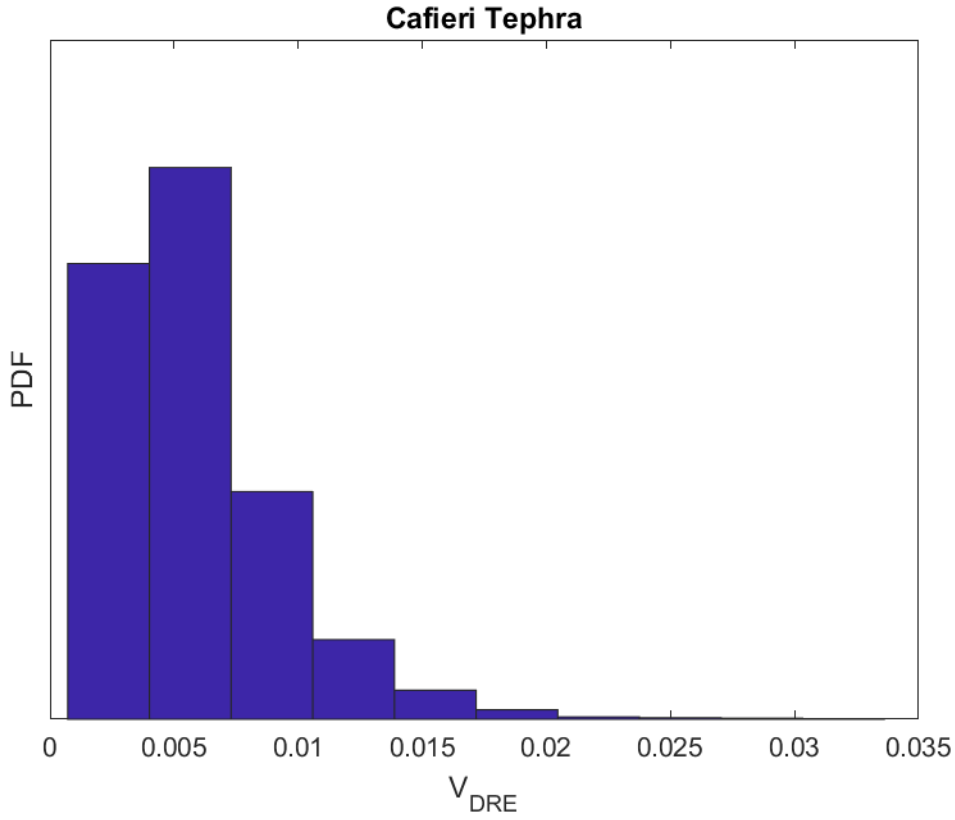
Cafieri Tephra
PDF
0
0.005
0.01
0.015
0.02
0.025
0.03
0.035
V_{DRE}

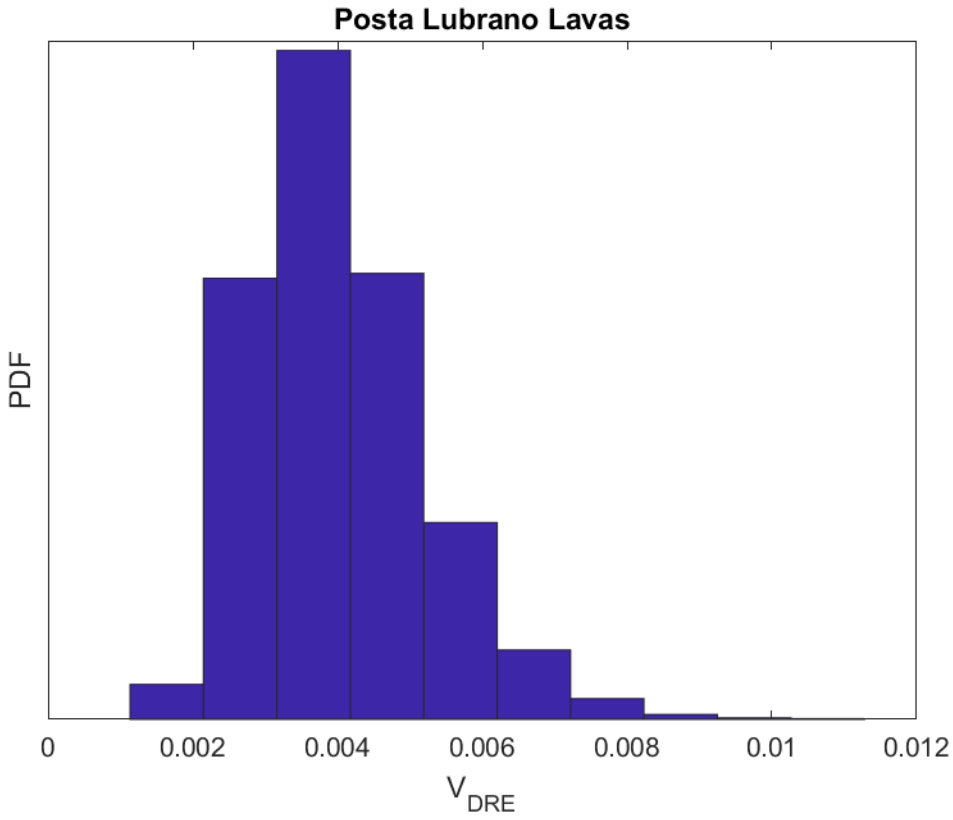
Posta Lubrano Lavas
PDF
0
0.002
0.004
0.006
0.008
0.01
0.012
V DRE

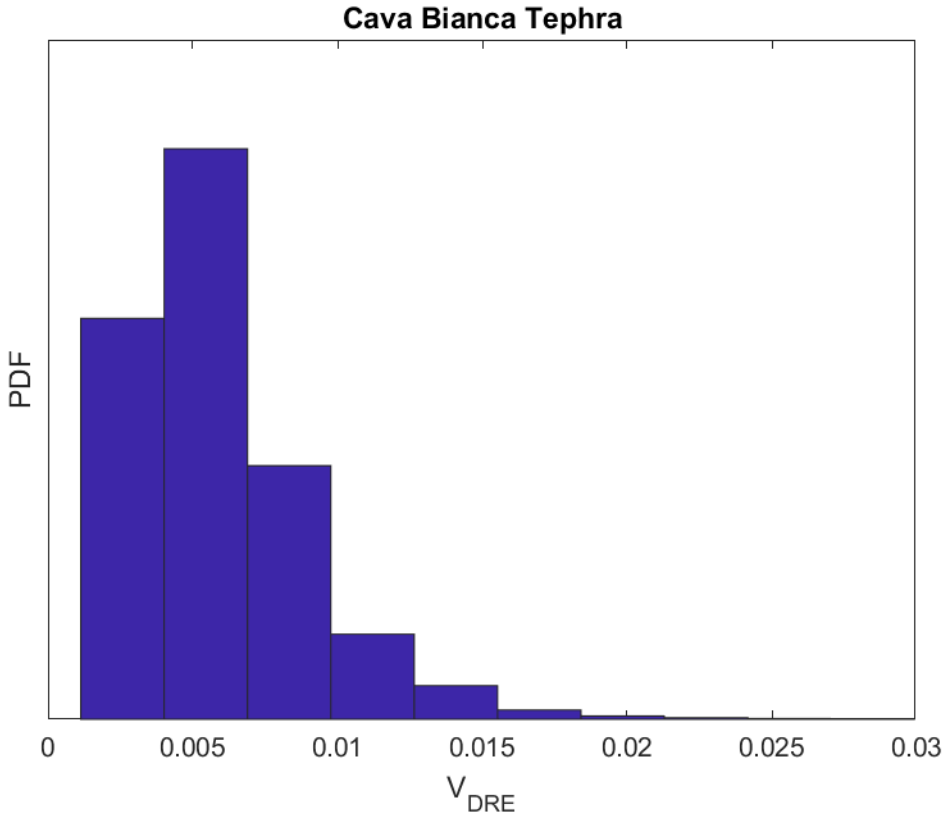
Cava Bianca Tephra
PDF
0
0.005
0.01
0.015
0.02
0.025
0.03
V DRE

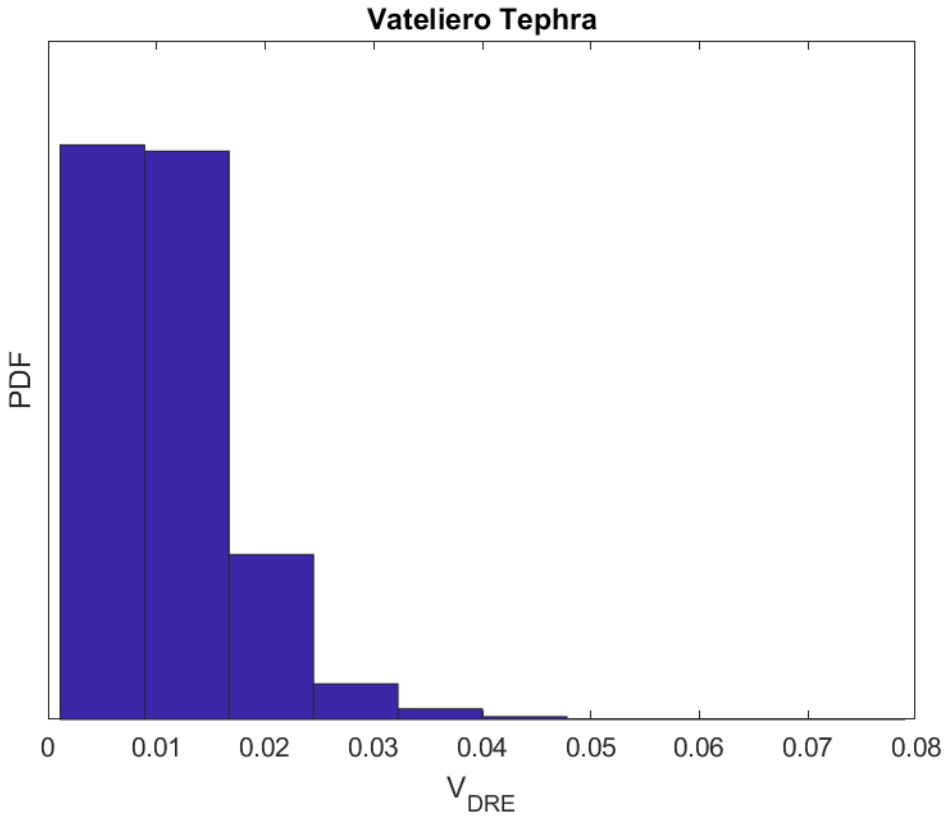
Vateliero Tephra
PDF
0
0.01
0.02
0.03
0.04
0.05
0.06
0.07
0.08
V DRE

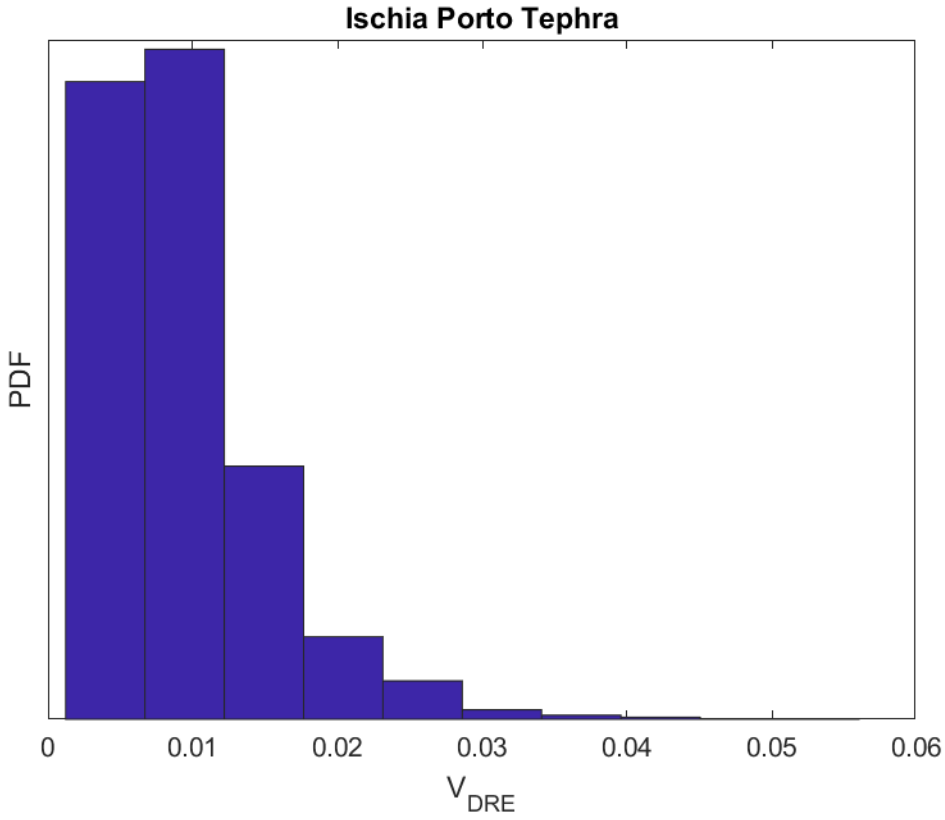
Ischia Porto Tephra
PDF
0
0.01
0.02
0.03
0.04
0.05
0.06
V DRE

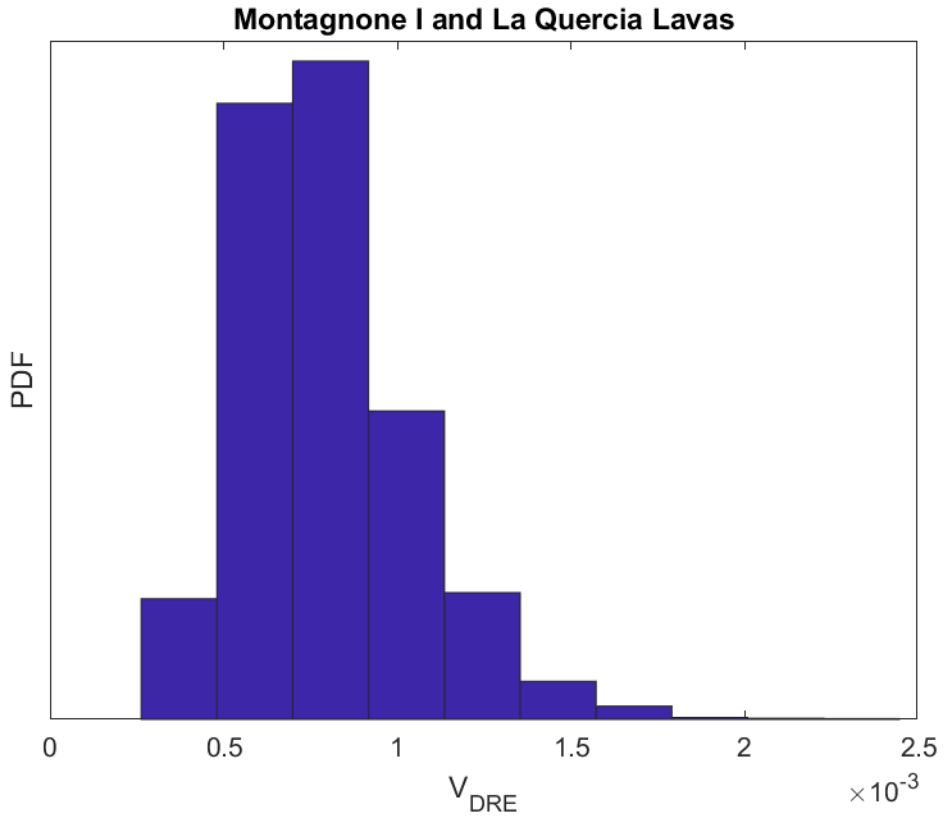
Montagnone I and La Quercia Lavas
PDF
0
0.5
1
1.5
2
2.5
V_{DRE}
$\times 10^{-3}$

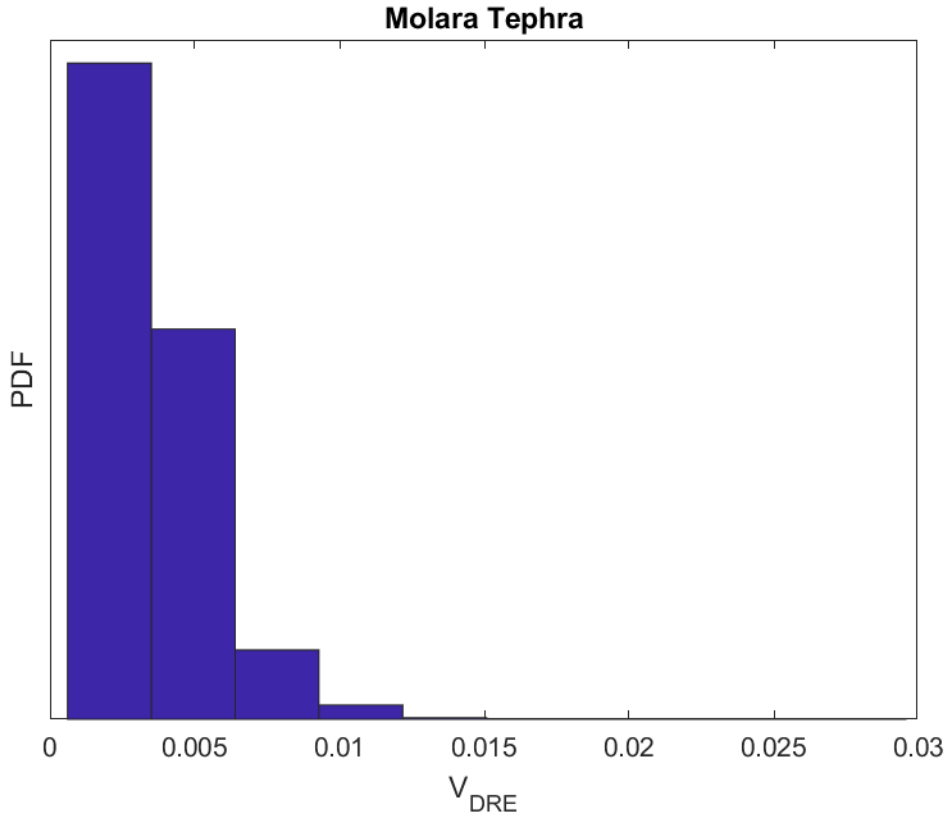
Molara Tephra
PDF
0
0.005
0.01
0.015
0.02
0.025
0.03
V_{DRE}

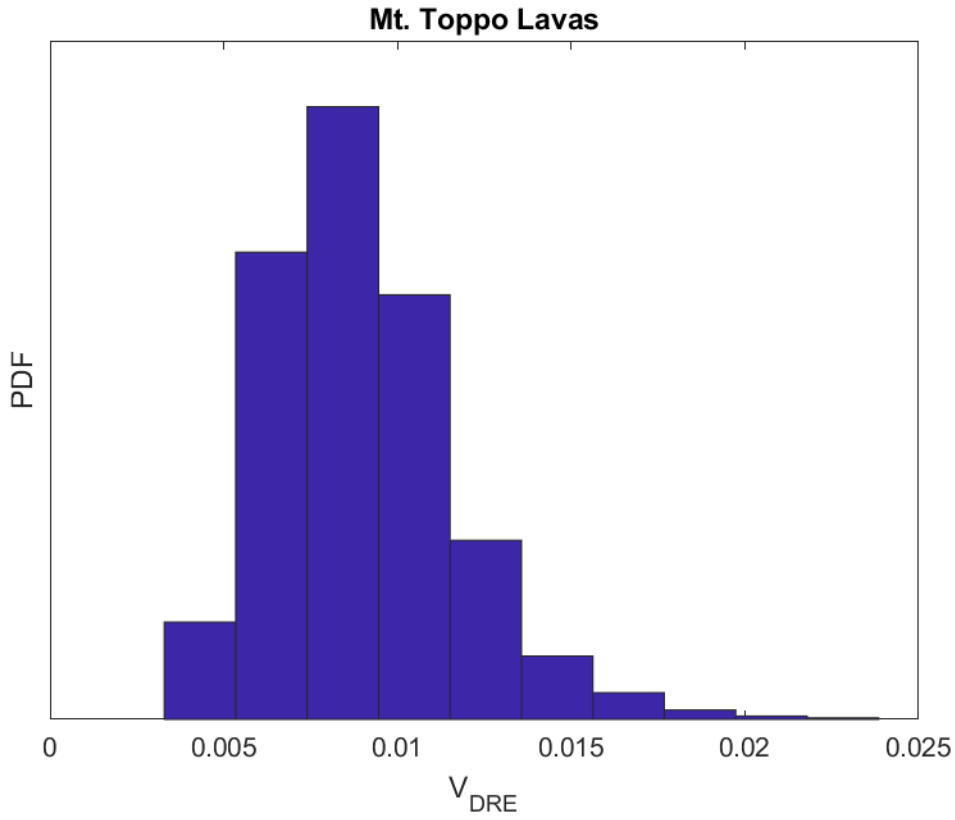
Mt. Toppo Lavas
PDF
0
0.005
0.01
0.015
0.02
0.025
V DRE

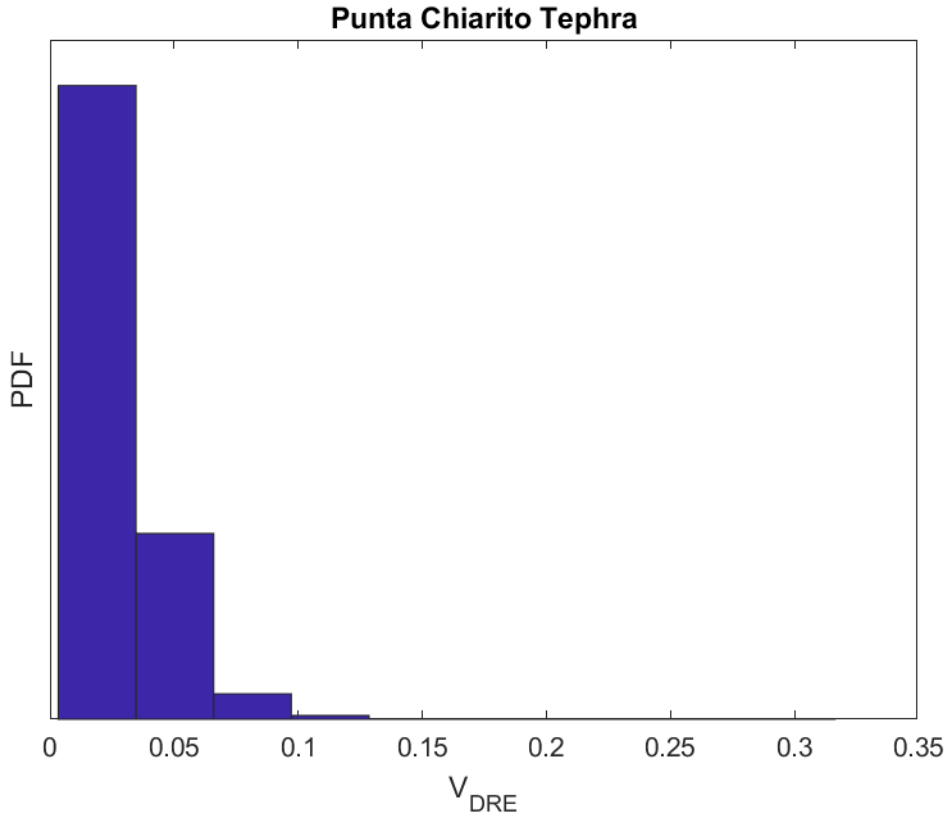
Punta Chiarito Tephra
PDF
0
0.05
0.1
0.15
0.2
0.25
0.3
0.35
V DRE

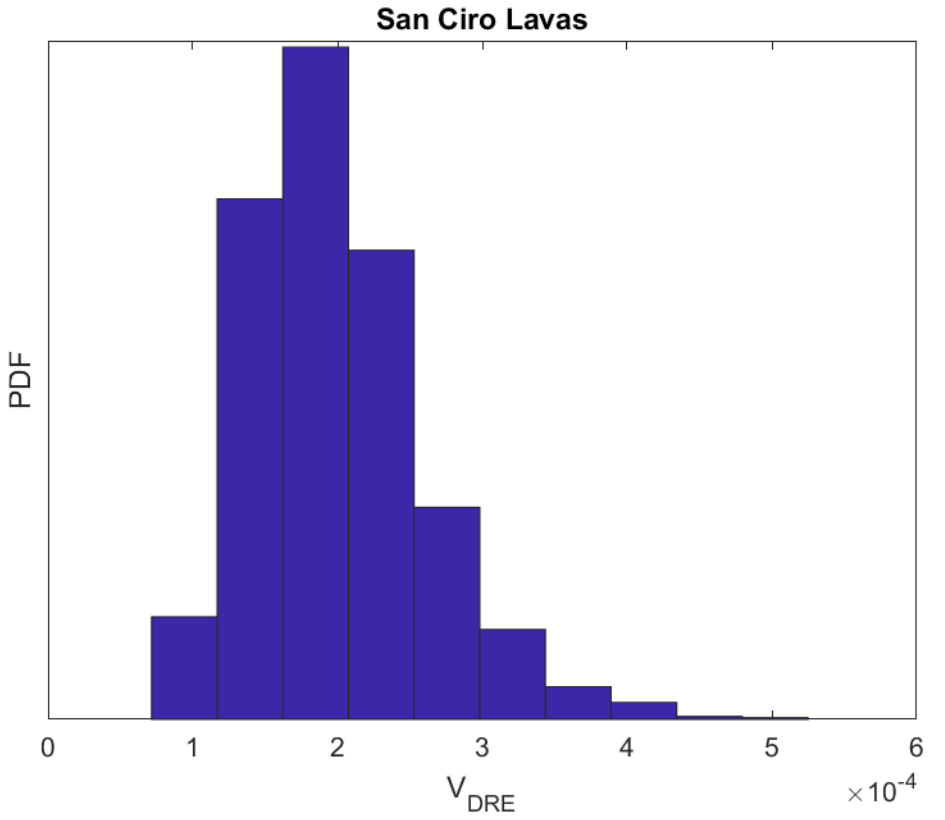
San Ciro Lavas
PDF
0
1
2
3
4
5
6
V_{DRE}
$\times 10^{-4}$

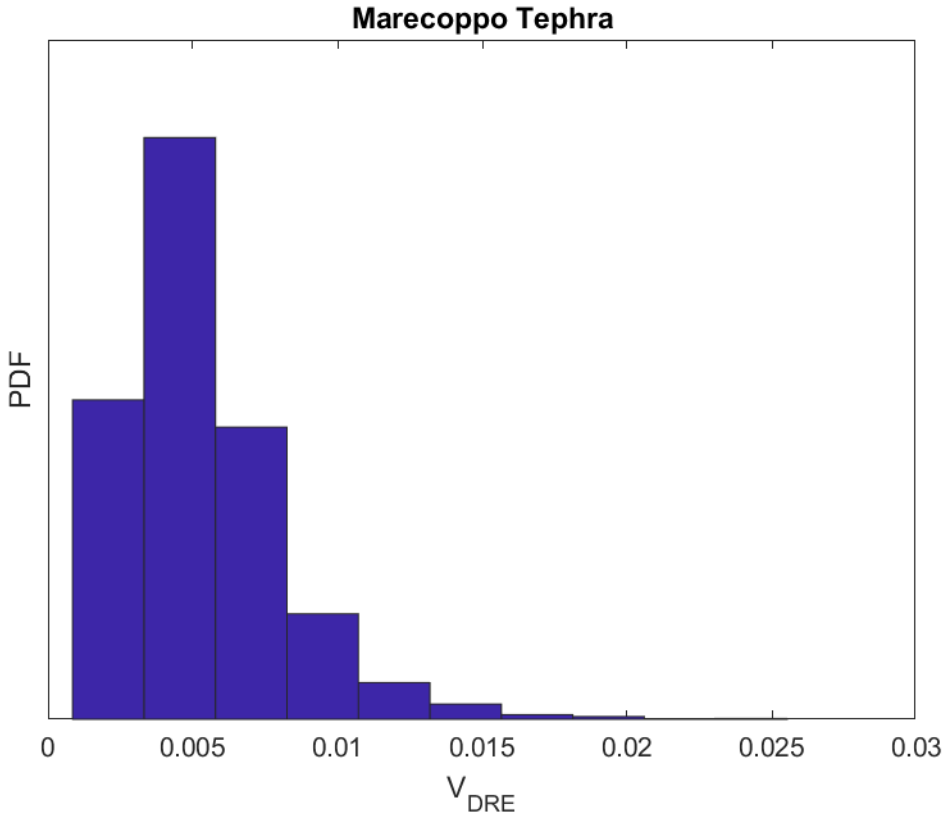
Marecoppo Tephra
PDF
0
0.005
0.01
0.015
0.02
0.025
0.03
V_{DRE}

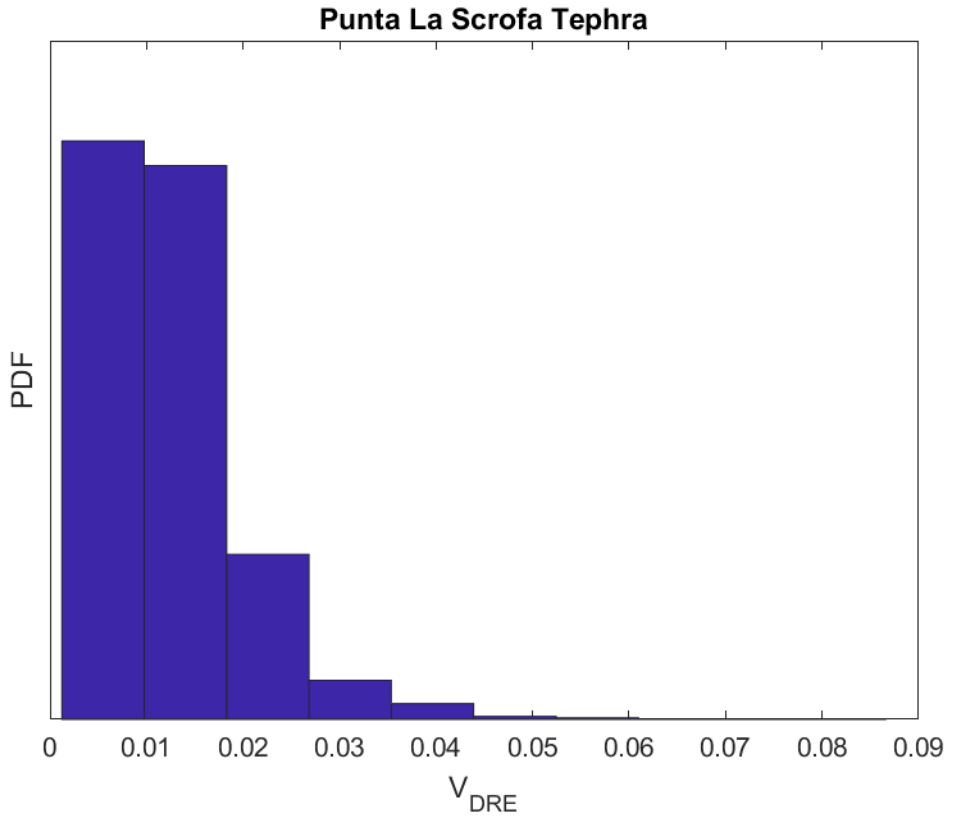
Punta La Scrofa Tephra
PDF
0
0.01
0.02
0.03
0.04
0.05
0.06
0.07
0.08
0.09
V DRE

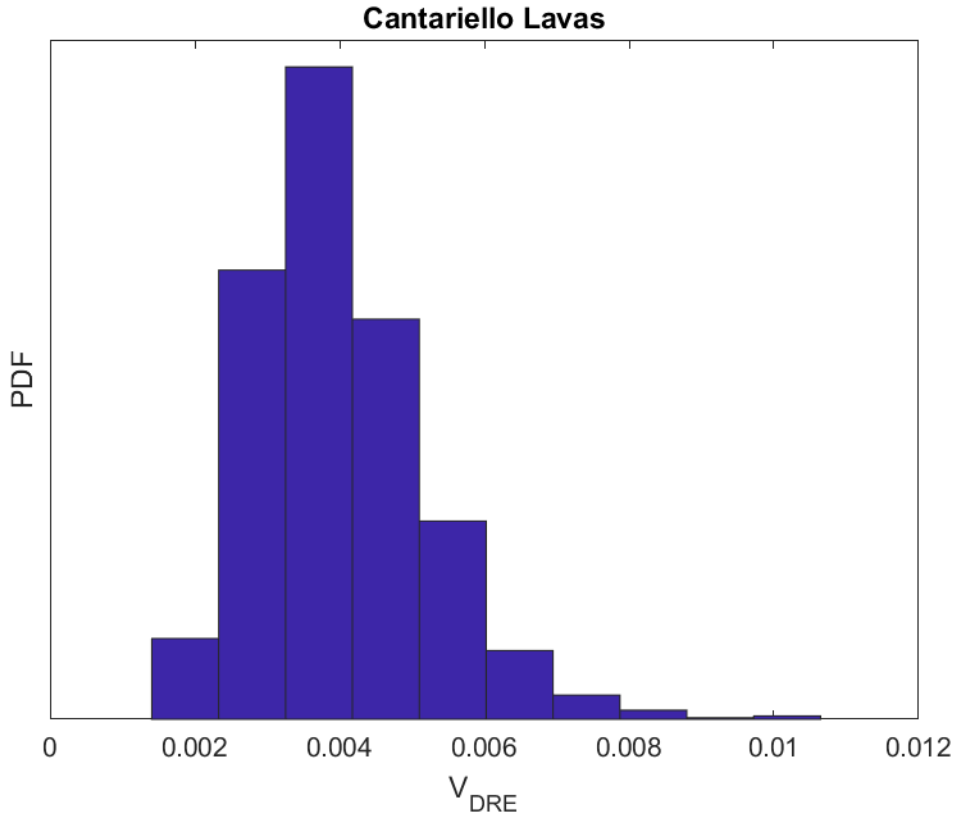
Cantariello Lavas
PDF
0
0.002
0.004
0.006
0.008
0.01
0.012
V DRE

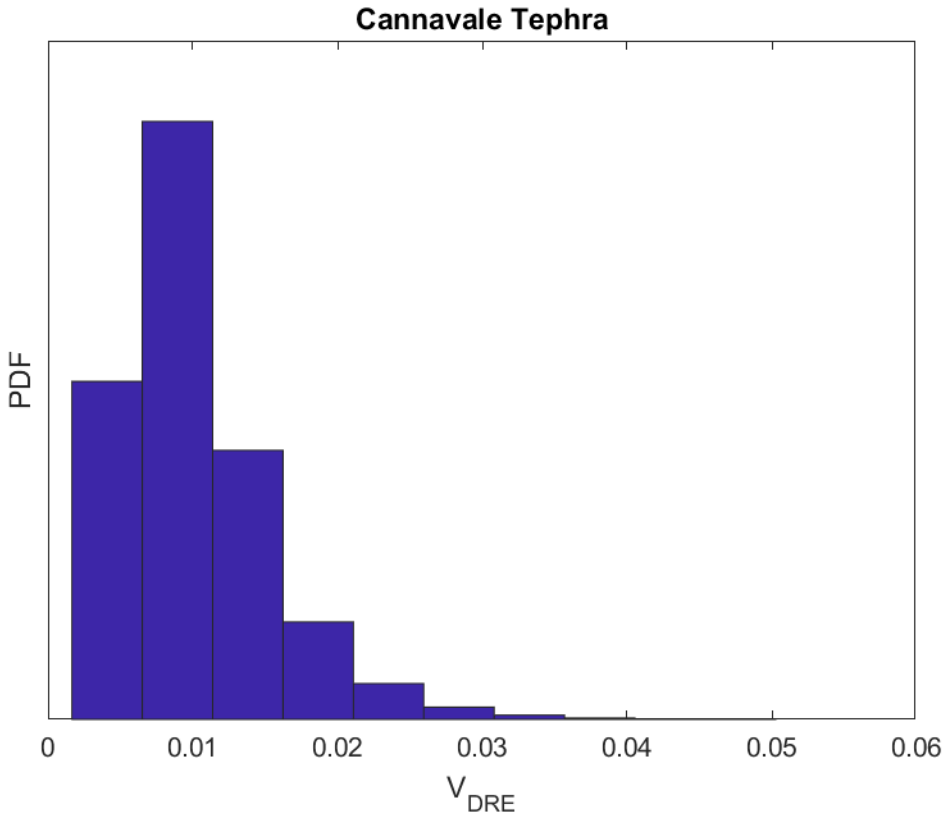
Cannavale Tephra
PDF
0
0.01
0.02
0.03
0.04
0.05
0.06
V DRE

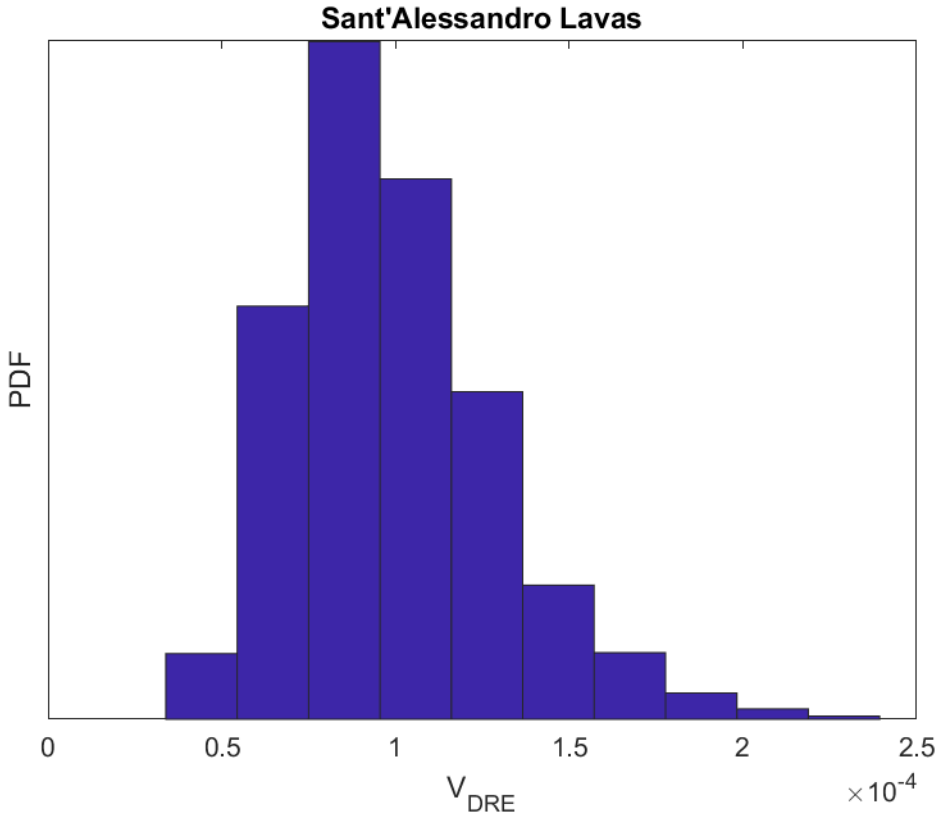
Sant'Alessandro Lavas
PDF
0
0.5
1
1.5
2
2.5
V DRE
×10-4

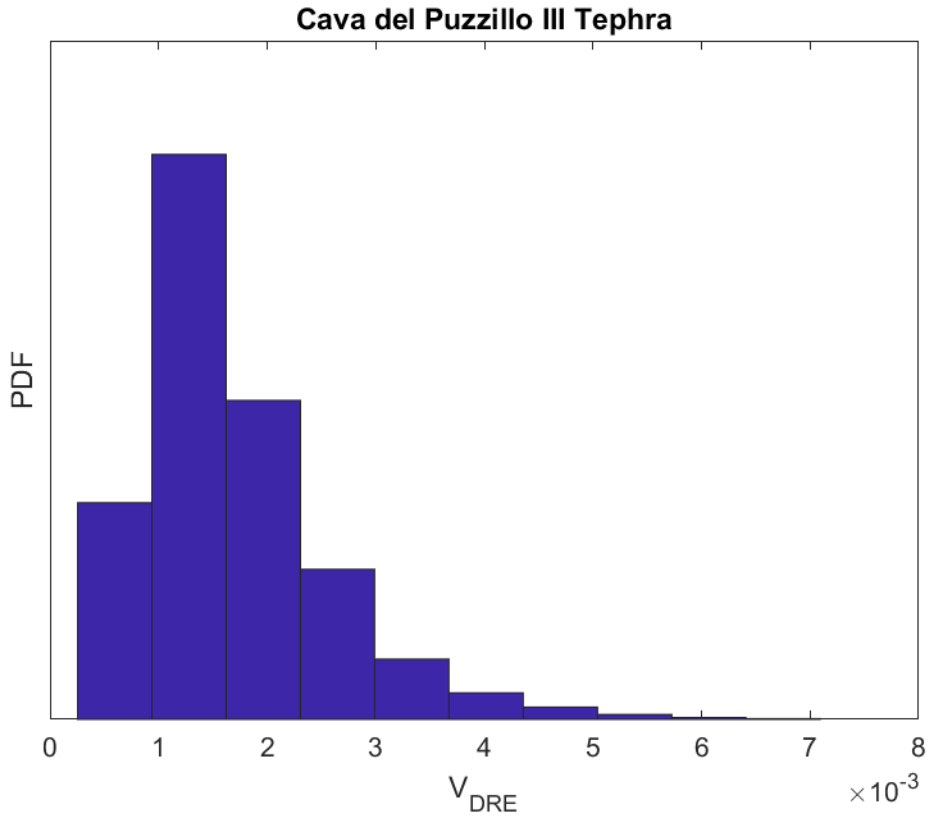
Cava del Puzzillo III Tephra
PDF
0
1
2
3
4
5
6
7
8
V DRE
×10-3

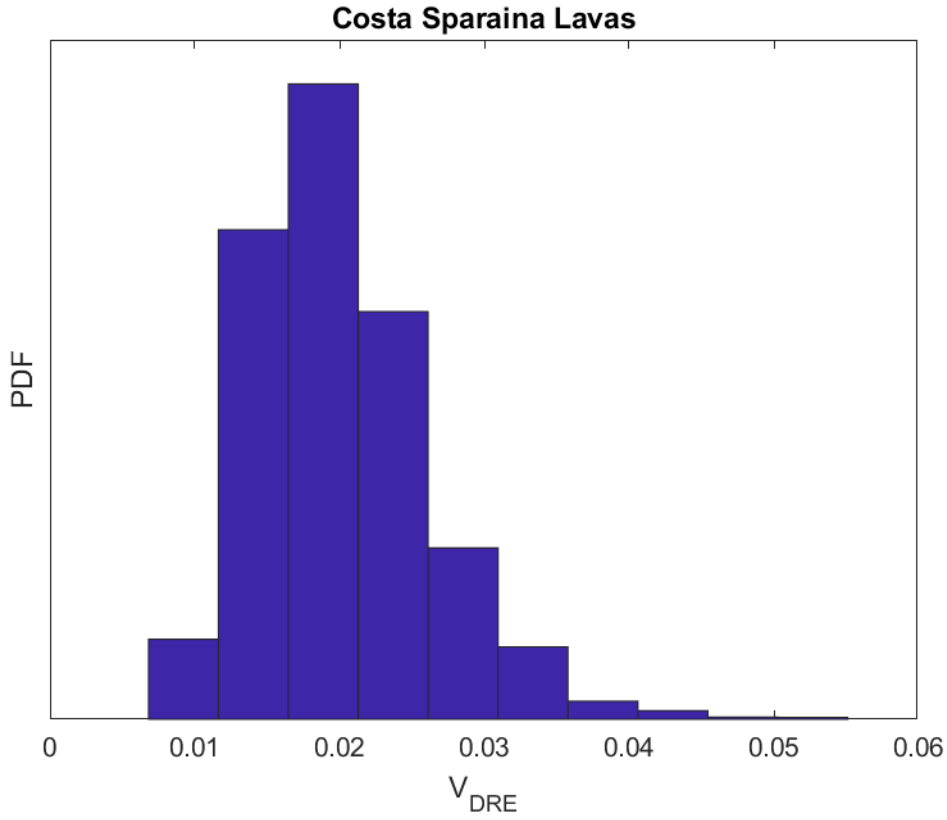
Costa Sparaina Lavas
PDF
0
0.01
0.02
0.03
0.04
0.05
0.06
V DRE

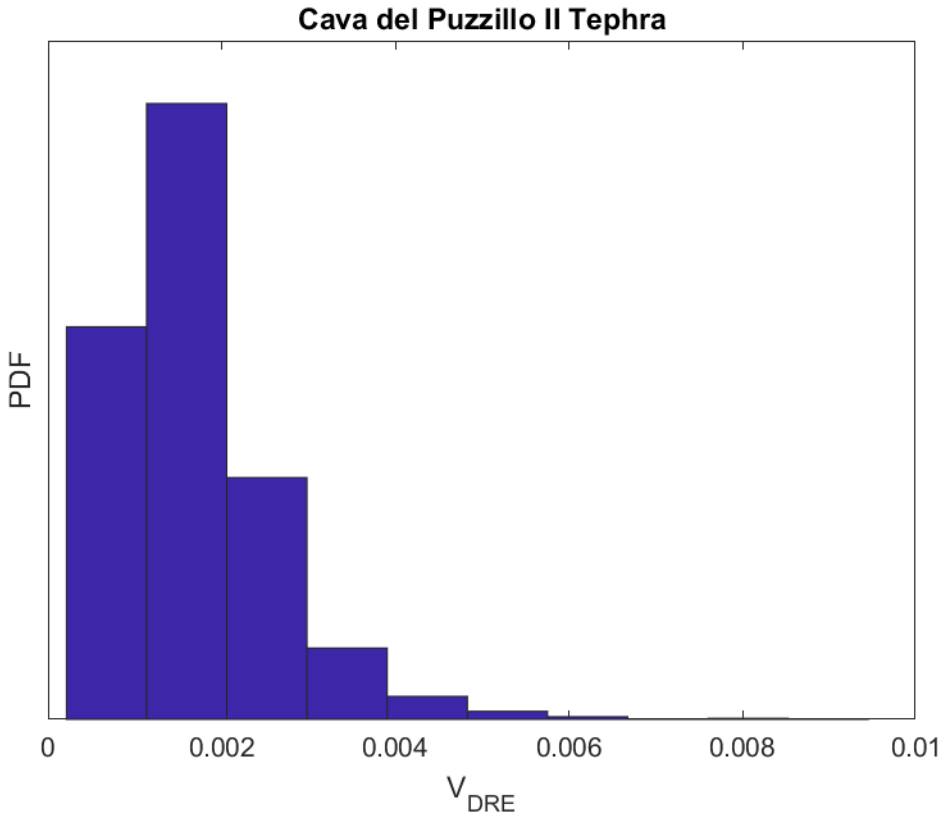
Cava del Puzzillo II Tephra
PDF
0
0.002
0.004
0.006
0.008
0.01
V_DRE

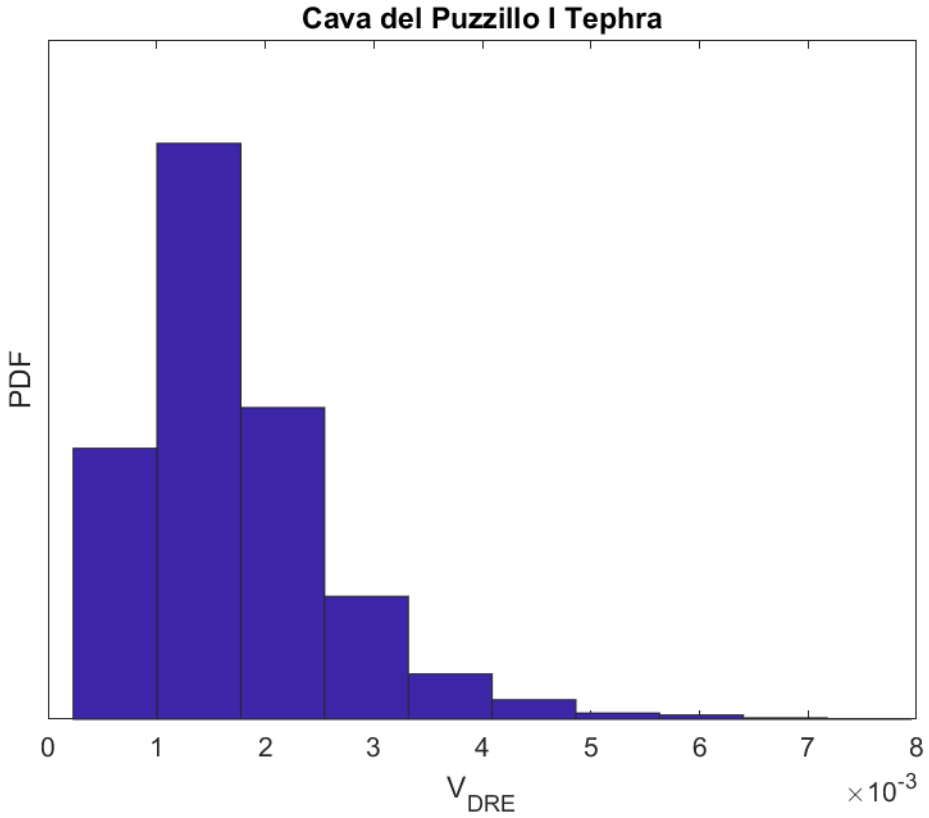
Cava del Puzzillo I Tephra
PDF
0
1
2
3
4
5
6
7
8
V_DRE
×10^-3

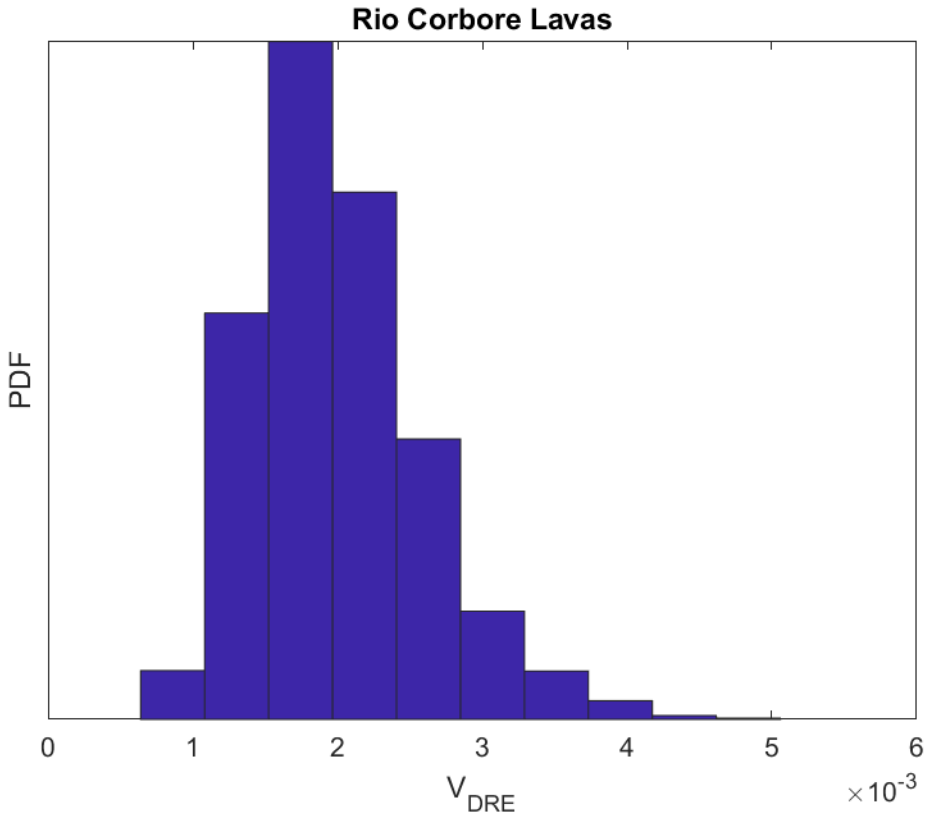
Rio Corbore Lavas
PDF
0
1
2
3
4
5
6
V_{DRE}
$\times 10^{-3}$

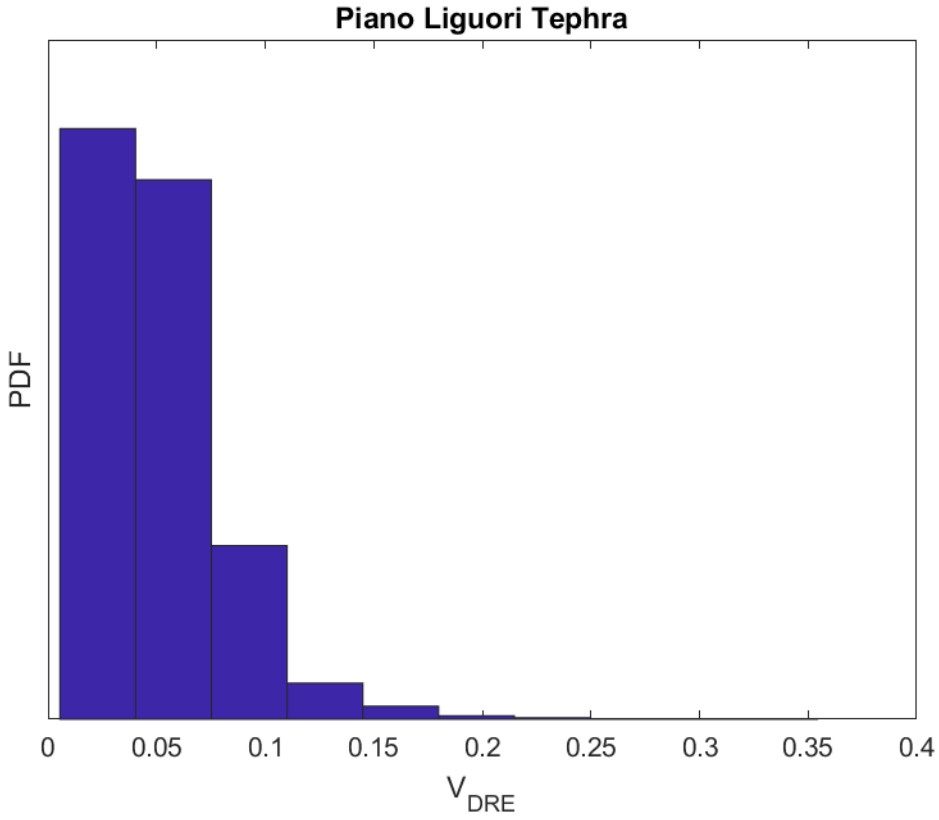
Piano Liguori Tephra
PDF
0
0.05
0.1
0.15
0.2
0.25
0.3
0.35
0.4
V_{DRE}

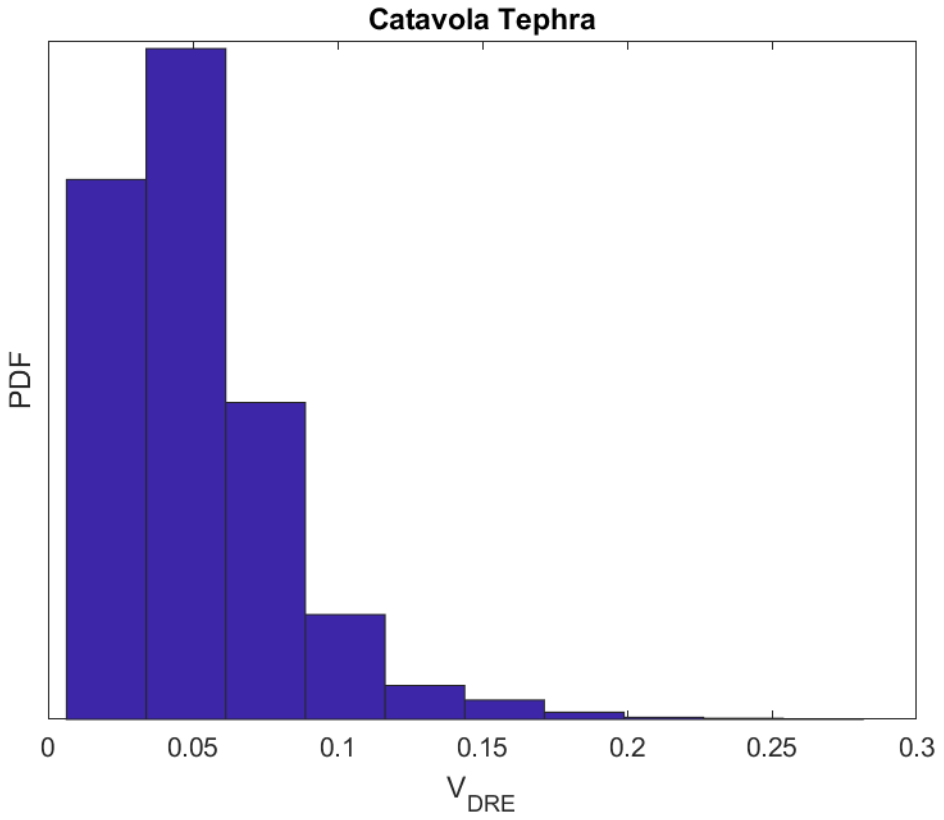
Catavola Tephra
PDF
0
0.05
0.1
0.15
0.2
0.25
0.3
V DRE

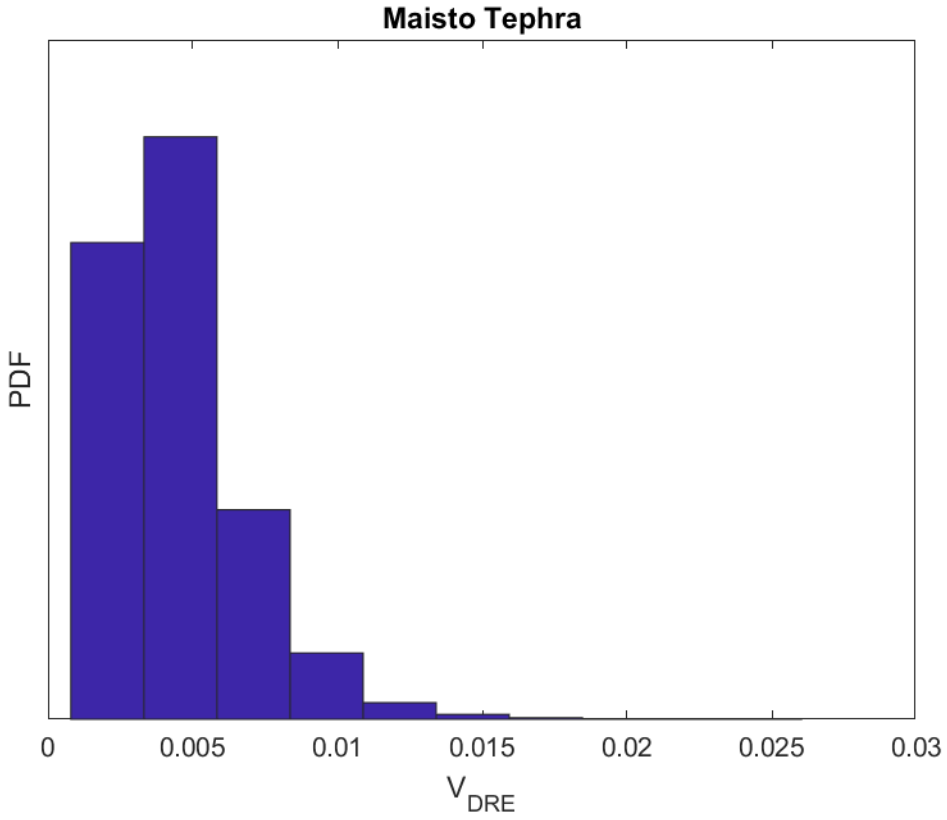
Maisto Tephra
PDF
0
0.005
0.01
0.015
0.02
0.025
0.03
V DRE

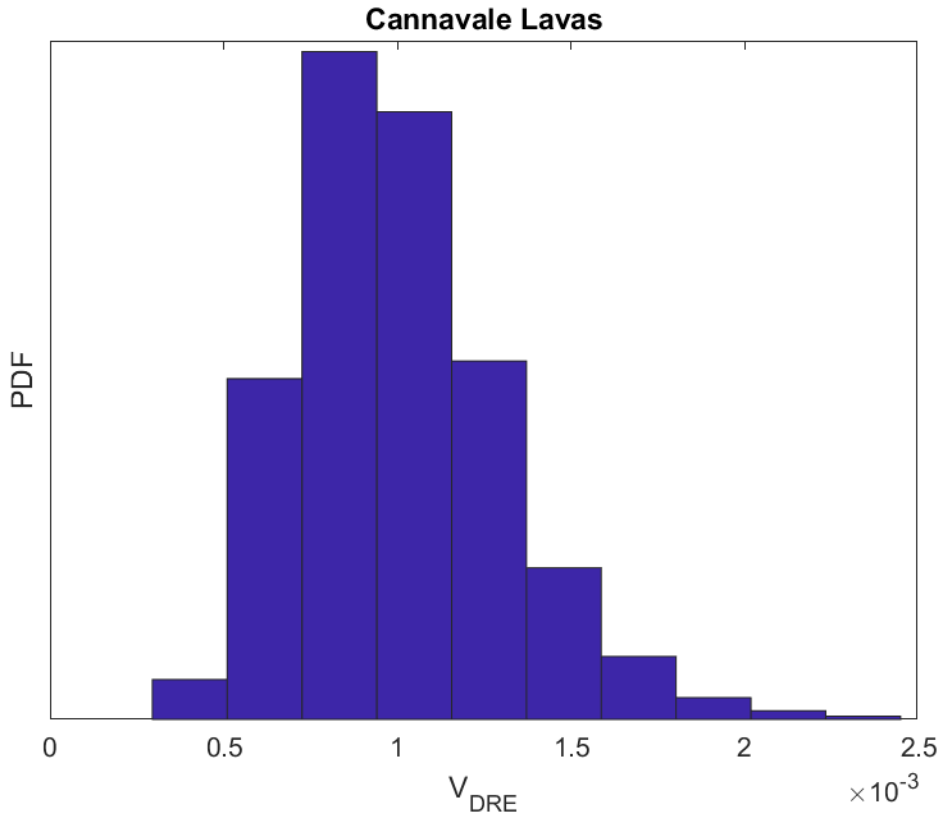
Cannavale Lavas
PDF
0
0.5
1
1.5
2
2.5
V_{DRE}
$\times 10^{-3}$

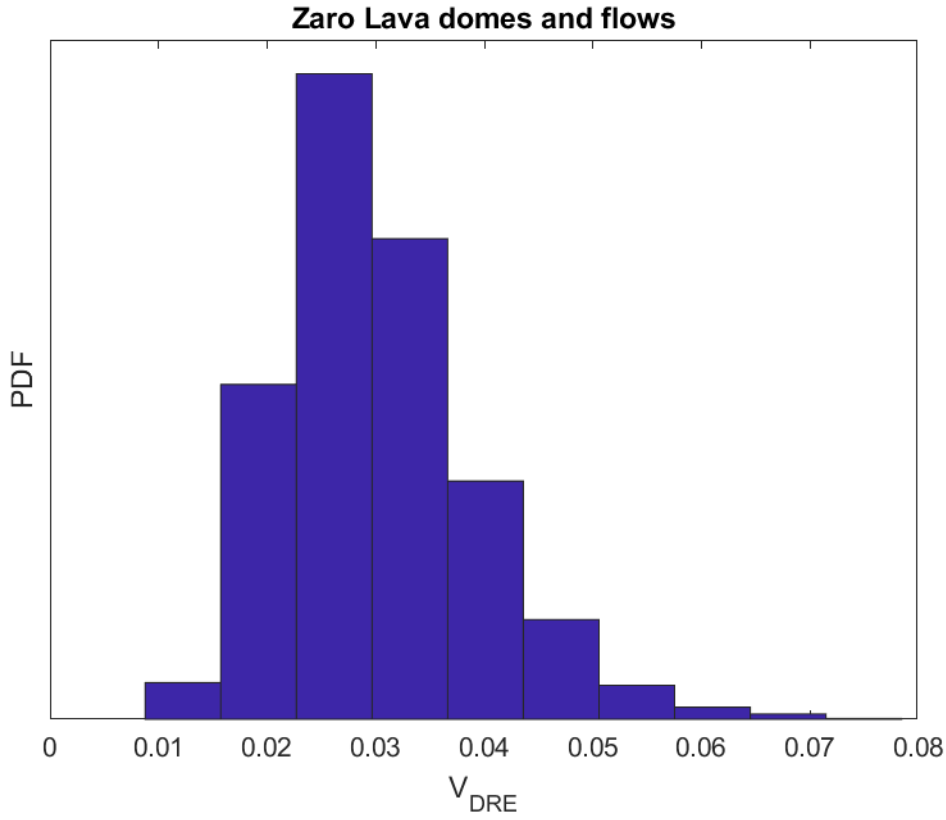
Zaro Lava domes and flows
PDF
0
0.01
0.02
0.03
0.04
0.05
0.06
0.07
0.08
V_{DRE}

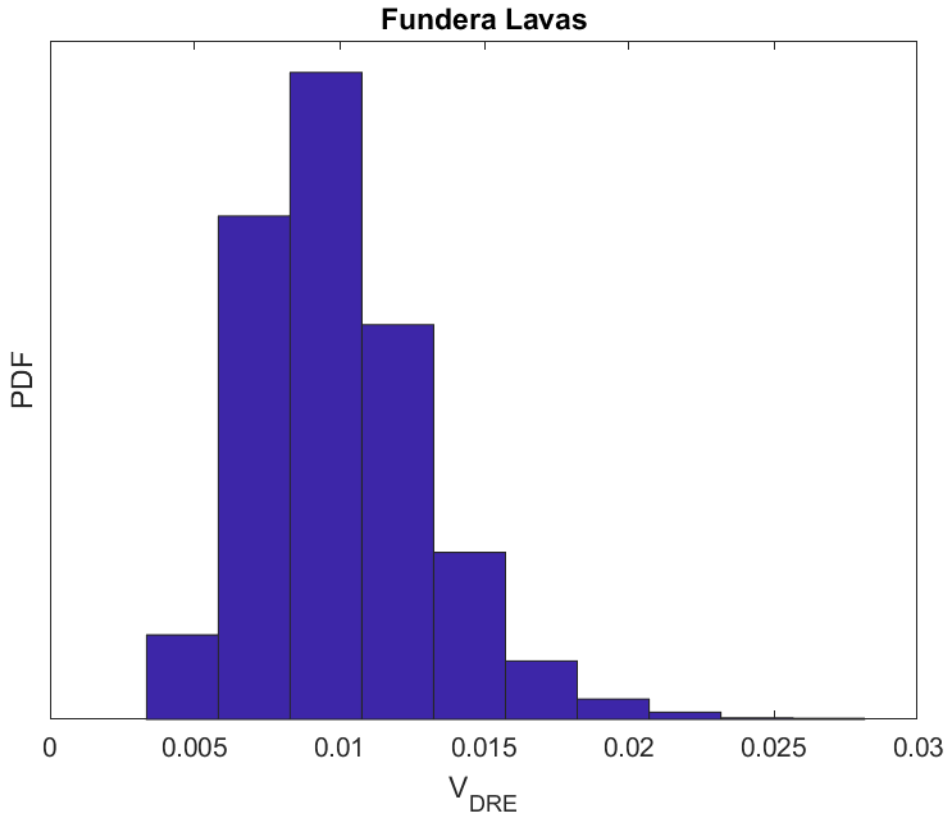
Fundera Lavas
PDF
0
0.005
0.01
0.015
0.02
0.025
0.03
V DRE

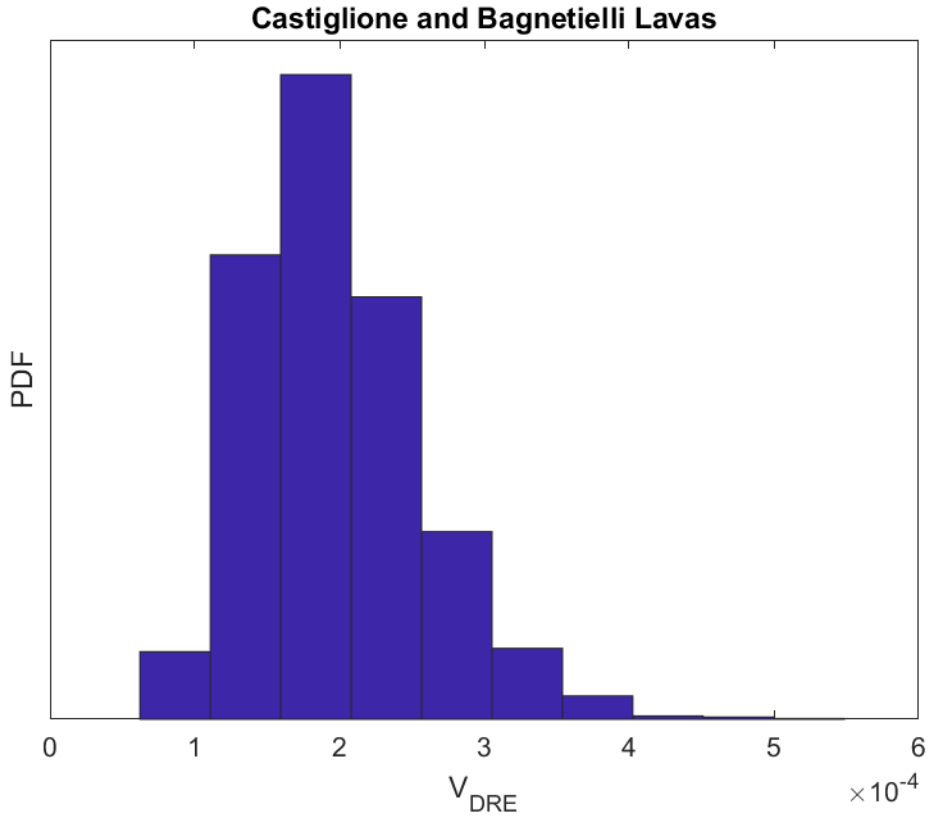
Castiglione and Bagnetielli Lavas
PDF
0
1
2
3
4
5
6
V DRE
×10-4

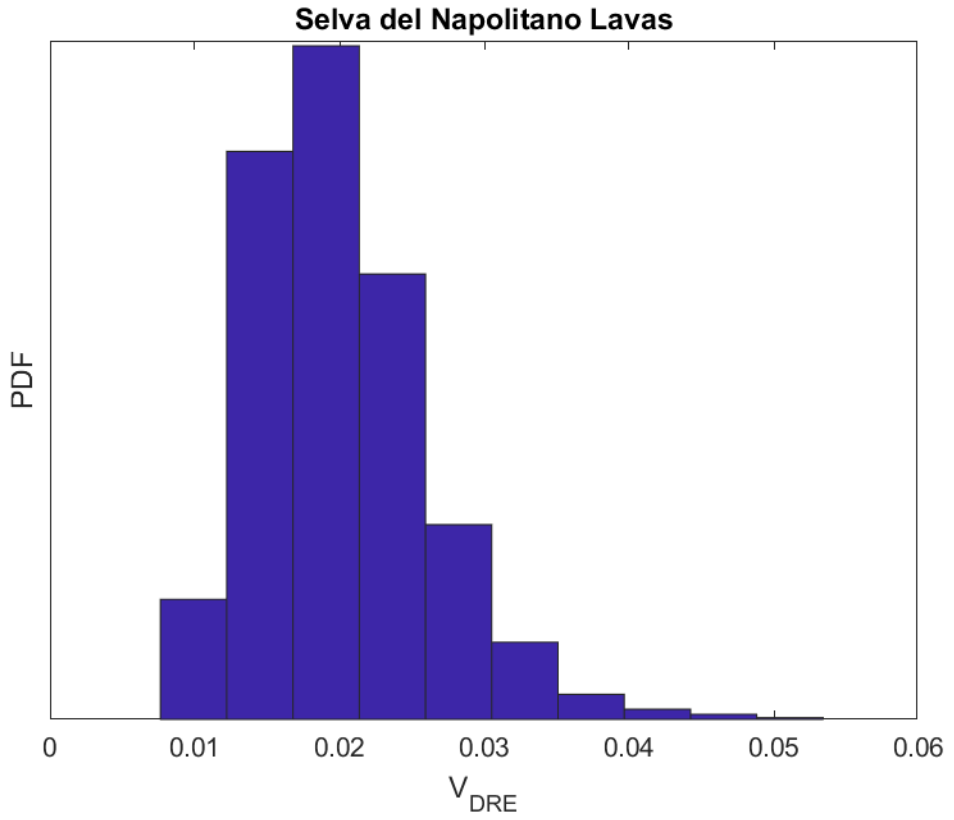
Selva del Napolitano Lavas
PDF
0
0.01
0.02
0.03
0.04
0.05
0.06
V DRE

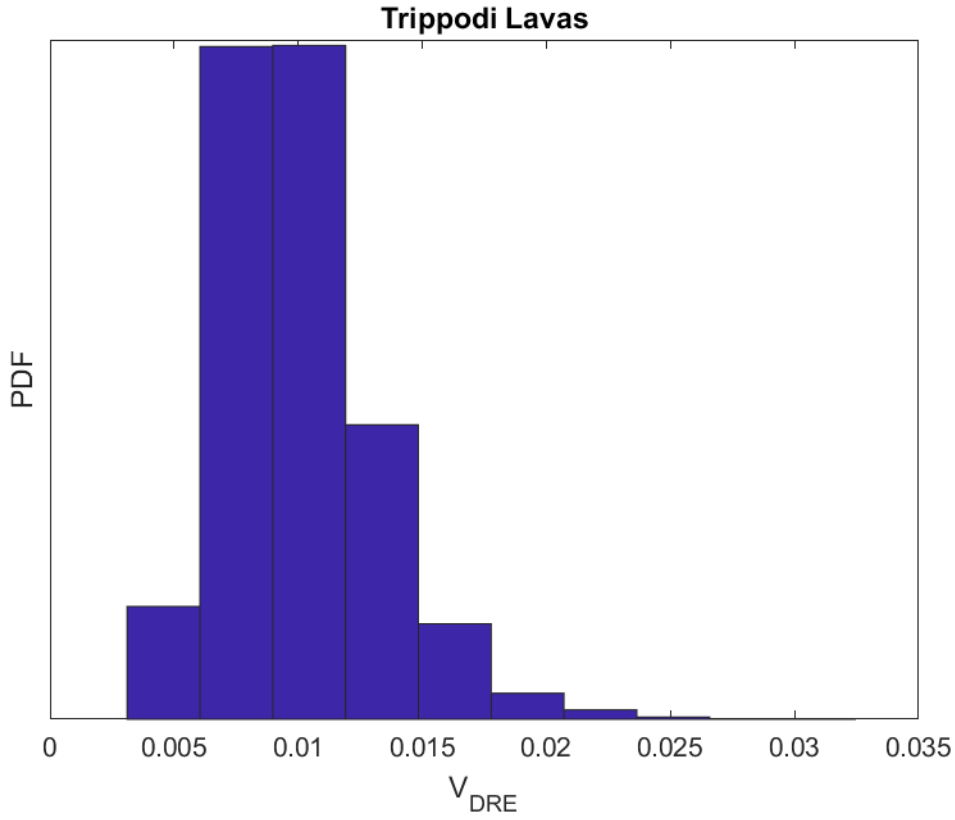
Trippodi Lavas
PDF
0
0.005
0.01
0.015
0.02
0.025
0.03
0.035
V DRE

References

Alberico, I., Lirer, L., Petrosino, P., & Scandone, R. (2008). Volcanic hazard and risk assessment from pyroclastic flows at Ischia island (southern Italy). *Journal of volcanology and geothermal research*, *171*(1-2), 118-136.

Alessio, G., Esposito, E., Ferranti, L., Mastrolorenzo, G., & Porfido, S. (1996). Correlazione tra sismicità ed elementi strutturali nell'isola d'Ischia. *Il Quaternario*, *9*(1), 303-308.

Bebbington M. (2008) Incorporating the eruptive history in a stochastic model for volcanic eruptions. J Volcanol Geotherm Res 175:325–333.

Bebbington, M. S. (2015). Spatio-volumetric hazard estimation in the Auckland volcanic field. *Bulletin of Volcanology*, *77*(5), 39.

Bonadonna, C., & Houghton, B. F. (2005). Total grain-size distribution and volume of tephra-fall deposits. Bulletin of Volcanology, 67(5), 441-456.

Bonadonna, C., Genco, R., Gouhier, M., Pistolesi, M., Cioni, R., Alfano, F., ... & Ripepe, M. (2011). Tephra sedimentation during the 2010 Eyjafjallajökull eruption (Iceland) from deposit, radar, and satellite observations. *Journal of Geophysical Research: Solid Earth*, *116*(B12).

Bonadonna, C., Biass, S., & Costa, A. (2015). Physical characterization of explosive volcanic eruptions based on tephra deposits: propagation of uncertainties and sensitivity analysis. *Journal of Volcanology and Geothermal Research*, *296*, 80-100.

Brown, S. K., Crosweller, H. S., Sparks, R. S. J., Cottrell, E., Deligne, N. I., Guerrero, N. O., ... & Takarada, S. (2014). Characterisation of the Quaternary eruption record: analysis of the Large Magnitude Explosive Volcanic Eruptions (LaMEVE) database. *Journal of Applied Volcanology*, *3*(1), 5.

Buchner G. Eruzioni vulcaniche e fenomeni vulcanotettonici di età preistorica e storica nell'isola d'Ischia. In: Centre Jean Bérard, Institut Français de Naples (ed), Tremblements de terre, eruptions volcaniques et vie des hommes dans la Campanie antique, vol. 7; 1986. p. 145–88.

Capaldi, G., Civetta, L., & Gasparini, P. (1976). Volcanic history of the island of Ischia (South Italy). Bulletin Volcanologique, 40(1), 11-22.

Carey, S. N., & Sigurdsson, H. (1982). Influence of particle aggregation on deposition of distal tephra from the May 18, 1980, eruption of Mount St. Helens volcano. *Journal of Geophysical Research: Solid Earth*, *87*(B8), 7061-7072.

Carey, S., & Sparks, R. S. J. (1986). Quantitative models of the fallout and dispersal of tephra from volcanic eruption columns. *Bulletin of volcanology*, *48*(2-3), 109-125.

Carlino, S., Cubellis, E., & Marturano, A. (2010). The catastrophic 1883 earthquake at the island of Ischia (southern Italy): macroseismic data and the role of geological conditions. *Natural hazards*, *52*(1), 231.

Casalini, M., R. Avanzinelli, et al. (2017). "Geochemical and radiogenic isotope probes of Ischia volcano, Southern Italy: Constraints on magma chamber dynamics and residence time." American Mineralogist 102(2): 262-274.

Castaldo, R., G. Gola, et al. (2017). "The role of thermo-rheological properties of the crust beneath Ischia Island (Southern Italy) in the modulation of the ground deformation pattern." Journal of Volcanology and Geothermal Research 344: 154-173.

Chester, D. K., Degg, M., Duncan, A. M., & Guest, J. E. (2000). The increasing exposure of cities to the effects of volcanic eruptions: a global survey. *Global Environmental Change Part B: Environmental Hazards*, *2*(3), 89-103.

Chiesa S, P. S., Vezzoli L. (1986). "Studio dell'ultima eruzione storica dell'isola di Ischia." Boll GNV: 153-166.

Civetta, L., G. Gallo, et al. (1991). "Sr-and Nd-isotope and trace-element constraints on the chemical evolution of the magmatic system of Ischia (Italy) in the last 55 ka." Journal of Volcanology and Geothermal Research 46(3-4): 213-230.

Coltelli, M., Proietti, C., Branca, S., Marsella, M., Andronico, D., & Lodato, L. (2007). Analysis of the 2001 lava flow eruption of Mt. Etna from three-dimensional mapping. *Journal of Geophysical Research: Earth Surface*, *112*(F2).

Costa, A., Suzuki, Y. J., Cerminara, M., Devenish, B. J., Ongaro, T. E., Herzog, M., ... & Engwell, S. (2016). Results of the eruptive column model inter-comparison study. Journal of Volcanology and Geothermal Research, 326, 2-25.

Cubellis E, Carlino S, Iannuzzi R, Luongo G, Obrizzo F. (2004) Management of historical seismic data using GIS: the island of Ischia (Southern Italy). Natural Hazard.

D'Antonio, M., Tonarini, S., Arienzo, I., Civetta, L., Di Renzo, V., (2007). Components and processes in the magma genesis of the Phlegrean Volcanic District (Southern Italy). In: Beccaluva, L., Bianchini, G., Wilson, M. (Eds.), Cenozoic volcanism in the Mediterranean area: GSA, Sp. Pap. 418, Boulder, pp. 203–220.

De Novellis, V., Carlino, S., Castaldo, R., Tramelli, A., De Luca, C., Pino, N. A., ... & Bonano, M. (2018). The 21 August 2017 Ischia (Italy) earthquake source model inferred from seismological, GPS, and DInSAR measurements. Geophysical Research Letters, 45(5), 2193-2202.

de Vita, S., Sansivero, F., Orsi, G., Marotta, E., & Piochi, M. (2010). Volcanological and structural evolution of the Ischia resurgent caldera (Italy) over the past 10 ky. *Geol. Soc. Am. Spec. Pap*, *464*, 193-239.

Del Gaudio, C., I. Aquino, et al. (2011). "Monitoraggio geodetico dell'isola d'Ischia: risultati della livellazione geometrica di precisione eseguita a giugno 2010." Quaderni di Geofisica 87: 1-17.

Di Vito, M.A., Isaia, R., Orsi, G., Southon, J., de Vita, S., D'antonio, M., Pappalardo, L., Piochi, M., (1999). Volcanism and deformation in the past 12 ka at the Campi Flegrei caldera (Italy). J. Volcanol. Geotherm. Res. 91, 221–246.

Dominey-Howes, D., & Minos-Minopoulos, D. (2004). Perceptions of hazard and risk on Santorini. *Journal of Volcanology and Geothermal Research*, *137*(4), 285-310.

Druitt, T.H., Edwards, L., Mellors, R.M., Pyle, D.M., Sparks, R.S.J., Lanphere, M., Davies, M., Barreiro, B., (1999). Santorini Volcano. Geological Society, London, Memoirs, vol. 19, 165 pp

Garcia-Aristizabal A, Marzocchi W, Fujita E (2012). A Brownian model for recurrent volcanic eruptions: an application to Miyakejima volcano (Japan). Bull Volcanol 74:545–558.

Iacono A. La "Guerra d'Ischia" nel De Bello Neapolitano di G. Pontano Quaderni dell'Accademia Pontaniana. 1996; 19:1–90.

Macedonio, G., Costa, A., & Folch, A. (2008). Ash fallout scenarios at Vesuvius: numerical simulations and implications for hazard assessment. *Journal of Volcanology and Geothermal Research*, *178*(3), 366-377.

Marti, J., Spence, R., Calogero, E., Ordoñez, A., Felpeto, A., & Baxter, P. (2008). Estimating building exposure and impact to volcanic hazards in Icod de los Vinos, Tenerife (Canary Islands). *Journal of Volcanology and Geothermal Research*, *178*(3), 553-561.

Marti, J., Sobradelo, R., & Felpeto, A. (2010, May). Hazard assessment at Teide-Pico Viejo volcanic complex (Tenerife, Canary Islands). In *EGU General Assembly Conference Abstracts* (Vol. 12, p. 5774).

Martini, F., Tassi, F., Vaselli, O., Del Potro, R., Martinez, M., Van del Laat, R., & Fernandez, E. (2010). Geophysical, geochemical and geodetical signals of reawakening at Turrialba volcano (Costa Rica) after almost 150 years of quiescence. *Journal of Volcanology and Geothermal Research*, *198*(3-4), 416-432.

Marzocchi W, Sandri L, Gasparini P, Newhall C, Boschi E (2004) Quantifying probabilities of volcanic events: the example of volcanic hazard at Mt Vesuvius. J Geophys Res 109: B11201

Marzocchi, W., & Zaccarelli, L. (2006). A quantitative model for the time-size distribution of eruptions. *Journal of Geophysical Research: Solid Earth*, *111*(B4).

Marzocchi, W., Sandri, L., & Selva, J. (2008). BET_EF: a probabilistic tool for long-and short-term eruption forecasting. *Bulletin of Volcanology*, *70*(5), 623-632.

Marzocchi, W., & Bebbington, M. S. (2012). Probabilistic eruption forecasting at short and long-time scales. *Bulletin of volcanology*, *74*(8), 1777-1805.

Morton, B., G. Taylor, et al. (1956). Turbulent gravitational convection from maintained and instantaneous sources. Proceedings of the Royal Society of London A: Mathematical, Physical and Engineering Sciences, The Royal Society.

Newhall, C., & Hoblitt, R. (2002). Constructing event trees for volcanic crises. *Bulletin of Volcanology*, *64*(1), 3-20.

Orsi, G., G. Gallo, et al. (1992). A comprehensive study of pumice formation and dispersal: the Cretaio Tephra of Ischia (Italy). Journal of Volcanology and Geothermal Research 53(1-4): 329-354.

Orsi, G., de Vita, S., Di Vito, M., (1996). The restless, resurgent Campi Flegrei nested caldera (Italy): constraints on its evolution and configuration. J. Volcanol. Geotherm. Res.
74, 179–214.

Orsi, G., Piochi, M., Campajola, L., D'Onofrio, A., Gialanella, L., & Terrasi, F. (1996). ^{14}C geochronological constraints for the volcanic history of the island of Ischia (Italy) over the last 5000 years. *Journal of Volcanology and Geothermal Research*, *71*(2-4), 249-257.

Orsi, G., M. A. Di Vito, et al. (2009). "Long-term forecast of eruption style and size at Campi Flegrei caldera (Italy)." Earth and Planetary Science Letters 287(1-2): 265-276.

Pecoraino, G., L. Brusca, et al. (2005). "Total CO2 output from Ischia Island volcano (Italy)." Geochemical Journal 39(5): 451-458.

Poli, S., S. Chiesa, et al. (1989). "Time dimension in the geochemical approach and hazard estimates of a volcanic area: The isle of Ischia case (Italy)." Journal of Volcanology and Geothermal Research 36(4): 327-335.

Pyle, D. M. (1989). The thickness, volume and grainsize of tephra fall deposits. Bulletin of Volcanology, 51(1), 1-15.

Rittmann, A., & Gottini, V. (1980). *L'isola d'Ischia: Geologia*.

Rosi, M., Pistolesi, M., Bertagnini, A., Landi, P., Pompilio, M., & Di Roberto, A. (2013). Stromboli volcano, Aeolian Islands (Italy): present eruptive activity and hazards. *Geological Society, London, Memoirs*, *37*(1), 473-490.

Sandri, L., Guidoboni, E., Marzocchi, W., & Selva, J. (2009). Bayesian event tree for eruption forecasting (BET_EF) at Vesuvius, Italy: a retrospective forward application to the 1631 eruption. *Bulletin of volcanology*, *71*(7), 729-745.

Sbrana, A., R. Toccaceli, et al. (2011). "Carta Geologica della Regione Campania, Note Illustrative della Carta Geologica alla scala 1: 10.000, Foglio 464 Isola di Ischia, Regione Campania-Assessorato Difesa del Suolo."

Scandone, R., Giacomelli, L., & Gasparini, P. (1993). Mount Vesuvius: 2000 years of volcanological observations. *Journal of volcanology and geothermal research*, *58*(1-4), 5-25.

Scott, W. E., Hoblitt, R. P., Torres, R. C., Self, S., Martinez, M. M. L., & Nillos, T. (1996). Pyroclastic flows of the June 15, 1991, climactic eruption of Mount Pinatubo. *Fire and Mud: Eruptions and Lahars of Mount Pinatubo, Philippines*, 545-570.

Selva, J., Orsi, G., Di Vito, M. A., Marzocchi, W., & Sandri, L. (2012). Probability hazard map for future vent opening at the Campi Flegrei caldera, Italy. *Bulletin of volcanology*, *74*(2), 497-510.

Selva, J., Costa, A., De Natale, G., Di Vito, M. A., Isaia, R., & Macedonio, G. (2018). Sensitivity test and ensemble hazard assessment for tephra fallout at Campi Flegrei, Italy. *Journal of Volcanology and Geothermal Research*, *351*, 1-28.

Selva, J et al., (2019) Multiple natural hazards at volcanic islands: a review for the Ischia volcano (Italy). Journal of Applied Volcanology.

Shimozuru, D. (1996). Volcanic emergency management in Japan: case histories of Izu-Oshima and Unzen. In *Monitoring and Mitigation of Volcano Hazards* (pp. 787-806). Springer, Berlin, Heidelberg.

Sparks, R. S. J. (2003). Forecasting volcanic eruptions. *Earth and Planetary Science Letters*, *210*(1-2), 1-15.

Sulpizio, R. (2005). Three empirical methods for the calculation of distal volume of tephra-fall deposits. Journal of volcanology and geothermal research, 145(3-4), 315-336.

Taddeucci, J., Scarlato, P., Montanaro, C., Cimarelli, C., Del Bello, E., Freda, C., ... & Dingwell, D. B. (2011). Aggregation-dominated ash settling from the Eyjafjallajökull volcanic cloud illuminated by field and laboratory high-speed imaging. *Geology*, *39*(9), 891-894.

Thouret, J. C. (1999). Urban hazards and risks; consequences of earthquakes and volcanic eruptions: an introduction. *GeoJournal*, *49*(2), 131-135.

Vezzoli, L., & Barberi, F. (1988). Progetto finalizzato geodinamica: monografie finali. X: Island of Ischia. *Quaderni de La ricerca scientifica*, (114).

Wallenstein, N., Duncan, A., Chester, D., & Marques, R. (2007). Fogo volcano (Sao Miguel, Azores): a hazardous edifice. *Géomorphologie: relief, processus, environnement*, *13*(3), 259-270.

Zaccarelli L, Sandri L, De Vita S, Di Vito M, Sansivero F (2018). Long-term eruption forecasting at Ischia volcano, cities on volcanoes 10, Naples, Italy, 2-7 September 2018.

Chapter 2: Reconstructing fallout dispersal and total grain-size distribution of Cretaio Tephra (60 A.D.) (Ischia Island, Italy) through field data analysis and numerical modelling

Paolo Primerano[1], Guido Giordano[1], Antonio Costa[2], Sandro de Vita[3], Mauro Antonio Di Vito[3]

[1]Dipartimento di Scienze, Università degli Studi Roma Tre, L.go San Leonardo Murialdo 1, 00146 Roma, Italy.
[2]Istituto Nazionale di Geofisica e Vulcanologia - Via Donato Creti, 12, 40126 Bologna, Italy.
[3]Istituto Nazionale di Geofisica e Vulcanologia - Osservatorio Vesuviano, Via Diocleziano 328, 80124 Napoli, Italy.

Abstract

Eruptive column numerical modelling has been applied to Cretaio Tephra that is the highest magnitude and intensity event in the last 10 kyrs in Ischia, in order to establish the dispersal of the fallout related to the climax phase of the eruption and characterize the physical parameters, such as magnitude and intensity, and impact parameters.
The fieldwork, aimed to validate the existent stratigraphy, had as its goal the samples collection in the proximal area of the buried vent, and in the island along and across the apparent dispersal axis.
Grain size distributions of the erupted products show a bimodal trend probably due first by the ballistic component, especially in the most proximal sampling sites and then to the aggregation processes of the finest particles by moisture in the plume.
Medial-distal points never considered before have been used in the analysis, and their contribution have been quantified through a sensitivity study.
The fine ash component has been characterized by a Mastersizer optical analysis and results used in the understanding of aggregation processes observed in the grain size distribution.
Dispersal, plume height, TGSD, mass distribution, wind profile and diffusion coefficient of the eruptive column of Cretaio Tephra eruption have been modelled using TOTGS and HAZMAP codes.
The comparison between the results obtained by numerical modelling with different datasets allows to understand how the results change as function of data availability.
This work allows to planning better the fieldwork aimed to volcanic island hazard eruptive column related. From this work is evident that the adding of new sampling point in the proximal areas will not improve significantly the final result, if these are already conspicuous.
Produced fallout hazard maps demonstrate that nowadays, an eruption like the Cretaio Tephra could have an impact of national significance that represents a new scenario which has not been fully considered by the volcanological community and authorities because recent tephras of Ischia island has never been founded or considered in the central mainland area.

Introduction

Ischia is a volcanic island located in the western part of the Gulf of Naples and it belongs to the Phlegraean volcanic district. Ischia island counts a large number of eruptions in historical times and the last event was in 1302 A.D. (Capaldi et al., 1976; Chiesa et al., 1986; Vezzoli 1988). It is a very densely inhabited active volcano, hosting a permanent population of about 65'000 people which increases considerably during summer; nonetheless, the volcanic risk in case of renewal of activity is relatively understudied and scientific literature about the quantification of the hazard is poor (Selva et al., 2019).

Like for all volcanic islands, such as the Eolian arc in the Tyrrhenian Sea (Rosi et al., 2013), Santorini (Druitt et al., 1999) and the Aegean arc in general (Dominey-Howes et al., 2004), Tenerife and Canary Island (Marti et al., 2008; Marti et al., 2010), and Fogo islands (Wallenstein et al., 2007), Ischia is subject to a series of volcanic related hazards (Selva et al., 2019; de Vita et al., 2006; Della Seta et al., 2012), which insist in a relatively small environment. Many of such volcanic islands have been designated as nature reserves, national parks, and consequently sites of tourism (Erfurt-Cooper, 2011).
Moreover, the peculiarity of Ischia is to be a volcanic island located near one of the most densely populated areas of the world, that is the Neapolitan district (Orsi et al., 2003, Alberico et al., 2011). In the world similar conditions can be found in Indonesia, Japan and Philippines and the problem of volcanic risk management is becoming more and more challenging (Sandri et al., 2012; Tilling, 1989; Nave et al., 2010; Paton et al., 2008; Perry et al., 2008; Woo, 2015; Hansell et al. 2006; Guffanti et al., 2009). In case of eruption, even if small, the number of people involved will be surely impressive.

On the other hand, for the estimation of the explosive eruption parameters pivotal for hazard assessment, volcanic islands suffer from a bias linked to the distribution of the available outcrops, typically concentrated in the area proximal to the vent and this means a lack in a complete dataset, in particular of data about distal products dispersed in the sea.
However, for the reconstruction of fallout processes, a complete and qualitatively valid dataset is fundamental for a good estimation of the total grain size distribution (TGSD) and total erupted mass. In particular, availability of distal samples has a great importance especially in the calculation of the magnitude of the eruption, particularly for eruptions that produce a significant amount of fine ash. In fact, the isopach maps tracked using a dataset relative only to proximal sites, are qualitatively not very reliable (Bonadonna et al., 2002; 2015), and this is particularly true in volcanic island where the isolines are generally limited to the onshore (e.g. Walker & Croasdale, 1971).

In the last few years there has been a great development in plume-related modelling. Starting from the description of a plume (Morton 1956) and the need to classify the volume and the explosivity of the volcanic eruptions (Walker, 1973; Newhall and Self, 1982; Pyle, 1989; Costa et al., 2016), we are now able to estimate the main eruptive and direct impact parameters related to volcanic plumes such as the ground load of tephra deposit (Bonadonna and Houghton, 2005), the height of the column (Woods 1988, Suzuki et al 2016), the dispersal (Carey & Sparks, 1986) and to describe an eruptive eruption column through the comparison of different methods (Bonadonna and Houghton, 2005; Sulpizio et al 2005; Costa et al., 2016). However, the accuracy of reconstructions derived from

the analysis of the deposits from the rock record strongly depends on the degree of preservation of the deposit, the number and areal distribution of the available outcrops, especially in distal settings, generally lacking for erosion or because very difficult to access (Pyle, 1989, 1995; Rose, 1993; Bonadonna et al., 2015). Furthermore, settling behaviour of distal ash may be affected by aggregation (Carey & Sigurdsson, 1982; Rose, 1993; Sparks et al., 1992; Cornel et al., 1983; Sorem et al., 1982; Taddeucci et al., 2011; Bonadonna et al., 2011).

This work concerns of the reconstruction of the main impact parameters associated with the Cretaio Tephra sub-Plinian eruption (ca 1950 BP; Orsi et al., 1996), which is the highest magnitude explosive eruption occurred on Ischia in the last 3 kyrs, chosen as the worst potential scenario in Ischia island (Orsi et al., 1992), in order to study the effect of a similar event nowadays in this kind of high-risk environment.

We have modelled Cretaio Tephra dispersal, plume height, TGSD, mass distribution, wind profile and diffusion coefficient of the eruptive column using HAZMAP (Macedonio et al., 2005; Pfeiffer et al., 2005) and also estimated the TGSD of Cretaio according to Biass & Bonadonna (2014)
We present also the associated hazard maps for the explosive scenarios based on the dispersal of Cretaio Tephra as the basis for the risk zonation for tephra fallout (Barberi et al., 1990) in the island and in the mainland. The tephra fallout hazard maps are based on an eruptive scenario obtained considering the best fit parameters obtained from the numerical simulations which best reproduce the Cretaio Tephra deposits and individual grain-sizes (Macedonio et al., 2005; Pfeiffer et al., 2005; Bonasia et al., 2010), together with a statistical set of wind profiles which account for the regional meteorological variability needed to construct tephra loading probability maps (Macedonio et al., 2008; Costa et al., 2009; Alberico et al., 2011; Macedonio et al., 2016) for different thresholds, which are representatives for potential roof collapses, shut down of airports, interruptions of the road system and other critical issues.

1. Geological background

The geological history of Ischia island has been characterized by an interplay among volcanism, tectonism, sedimentation and erosion (Capaldi 1976; Rittmann & Gottini, 1980; Buchner 1986; Vezzoli 1988; Orsi et al. 1991, 1996; Acocella & Funiciello, 1999; Molin et al., 2003; Tibaldi & Vezzoli, 2004; de Vita et al. 2006, 2010; Brown et al. 2008, 2014; Della Seta et al. 2012, 2015; Sbrana et al. 2011, 2018). Ischia is composed of volcanic rocks and epiclastic sediments, which reflect constructive and destructive phases (Vezzoli 1988; Orsi et al. 1991, 2003; de Vita et al. 2006; Della Seta et al. 2012).

The oldest outcrops date back to about 150 kyrs BP, while the most recent eruption occurred in 1302 A.D. in the eastern sector of the island (Chiesa et al., 1986; Vezzoli 1988; Civetta et al., 1991). During this period, five phases of activity have been distinguished (Poli 1989; Civetta et al., 1991; Casalini et al., 2017).

The last period of activity in the island began at about 10 kyrs (Selva et al., 2019 and reference therein) and is still active with the last historic lava flow eruption recorded at Arso in 1302 A.D. (Chiesa et al., 1986). This period is characterized by mainly latitic to trachytic monogenetic volcanic activity and ongoing Mt. Epomeo caldera resurgence (Orsi et al. 1991, 1996; de Vita et al. 2006, 2010). Caldera resurgence almost restricted eruptions to the eastern sector of the island with only a few vents located outside this sector, along regional and volcano-tectonic fault systems. The volcanic activity was characterized by lava domes and high aspect ratio lava flows, and magmatic and phreatomagmatic explosive eruptions that generated variably dispersed pyroclastic fall and PDC deposits (de Vita et al. 2010).

The last 10 kyrs of volcanic activity can be differentiated with respect to the previous period for a series of characteristics (Selva et al., 2019). First of all, there was a clear acceleration in the recorded eruptive activity with respect to the previous period. In this phase the magma chemistry shows a change with respect to the preceding periods, with a change of isotopic signatures (Civetta et al., 1991; Casalini et al., 2017) and most of the eruptive vents were located within the morphological depression to the east of Monte Epomeo. Only a few eruptions occurred to the west, at Zaro and at Punta Chiarito promontory and to the north, along a volcano-tectonic fault-system (Fig.1). This because the absence of volcanic activity in the Monte Epomeo area might be related to the occurrence of the resurgence (Acocella & Funiciello, 1999).

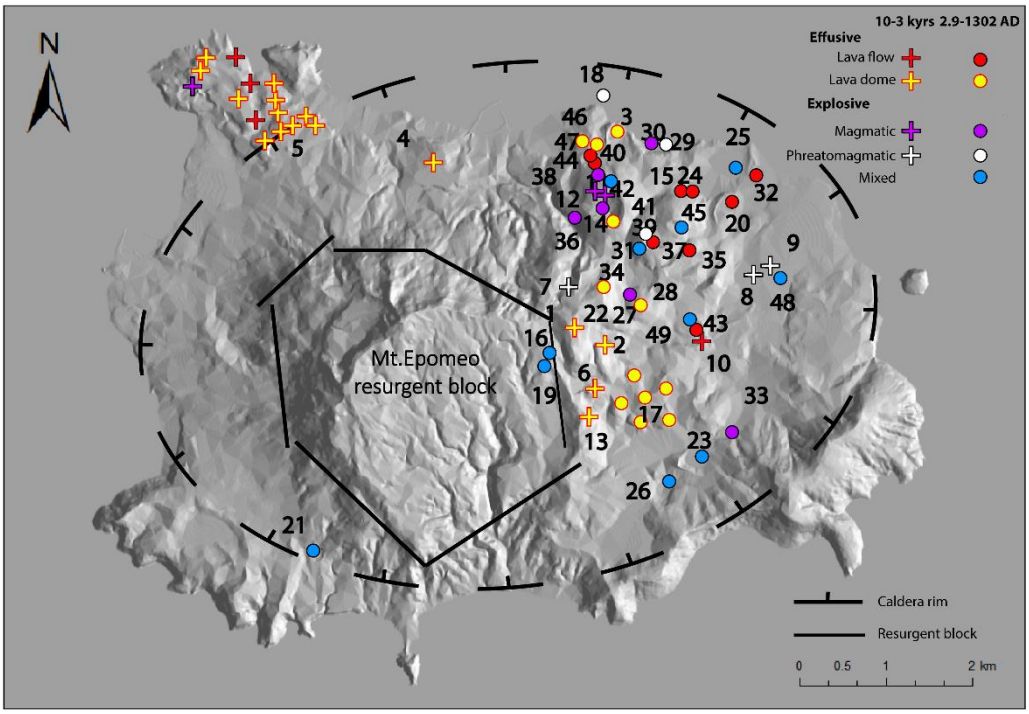

1	Trippodi Lavas	14	Cava del Puzzillo III Tephra	27	Cava Bianca Tephra	40	Villammare Tephra
2	Selva del Napolitano Lavas	15	Sant'Alessandro Lavas	28	Posta Lubrano Lavas	41	Fondo d'Oglio Tephra
3	Castiglione and Bagnetielli Lavas	16	Cannavale Tephra	29	Cafieri Tephra	42	Bosco della Maddalena Tephra
4	Fundera Lavas	17	Cantariello Lavas	30	Cafieri Lavas	43	Fiaiano Tephra
5	Zaro Lava domes and flows	18	Punta La Scrofa Tephra	31	Posta Lubrano Tephra	44	Rotaro Lavas
6	Cannavale Lavas	19	Marecoppo Tephra	32	San Pietro Lavas	45	Montagnone-Maschiata Lavas
7	Maisto Tephra	20	San Ciro Lavas	33	Cava Nocelle Tephra	46	Punta La Scrofa Lavas
8	Catavola Tephra	21	Punta Chiarito Tephra	34	Cretaio Tephra	47	Pietra Vono Lavas
9	Piano Liguori Tephra	22	Mt. Toppo Lavas	35	Arcamone-Sacchetta Lavas	48	Fondo Bosso Tephra
10	Rio Corbore Lavas	23	Molara Tephra	36	Cava Buceto Tephra	49	Arso Lavas and Tephra
11	Cava del Puzzillo I Tephra	24	Montagnone I and La Quercia Lavas	37	Bosco dei Conti Tephra		
12	Cava del Puzzillo II Tephra	25	Ischia Porto Tephra	38	Mt. Tabor Lavas		
13	Costa Sparaina Lavas	26	Vateliero Tephra	39	Bosco della Maddalena Lavas		

Fig.1 – DEM of ischia island. With different colour, the volcanic vents with their typology of activity have been reported. Plus and dots indicate different times of activity (modified from Selva et al., 2019).

1.1 The Cretaio Tephra

The Cretaio Tephra is a violent strombolian to sub-Plinian eruption (Orsi et al., 1992) and it is the highest magnitude and intensity event in the chosen reference period of 10 kyrs occurred in Ischia. The eruption covered almost all the eastern sector of the island. It consists in a sequence of pyroclastic fall and surge deposits that are dispersed over a wide area in the eastern part of the island (Fig. 2). Areas like Monte Trippodi, Piani di San Paolo, Selva del Napolitano and even Monte dei Vezzi were covered (Sbrana & Toccaceli, 2011).

It was erupted in Roman times (Rittmann & Gottini, 1980; Buchner, 1986) between the 1st century BC and the 1st century A.D., likely around 60 A.D. (Orsi et al., 1996), dating obtained as the middle value of two different samples, the first one between 162 BC - 207 A.D. and the second one between 114 A.D. - 424 A.D.. It overlies a paleosol with a ^{14}C age of 1.97±0.07 kyrs (Orsi et al., 1992, 1996) that contains pieces of Roman-age pottery and is developed above variable volcanic deposits of different ages. The Cretaio Tephra is in turn overlain by the Bosco dei Conti Tephra, from which it is separated by a centimetric humified horizon (Orsi et al., 1996; de Vita et al., 2010).

The eruption started with a phreatomagmatic phase that produced directional base surges, and was followed by the formation of a pulsating violent strombolian to sub-Plinian eruption column (de Vita et al., 2010).

The vent is buried by tephra deposits originated from later eruptions and are no morphological evidences of an edifice that could be related to this eruption. On the basis of dispersal area, thickness variation of the deposit, and size variation of its components (Orsi et al., 1992), it is hypothesized that the eruption vent was located in the area between Bosco della Maddalena and Monte Maschiata (Fig. 2) (de Vita et al., 2010).

The maximum thickness of the Cretaio Tephra is ~3 m in the area of Cretaio, decreasing to 0.7 m over a distance of ~4 km toward the South (Orsi et al., 1992; de Vita et al., 2010).

The volume of erupted magma, although difficult to measure, because most was deposited offshore, was calculated to be <0.02 km^3 DRE by Orsi et al., (1992). The deposit was subdivided into seven subunits. Five are pumice and ash fallout deposits and two are hydrovolcanic surge deposits (Orsi et al., 1992; de Vita et al., 2010).

de Vita et al. (2010) described the eruption stratigraphy in the following way:

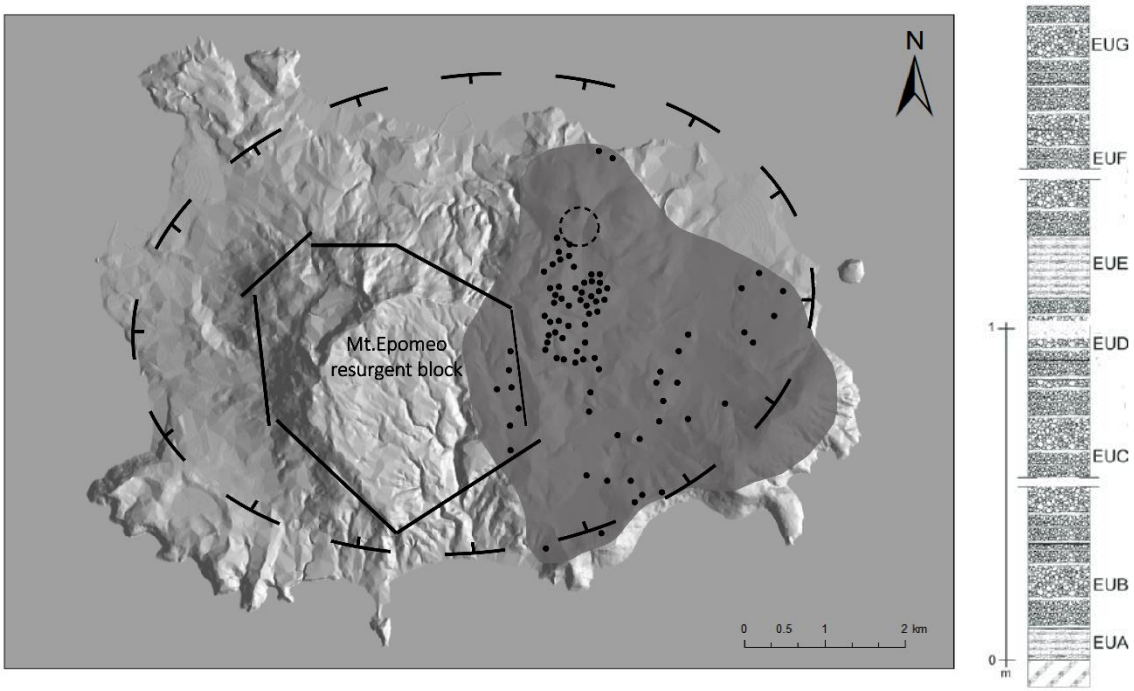

Fig. 2 – Cretaio Tephra vent area and outcrops reported in Orsi et al. (1992) and de Vita et al. (2010), with the stratigraphic section (modified from de Vita et al., 2010).

Eruption Unit A (EUA): this unit is an ash-surge deposit which occurs only in proximal area and reaches a maximum thickness of 53 cm. It is whitish grey in colour and composed of ash- to lapilli-sized particles with scattered and rounded pumice clasts and about 20% lithic clasts.

EUB: this unit is a fallout deposit found in almost all the measured sections by Orsi et al. (1992) and attains a maximum thickness of 33 cm. It is massive and composed of pinkish pumice with subordinate lithic clasts. Both juvenile and lithic clasts are angular. Fine ash is dispersed throughout the deposit.

EUC: this unit is a normal graded fallout deposit, its maximum thickness is 130 cm in the area of Mt. Trippodi; it is present in all the measured sections, and represents the climactic phase of the eruption. It is made of well vesicular white, black and banded pumice fragments and smaller grey lithic clasts.

EUD: this fallout member is composed of greenish-grey vesicular juvenile fragments and lithic clasts. It consists of three massive layers, and the intermediate layer is the finest grained. The juvenile fragments, representing parts of broken pumice and/or bombs are less vesicular than the pumice fragments of the other units. The lithic clasts are smaller than a few millimetres. The maximum thickness in proximal area is 50 cm.

EUE: is a pyroclastic surge deposit subdivided into three parts, with the lower and upper parts composed of fine ash- to lapilli-sized particles with few small rounded pumices, while the middle layer is made up mostly of rounded pumice fragments in a fine matrix. The maximum thickness is 20 cm.

EUF: this fallout unit has been subdivided into four normally graded beds. Each bed is composed of pumice fragments and lithic clasts. Pumice fragments, accounting for 60% of the deposit, are angular and whitish-grey in colour. Angular lithic clasts are abundant, and make up the remaining part of the deposit. Maximum thickness is 1 m.

EUG: this fallout unit only crops out in few sections in the western part of the outcrop area. It is composed of yellowish-white pumice fragments and subordinate grey lava lithic clasts. In many of the measured sections by Orsi et al. (1992) this member has been eroded and humified at the top (de Vita et al., 2010).

The field data available on the Cretaio Tephra are found in Orsi et al., (1992) and de Vita et al., (2010), but the information about the exactly location, typology, thickness and grain sizes of the outcrops are not present, and moreover, the isopach maps produced by Orsi et. al, (1992) seems to be unusual and relatively poorly constrained. A work on availability check of the outcrop and a fieldwork based on the measurement relatives to the data collection, useful for impact parameters estimation, such as the validation of the stratigraphy and the realization of isopach and isopleth maps, has been performed.
The present work aims also to quantify the differences between the resulting models, using the dataset available by Orsi et al., (1992), a sub-dataset relative only to the proximal area, and a complete dataset which take into account a few medial and distal points, showing the possibility to realize a complete and reliable isopach map.
Cretaio Tephra fallout deposit has been previously modelled by INGV-DPC-V3 (2005–2007) only on the basis of the proximal on-land data of Orsi et al., (1992). Figure 3 shows the reconstructed distribution of pyroclastic fall-out deposits. According to that reconstruction, the eruptive column, dispersed toward S-SW.

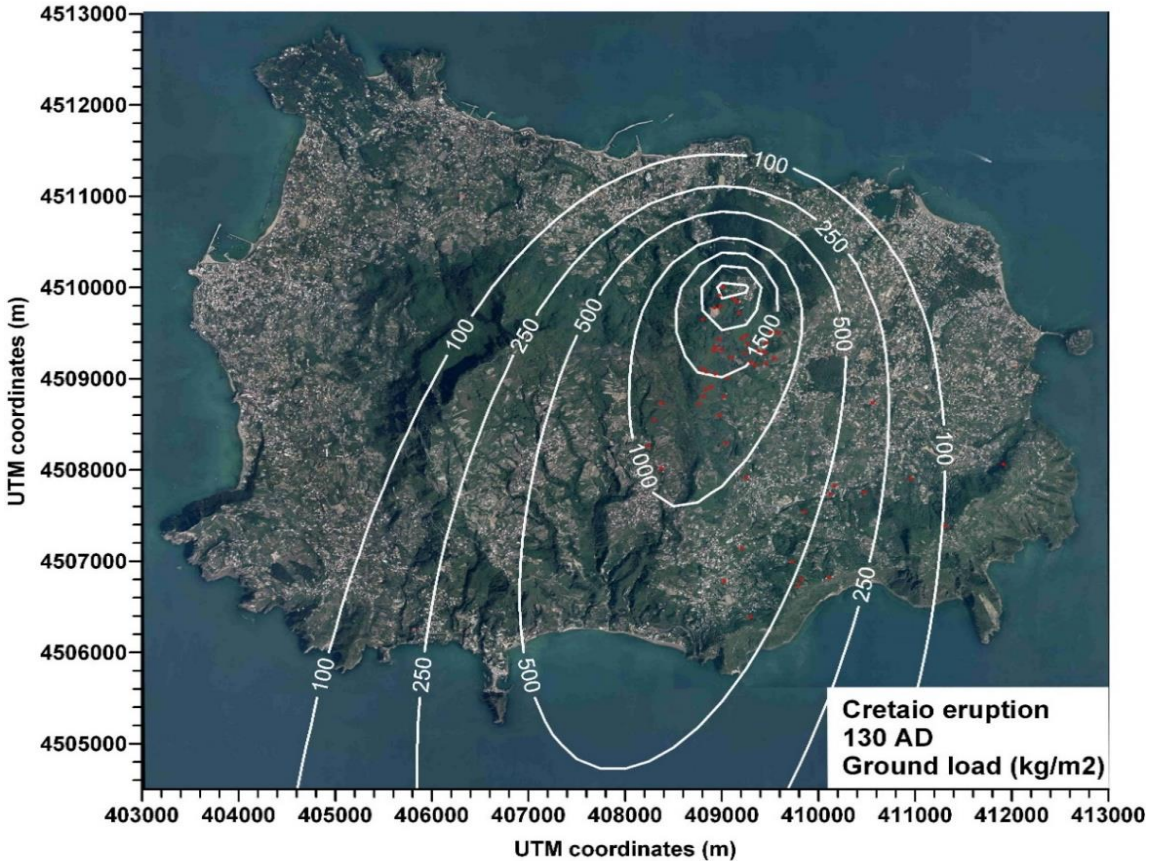

Fig.3 – Ground deposit isomass lines of Cretaio Tephra (Selva et al., 2019)., simulated by INGV-DPC-V3 (2005–2007) using the data in Orsi et al., (1992).

2. Data Presentation

In this chapter we present all the data and their acquisition processes useful for the application of numerical modelling, to reconstruct the dispersal of the fallout related to the climactic phase of the eruption, i.e. the EUC member, and characterize physical parameters, such as magnitude and intensity.

2.1 On-shore deposits

We have carefully analysed all outcrops preserved on the island. All available deposits locations are reported in Appendix A. These represent only a subset of those reported in Orsi et al., (1992) and de Vita et al., (2010) due to the very intense urbanization of the area (Fig 4).
Samples were collected with a relatively good distribution, in the proximal area near the buried vent, and in the island along and across the apparent dispersal axis.

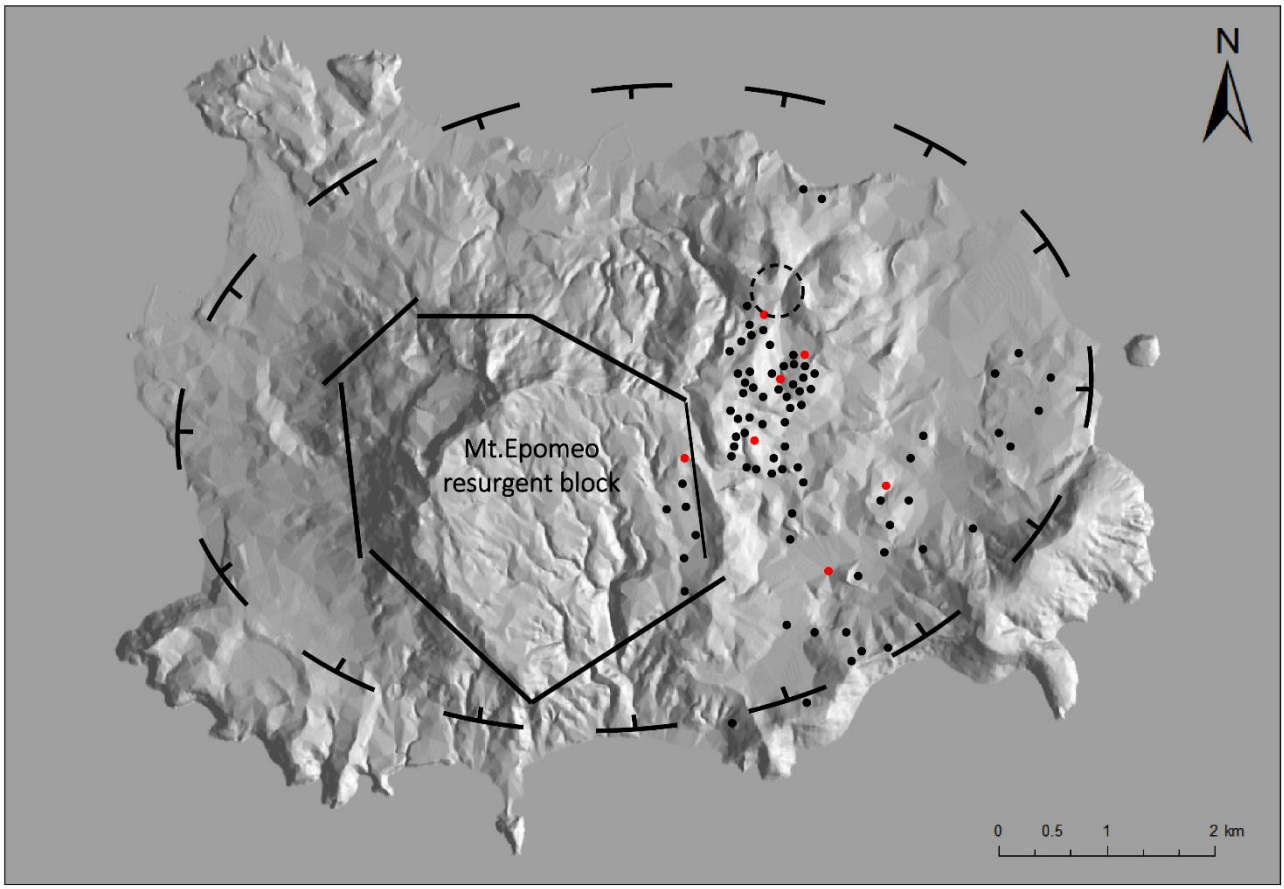

Fig. 4 – Outcrop and studied sections of Cretaio Tephra by Orsi et al. (1992) and de Vita et al. (2010) (black dots). Red dots: currently available outcrops studied in this work.

In the stratigraphy of the eruption, EUC has been chosen and sampled for the analysis, because it represents the climactic phase of the eruption, it is the only member present in all the measured sections, and most importantly, it is easily recognizable.

In the fieldwork, the outcrops have been described by logs (Fig. 5), sampled and analysed. Information about ballistic, max pumices and lithics components in the deposit have been estimated by measuring the 5 largest ones in a squared meter area.

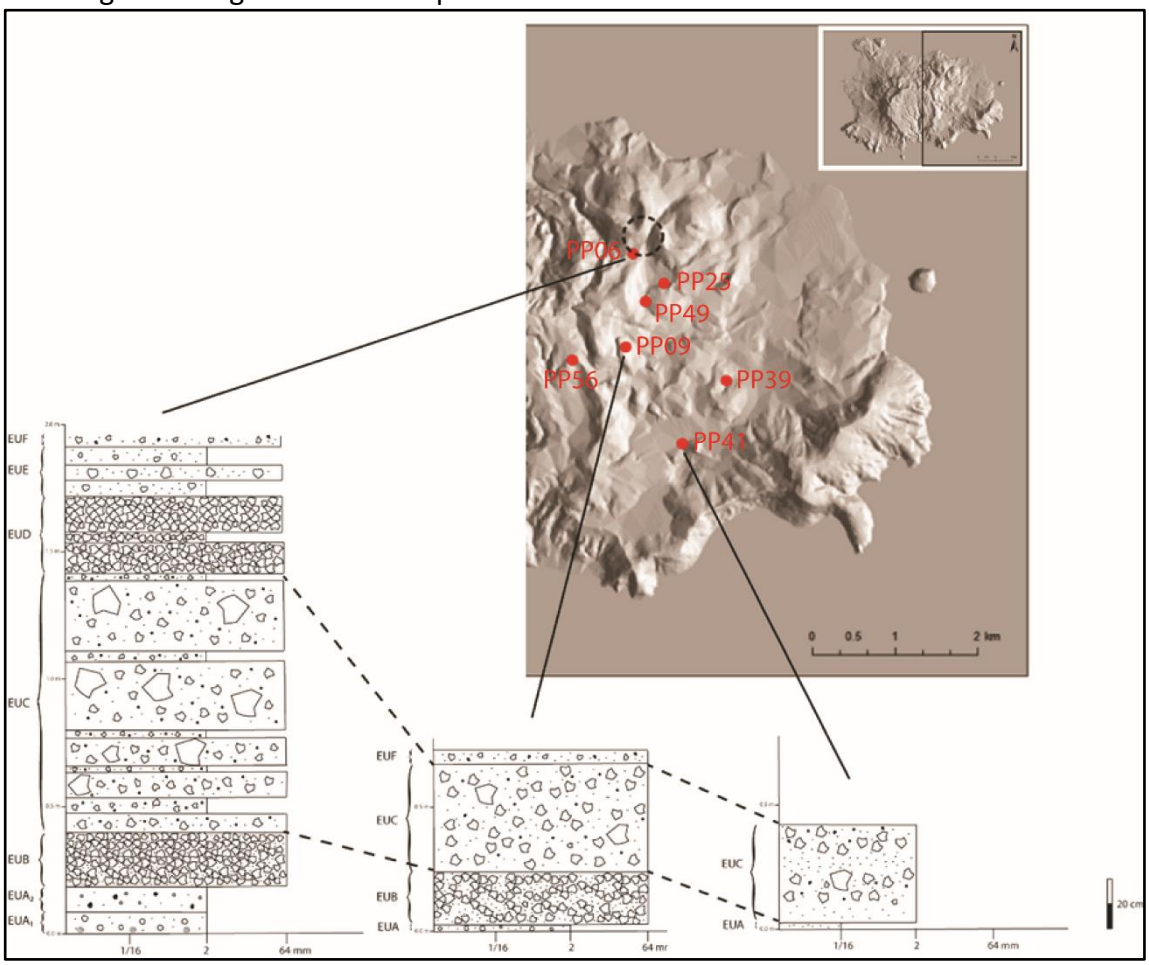

Fig.5 – Correlation of some measured stratigraphic sections of Cretaio Tephra along the dispersal axis.

The grain size distribution analysis has been performed at University of Roma Tre (Laboratorio di Geofisica e Geotecnica) and at Istituto Nazionale di Geofisica e Vulcanologia – Osservatorio Vesuviano. The methodology is described in Appendix B.

Figure 6 shows grain size distributions for each sampling point in Ischia island. The histograms show a more or less pronounced bimodal distribution in all the samples. The grain size subpopulation characterized by the coarsest mode is due to the ballistic component. If removed, the rest of the deposit shows a rather well-defined Gaussian distribution around a central mode. In some samples, the fine grain sizes show a tail which can be interpreted as the results of aggregation of the finest particles by moisture in the plume, according to the partially phreatomagmatic nature of the eruption.

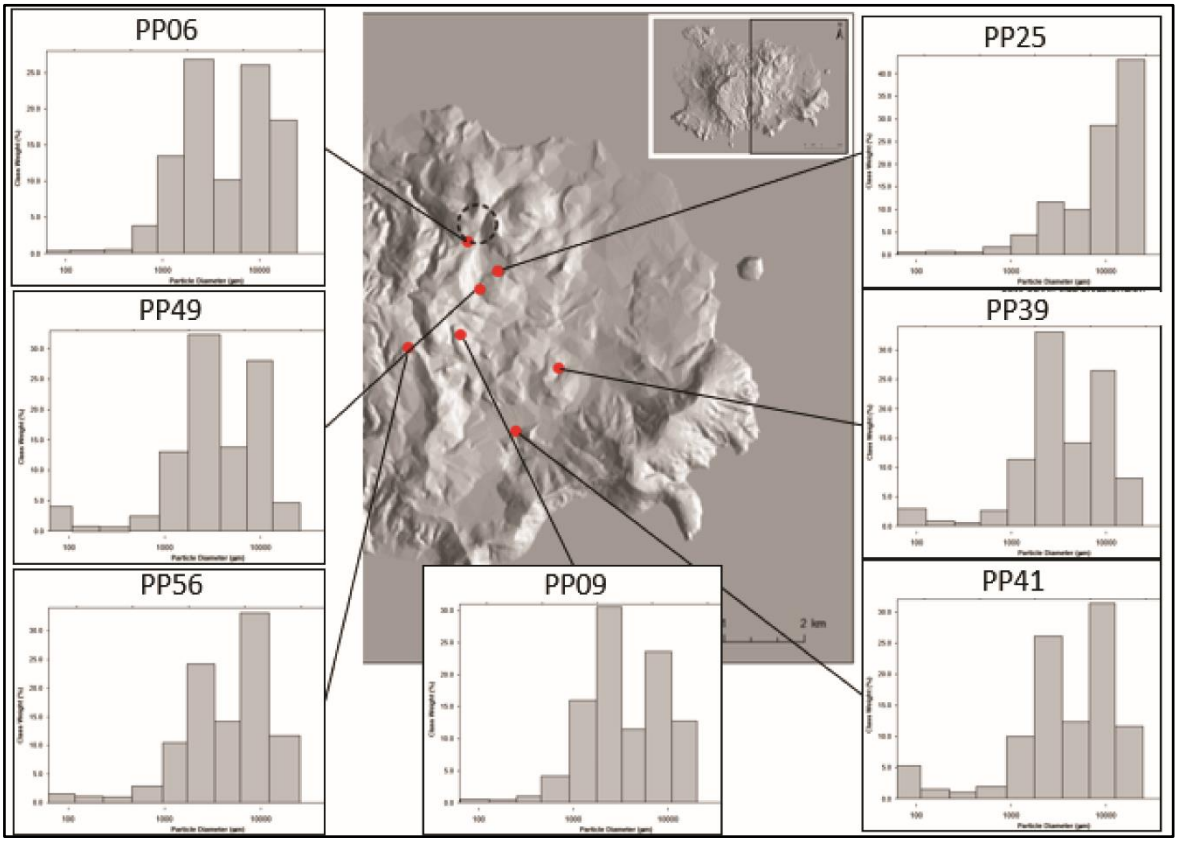

Fig. 6 – Sampling sites in Ischia and relative grain size distributions.

Figure 7 shows the grain size distributions obtained at University of Roma Tre (Laboratorio di Geofisica e Geotecnica) by a Mastersizer 2000 for the fine ash component.

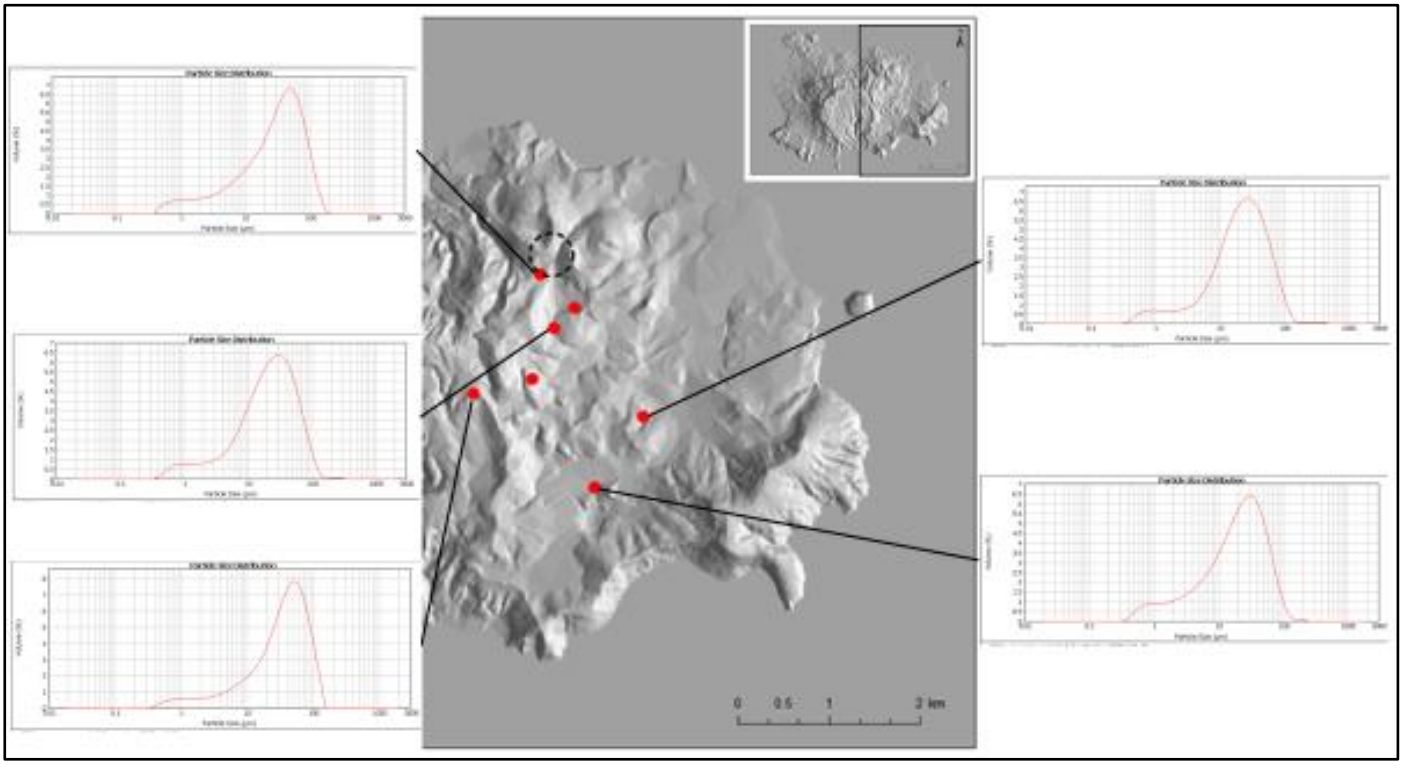

Fig.7 - Sampling sites in Ischia and relative fine ash grain size distributions.

Isopleth maps have been drawn and thickness and outsized pumice clasts distribution are shown in Fig. 8. These maps take into account only the on-land outcrops distribution.

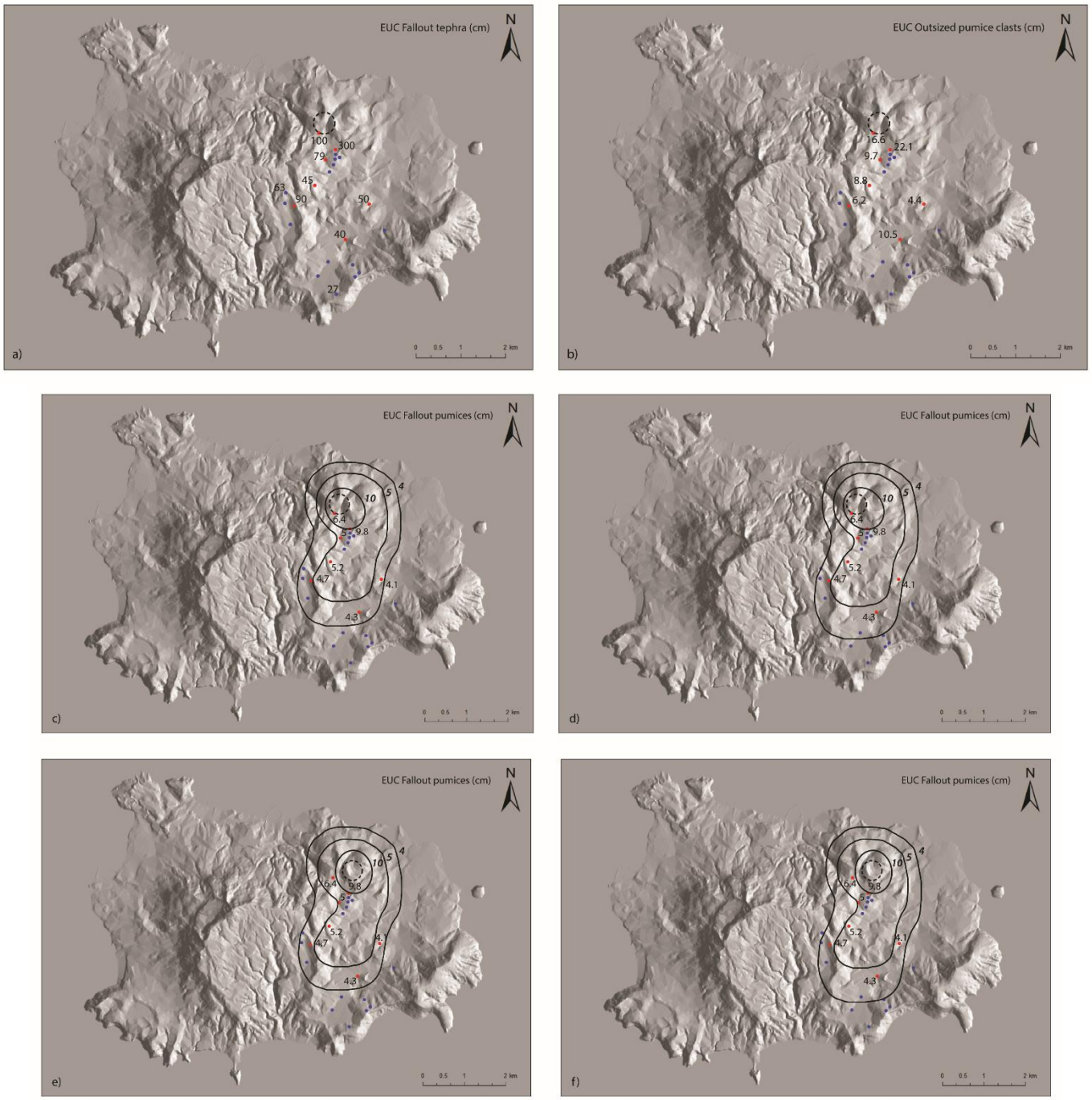

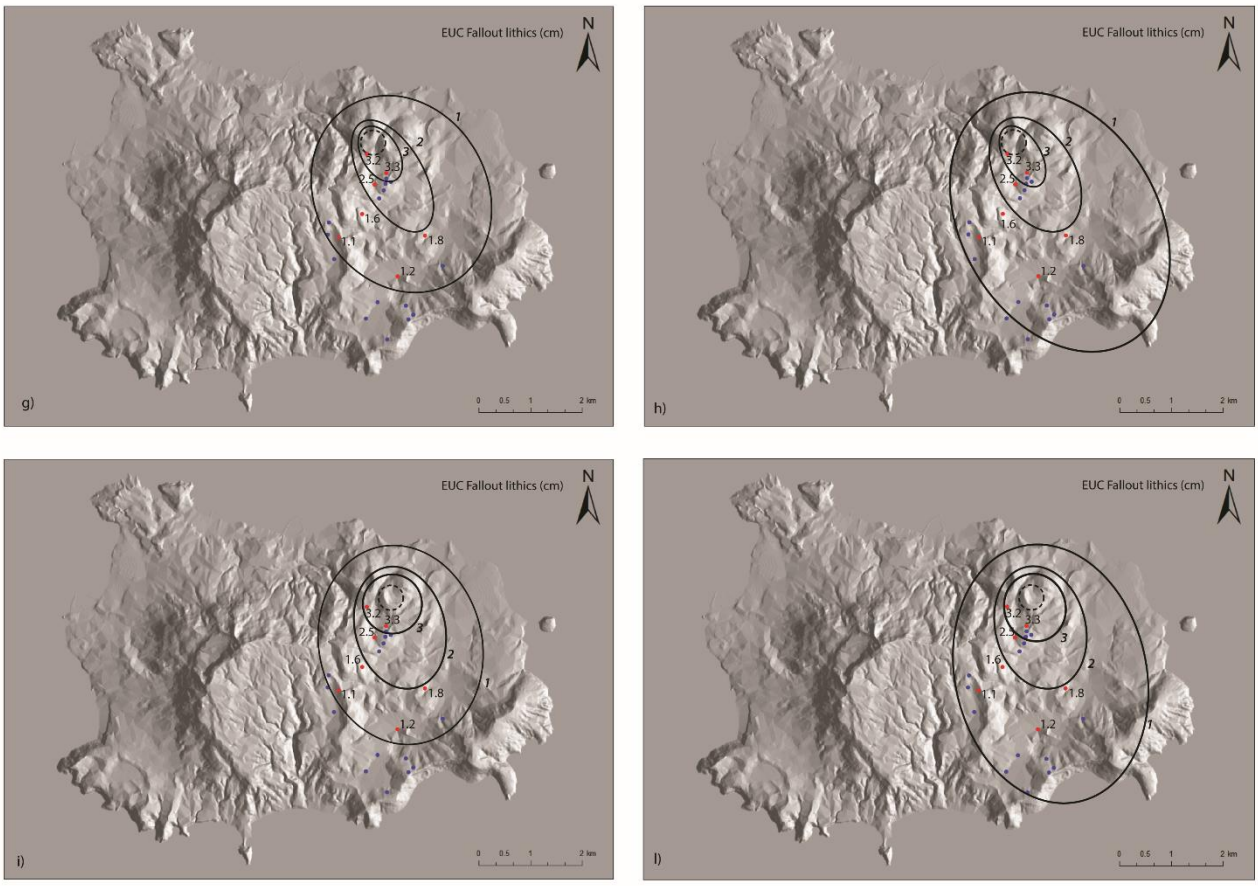

Fig.8 –EUC pumice and ballistic isopleth maps (c;g) with different vent position (e;i) and extrapolation (d;f;h;l), thickness (a) and outsized pumice clasts (b) distribution in cm.
Red dots: outcrops studied in this work. Blue dots: literature available outcrops selected for the analysis (Orsi et al., 1992).

	Figure	isopleth (cm)	crosswind range (km)	downwind range (km)	isopleth area (km^2)
Pumices	c	10	0.4	0.8	0.4
		5	0.8	2.8	3.7
		4	1.4	3.6	6.7
	d	10	0.5	1.0	0.7
		5	1.0	3.0	4.2
		4	1.3	4.3	8.2
	e	10	0.5	1.0	0.7
		5	0.9	3.1	4.0
		4	1.2	4.0	7.4
	f	10	0.4	1.0	0.7
		5	0.8	3.1	4.1
		4	1.1	4.3	8.3
Lithics	g	3	0.4	1.1	0.6
		2	0.7	2.4	2.3
		1	1.7	3.9	10.3
	h	3	0.4	1.3	0.7
		2	0.9	2.4	2.8
		1	2.0	5.4	16.0
	i	3	0.7	1.1	0.9
		2	1.0	2.4	3.3
		1	1.7	3.8	9.5
	l	3	0.6	1.3	1.1
		2	1.0	2.4	3.2
		1	2.0	5.0	14.4

Table 1 – Isopleths characterization for each figure of Fig.8: thickness, crosswind and downwind range, area.

The maximum thickness of EUC is 300 cm, which decreases rapidly towards NW to 100 cm and towards S/SE to 20 cm. EUC thickness in PP56 site is to be considered overthickened because on a steep slope, even if it does not seem to be reworked. Outsized pumice clasts map shows an axis oriented toward approximately N-S, strongly constrained by a 10.5 cm average diameter outsized pumice clast in PP41 site, at 2.5 km from the inferred vent. The largest average outsized pumice clast is in the PP25 site, with a diameter of 22.1 cm. Isopleth map of fallout pumices is much noisier than the fallout lithics one, but both suggest a dispersal axis toward S-SE. According with these data, about one third of the island has been covered by a deposit with a thickness greater than 50 cm. Pumice ballistics of 12 cm of diameter until 2.5 km far from the vent represent an important source of hazard. Large momentum and high temperatures give to the ballistics a great potential for damages and fires in half of the island.
Regarding the pumices and lithics isopleth maps, several scenarios have been proposed using the field data. Low on-land data availability entails to produce a more than one best data fitting, which can express as a range (Fig. 8c and 8d for pumice fallout and Fig. 8g and 8h for the lithic component). Moreover, in the Fig. 8e, 8f, 8i, 8l, has been presented the same dataset for pumice and lithics fallout, using a vent position which seems more appropriate, in respect to the new data about EUC thickness, than the one reported in de Vita et al., (2010). By this change, the dispersal axis rotates slightly toward a southern direction. In Table 1 are reported the characterization for each isopleth in terms of crosswind, downwind range (Carey & Sparks, 1986) and area.

Concerning the total grain size distribution, the HAZMAP model does not take into consideration the emplacement mechanism of the ballistic component, but it treats only the fallout related component. So, the ballistic component has been removed from the grain size distributions and the deposit thickness by fitting the proximal granulometric distribution as two gaussian subpopulations, the coarser and the finer one, rescaling the deposit thickness according to the relative fraction.

2.2 Medial-distal deposits

Fieldwork has been conducted in the continental and in the surrounding areas to find medial-distal outcrops of the Cretaio Tephra to better constrain the model.
On the mainland, the main problem is that the 60 A.D. Cretaio Tephra have to be distinguished from the potentially very similar fall deposits of the 79 A.D. eruption of Vesuvius (Giacomelli et al., 2003). Historical chronicles about the Cretaio eruption does not exist, although it occurred in Roman times, and since the uncertainty interval on the dating of the Cretaio eruption includes 79 A.D., a lot of care is needed to distinguish between the two as they are similar in lithology and their stratigraphic relationships are unknown. For these reasons several outcrops have been studied where tephra candidates are present in Sorrento Peninsula and Capri Island; samples have been collected and analysed.

A potential sampling sites of Cretaio Tephra has been found in Capri island (Fig. 9), where an ash layer has been sampled (Fig. 10).

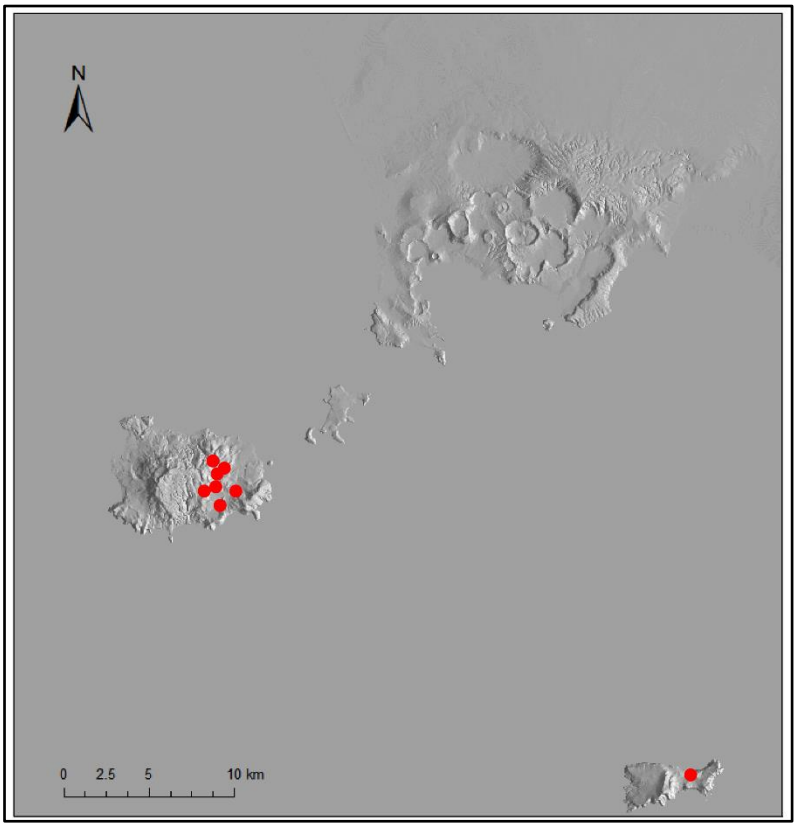

Fig.9 – Cretaio Tephra: Capri island sampling site in respect to those in Ischia island.

Fig.10 - Outcrop of Cretaio Tephra in Capri Island. The ash layer has been sampled.

Cretaio Tephra in Capri island consists in a laterally discontinuous laminated ash layer with granulometric alternations of fine-coarse and fine ash. Subcircular grey pumices with variable vesiculation are present. The maximum thickness is 15 cm and decreases to the North.

In order to be sure that the deposit found in Capri actually belongs to the Cretaio Tephra, and therefore include our sample to the dataset, particles of 0ϕ, 1ϕ and 2ϕ have been characterized by a microprobe analysis to study the intraclast and interclast compositional variability (Fig. 11). The characterization has been performed at Istituto Nazionale di Geofisica e Vulcanologia – Sezione di Roma where 8 spots in 0ϕ, 7 spots in 1ϕ and 20 spots in 2ϕ diameter ash particles have been investigated (Table 2). The comparisons to Cretaio composition published in Petrini et al. (2001), and to 79 A.D. eruption in Marianelli et al. (1995), confirm that the Capri sample belongs effectively to Cretaio Tephra (Fig. 12).

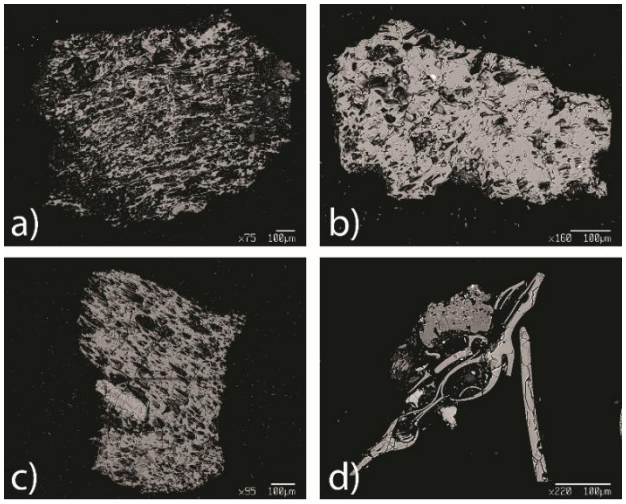

Fig.11 – Some of the BSE images of pumices (a, b, c) and ash shards (d) of Cretaio Tephra collected in Capri island. Particles have been studied by a microprobe analysis.

N. Spot	Al2O3	Na2O	K2O	Cl	FeO	SrO	MgO	CaO	SiO2	TiO2	Total	Grain size
1	18.960	6.260	7.070	0.779	2.760	0.201	0.339	1.560	60.900	0.435	99.263	
2	18.660	6.400	7.290	0.786	2.950	0.082	0.411	1.690	61.600	0.312	100.180	
3	18.680	6.420	7.190	0.798	3.050	0.060	0.285	1.680	60.650	0.385	99.199	
4	18.950	6.620	7.110	0.812	2.850	0.073	0.393	1.650	60.540	0.465	99.463	
5	19.570	5.950	6.620	0.237	1.650	0.119	0.246	1.800	63.690	0.454	100.336	
6	18.440	5.930	6.580	0.550	2.730	0.044	0.382	1.215	61.760	0.655	98.286	
7	19.270	3.380	10.580	0.580	2.870	0.229	0.497	2.240	57.230	0.393	97.269	
8	19.840	1.490	12.610	0.018	0.248	0.483	0.023	0.507	61.220	0.099	96.539	
9	18.970	3.580	9.310	0.749	3.620	0.192	0.535	2.880	58.090	0.435	98.360	
10	18.050	6.070	7.050	0.786	2.890	0.141	0.360	1.760	60.890	0.300	98.296	2ϕ
11	18.470	6.450	7.400	0.827	2.780	0.123	0.353	1.680	61.220	0.367	99.671	
12	18.600	3.580	9.480	0.684	3.470	0.051	0.712	2.630	58.280	0.630	98.117	
13	18.360	7.210	5.740	0.699	2.690	0.075	0.282	0.879	60.450	0.513	96.898	
14	18.090	7.280	5.770	0.729	2.800	-	0.279	0.882	61.880	0.495	98.204	
15	18.310	8.140	5.780	0.779	2.710	0.089	0.228	0.875	61.710	0.562	99.183	
16	18.510	6.430	7.120	0.820	2.860	0.113	0.355	1.740	61.190	0.312	99.450	
17	18.900	6.360	7.170	0.752	2.890	0.080	0.362	1.640	60.770	0.526	99.450	
18	18.890	6.530	7.030	0.803	2.760	0.095	0.299	1.630	60.600	0.429	99.066	
19	18.620	6.470	6.770	0.815	2.780	-	0.361	1.710	60.870	0.435	98.831	
20	18.610	6.270	6.940	0.817	3.090	0.075	0.306	1.810	60.170	0.428	98.516	
34	19.010	5.770	7.250	0.415	2.710	0.069	0.412	1.470	62.150	0.497	99.752	
35	18.950	5.860	7.310	0.374	2.560	0.133	0.503	1.540	61.660	0.429	99.319	
36	18.960	3.900	9.350	0.566	3.450	0.201	0.608	2.620	58.560	0.466	98.681	
37	19.060	3.920	8.880	0.672	3.260	0.181	0.604	2.760	59.250	0.515	99.102	1ϕ
38	18.750	3.900	9.210	0.621	3.540	0.200	0.659	2.740	59.400	0.478	99.498	
39	18.790	3.830	9.100	0.622	3.400	0.082	0.579	2.630	59.140	0.288	98.460	
40	18.920	3.750	9.220	0.677	3.320	0.115	0.591	2.890	58.900	0.398	98.781	
21	19.320	3.700	9.510	0.696	3.430	0.095	0.631	2.820	59.420	0.435	100.057	
22	18.950	3.620	9.460	0.664	3.600	0.156	0.662	2.900	58.170	0.441	98.623	
23	18.880	3.610	9.380	0.660	3.560	0.191	0.609	2.820	58.440	0.386	98.536	
24	18.710	3.600	9.290	0.654	3.660	0.229	0.762	3.190	56.580	0.477	97.152	
25	19.010	3.460	9.490	0.636	3.820	0.181	0.817	3.220	57.010	0.477	98.121	
26	18.760	3.620	9.440	0.620	3.760	0.211	0.771	3.160	57.400	0.483	98.226	
27	17.590	5.990	6.010	0.908	2.440	0.088	0.240	1.337	63.730	0.392	98.725	0ϕ
28	17.840	6.310	6.310	0.713	2.440	-	0.118	1.550	64.740	0.410	100.432	
29	17.540	6.030	6.150	0.781	2.240	0.127	0.186	1.440	65.020	0.405	99.919	
30	16.910	5.310	6.020	0.733	2.310	0.081	0.193	1.310	60.910	0.392	94.170	
31	16.550	5.420	6.130	0.701	2.360	0.096	0.200	1.326	61.730	0.331	94.845	
32	16.420	5.460	5.880	0.716	2.280	0.042	0.215	1.318	62.640	0.417	95.387	
33	18.820	5.590	7.260	0.417	2.660	0.079	0.441	1.600	62.660	0.570	100.098	

Table 2 - Microprobe analysis of Capri tephra deposit, divided by grain size particles.

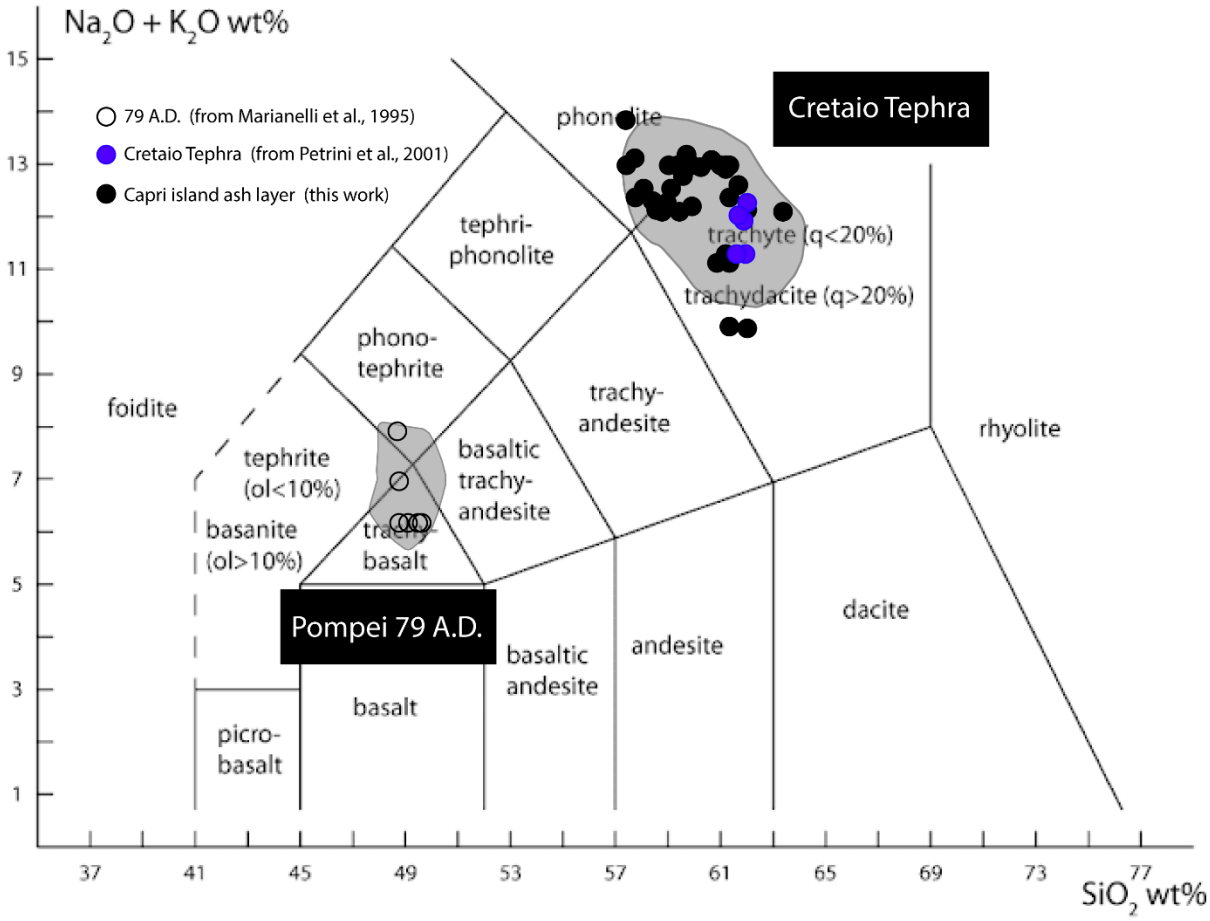

Fig.12 - Compositions of Cretaio Tephra (blue dots) and 79 A.D. (empty dots) eruptions (published in Petrini et al, 2001 and Marianelli et al., 1995, respectively), plotted in a TAS classificative diagram (modified after Le Bas et al., 1986) to compare the ash layer sampled in Capri island (black dots).

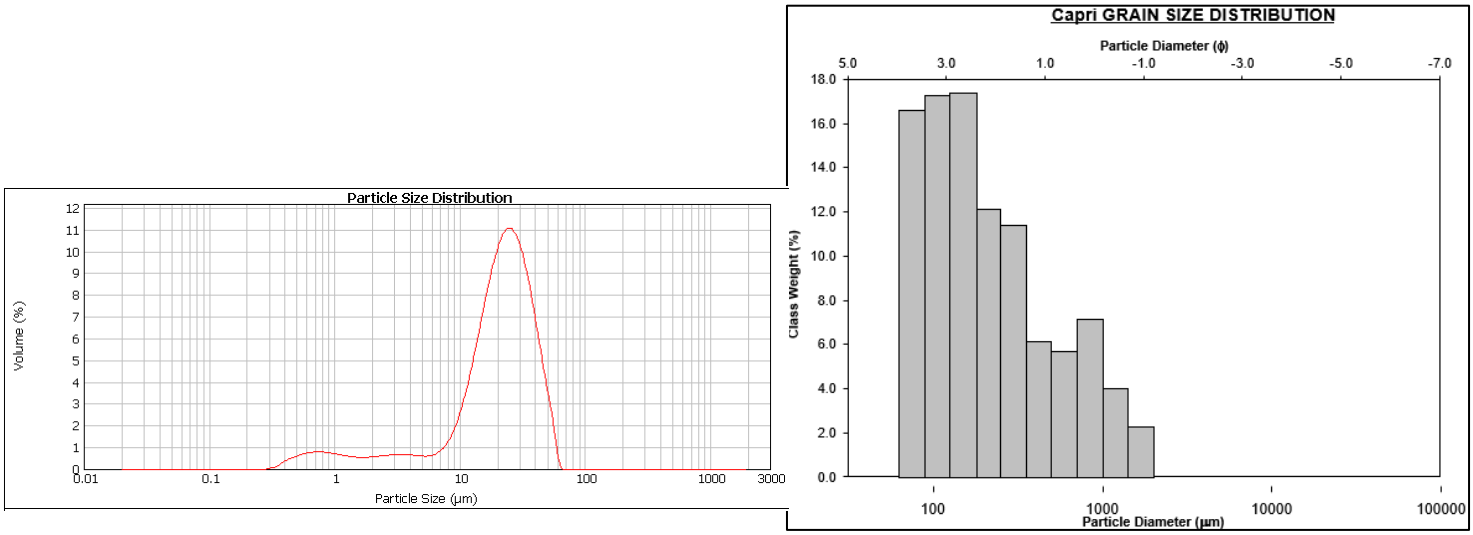

Fig. 13 – Grain size distribution of Cretaio Tephra sampled in Capri Island, obtained by sieving and Mastersizer.

Figure 13, shows the grain size distribution of Cretaio Tephra in Capri Island obtained by sieving and Mastersizer optical analysis of the finer grain sizes. The sample is characterized by a greater fine ash content with respect to proximal sample collected in Ischia.

Another sampling point outside Ischia island is CET1 (found and correlated to Cretaio Tephra on a compositional basis by Morabito et al., 2014). This represents the farthest site of Cretaio Tephra and has been found in the Eastern Tyrrhenian Sea. CET1 (Fig. 14) is a sample of microtephra with a thickness of 1 cm and a maximum clasts diameter of 250 µm.

These two deposits of Cretaio in Capri and in the eastern Tyrrhenian Sea allow us to better constrain the dispersal area of the Cretaio eruption.

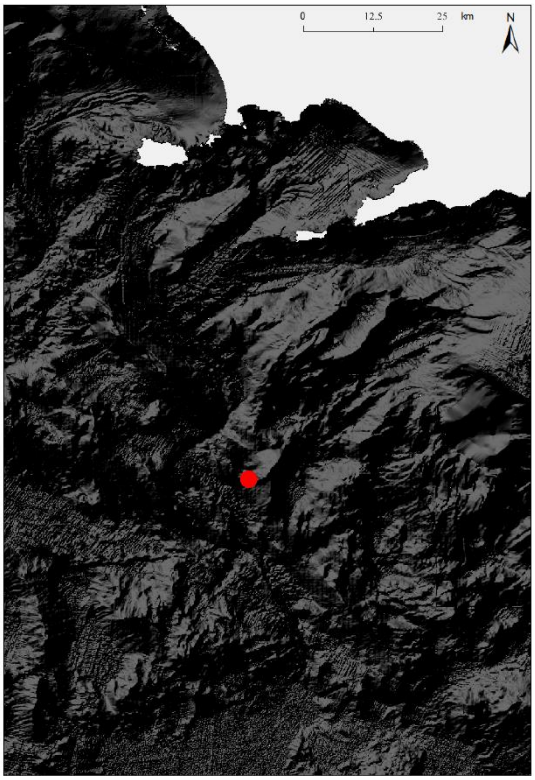

Fig. 14 – Location map of CET1 (red dot) in respect to Italian peninsula, Capri and Ischia islands.

CET1 sample is not available, so the grain size distribution has been inferred using the maximum clasts diameter of 250 µm reported in Morabito et al., (2014) and the same shape of the grain size distribution of the Capri deposit histogram. It has been treated in this way because we think it is reasonable to assume that the Capri deposit and CET1 share the same emplacement physics conditions relative to the umbrella region of the eruptive plume.
The inferred grain size distribution of CET1 is showed in Figure 15.

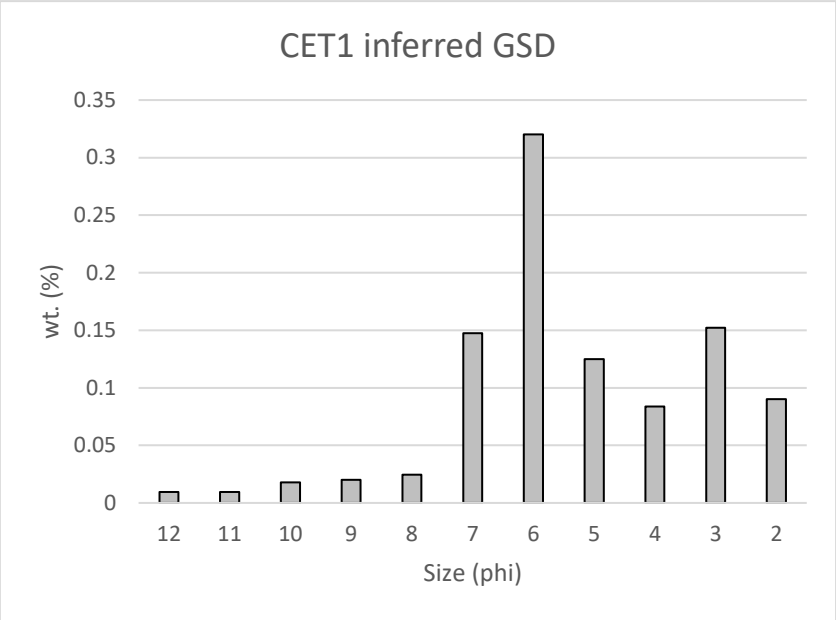

Fig. 15 – Grain size distribution of CET1, inferred by Capri deposit.

In order to better understand the behaviour of the particles in the plume and to describe the settling mechanisms, a set of measurement and estimation about densities have been performed.
Density of clasts >5mm has been measured by the methodology described in Appendix B and the mean value used in HAZMAP is 0.6 g/cm^3.
The dense rock equivalent (DRE) density has been obtained by helium-pycnometer by crushing the pumice to fine ash and it is 2.46 g/cm^3.
Deposit density has been assumed at 1000 kg/m^3 (Cioni et al., 2003; Costa et al., 2009).

3. Modelling

Grain size distributions (GSD) obtained and used in the analysis are reported in the following Table (3).

	-4	-3	-2	-1	0	1	2	3	4	5	6	7	8	9	10	11	12
PP06	1.059917	9.444136	28.40035	34.06694	17.08687	7.439906	0.720852	0.45387	0.329278	0.368864	0.267401	0.156692	0.092716	0.05448	0.041235	0.014629	0.001868
PP41	1.048064	11.08741	31.70394	33.07862	12.66937	3.167342	0.675271	1.8168	3.678618	0.263672	0.312228	0.210868	0.118348	0.093314	0.04936	0.017359	0.009413
PP25	11.96318	23.67885	26.00961	22.79167	8.666481	5.568632	0.996808	0.269813	0.024983	0	0	0	0	0	0	0	0
PP49	0.977398	11.981	38.41803	20.22122	17.0157	4.922087	0.956817	1.462826	2.85205	0.314252	0.364274	0.259875	0.125648	0.059128	0.045006	0.016633	0.008051
PP39	0.61715	9.546931	33.23793	35.67681	12.23103	4.289797	0.714966	0.855406	1.723579	0.289138	0.357783	0.251329	0.105597	0.045029	0.035118	0.014326	0.008076
PP09	1.043921	9.347289	28.31785	34.25512	17.97251	7.18796	1.392145	0.423128	0.052238	0	0	0	0	0	0	0	0
PP56	3.648739	15.92536	29.05819	29.02909	12.61817	4.920598	1.322715	1.320279	1.12784	0.441725	0.282202	0.137182	0.074339	0.042592	0.031878	0.011791	0.007316
Capri	0	0	0	0	2.908098	5.976864	8.202121	13.87371	7.631748	11.39404	29.18077	13.43093	2.24371	1.823798	1.616976	0.858611	0.858627
CET1	0	0	0	0	0	0	9.00194	15.22659	8.375948	12.50511	32.02629	14.74062	2.462503	2.001643	1.774653	0.942337	0.942354

Table 3 – Grain size distributions used in the analysis.

The total grain-size distribution (TGSD) has been estimated using the Voronoi tessellation method (Bonadonna & Houghton, 2005) starting from the GSDs of each sample, and then compared with that obtained by HAZMAP model (Macedonio et al., 2005; Pfeiffer et al., 2005).

The Voronoi tessellation is a method of spatial analysis and can be defined as the partitioning of the plane such that, for any set of distinct data points, the cell associated with a particular data point contains all spatial locations closer to that point than to any other. In particular in this work the dataset associated to each point of sampling (centre of each Voronoi cell) is the weighted average of the percentage retained weight for each granulometric class on the eruption unit thickness in the outcrop.

This technique of spatial analysis has been chosen because, with respect to other techniques reported in literature (such as Walker 1980; Murrow et al., 1980; Sparks et al., 1981; Carey and Sigurdsonn 1982; Parfitt 1998) for the determination of the total grain size distribution, do not introduce arbitrary sectors and allows to work with non-uniform data sets (Bonadonna & Houghton, 2005).

The Voronoi tessellation method needs the definition of the zero-mass contour through the reconstruction of the prevailing wind during the eruption.

In a first approach strong and weak wind conditions have been assumed by changing the shape and the aspect-ratio of the zero-mass contour, considering the apparent dispersal axis.

TOTGS code (Biass & Bonadonna, 2014) has been used to calculate the direction of the dispersal axis of the fallout and the TGSD. Several runs have been performed, considering the effect of the addition of the sea samples and the characterization of the granulometric amount of fine ash in the model, in order to study even the variability of the results changing as much as possible the data set and sub-data set.

The total grain size distributions obtained by TOTGS code, with the characterization of the fine ash component in the deposits and the contribution of the sampling site outside Ischia island, without the ballistic component, is shown in Figure 16, in order to be compared with the one obtained by HAZMAP simulation (Table 4).

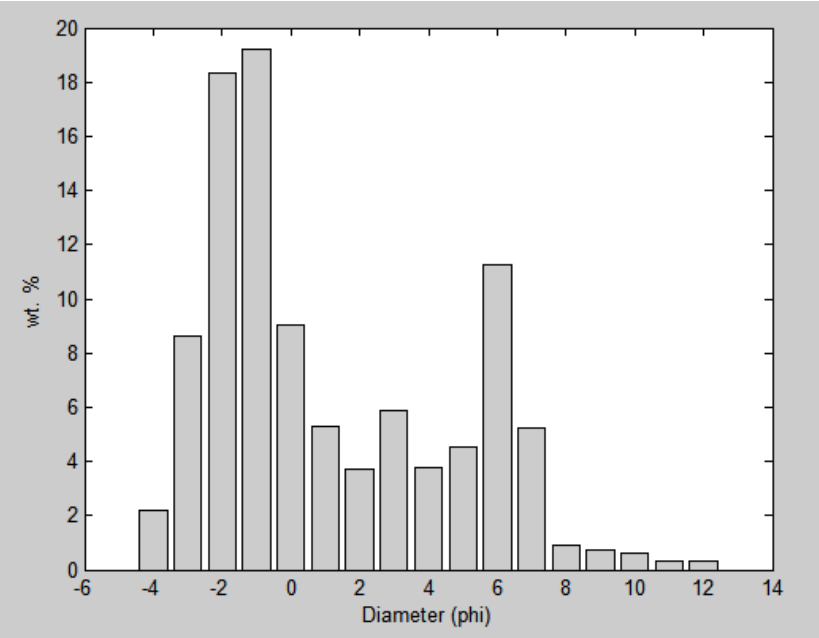

Fig.16 – TGSD obtained by TOTGS code.

phi	diameter (mm)	density (kg/m$^{3)}$	shape	%
-4	16	740	0.85	0.2519
-3	8	770	0.85	0.845
-2	4	790	0.85	1.7822
-1	2	1080	0.85	1.8186
0	1	1320	0.85	1.0201
1	0.5	1630	0.85	0.6274
2	0.25	1780	0.83	0.2777
3	0.125	2100	0.81	0.7515
4	0.625	2460	0.8	3.6259
5	0.4455	2460	0.8	5.9116
6	0.3125	2460	0.8	42.1329
Aggregates (7-12)	0.2	50	1.0	40.9552

Table 4 – TGSD obtained by HAZMAP.

The eruptive source parameters such as emitted volume, dispersal axis direction and column height have been calculated by HAZMAP by solving an inverse problem. The assumptions of the model are a horizontally uniform wind and a deposit formed by the sum of several gaussian distributions for each granulometric class.
The input interval values needed for the model are:

- Height of the tropopause;
- Wind direction;

- Vertical wind velocity profile;
- Vent position;
- Minimum and maximum height of the eruptive column;
- Suzuki's coefficient;
- Plume diffusion in the atmosphere;
- Compositional based deposit density and particle sphericity (the same of Astroni, from Mele et al, 2018);

Besides solving the inverse problem using all the available data, a sensitivity study was also performed in order to understand how the results change as function of data availability.
We considered the case using proximal data only, proximal and distal only, and proximal, medial, and distal. Moreover, by considering that fine ash can settle as aggregate particles using the parametrization by Cornell et al. (1983), we also estimated how results change either accounting for or neglecting ash aggregation.

The results are summarized in the following Table (5):

Used dataset				Intermediate results				
Used sampling point	Ballistic component	Fine ash grain size characterization	Fine ash aggregation	Tephra Volume (km^3 DRE)	Column height (km)	Dispersal direction 0° EST, CCW; (°)	Wind velocity at tropopause (m/s)	Diffusion coefficient (m^2/s)
Proximal only (Ischia)	Excluded	No	No	0.06	20	100	6	5000
Proximal only (Ischia)	Excluded	No	Yes	0.06	20	100	6	5000
Proximal only (Ischia)	Excluded	< 5 phi	Yes	0.05	18	105	5	4000
Proximal+distal (Ischia + CET1)	Excluded	< 5 phi	No	0.06	4	280	9	2000
Proximal+ medial+distal (Ischia + CET1 + Capri)	Excluded	< 5 phi	No	0.056	5	293	9	2000
Proximal+ medial+distal (Ischia + CET1 + Capri)	Excluded	< 5 phi	Yes	0.075	5/13	295	5	2000

Table 5 – Result sensitivity as function of the used sub-dataset.

3.1 Best fit scenarios

In this paragraph are shown in details the two best fit scenarios, both obtained through the integration of data relatives to the subtraction of the contribution on the island of the ballistic component and the characterization of fine ash up to 12 phi useful to the estimation of the aggregational effect at the distal locations. These differ from each other in the completeness of the sampling point dataset. The first presented scenario uses only the proximal data in Ischia, the second one the GSD of each sampling location in Ischia, Capri and the inferred sample of CET1.

For the first scenario the parameters treated in the previous discussed methodology, has rendered these eruptive parameters:
Volume (DRE): 0.05 km^3;
Wind velocity: 5 km/h;
Wind direction: 105° (Toward N-NW);
Column height: 18 km;
Diffusion coefficient: 4000 m^2/s.

The second most complete dataset scenario has rendered these eruptive parameters:
Volume (DRE): 0.075 km^3;
Wind velocity: 5-11 km/h;
Wind direction: 295° (Toward S-SE);
Column height: 5/13 km;
Suzuki's coefficient: 9;
Diffusion coefficient: 2000 m^2/s.

The particles aggregation assumptions variability, made on the basis of Cornel et al. (1983), has an effect on the column height that range between 5 and 13 km. The mass eruption rate (MER) provided by the numerical modelling is 10^5 kg/s, which means, on the basis of the calculated erupted volume, a duration of the eruption from one day to one week, likely few days.

Figure 17 shows the obtained area affected by Cretaio Tephra deposition. The dispersal axis is toward S-SE. The fallout related to the climactic phase of Cretaio Tephra affected, according to previous reports by Buchner, (1986), entirely Ischia and Capri Island and partially the surrounding area of Napoli and Sorrento Peninsula.

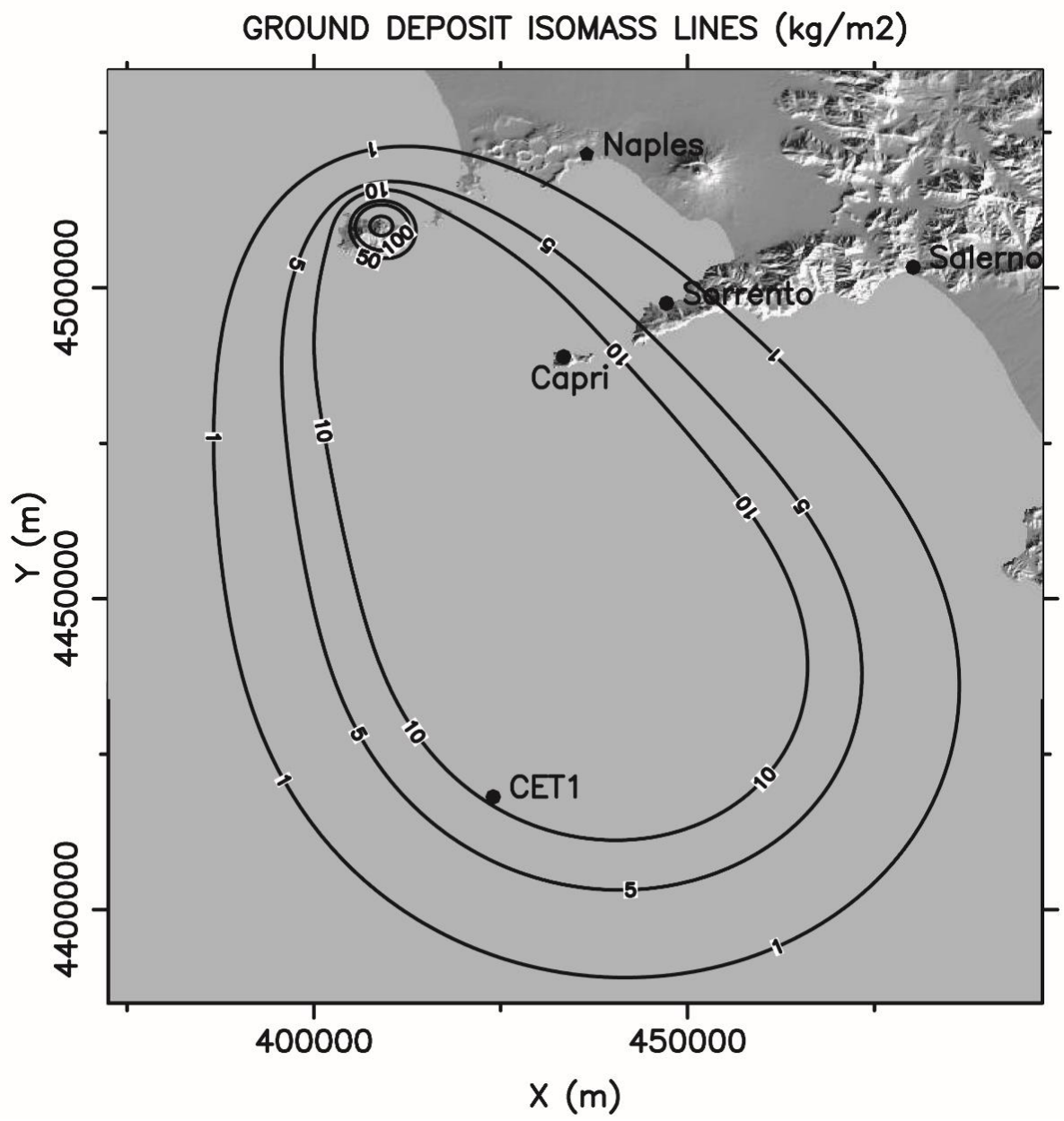

Fig. 17 – Ground deposit isomass lines (kg/m²) and deposit thickness (mm) in the involved area of Cretaio Tephra eruption, obtained using the most complete dataset scenario.

3.2 Hazard maps

The best fit solution which takes into account the complete dataset has been fixed as reference scenario to produce probability maps, obtained by considering tens of thousands of simulations which use a 36 years wind profiles database from NOAA (since 1968 to 2003) corresponding to a location in the Gulf of Salerno (Costa et al., 2009).
Probability maps have been obtained for several tephra loads thresholds, such as 1, 10, 100 and 300 kg/m^2. Results and impact on the different areas are shown in Figure 18.
An eruption like Cretaio Tephra, nowadays could involve the Phlegraean area, having the 5% probability of a deposit of more than 1 cm and causing a serious problem for the road and airport systems. Procida island is within the 5% probability of having a tephra loading of 100 kg/m^2. The whole north-eastern part of Ischia island is within the curve of 5% for the tephra loading of 300 kg/m^2 which represents the threshold for roof collapse.

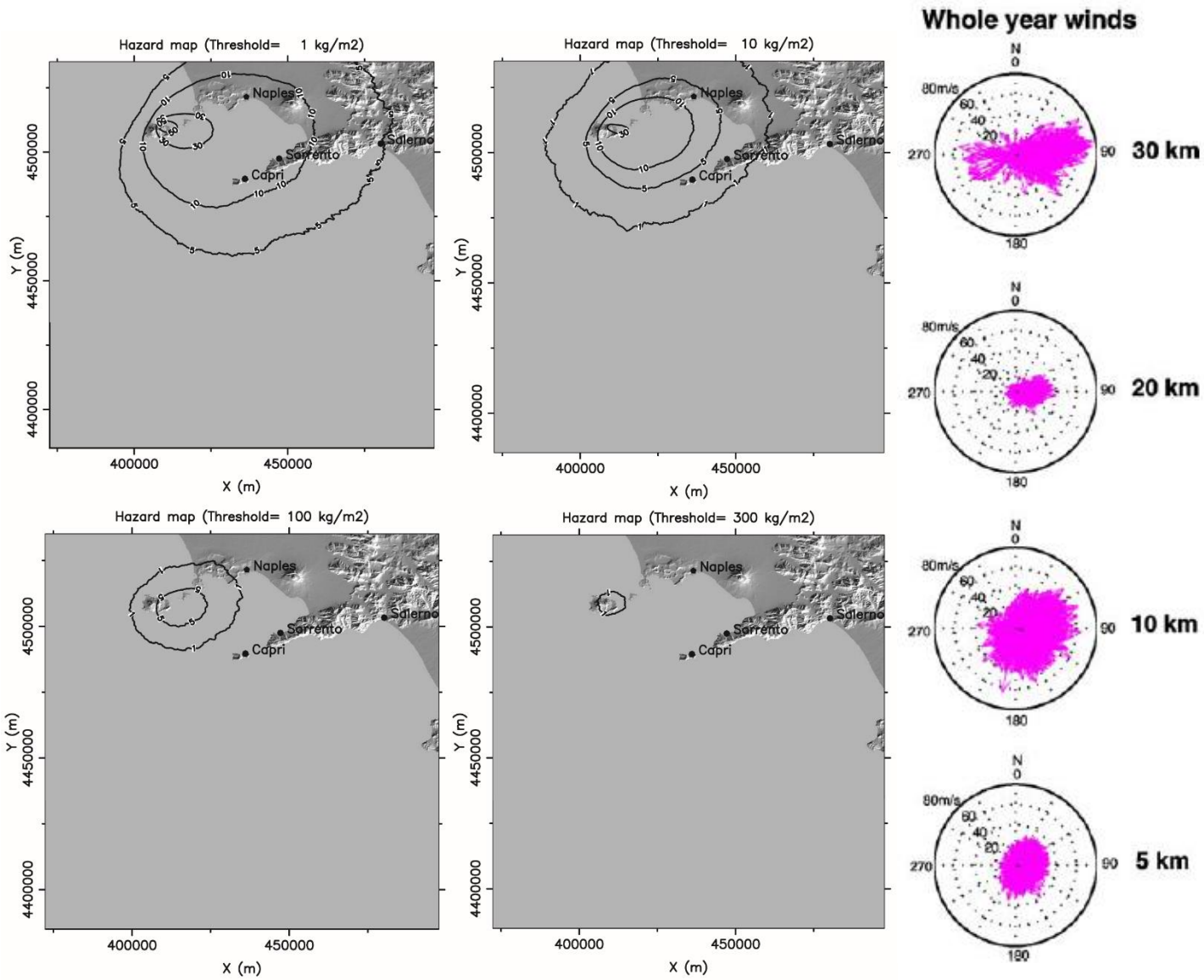

Fig. 18 – Hazard maps based on Cretaio Tephra scenario. On the right: wind distribution diagrams corresponding to the point of the NOOA global mesh nearest to Naples (l40°, 15°) for the 36 years period 1968–2003 (modified from Costa et al., 2009).

3.3 Uncertainties

A quantification of the uncertainties of the physical parameters which describe volcanic explosive eruptions is crucial to both the characterization of explosive volcanism and the assessment of associated hazards (Bonadonna et al., 2015).

Tephra thickness is a data useful for the TGSD analysis. Thickness of the analysed outcrop may be affected by uncertainties related to depositional and post-depositional processes, such as variation in topography, compaction and erosion (Engwell et al., 2013). Thickness measurement uncertainties is a source of volume uncertainty up to 5-10%, but it decreases substantially with the increasing of data points collected (Engwell et al., 2013). TGSD itself may have large uncertainties (Bonadonna and Houghton, 2005; Bonadonna et al., 2015). The determination of the erupted volume could have uncertainties up to 70% depending on the deposit exposure, distribution of the sampling points and eruption magnitude (Bonadonna et al., 2015). In this work the uncertainty about the volume calculation could be quite high because of the poor distal dataset. The lack of a distal dataset can produce an associated uncertainty up to 50% on the fine-ash content determination (Volentik et al., 2010).

4. Discussion

The research about the volcanic plumes and tephra dispersal has developed enormously especially in the last decades. (Morton 1956; Walker, 1973; Newhall and Self, 1982; Sorem et al., 1982; Carey & Sigurdsson, 1982; Cornel et al., 1983; Woods 1988; Pyle, 1989, 1995; Sparks et al., 1992; Rose, 1993; Bonadonna et al., 2002, 2011; Bonadonna and Houghton, 2005; Sulpizio et al 2005; Suzuki et al 2016; Costa et al., 2016). Nevertheless, to reconstruct features of very old eruptions as much as possible field data are needed, however, many of the active volcanoes in the world are islands and reconstruction of impact parameters of explosive plume rely usually on highly incomplete datasets, as most of the dispersal is offshore. Ischia island is one of such active volcanic islands and the expected explosive scenario is similar to the 60 A.D. violent strombolian - sub-Plinian eruption of the Cretaio Tephra (Orsi et al., 1996; de Vita et al., 2010).

In this work we have specifically addressed the reconstruction of the Cretaio tephra fallout dispersal by characterizing the eruption source parameters and showed the importance of medial-distal data to better constrain the dispersal area, the total erupted mass, the column height and the total grain size distribution. All these parameters are important in order to perform models capable to simulate the impact of an eruption similar to Cretaio Tephra and consequently to analyse the related hazard. The so far most complete dataset presented in this paper, it gives an erupted volume of magma of 0.075 km^3, an eruptive column height between 5-13 km (depending on the particles aggregation assumptions) which disperses the products toward S-SE. Such column would correspond to a MER of 10^5 kg/s which would indicate an eruption of some days.
In order to validate the obtained result about the eruption column height, a second independent methodology proposed by Carey & Sparks, (1986) has been applied using the isopleth characterization reported in Table 1. Carey & Sparks, (1986) proposed two methodology: the first one is based on the relationship between the isopleth area and the maximum pumice and lithic; the second one, on a combination of the crosswind range versus maximum downwind range of the lithics isopleths. The result, obtained by using the isopleth maps in Fig. 8, is an eruptive column height between 5 and 10 km. This range values, obtained by the field data is coherent with the obtained result of the numerical modelling.
The application of the independent methodology allows us to estimate the uncertainty of the numerical method and to identify a more plausible range among the values obtained by the numerical modelling.

We show that the main source of improvement in the calculation of the eruptive parameters is given by the adding of just two samples located in the medial-distal areas. These may seem only few, but this work shows they have a great power to change the final result.
Having some (as first scenario in this work) or even a lot (as the simulation based on Orsi et al., 1992) available sampling points but only from the proximal deposition, may not increase the accuracy of the reconstruction.
Actually, we show that our final result shown in Fig. 17 is substantially different from the one obtained with the same method but relying only on outcrops on the island (Orsi et al., 1992) shown in Fig. 3, as well as all the related eruption parameters shown in Table 4.

Eruptive parameters, such as the column height, may change of one order of magnitude, with the addition of two samples located in the medial-distal areas.
Results shown in Table 4, also show that the grain size characterization of the finest particles which we have obtained by optical grain size analysis, have a great importance for the reconstruction of the eruption parameters, in fact they offer strong constraints on the column itself and on the dispersal axis direction.

The plume dispersal axis of the Cretaio Tephra eruption is now estimated toward S-SE. The fallout related to the climactic phase of Cretaio Tephra affected entirely Ischia and Capri Island and partially the surrounding area of Napoli and Sorrento Peninsula. This is a new scenario which has so far not been fully considered by the volcanological community and authorities. Recent tephras of Ischia island has never been founded or considered in the Campanian or in the central mainland area.
From the hazard maps is clear that in case of an eruption like Cretaio Tephra, the Phlegraen area could be involved and the airport system could be affected. Ischia and probably Procida islands will have to be evacuated and central-southern Italy will be affected by the effects of the eruption.

For the first time, this work rises the attention on this new scenario of an explosive eruption which may affect and damage the Phlegrean archipelago and even the Gulf of Naples.

A general consideration grounded on the results presented in this paper, is that for hazard studies, the field time invested on the search of new sampling point in the proximal areas (which for many volcanic islands more or less coincides with the island itself) if these are already conspicuous, will not change or improve significantly the final result. It would be better instead to look for distal points in the offshore, and financing new sea core production or interpreting the existing ones.

5. Conclusions

In this paper the best fit solution of the modelling of the Cretaio Tephra fall deposit has been presented in order to study the volcanic hazard in Ischia island and in the surrounding area associated with the scenario of an explosive eruption of sub-Plinian intensity.
Cretaio Tephra, although is a relatively small eruption, is the largest in magnitude eruption occurred at Ischia in the last 3 kyrs, which is considered the reference period for hazard studies (Selva et al., 2019). Nowadays, an eruption like the Cretaio Tephra could have an enormous impact in the island and in the mainland, not only in the short term in terms of casualties and damage to buildings and to woodland heritage but also in the socio-economic terms and managerial energies. This characterization of Cretaio Tephra represents a likely scenario of the greatest explosive eruption that can be used to project an evacuation plan, which may probably regard all the island. This new scenario has not been fully considered by the volcanological community and authorities, because recent tephras of Ischia island has never been founded or considered in the Campanian or in the central mainland area.

Volcano risk management procedures need to involve an economically and socially realistic assessment of risk (Woo, 2008). The explosive eruption hazard assessment must be necessarily completed with the information about the risk in the island. The presence at the moment of the eruption of residents and tourists in Ischia it should be reduced as much as possible. A study on the location of the harbours, present and serviceable in the larger municipalities throughout the coast, and their capacity is fundamental.

Appendix A

Informations about EUC outcrop positions and thickness have been reported:

Sample	UTM (33 T Zone)		Latitude	Longitude	EUC thickness (m)
PP06	409072.59 m E	4509849.74 m N	40°44'4.44"N	13°55'23.36"E	1.00
PP41	409520.86 m E	4507539.35 m N	40°42'49.70"N	13°55'43.67"E	0.40
PP25	409524.22 m E	4509533.19 m N	40°43'54.35"N	13°55'42.78"E	3.00
PP49	409231.81 m E	4509289.11 m N	40°43'46.32"N	13°55'30.44"E	0.79
PP39	410372.61 m E	4508205.38 m N	40°43'11.63"N	13°56'19.62"E	0.50
PP09	409220.66 m E	4508608.61 m N	40°43'24.25"N	13°55'30.32"E	0.45
PP56	408402.22 m E	4508490.55 m N	40°43'20.10" N	13°54'55.50" E	0.90
Capri	436062.00 m E	4489650.00 m N	40°33'18.53"N	14°14'41.32"E	0.15
	UTM (Zona 33 S)				
CET1	424000.01 m E	4418146.00 m N	39°54'35.98"N	14° 6'38.96"E	0.01

Appendix B

Methodologies:

Grain size distributions, have been obtained for each of the samples by sieving and Mastersizer 2000 (Model APA2000). Several sieves with 16 mm, 8 mm, 5 mm, 2 mm, 1 mm, 425 µm, 250 µm, 125 µm and 75 µm meshes have been used. Vibrating screen has been setted to 4 in the scale of vibration that goes from 1 to 10, in order to not damage breakable pumices, for 10 minutes in dry conditions. The content of the last mesh has been analysed with an optical grain-meter Mastersizer 2000 to reconstruct the finest particle from 5 phi to 12 phi. The result of the Mastersizer analysis is a mean value diagram particle size (µm) vs volume (%) of 30 measurement cycles for each sample, and converting the percentage volume to weight is possible to merge the two information in a unique GSD diagram.

To obtain the clast densities, useful for HAZMAP model, more than 400 pumices and lithics within the granulometric classes of 32-16mm, 16-8mm and 8-5mm have been analysed by the method proposed by Houghton & Wilson, (1989). This method based on the Archimedes' principle, consists of weighing the selected clasts in air, in water and again in water after having coated them with a film of cellulose acetate which makes them impermeable, in order to isolate the connected porosity. The cellulose acetate density is known (1.3 g/cm^3) and comparing the different weights is possible to obtain the density of each clast. This method has an accuracy within 30 kg m^{-3} (Gurioli et al., 2015).

References

Acocella, V. and R. Funiciello (1999). The interaction between regional and local tectonics during resurgent doming: the case of the island of Ischia, Italy. Journal of Volcanology and Geothermal Research 88(1): 109-123.

Alberico, I., Petrosino, P., & Lirer, L. (2011). Volcanic hazard and risk assessment in a multi-source volcanic area: the example of Napoli city (Southern Italy). *Natural Hazards and Earth System Sciences*, *11*(4), 1057-1070.

Barberi, F., Macedonio, G., Pareschi, M. T., & Santacroce, R. (1990). Mapping the tephra fallout risk: an example from Vesuvius, Italy. *Nature*, *344*(6262), 142.

Biass, S., Bonadonna, C., 2014, TOTGS: Total grainsize distribution of tephra fallout.

Bonadonna, C., Macedonio, G., & Sparks, R. S. J. (2002). Numerical modelling of tephra fallout associated with dome collapses and Vulcanian explosions: application to hazard assessment on Montserrat. *Geological Society, London, Memoirs*, *21*(1), 517-537.

Bonadonna, C., Mayberry, G. C., Calder, E. S., Sparks, R. S. J., Choux, C., Jackson, P., ... & Ryan, G. (2002). Tephra fallout in the eruption of Soufrière Hills Volcano, Montserrat. *Geological Society, London, Memoirs*, *21*(1), 483-516.

Bonadonna, C., & Houghton, B. F. (2005). Total grain-size distribution and volume of tephra-fall deposits. *Bulletin of Volcanology*, *67*(5), 441-456.

Bonadonna, C., Genco, R., Gouhier, M., Pistolesi, M., Cioni, R., Alfano, F., ... & Ripepe, M. (2011). Tephra sedimentation during the 2010 Eyjafjallajökull eruption (Iceland) from deposit, radar, and satellite observations. *Journal of Geophysical Research: Solid Earth*, *116*(B12).

Bonadonna, C., Biass, S., & Costa, A. (2015). Physical characterization of explosive volcanic eruptions based on tephra deposits: propagation of uncertainties and sensitivity analysis. *Journal of Volcanology and Geothermal Research*, *296*, 80-100.

Bonasia, R., Macedonio, G., Costa, A., Mele, D., & Sulpizio, R. (2010). Numerical inversion and analysis of tephra fallout deposits from the 472 AD sub-Plinian eruption at Vesuvius (Italy) through a new best-fit procedure. *Journal of Volcanology and Geothermal Research*, *189*(3-4), 238-246.

Brown, R. J., G. Orsi, et al. (2008). "New insights into Late Pleistocene explosive volcanic activity and caldera formation on Ischia (southern Italy)." Bulletin of Volcanology 70(5): 583-603.

Brown, R., L. Civetta, et al. (2014). "Geochemical and isotopic insights into the assembly, evolution and disruption of a magmatic plumbing system before and after a cataclysmic caldera-collapse eruption at Ischia volcano (Italy)." Contributions to Mineralogy and Petrology 168(3): 1035.

Buchner, G. (1986). Eruzioni vulcaniche e fenomeni vulcanotettonici di età preistorica e storica nell'isola d'Ischia. *Tremblements de terre, eruptions volcaniques et vie des hommes dans la Campanie antique*, *7*, 145-188.

Capaldi, G., Civetta, L., & Gasparini, P. (1976). Volcanic history of the island of Ischia (South Italy). Bulletin Volcanologique, 40(1), 11-22.

Carey, S. N., & Sigurdsson, H. (1982). Influence of particle aggregation on deposition of distal tephra from the May 18, 1980, eruption of Mount St. Helens volcano. *Journal of Geophysical Research: Solid Earth*, *87*(B8), 7061-7072.

Carey, S., & Sparks, R. S. J. (1986). Quantitative models of the fallout and dispersal of tephra from volcanic eruption columns. *Bulletin of volcanology*, *48*(2-3), 109-125.

Casalini, M., R. Avanzinelli, et al. (2017). "Geochemical and radiogenic isotope probes of Ischia volcano, Southern Italy: Constraints on magma chamber dynamics and residence time." American Mineralogist 102(2): 262-274.

Chiesa, S., Poli, S., & Vezzoli, L. (1986). Studio dell'ultima eruzione storica dell'isola di Ischia. Bollettino GNV, 1, 153-166.

Cioni, R., Longo, A., Macedonio, G., Santacroce, R., Sbrana, A., Sulpizio, R., & Andronico, D. (2003). Assessing pyroclastic fall hazard through field data and numerical simulations: example from Vesuvius. *Journal of Geophysical Research: Solid Earth*, *108*(B2).

Civetta, L., G. Gallo, et al. (1991). "Sr-and Nd-isotope and trace-element constraints on the chemical evolution of the magmatic system of Ischia (Italy) in the last 55 ka." Journal of Volcanology and Geothermal Research 46(3-4): 213-230.

Costa, A., Dell'Erba, F., Di Vito, M. A., Isaia, R., Macedonio, G., Orsi, G., & Pfeiffer, T. (2009). Tephra fallout hazard assessment at the Campi Flegrei caldera (Italy). *Bulletin of Volcanology*, *71*(3), 259.

Costa, A., Suzuki, Y. J., Cerminara, M., Devenish, B. J., Ongaro, T. E., Herzog, M., ... & Engwell, S. (2016). Results of the eruptive column model inter-comparison study. *Journal of Volcanology and Geothermal Research*, *326*, 2-25.

Cornell, W., Carey, S., & Sigurdsson, H. (1983). Computer simulation of transport and deposition of the Campanian Y-5 ash. *Journal of Volcanology and Geothermal Research*, *17*(1-4), 89-109.

Della Seta, M., E. Marotta, et al. (2012). "Slope instability induced by volcano-tectonics as an additional source of hazard in active volcanic areas: the case of Ischia island (Italy)." Bulletin of Volcanology 74(1): 79-106.

Della Seta, M., Marmoni, G. M., Martino, S., Paciello, A., Perinelli, C., & Sottili, G. (2015). Geological constraints for a conceptual evolutionary model of the slope deformations affecting Mt. Nuovo at Ischia (Italy). *Italian Journal of Engineering Geology and Environment*, *15*(2), 15-28.

de Vita, S., Sansivero, F., Orsi, G., & Marotta, E. (2006). Cyclical slope instability and volcanism related to volcano-tectonism in resurgent calderas: the Ischia island (Italy) case study. *Engineering Geology*, *86*(2-3), 148-165.

de Vita, S., Sansivero, F., Orsi, G., Marotta, E., & Piochi, M. (2010). Volcanological and structural evolution of the Ischia resurgent caldera (Italy) over the past 10 ky. *Geol. Soc. Am. Spec. Pap*, *464*, 193-239.

Dominey-Howes, D., & Minos-Minopoulos, D. (2004). Perceptions of hazard and risk on Santorini. *Journal of Volcanology and Geothermal Research*, *137*(4), 285-310.

Druitt, T.H., Edwards, L., Mellors, R.M., Pyle, D.M., Sparks, R.S.J., Lanphere, M., Davies, M., Barreiro, B., (1999). Santorini Volcano. Geological Society, London, Memoirs, vol. 19, 165 pp.

Engwell, S. L., Sparks, R. S. J., & Aspinall, W. P. (2013). Quantifying uncertainties in the measurement of tephra fall thickness. *Journal of Applied Volcanology*, *2*(1), 5.

Erfurt-Cooper, P. (2011). Geotourism in volcanic and geothermal environments: playing with fire? *Geoheritage*, *3*(3), 187-193.

Giacomelli, L., Perrotta, A., Scandone, R., & Scarpati, C. (2003). The eruption of Vesuvius of 79 AD and its impact on human environment in Pompeii. *Episodes-Newsmagazine of the International Union of Geological Sciences*, *26*(3), 235-238.

Guffanti, M., Mayberry, G. C., Casadevall, T. J., & Wunderman, R. (2009). Volcanic hazards to airports. *Natural hazards*, *51*(2), 287-302.

Gurioli, L., D. Andronico, et al. (2015). "MeMoVolc consensual document: a review of cross-disciplinary approaches to characterizing small explosive magmatic eruptions." Bulletin of Volcanology 77(6): 49.

Hansell, A. L., Horwell, C. J., & Oppenheimer, C. (2006). The health hazards of volcanoes and geothermal areas. *Occupational and environmental medicine*, *63*(2), 149-156.

Houghton, B. F., & Wilson, C. J. N. (1989). A vesicularity index for pyroclastic deposits. *Bulletin of volcanology*, *51*(6), 451-462.

INGV-DPC-V3. Ricerche sui vulcani attivi, precursori, scenari, pericolosità e rischio, UR Orsi (Campi Flegrei and Ischia). Roma: Internal Report, INGV; 2005-2007.

Le Bas MJ, Lemaitre RW, Streckeisen A, Zanettin B (1986) A chemical classification of volcanic rocks based on the total alkali-silica diagram. J Petrol 27:745-750.

Macedonio G., Costa A., Longo A. (2005) A computer model for volcanic ash fallout and assessment of subsequent hazard, Comput. Geosci., 31 (7), 837-845.

Macedonio, G., Costa, A., & Folch, A. (2008). Ash fallout scenarios at Vesuvius: numerical simulations and implications for hazard assessment. *Journal of Volcanology and Geothermal Research*, *178*(3), 366-377.

Macedonio, G., Costa, A., Scollo, S., & Neri, A. (2016). Effects of eruption source parameter variation and meteorological dataset on tephra fallout hazard assessment: example from Vesuvius (Italy). *Journal of Applied Volcanology*, *5*(1), 5.

Marianelli, P., Metrich, N., Santacroce, R., & Sbrana, A. (1995). Mafic magma batches at Vesuvius: a glass inclusion approach to the modalities of feeding stratovolcanoes. *Contributions to Mineralogy and Petrology*, *120*(2), 159-169.

Marti, J., Spence, R., Calogero, E., Ordoñez, A., Felpeto, A., & Baxter, P. (2008). Estimating building exposure and impact to volcanic hazards in Icod de los Vinos, Tenerife (Canary Islands). *Journal of Volcanology and Geothermal Research*, *178*(3), 553-561.

Marti, J., Sobradelo, R., & Felpeto, A. (2010, May). Hazard assessment at Teide-Pico Viejo volcanic complex (Tenerife, Canary Islands). In *EGU General Assembly Conference Abstracts* (Vol. 12, p. 5774).

Mele, D., & Dioguardi, F. (2018). The grain size dependency of vesicular particle shapes strongly affects the drag of particles. First results from microtomography investigations of Campi Flegrei fallout deposits. *Journal of Volcanology and Geothermal Research*, *353*, 18-24.

Molin, P., Acocella, V., & Funiciello, R. (2003). Structural, seismic and hydrothermal features at the border of an active intermittent resurgent block: Ischia Island (Italy). *Journal of Volcanology and Geothermal Research*, *121*(1-2), 65-81.

Morabito, S., P. Petrosino, et al. (2014). A multidisciplinary approach for reconstructing the stratigraphic framework of the last 40 ka in a bathyal area of the eastern Tyrrhenian Sea. Global and Planetary Change 123: 121-138.

Morton, B. R., Taylor, G. I., & Turner, J. S. (1956). Turbulent gravitational convection from maintained and instantaneous sources. *Proceedings of the Royal Society of London. Series A. Mathematical and Physical Sciences*, *234*(1196), 1-23.

Murrow PJ, Rose WI, Self S (1980) Determination of the total grain size distribution in a Vulcanian eruption column, and its implications to stratospheric aerosol perturbation. Geophys Res Lett 7:893–896

Nave, R., Isaia, R., Vilardo, G., & Barclay, J. (2010). Re-assessing volcanic hazard maps for improving volcanic risk communication: application to Stromboli Island, Italy. *Journal of Maps*, *6*(1), 260-269.

Newhall, C. G., & Self, S. (1982). The volcanic explosivity index (VEI) an estimate of explosive magnitude for historical volcanism. *Journal of Geophysical Research: Oceans*, *87*(C2), 1231-1238.

Orsi, G., Gallo, G., & Zanchi, A. (1991). Simple-shearing block resurgence in caldera depressions. A model from Pantelleria and Ischia. *Journal of Volcanology and Geothermal Research*, *47*(1-2), 1-11.

Orsi, G., G. Gallo, et al. (1992). A comprehensive study of pumice formation and dispersal: the Cretaio Tephra of Ischia (Italy). Journal of Volcanology and Geothermal Research 53(1-4): 329-354.

Orsi, G., Piochi, M., Campajola, L., D'Onofrio, A., Gialanella, L., & Terrasi, F. (1996). ^{14}C geochronological constraints for the volcanic history of the island of Ischia (Italy) over the last 5000 years. *Journal of Volcanology and Geothermal Research*, *71*(2-4), 249-257.

Orsi, G., de Vita, S., Di Vito, M., Isaia, R., Nave, R., & Heiken, G. (2003). Facing volcanic and related hazards in the Neapolitan area. *Earth Sciences in Cities*, *56*, 121-170.

Parfitt EA (1998) A study of clast size distribution, ash deposition and fragmentation in a Hawaiian-style volcanic eruption. J Volcanol Geotherm Res 84:197–208

Paton, D., Smith, L., Daly, M., & Johnston, D. (2008). Risk perception and volcanic hazard mitigation: Individual and social perspectives. *Journal of Volcanology and Geothermal Research*, *172*(3-4), 179-188.

Perry, R. W., & Lindell, M. K. (2008). Volcanic risk perception and adjustment in a multi-hazard environment. *Journal of Volcanology and Geothermal Research*, *172*(3-4), 170-178.

Petrini, R., Forte, C., Orsi, G., & Piochi, M. (2001). Influence of magma dynamics on melt structure: spectroscopic studies on volcanic glasses from the Cretaio Tephra of Ischia (Italy). *Contributions to Mineralogy and Petrology*, *140*(5), 532.

Pfeiffer T., Costa A., Macedonio G. (2005). A model for the numerical simulation of tephra fall deposits, J. Volcanol. Geotherm. Res., 140, 273.

Pyle, D. M. (1989). The thickness, volume and grainsize of tephra fall deposits. Bulletin of Volcanology, 51(1), 1-15.

Pyle, D.M., 1995, Assessment of the minimum volume of tephra fall deposits: Journal of Volcanology and Geothermal Research, v. 69, p. 379– 382.

Poli, S., S. Chiesa, et al. (1989). "Time dimension in the geochemical approach and hazard estimates of a volcanic area: The isle of Ischia case (Italy)." Journal of Volcanology and Geothermal Research 36(4): 327-335.

Rittmann, A., & Gottini, V. (1980). *L'isola d'Ischia: Geologia*.

Rose, W.I., 1993, Comment on another look at the calculation of fallout tephra volumes' by Judy Fierstein and Manuel Nathenson: Bulletin of Volcanology, v. 55, p. 372–374.

Rosi, M., Pistolesi, M., Bertagnini, A., Landi, P., Pompilio, M., & Di Roberto, A. (2013). Stromboli volcano, Aeolian Islands (Italy): present eruptive activity and hazards. *Geological Society, London, Memoirs*, *37*(1), 473-490.

Sandri, L., Jolly, G., Lindsay, J., Howe, T., & Marzocchi, W. (2012). Combining long-and short-term probabilistic volcanic hazard assessment with cost-benefit analysis to support decision making in a volcanic crisis from the Auckland Volcanic Field, New Zealand. *Bulletin of volcanology*, *74*(3), 705-723.

Sbrana, A., R. Toccaceli, et al. (2011). "Carta Geologica della Regione Campania, Note Illustrative della Carta Geologica alla scala 1: 10.000, Foglio 464 Isola di Ischia, Regione Campania-Assessorato Difesa del Suolo."

Sbrana, A., P. Marianelli, et al. (2018). "Volcanology of Ischia (Italy)." Journal of Maps 14(2): 494-503.

Selva, J. et al., (2019) Multiple natural hazards at volcanic islands: a review for the Ischia volcano (Italy). Journal of Applied Volcanology.

Sorem, R. K. (1982). Volcanic ash clusters: tephra rafts and scavengers. *Journal of Volcanology and Geothermal Research*, *13*(1-2), 63-71.

Sparks RSJ, Wilson L, Sigurdsson H (1981) The pyroclastic deposits of the 1875 eruption of Askja, Iceland. Phil Trans R Soc Lond 229:241–273.

Sulpizio, R. (2005). Three empirical methods for the calculation of distal volume of tephra-fall deposits. Journal of volcanology and geothermal research, 145(3-4), 315-336.

Taddeucci, J., Scarlato, P., Montanaro, C., Cimarelli, C., Del Bello, E., Freda, C., ... & Dingwell, D. B. (2011). Aggregation-dominated ash settling from the Eyjafjallajökull volcanic cloud illuminated by field and laboratory high-speed imaging. *Geology*, *39*(9), 891-894.

Thomas, R. M. E., & Sparks, R. S. J. (1992). Cooling of tephra during fallout from eruption columns. *Bulletin of Volcanology*, *54*(7), 542-553.

Tibaldi, A. and L. Vezzoli (2004). "A new type of volcano flank failure: the resurgent caldera sector collapse, Ischia, Italy." Geophysical Research Letters 31(14).

Tilling, R. I. (1989). Volcanic hazards and their mitigation: progress and problems. *Reviews of Geophysics*, *27*(2), 237-269.

Vezzoli, L., & Barberi, F. (1988). Progetto finalizzato geodinamica: monografie finali. X: Island of Ischia. *Quaderni de La ricerca scientifica*, (114).

Volentik, A. C., Bonadonna, C., Connor, C. B., Connor, L. J., & Rosi, M. (2010). Modeling tephra dispersal in absence of wind: Insights from the climactic phase of the 2450 BP Plinian eruption of Pululagua volcano (Ecuador). *Journal of Volcanology and Geothermal Research*, *193*(1-2), 117-136.

Walker, G. P. L., & Croasdale, R. (1971). Two Plinian-type eruptions in the Azores. *Journal of the Geological Society*, *127*(1), 17-55.

Walker, G. P. (1973). Explosive volcanic eruptions—a new classification scheme. *Geo*logische Rundschau, 62(2), 431-446.

Walker GPL (1980) The Taupo Pumice: product of the most powerful known (Ultraplinian) eruption? J Volcanol Geotherm Res 8:69–94.

Wallenstein, N., Duncan, A., Chester, D., & Marques, R. (2007). Fogo volcano (Sao Miguel, Azores): a hazardous edifice. *Géomorphologie: relief, processus, environnement*, *13*(3), 259-270.

Woo, G. (2008). Probabilistic criteria for volcano evacuation decisions. Natural Hazards, 45(1), 87-97.

Woo, G. (2015). Cost–benefit analysis in volcanic risk. In *Volcanic Hazards, Risks and Disasters* (pp. 289-300). Elsevier.

Woods, A.W., 1988. The fluid dynamics and thermodynamics of eruption columns. Bull. Volcanol. 50 (3), 169–193.

Chapter 3: Rheological behavior of Ischia Island lava flows (Campania, Italy)

Paolo Primerano[1], Guido Giordano[1], Alessandro Vona[1], Sandro de Vita[2]

[1]Dipartimento di Scienze, Università degli Studi Roma Tre, L.go San Leonardo Murialdo 1, 00146 Roma, Italy.
[2]Istituto Nazionale di Geofisica e Vulcanologia - Osservatorio Vesuviano, Via Diocleziano 328, 80124 Napoli, Italy.

Abstract

Starting from the characterization of the last period of volcanic history of Ischia island, two end-member lava flows, in terms of compositional and morphological features, have been selected in order to propose a process useful to reconstruct the syneruptive rheology of the lavas that can be applicable to estimate impact parameters on which to base a potential effusive scenario. A textural analysis and a rheological study of natural and partially-crystallized magma from Arso Lavas (1302 A.D) and Zaro Lava domes and flows (6 ± 2.2 kyrs) have been performed. The present work aims at investigating the role of the high crystal cargo (up to 75% for Arso and 87% for Zaro) in the rheological behaviour of these lava flows. Three Gaussian-shaped peaks observed in both CSDs can be interpreted as the magma chamber crystallization phase with rise of magma to surface in at least one stage. The syn-emplacement temperature and crystallinity conditions have been established by removing only the microcrystal population in a temperature-controlled furnace. The rheological flow properties are determined by a series of high-temperature deformation experiments in a uniaxial press. The experimental results have been validated and compared with the numerical ones, to describe the uncertainties of each model.

One of the important targets for this work is to investigate the relationship between the velocity of the lava flows and the ground slope. All the data necessary to apply the Jeffreys equation, relative to the environment and to the area of emplacement, like position, geometry and slope of the channel, have been evaluated by a GIS analysis.

The eruption duration of Arso Lavas is known because it is the last eruption at Ischia, occurred in 1302 A.D. This information makes it possible to constrain the methodological process that can be extended to estimate the impact parameters of other similar lava flows.

Introduction

Ischia is a volcanic island located in the western part of the Gulf of Naples and it belongs to the Phlegraean volcanic district. Ischia island counts a large number of eruptions in historical times and the last event was in 1302 A.D. (Capaldi et al., 1976; Chiesa et al., 1986; Vezzoli 1988). It is a very densely inhabited active volcano, hosting a permanent population of about 65'000 people which increases considerably during summer; nonetheless, the risk associated with lava flows in case of renewal of activity is relatively understudied and scientific literature about the quantification of the hazard is poor (Selva et al., 2019).
In the last years there has been a great development in lava flow-related modelling. Lava flows (Griffiths et al., 1993; Latutrie et al., 2017; Vona et al., 2017) and lava domes (Williams, 1932; Sparks et al., 1988; Fink et al., 1990; Nakada et al., 1995; Nakada & Motomura, 1999; Watts et al., 2002) have been described through numerical and analogue models and rheological properties have been calculated taking into account both chemical properties and components content (Moore 1987; Whittington et al., 2001; Giordano et al., 2004; Caricchi et al., 2007; Giordano et al., 2008; Cimarelli et al., 2011; Vona et al., 2013; Castruccio et al., 2014; Gualda & Ghiorso, 2015; Vona et al., 2017; Klein et al., 2018) in order to describe the rheological behaviour of the lava also in the structure of the magmatic systems (Andronico et al., 2005; Landi et al., 2006; Morgavi et al., 2016; Cashman et al., 2017).

We present a reconstruction of the syneruptive rheology of the lava of Arso Lavas (1302 A.D, Chiesa et al., 1986) and Zaro Lava domes and flows (6 ± 2.2 kyrs, Vezzoli, 1988). These two effusive eruptions have been chosen because in the selected reference period for Ischia island, that is the last 10 kyrs, represent the compositional and morphological end members of the most recent activity of Ischia. Zaro Lava domes and flows (de Vita et al., 2010) are made of highly porphyric trachytic lava with a high aspect ratio; by contrast Arso Lava flow has a relatively lower degree of porphyricity and aspect ratio.
The present work aims at investigating the role of the crystal cargo in the rheological behaviour of these alkali-trachytic lava flows.
Arso Lavas is the last eruption in Ischia, which occurred in 1302 A.D., so the information about the duration of the eruption is known from the historical chronicles (Chiesa et al., 1986). This information makes it possible to reconstruct the syneruptive rheology of the lava that can be applicable to estimate the impact parameters.

1. Geological background

Volcanism, tectonism, sedimentation and erosion characterized the geological history of Ischia island (Capaldi 1976; Rittmann & Gottini, 1980; Buchner 1986; Vezzoli 1988; Orsi et al. 1991, 1996; Acocella & Funiciello, 1999; Molin et al., 2003; Tibaldi & Vezzoli, 2004; de Vita et al. 2006, 2010; Brown et al. 2008, 2014; Della Seta et al. 2012, 2015; Sbrana et al. 2011, 2018). Ischia is composed of volcanic rocks and epiclastic sediments, which reflect constructive and destructive phases (Vezzoli 1988; Orsi et al. 1991, 2003; de Vita et al. 2006; Della Seta et al. 2012).

The oldest outcrops are around at 150 kyrs BP, and the most recent eruption occurred in 1302 A.D. (Chiesa et al., 1986; Vezzoli 1988; Civetta et al., 1991). The period since at least 150 kyrs to present, has been divided in five phases of activity (Poli 1989; Civetta et al., 1991; Casalini et al., 2017).

The begin of the last period of activity in the island has been identified at about 10 kyrs (Selva et al., 2019 and reference therein). The volcanic system is still active with the last historic lava flow eruption recorded at Arso in 1302 A.D. (Chiesa et al., 1986). This period is characterized by an ongoing Mt. Epomeo caldera resurgence and by a mainly latitic to trachytic monogenetic volcanic activity (Orsi et al. 1991, 1996; de Vita et al. 2006, 2010). The resurgence almost restricted eruptions to the eastern sector of the island, along regional and volcano-tectonic fault systems with only a few vents located outside this sector. The volcanic activity was characterized by lava domes and high aspect ratio lava flows, and magmatic and phreatomagmatic explosive eruptions that generated variably dispersed pyroclastic fall and PDC deposits (de Vita et al. 2010).

The last 10 kyrs of volcanic activity can be differentiated with respect to the previous period for a series of specific characteristics (Selva et al., 2019), which consist in a clear acceleration in the recorded eruptive activity with respect to the previous period of quiescence or very reduced volcanic activity. In this last phase the magma chemistry shows a change with respect to the preceding periods, especially in the isotopic signatures (Civetta et al., 1991; Casalini et al., 2017) and in the concentration of most of the eruptive vents within the morphological depression to the east of Monte Epomeo. Only a few eruptions occurred to the west, at Zaro and at Punta Chiarito promontory and to the north, along a volcano-tectonic fault-system (Fig.1). This because the occurrence of the resurgence may have caused the absence of volcanic activity in the Monte Epomeo area (Acocella & Funiciello, 1999).

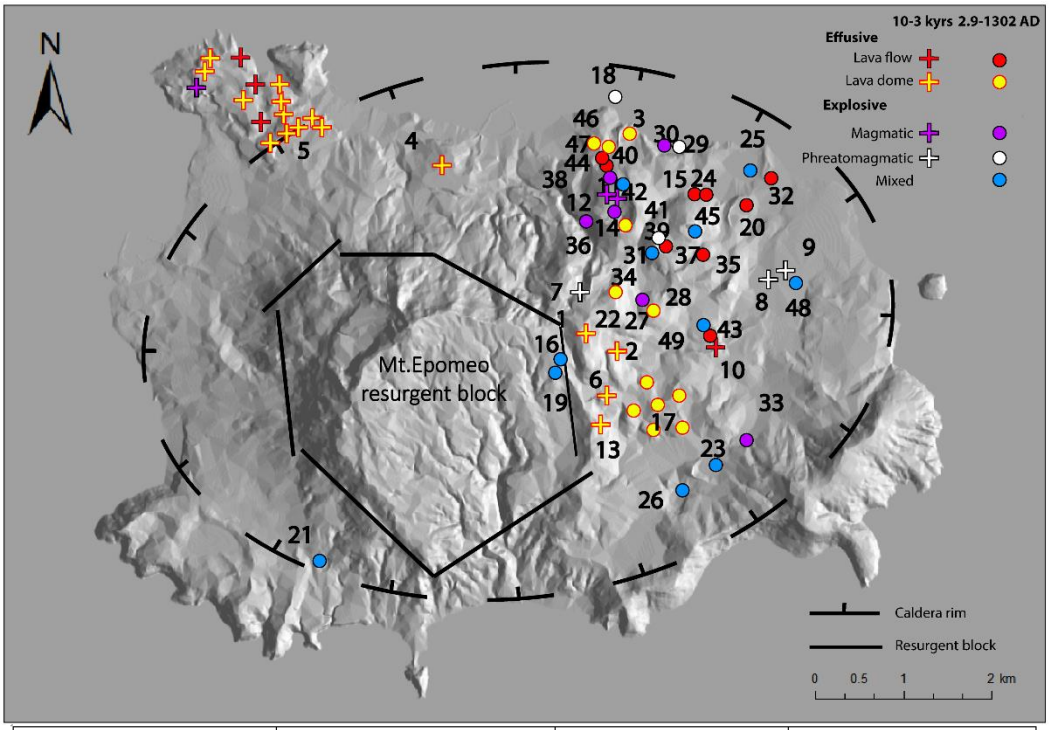

1	Trippodi Lavas	14	Cava del Puzzillo III Tephra	27	Cava Bianca Tephra	40	Villammare Tephra
2	Selva del Napolitano Lavas	15	Sant'Alessandro Lavas	28	Posta Lubrano Lavas	41	Fondo d'Oglio Tephra
3	Castiglione and Bagnetielli Lavas	16	Cannavale Tephra	29	Cafieri Tephra	42	Bosco della Maddalena Tephra
4	Fundera Lavas	17	Cantariello Lavas	30	Cafieri Lavas	43	Fiaiano Tephra
5	Zaro Lava domes and flows	18	Punta La Scrofa Tephra	31	Posta Lubrano Tephra	44	Rotaro Lavas
6	Cannavale Lavas	19	Marecoppo Tephra	32	San Pietro Lavas	45	Montagnone-Maschiata Lavas
7	Maisto Tephra	20	San Ciro Lavas	33	Cava Nocelle Tephra	46	Punta La Scrofa Lavas
8	Catavola Tephra	21	Punta Chiarito Tephra	34	Cretaio Tephra	47	Pietra Vono Lavas
9	Piano Liguori Tephra	22	Mt. Toppo Lavas	35	Arcamone-Sacchetta Lavas	48	Fondo Bosso Tephra
10	Rio Corbore Lavas	23	Molara Tephra	36	Cava Buceto Tephra	49	Arso Lavas and Tephra
11	Cava del Puzzillo I Tephra	24	Montagnone I and La Quercia Lavas	37	Bosco dei Conti Tephra		
12	Cava del Puzzillo II Tephra	25	Ischia Porto Tephra	38	Mt. Tabor Lavas		
13	Costa Sparaina Lavas	26	Vateliero Tephra	39	Bosco della Maddalena Lavas		

Fig.1 – DEM of ischia island. With different colour, the volcanic vents with their typology of activity have been reported. Plus and dots indicate different times of activity (modified from Selva et al., 2019).

1.1 Zaro Lava domes and flows eruption

Zaro Lava Domes and Flows (6 ± 2.2 kyrs, Vezzoli, 1988) are located in the north-western portion of the island (Fig. 2). The activity of this eruption is characterized by an initial explosive phase named La Sciavica Member, described by Sbrana & Toccaceli, (2011). The lava flow analysed in this work is the Punta Caruso Member (Sbrana & Toccaceli, 2011). The volcanic activity produced a series of exogenous lava domes and a lava flows interpreted as unique by Vezzoli, (1988) and Sbrana & Toccaceli, (2011) and as a superimposition of at least 3 lava flow events (Fig. 2) emplaced in a short time span by de Vita et al., (2010).

Lava flows are about 1500 m in length and 800-1000 m wide (Vezzoli, 1988). The very viscous extrusions, occurred along the flanks of pre-existing hills, producing lava flows with low mobility and high aspect ratio (de Vita et al., 2010; Vezzoli et al., 2009).

Zaro lava has a high porphyricity, characterized by a high crystal cargo of feldspar which often appears as a very dense cluster of sanidine phenocrysts (Vezzoli, 1988; Vezzoli et al., 2009; de Vita et al., 2010).

The resulting morphologies deriving from the superimposition of different lava and dome units (de Vita et al., 2010) have been interpreted as due to a series of regional and local faults by Vezzoli, (1988) or alternatively as an articulated morphology of a single lava flow by Sbrana & Toccaceli, (2011).

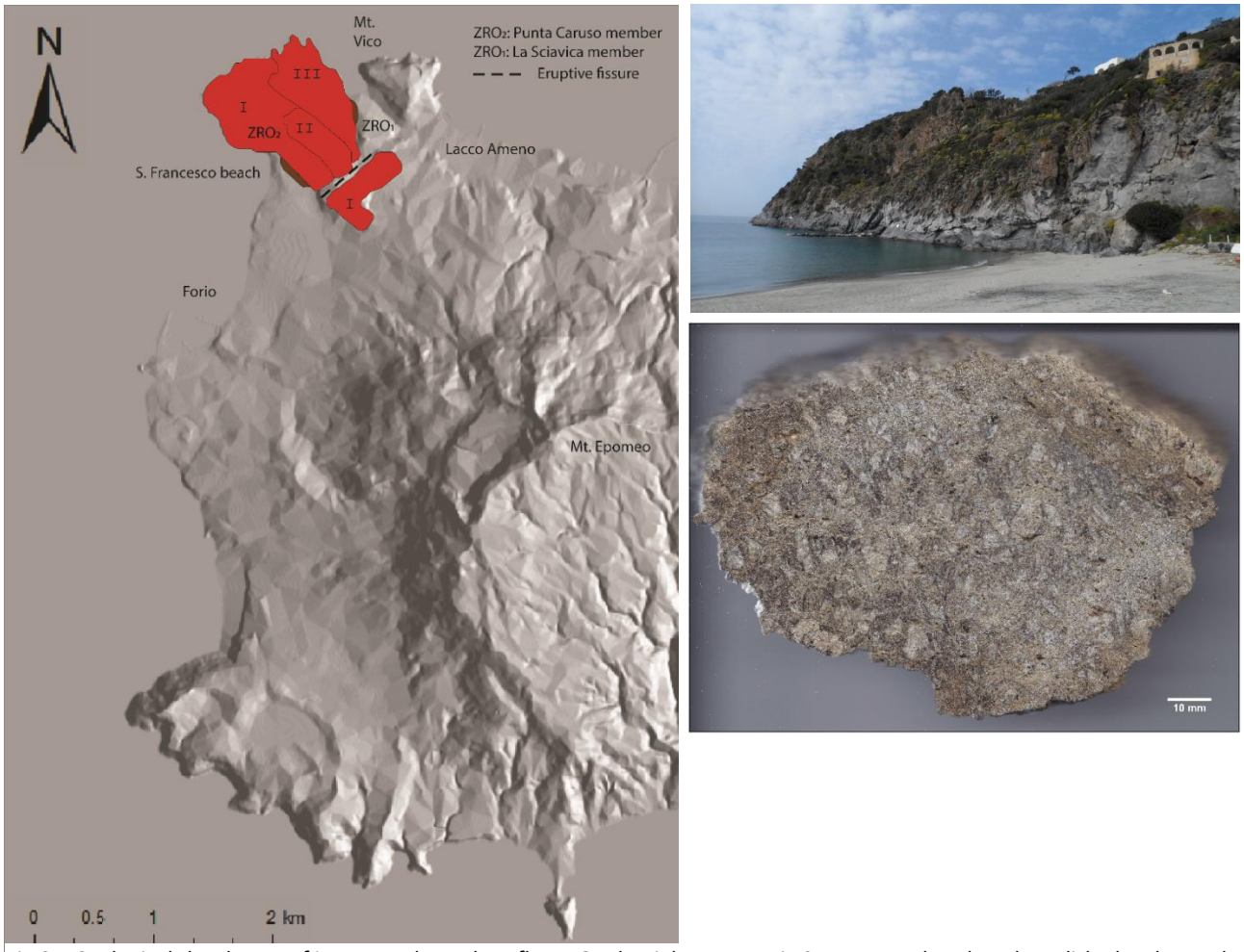

Fig.2 – Geological sketch map of interpreted Zaro lava flows. On the right: outcrop in S. Francesco beach and a polished rock sample.

1.2 Arso Lavas eruption

Arso Lava flow is the last eruption in Ischia Island, which occurred in 1302 A.D. (Chiesa et al., 1986) in the Arso crater, near Fiaiano. During the eruption, the lava flow (named Bosco d'Argento Member by Sbrana & Toccaceli, 2011), preceded by a scoria-fall deposit (named Fasolara Member by Sbrana & Toccaceli, 2011) reached the sea at Punta Molina, flowing for 2.7 km (Fig.3). Thickness of 15-20 m remains constant for the entire length of the flow and near the coast it reduces to 4 m (Sbrana & Toccaceli, 2011).
Into the crater, scoriae of the Bosco di Spalatriello Member are locally welded and sometimes intercalated with ash beds (Sbrana & Toccaceli, 2011).
The lava flow is well vesiculated, rich in sanidine phenocrysts in a black/reddish groundmass (Vezzoli, 1988; de Vita et al., 2010). Arso Lava shows a vertical chemical variability from latite to trachyte (Civetta et al., 1991).
The eruption began on the 18th of January 1302 A.D. (Buchner, 1986) and lasted for 2 months (Chiesa et al., 1986). The historical chronicles described the eruption as an extraordinary event as a "Fire with the strong of sulfur with mistiness which afflicted the whole region. Ash fell in the Cava dei Terreni, at 65 km away, toward E from the vent" (Buchner, 1986). Pumices, floating in the sea, reached more than 300 km away (Chiesa et al., 1986).
According to Rittmann & Gottini (1980) the lava flow was generated at the base of a lava dome.

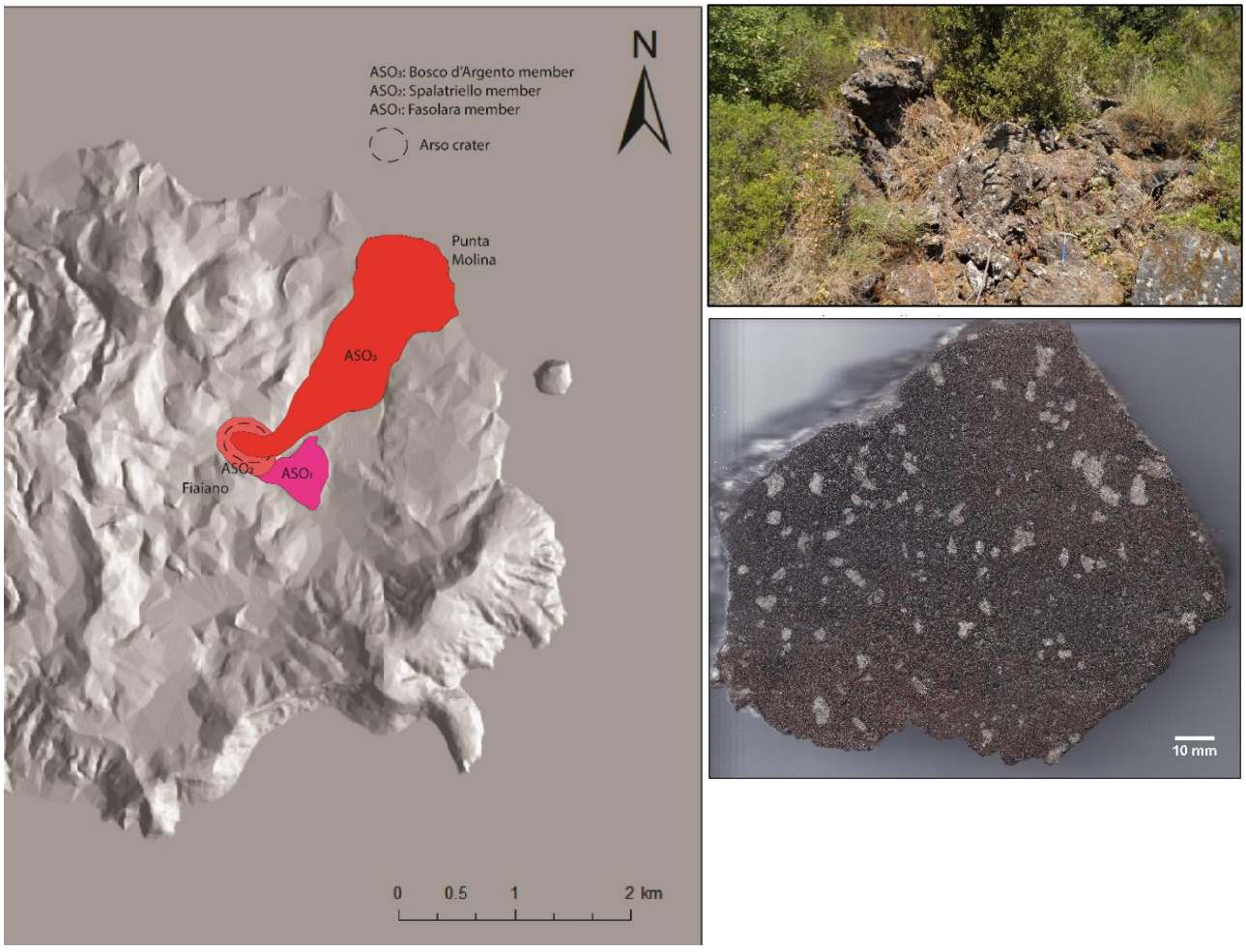

Fig.3 – Geological sketch map of Arso lava flow. On the right: outcrop in Arso crater and a polished rock sample.

2. Methodological strategy

In this paper a method to reproduce the syneruptive rheological conditions is proposed. A textural analysis, based on the crystal size distribution, has been used to characterize lava flows at natural post-depositional conditions. In this way, the number of nucleation and crystallization events have been identified.

In order to understand which event of nucleation is proper to the last phase of crystallization, due to the syn- and post-depositional cooling, a 3D textural analysis has been performed to identify the existence of fluidal textures in the microcrystal population, assumed as the last event of crystallization.

Once constrained the formation period of the microlite crystal cargo, a set of EDS measurement have been performed along the crystal axis in order to quantify the overgrowth in the other crystal populations. This has been useful because only a part of the remaining crystal populations may have contributed to the crystal cargo in the syneruptive rheological conditions.

Therefore, the crystal cargo has been brought back to emplacement conditions trough the estimation of the T window of lava emplacement. In this T range, the rheological response of the lavas has been studied through deformation experiments in a high-T uniaxial press where several compression experiments at different strain rates have been performed.

Experimental rheological results have been compared with the results predicted by the viscosity model proposed by Giordano et al., (2008) taking into account the effects of melt composition and temperature as well as that of the suspended crystalline phases (Vona et al., 2011).

3. Data Presentation

This chapter gathers the sampling criteria, all the textural and rheological data and their acquisition processes useful for the construction of the syneruptive rheological characteristics with an approach that can be applicable to other similar lava flows.

3.1 Textural analysis

Zaro Lava domes and flows have been interpreted in the field as a lava field with three different lava flows according to de Vita et al., (2010). The complex morphologies that can be observed especially in the northern part of the Unit have been interpreted due to the ogives formed in response to the compression during the first stages of the cooling (Nakada et al., 1995) as suggested by Vezzoli et al., (2009) and according to evidences in the field and morphology cross-checked by both DEM and aerial photos (1955, 1990, 2003 surveys).

Eight samples have been collected from different vertical position and distance from the vent, in order to describe all the Unit. Moreover, we sample a mafic enclave and a dyke in the San Francesco Beach, in the southern part of the lowest lava flow. For the Arso Lavas three samples have been collected in proximal, medial and distal position from the vent.

Textural analyses have been performed following the same approach proposed for vesicles by Shea et al., (2010) and by Vona et al., (2017), in order to quantify and describe the role of the crystal cargo. This kind of information can be useful to characterize the physical processes that drive the magma ascent and the subsequent eruption (Marsh, 1988; Marsh 1998).

This methodology is based on the acquisition of images of polished rocks and thin section of natural samples by scanner and SEM (through BSE image acquisition). Magnifications at 20x (115 px/mm), 60x (344 px/mm), 240x (1380 px/mm) and 480x (2735 px/mm) have been collected to represent the full-size range of crystal and vesicle populations and edited and binarized with an image analysis software (Image J 1.51j8®) (Fig. 4, 5).

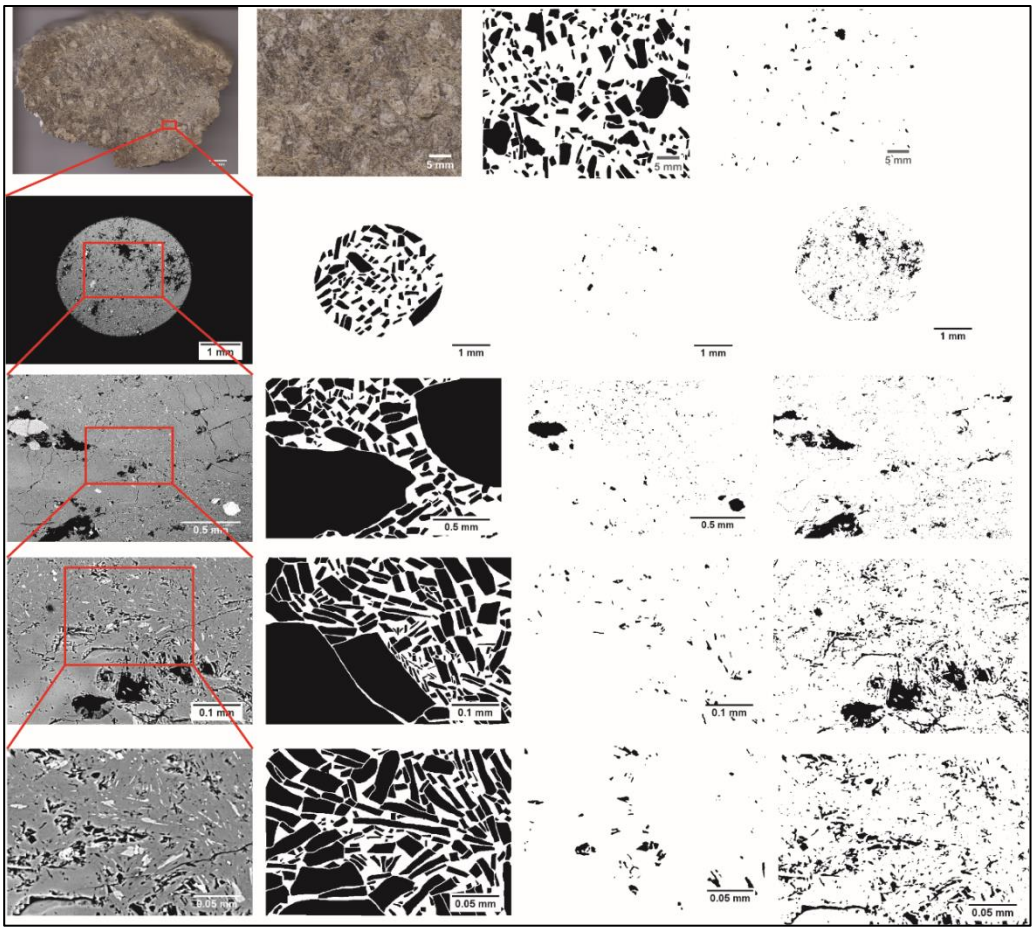

Fig.4 – Zaro, PP23 image acquisition and felsic, mafic and vesicle binarization, respectively.

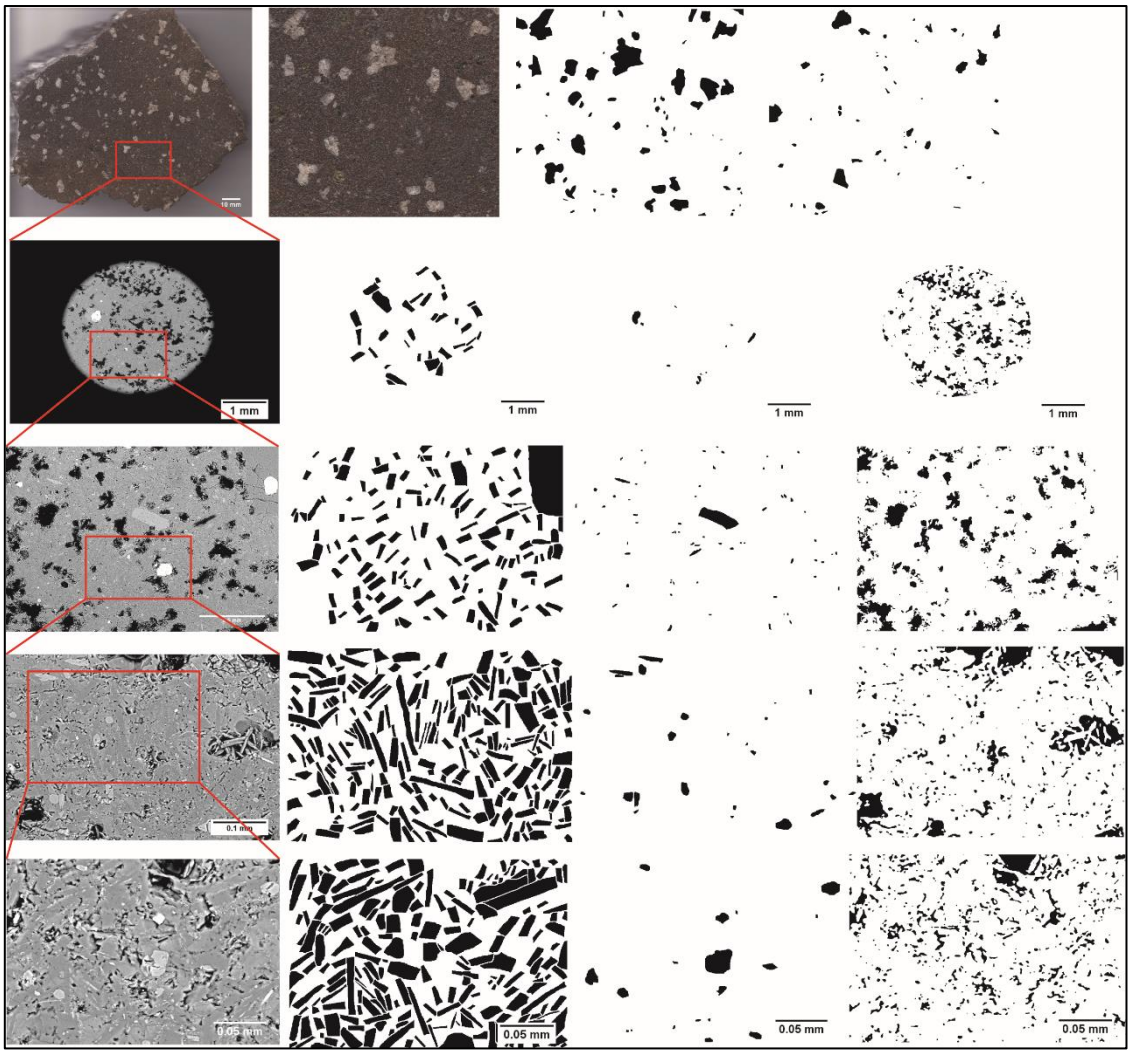

Fig.5 – Arso, PP32 image acquisition and felsic, mafic and vesicle binarization, respectively.

Distribution of major axis length of each population versus phase fraction were quantified by excluding the overlapping size between the magnification (Fig.6, 7) and by a correction by a factor which takes into account the space already occupied by larger particles. In this way, melt referenced crystal and vesicle fractions (Shea et al., 2010) were obtained from the 2D images as area ratios.
Textural analyses have been performed through the acquisition and processing of a large number of images (165), so the results obtained can be considered statistically valid. In Appendix A all the magnifications for crystal phases images binarization are reported for each sample.

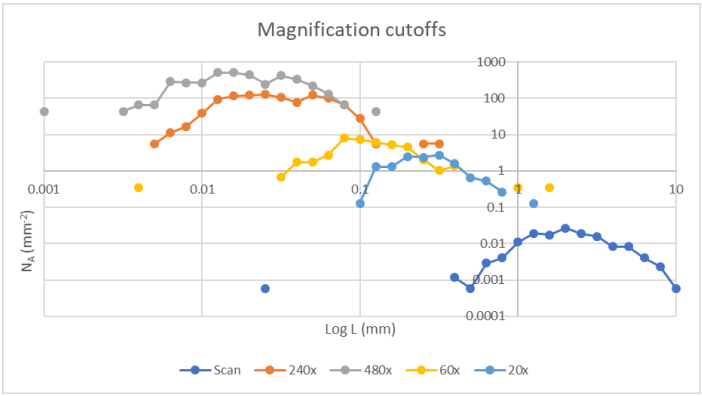

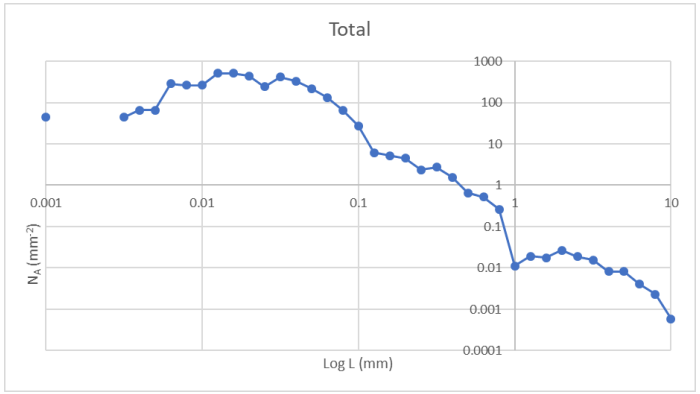

Fig.6 – Zaro, PP23 chosen magnifications cutoffs for felsic component in number of objects per melt area for different size classes diagram.

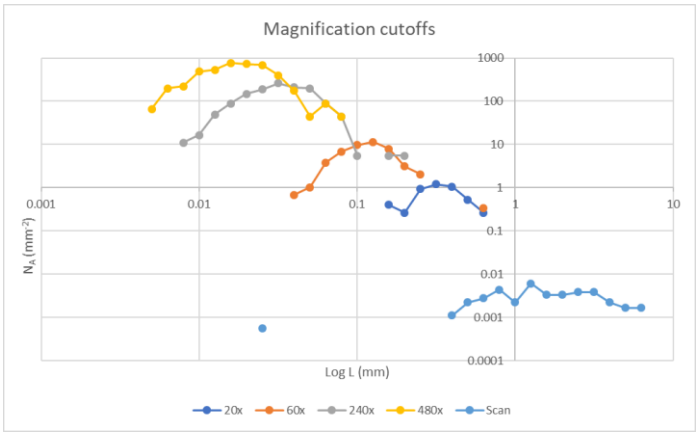

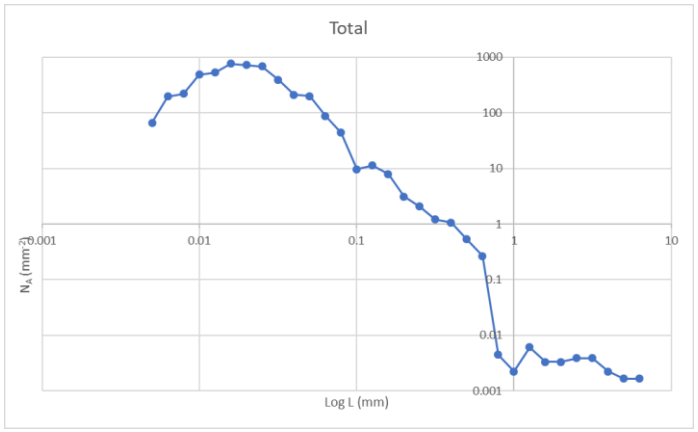

Fig.7 – Arso, PP32 chosen magnifications cutoffs for felsic componen in number of objects per melt area for different size classes diagram.

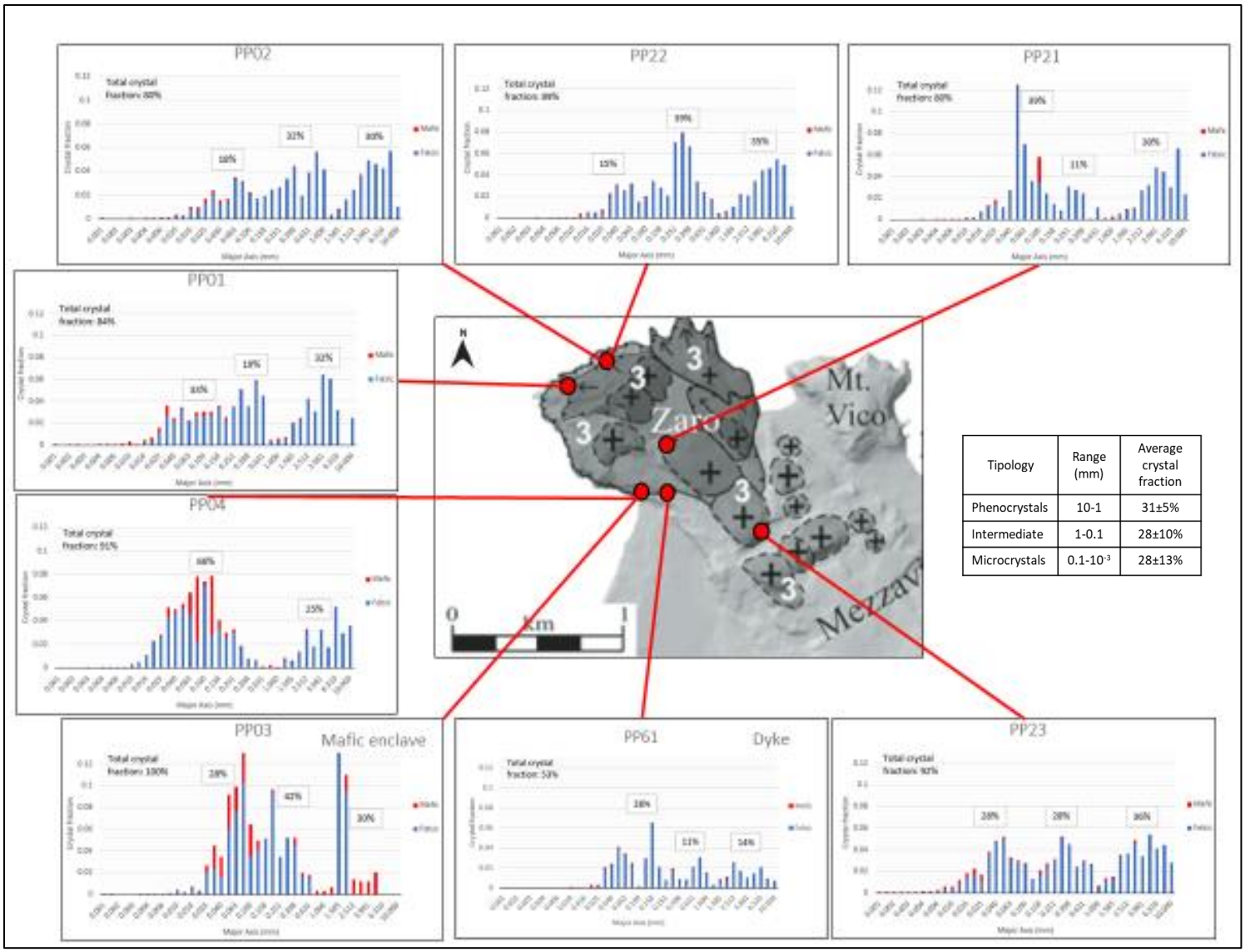

Tipology	Range (mm)	Average crystal fraction
Phenocrystals	10-1	31±5%
Intermediate	1-0.1	28±10%
Microcrystals	$0.1\text{-}10^{-3}$	28±13%

Fig.8– Zaro Lava Domes and Flows CSDs for each sample, further subdivided in relative percentages of the sanidine (blue) and mafic (red) crystal fractions.

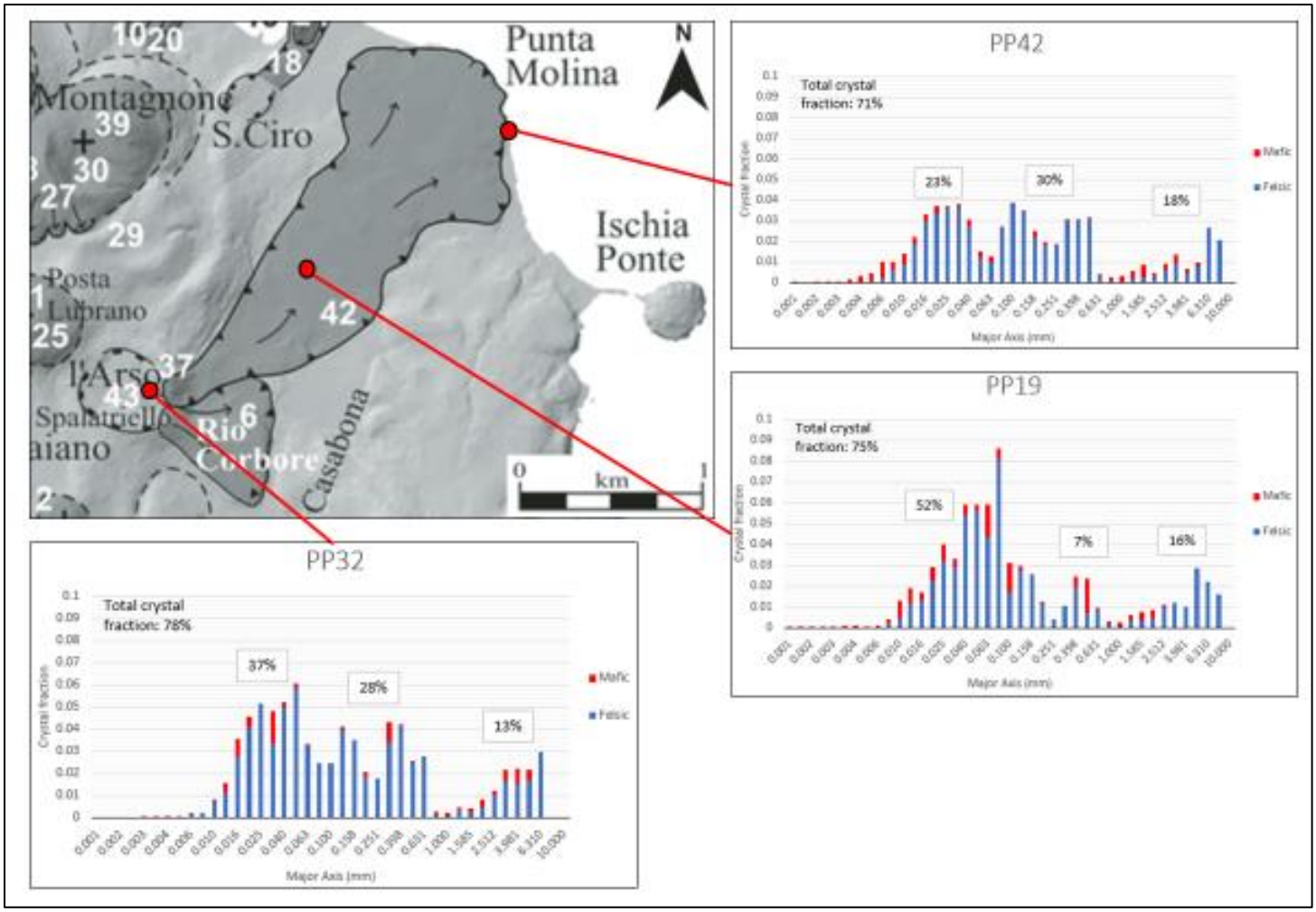

Fig.9 – Arso Lavas CSDs for each sample, further subdivided in relative percentages of the sanidine (blue) and mafic (red) crystal fractions.

The crystal size distributions (Fig. 8, 9) are characterized by the presence of three distinct modes at 5, 0.3 and 0.06 mm for both lava flows around well separated Gaussian distributions. The samples which show the most defined Gaussian distributions are the closest to the vent (PP23 and PP32) and those in the central portion of the lava flow (PP02, PP21, PP22 and PP19). The largest population includes mm-sized phenocrystals. In PP23 each Gaussian distribution represent approximately 1/3 of the total crystallinity (as in PP02, PP22, PP42), whereas in PP32, PP01, PP21, PP04 the largest part of crystallinity is represented by the microcrystal population that range between 40% and 70%.
The total CSDs diagrams (ln(n) vs size in mm plots) relative to the entire formations (Fig. 10, 11) show three different linear distributions.
The total crystallinity is considered 87% for Zaro, with a variability between 80% and 92% and for Arso is 74% with a variability between 71% and 78%. The contribution of the mafic phases is up to 6% for Zaro and up to 10% for Arso.

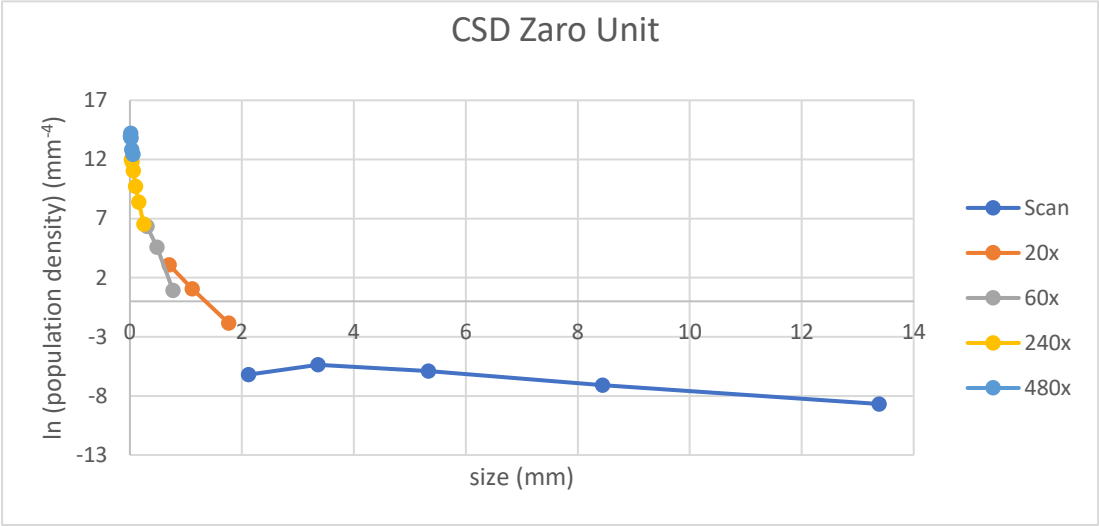

Fig.10 – Total CSD of Zaro Lava Domes and Flows, calculated using all the collected samples.

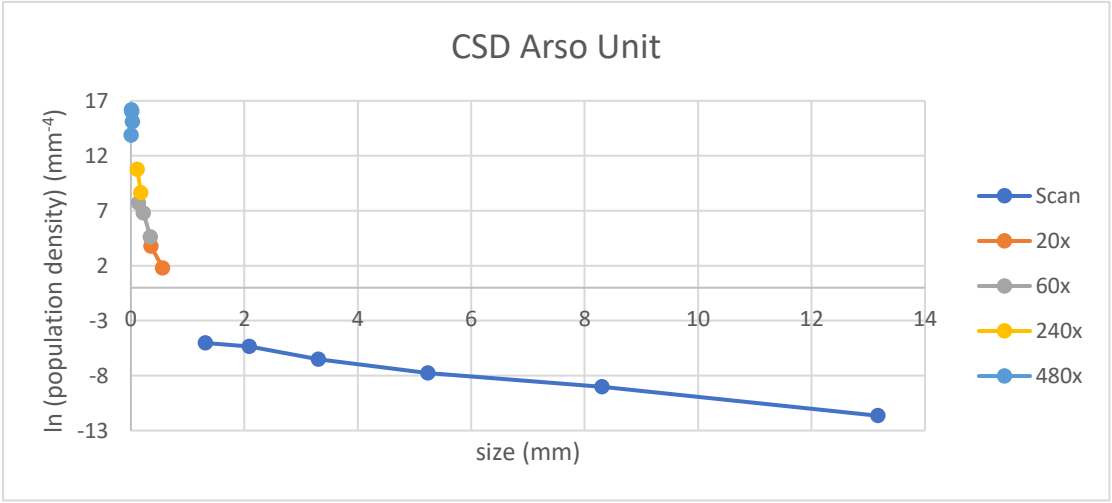

Fig. 11 - Total CSD of Arso Lavas, calculated using all the collected samples.

3.1.1 Textural analysis interpretation

The three Gaussian population identified by CSDs (Fig. 8, 9, 10, 11) can be interpreted as a polyphase history of crystallization with the nucleation and growth of three distinct crystal populations: phenocrystal, micro-phenocrystal and microcrystal population (Marsh, 1988, 1998; Mangan & Cashman, 1996; Shea et al., 2010).
An interpretation for such CSDs could be that magma rose from shallow reservoirs (Orsi et al., 1999), where phenocrystal population could nucleate and grow, to surface in at least one stage where degassed and crystallized before eruption.

3.2 3D imaging of microlites population

From the 2D images of the microcrystal population a fluidal texture seems to appear (Appendix A). In order to constrain its formation, is fundamental to understand if the microlites are affected by flowage diffusely in the rock texture or only in locally domains.
In order to understand which event of nucleation is proper of the last phase of crystallization, with the support of a master student, a 3D finalized reconstruction textural analysis has been performed.

Samples chosen for the analysis have been collected during the fieldwork in respect to an absolute reference system, in such a way as to be reoriented in the laboratory. Samples have been cut on three different orthogonal sections in respect to the lava flow direction. X plain has been considered perpendicular to flow direction, Y parallel and Z the basal plain.
Polished sample rocks and thin section have been analysed by scanner and SEM (BSE) images using the software (ImageJ 1.51j8®). For each sample, only the microcrystal population has been analysed, because that is which attributes the high values component of crystallinity to the flow, theoretically incompatible with a flow able to reorient the direction of the crystal axis (Cimarelli et al., 2011; Mader et al., 2013; Vona et al., 2011, 2013, 2017). Calculating the angular value of each microlite, it has been possible to determine for each section the axial crystal orientation in respect to the lava flow. The software Daisy 3 (5.3fd) has been used for the analysis.

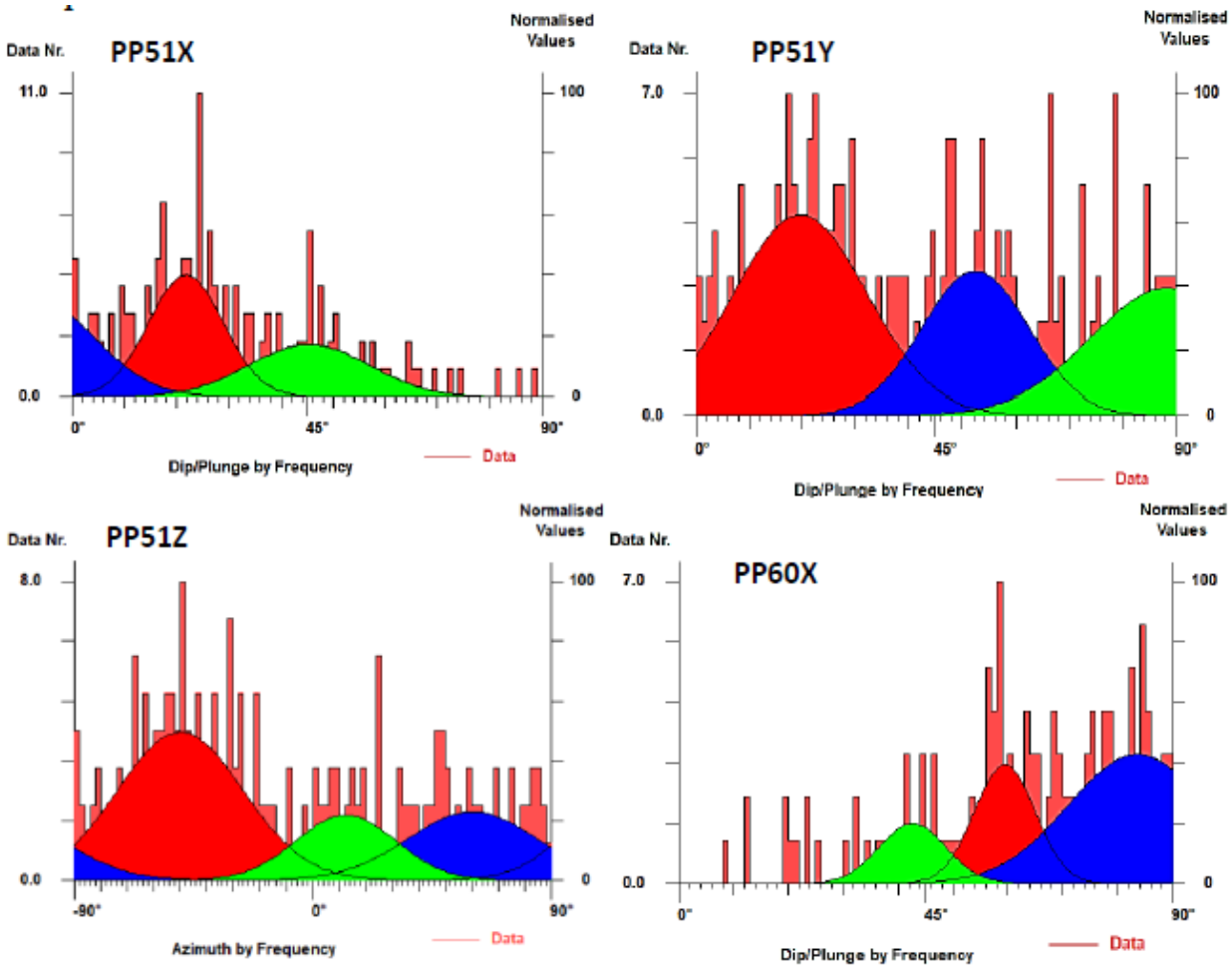

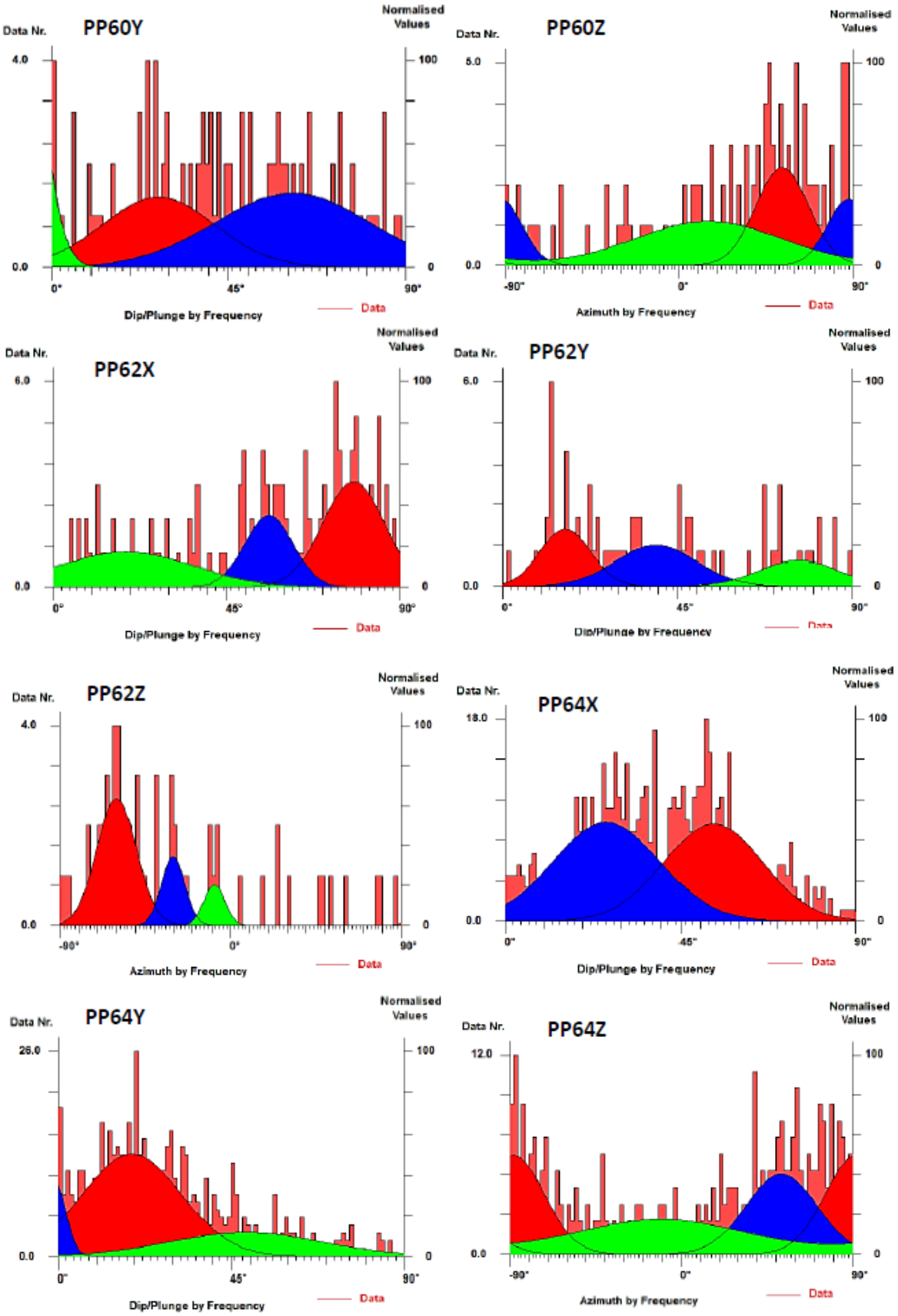

Fig.12 - Representative histograms of the X, Y and Z sections of the samples. Different colours indicate different frequency values (in red the most frequent angles, in blue the intermediate ones and in green the less frequent.

Histograms of each section of the samples (Fig. 12) show the normalized values slope of the crystals. More than the 50% have different orientations and only a small percentage of crystals has a marked orientation. Therefore, a significant preferential orientation of the crystals within the samples can be excluded.

3.2.1 3D imaging of microlites population interpretation

Through a 3D textural analysis, we have demonstrated that the growth of the microcrystal population is a post-depositional process due to the cooling after emplacement, since the apparent fluidal textures found in 2D do not appear to be statistically present on a large scale, but are locally domains proper of a trachytic texture, in accord to MacKenzie et al. (1982).
Therefore, the microlites population does not contribute to the crystal cargo during the emplacement and for this it can be declared removable to reconstruct the syneruptive rheology of the lavas.

3.3 Chemical overgrowth analysis

Once established that the microcrystal population does not contribute to the syn-emplacement crystal cargo, we have to know if also the overgrowth on the other crystal populations has to be removed in order to have a better reconstruction of the syneruptive rheology of the lavas.
The possible effect of crystal overgrowth has been assessed by analyzing the crystals populations for their zoning (Fig. 13) on a statistically valid set of measurement (150, reported in Appendix B) of chemical composition performed by an EDS at Istituto Nazionale di Geofisica e Vulcanologia – Sezione di Roma, along the crystal axis from core to rim.

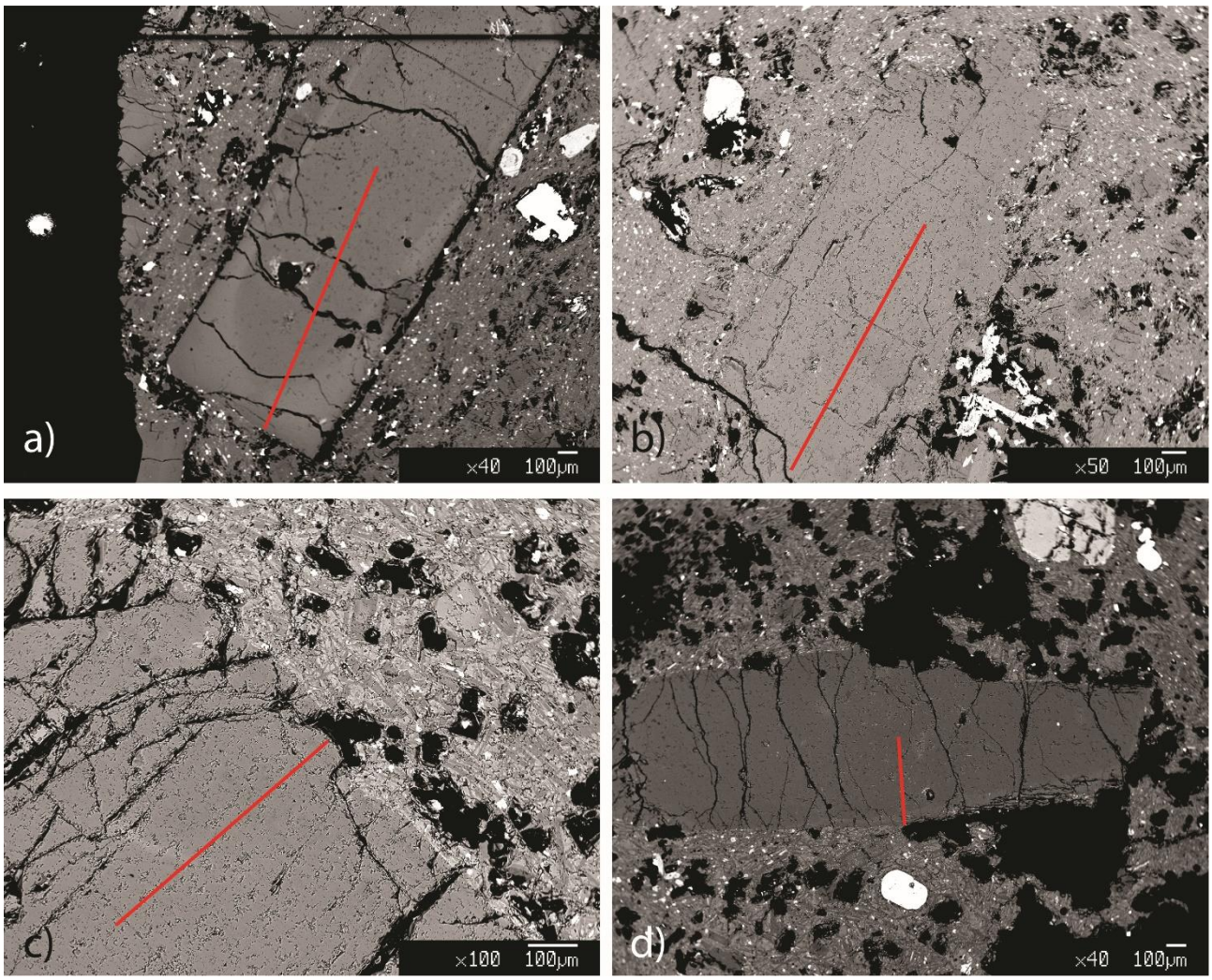

Fig.13 – Core to rim transect of Zaro phenocrystals (a, b) and Arso phenocrystals (c,d).

The ternary diagrams (Fig. 14), obtained by CALCMIN (Brandelik, 2009) and the compositional profiles (Fig. 15) show an unappreciable internal core to rim variability in the phenocrystal population.

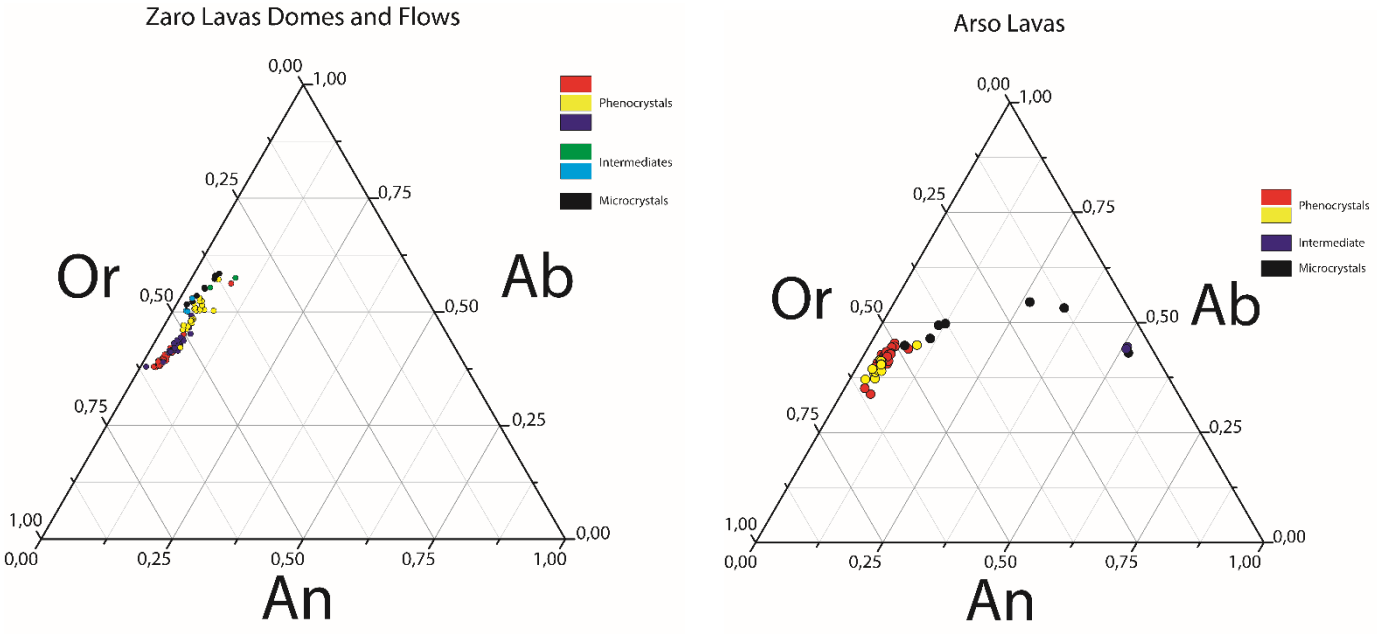

Fig.14 – Ternary diagrams of plagioclase of Zaro Lavas Domes and Flows and Arso Lavas.

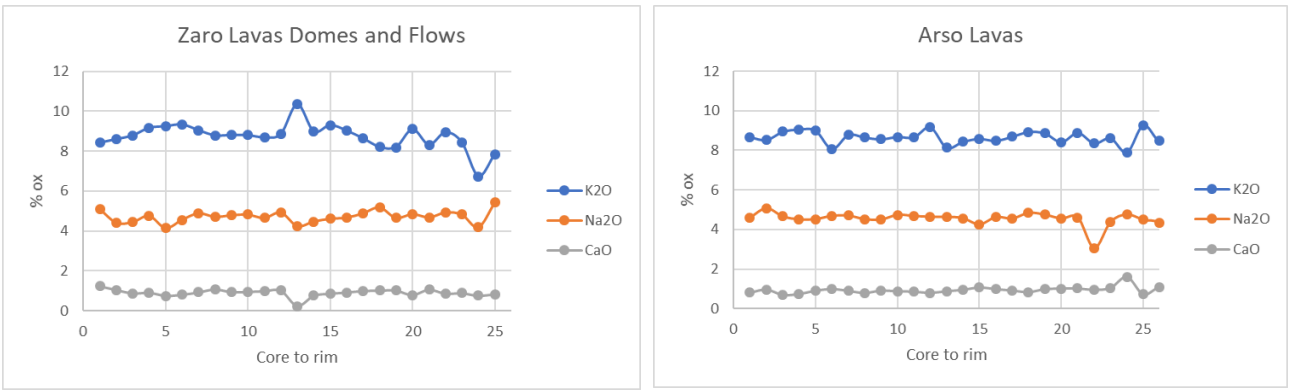

Fig.15 – Core to rim compositional profiles of phenocrystals from Zaro Lavas Domes and Flows and Arso Lavas.

3.3.1 Chemical overgrowth analysis interpretation

Ternary diagrams show that the overgrowth rate of the pre-existent crystals at the cooling time is close to zero, or in any case is not visible from microprobe analysis since the composition of phenocrysts and microphenocysts are too similar to the composition of microlites. This could be due to the low diffusivity of the elements, a characteristic of high viscosity systems.
From this analysis we can assert that the total crystal cargo at the emplacement time is represented by the phenocryst and microphenocryst populations and then, the remaining crystal cargo, once the microlite component has been removed, is a representative quantity at the time of eruption.

3.4 Experimental modelling

In order to correctly characterize the rheology of a lava flow, it is fundamental to bring the crystal cargo, back to emplacement conditions. To do this, it is necessary to remove the post-depositional crystal cargo, formed during cooling of the lava, that we have interpreted previously as the microcrystal population. Experiments in a temperature-controlled furnace have been performed to individuate at which temperature this population begins to be reabsorbed.
For both the lava Units, rheological experiments have been conducted on samples closest to vents (PP23 for Zaro and PP32 for Arso), because of the more easily recognisable shapes of the Gaussian populations and minor intensity of secondary post-depositional processes.
Several samples have been exposed to high temperature in a Nabertherm HT17/16 furnace set to incremental steps of 960 °C, 1000 °C, 1050 °C, 1075 °C e 1100 °C. At every incremental step of temperature, samples show a decrement of the total crystal fraction, with a consequent increment in the glass portion. For both lavas, at 1075 °C the microlite population is removed and we choose this temperature as the one that can be associated to eruptive conditions. At this temperature the crystal fraction for both lavas, is around 35%.
1075°C is the temperature at which the microcrystal population has been reabsorbed and then assumable as a temperature at which the flows were emplaced. Moreover, the considered emplacement temperature may seem too high for a trachytic composition, but considering that the natural samples can be assumed anhydrous, this condition is reflected by an increment of the melting temperature. Anyway, rheological experiments have been performed also at 900°C, after the removing of the microcrystal population at 1075°C, which represents a more suitable temperature for the emplacement of a trachyte.
In these T range, the rheological response of the lavas has been studied through deformation experiments in a high-T uniaxial press. Several compression experiments have been performed at constant strain rates of $5x10^{-5}$ s^{-1} and $1x10^{-4}$ s^{-1} following two different strategies:

1) Samples were held at 1075°C for 1 hour and then deformed;
2) Samples were held at 1075°C for 1 hour, rapidly cooled to 900°C, and then deformed.

Applied constant strain rates represent the end members which natural lavas could experience in Ischia terrain conditions. The end of the measurement has been imposed to a 20% of sample total strain.
Samples names and applied conditions are summarized in the following table (Tab.1).

	Sample	T (°C)	Applied constant strain rate (s^{-1})
Zaro	PP23-1	1075	$5*10^{-5}$
	PP23-3	900	$5*10^{-5}$
	PP23-4	1075	$1*10^{-4}$
	PP23-5	900	$1*10^{-4}$
Arso	PP32-1	1075	$5*10^{-5}$
	PP32-3	900	$5*10^{-5}$
	PP32-4	1075	$1*10^{-4}$
	PP32-5	900	$1*10^{-4}$

Tab. 1 – Sample name and condition applied in high-T uniaxial press.

In the following Figure (16) have been reported the stress vs strain diagrams relative to both lava flows.

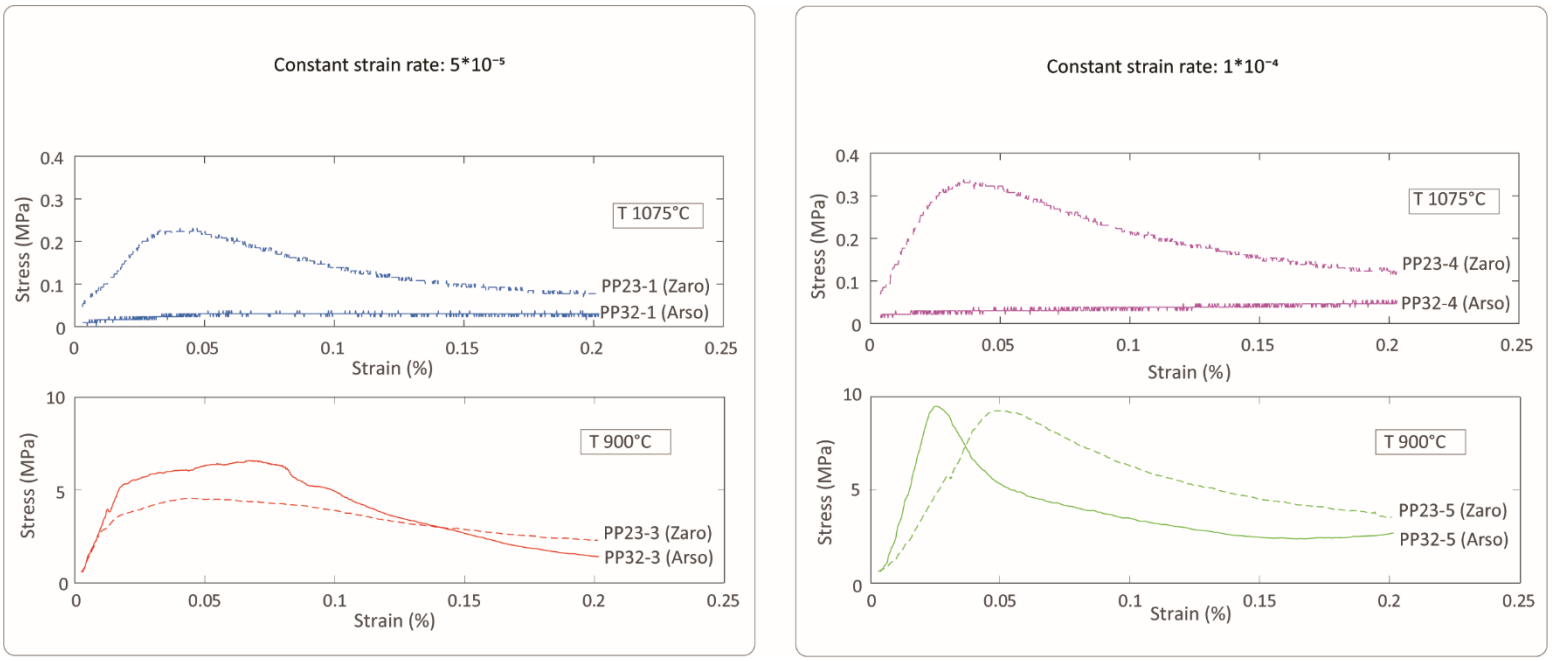

Fig.16 – Stress vs strain % diagrams subdivided by temperature and applied constant strain rate for Zaro and Arso lavas.

The diagrams allow to recognise the viscous/brittle transition and the value of the stress peak and drop, which identify the brittle behaviour at different stress values, depending on temperature. Viscosity values at the experimental conditions are presented in Figure 17.

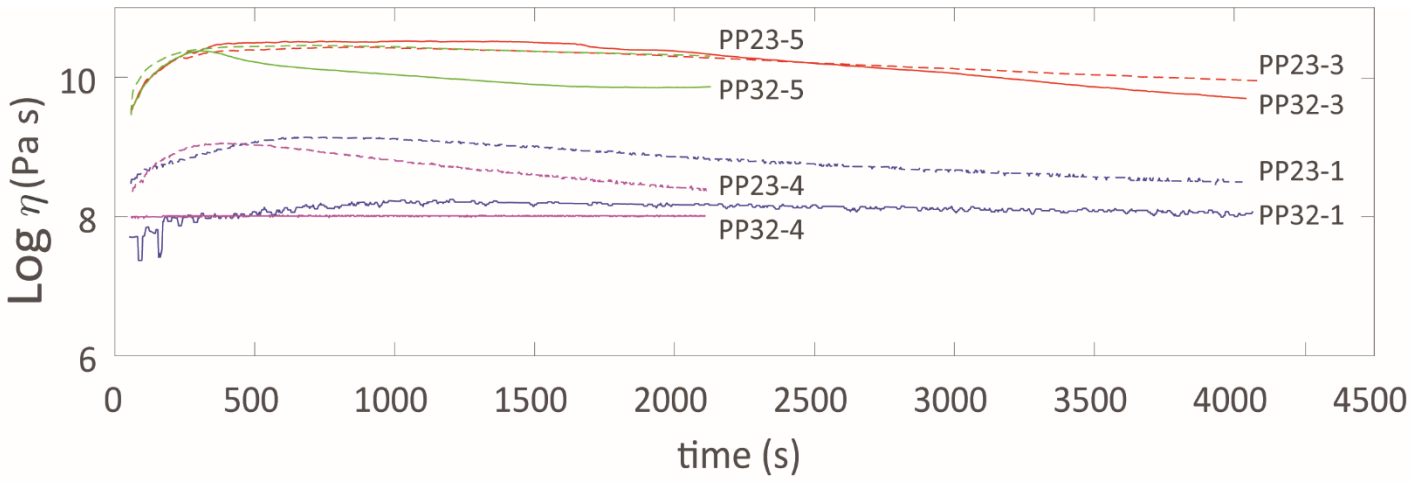

Fig. 17 – Viscosity diagrams for each sample analysed.

Zaro lavas display brittle dominated behaviour at both high and low T. Arso lava shows pure viscous deformation at high-T. Apparent viscosity is mainly controlled by the experimental T rather than from the imposed strain rate, and ranges between 8-10 log units Pa s. Arso lava shows lower apparent viscosity than Zaro lavas.

At the end of each experiment, post-run cores (Fig. 18) have been analysed to determine if the imposed instrumental strain has been correctly applied to the samples and how this has been distributed in the cores. This information and the change in core geometry (length L and radius r) are reported in Table 2, where there are also the textural analysis results.

Fig.18 – Zaro and Arso lavas post-run samples.

		Pre-run			Post-run		instrumental strain	sample strain	radial strain	total crystal fraction	vesicle content
Eruption	Sample	L_i	r_i	ρ_b	L_f	r_f	ε_m	ε_s	ε_r		
Zaro	PP23-1	41.70	9.95	2.14	33.14	11.45	0.20	0.21	0.24	27	15
	PP23-3	42.71	10.03	2.06	35.55	11.19	0.20	0.17	0.20	32	26
	PP23-4	41.21	9.96	2.07	32.92	11.44	0.20	0.20	0.24	30	10
	PP23-5	40.87	10.02	2.04	33.19	11.75	0.20	0.19	0.27	39	18
Arso	PP32-1	42.34	10.40	1.62	33.83	10.50	0.20	0.20	0.02	16	21
	PP32-3	39.23	10.06	1.97	33.44	12.05	0.20	0.15	0.30	24	40
	PP32-4	43.23	10.02	1.65	33.05	10.62	0.20	0.24	0.11	30	33
	PP32-5	41.73	10.06	2.00	33.25	12.16	0.20	0.20	0.32	23	9

Tab.2 - Pre- and post-run core geometry. L and r are expressed in mm. ρ_b is expressed in g/cm³. Total crystal fraction and vesicle content are expressed in %. Strain parameters are: instrumental strain, sample strain and radial strain.

The density values have to be compared with the dense rock equivalent (DRE) densities obtained by helium-pycnometer on samples powders and it is 2.65 g/cm^3 for Zaro Lavas and 2.69 g/cm^3 for Arso Lavas. Total crystal fraction refers to phenocrystal and micro-phenocrystal populations because the microcrystal one has been reabsorbed. These data have been used in the numerical modelling.

3.5 Numerical modelling

In order to validate the experimental results and to ascertain that the rheological behaviour of Ischia lava flows can be forecasted by the existent numerical models Vona et al., (2011) and Giordano et al., (2008), without showing unexpected behaviour, a set of simulations have been conducted.

In a first stage of modelling the MELTS calculator (Gualda & Ghiorso, 2015) has been used. The output used in this first stage is the liquid compositions corresponding to crystallinities observed in post-run samples. 31% of total crystal fraction in Zaro Lavas, corresponds in the GRD model at 1036 °C and 23% of total crystal fraction in Arso Lavas, corresponds in the GRD model at 1026 °C. This data allows to make an idea on how the model works, describing also correctly the crystalline phases that form the solid phase, in accord with the performed XRD analysis (reported in Appendix C).
Once verified that the model predicts the total crystallinity within an acceptable error, EDS measurements of wt% oxides in the glass on the post-run samples thin sections, have been performed and used to calculate the compositional controls on viscosity (A-B-C parameters) by the GRD model.
The viscosity modelling has been performed using the model of Vona et al., (2011) "model for predicting crystal bearing magma viscosity". This provides as input calculated A-B-C parameters, the system temperature and strain rate applied (the same of the uniaxial press), crystal content calculated by textural analysis on post-run samples and the aspect ratio of the different phases calculated by CSDslice 5 (Morgan & Jerram, 2006) and CSDCorrection 1.6 (Higgins, 2000).
Moreover, at the obtained viscosity values have been added the maximum and the minimum influence of the vesicle content by the Llewellin & Manga, (2005) calculations, applying the Regime 1, for Capillary number (Ca) <1.
Input required by the model and output produced have been reported in the Tab. 3.

		INPUT								
							input crystal content and aspect ratio of the different phases			
							Felsic phase		Mafic phase	
Eruption	Sample	T (°C)	A	B	C	Constant strain rate (s^{-1})	ϕ1	R1	ϕ2	R2
Zaro Lavas	PP23-1	1075	-4.55	10015.81	361.9162	5.00E-05	0.24	5.9	0.02	2.7
	PP23-3	900	-4.55	10565.89	340.7949	5.00E-05	0.29	5.9	0.03	2.7
	PP23-4	1075	-4.55	10304.39	347.1236	1.00E-04	0.28	5.9	0.02	2.7
	PP23-5	900	-4.55	10007.27	366.7635	1.00E-04	0.36	5.9	0.03	2.7
Arso Lavas	PP32-1	1075	-4.55	9539.889	387.4022	5.00E-05	0.13	5.7	0.03	2.8
	PP32-3	900	-4.55	9081.628	408.9267	5.00E-05	0.22	5.7	0.02	2.8
	PP32-4	1075	-4.55	9286.168	440.922	1.00E-04	0.18	5.7	0.12	2.8
	PP32-5	900	-4.55	9356.776	404.2137	1.00E-04	0.2	5.7	0.03	2.8

		OUTPUT											
						Power law flow parameters		(effect of crystals)	liquid + crystals			Vesicle influence	
					Relative consistency	Consistency (Pa s)n	Flow Index	Relative Viscosity	Apparent Viscosity			Minimun influence	Maximum influence
Eruption	Sample	ϕtot	R(mean)	ϕmax	Kr	K	n	η_r	η_{app}	log η_{app}	vesicle content (%)	log η_{app}	log η_{app}
Zaro Lavas	PP23-1	0.26	5.65	0.41	7.25	2922695.94	0.95	12.08	4872582.013	6.69	0.15	6.76	7.05
	PP23-3	0.32	5.60	0.42	19.04	2652187439	0.92	40.72	5673201362	9.75	0.26	9.88	10.27
	PP23-4	0.3	5.69	0.41	13.40	7428486.978	0.93	24.98	13848398.51	7.14	0.10	7.19	7.43
	PP23-5	0.39	5.65	0.41	305.67	22144217477	0.85	1338.42	96963295905	10.99	0.18	11.07	11.40
Arso Lavas	PP32-1	0.16	5.16	0.43	2.55	611671.0022	0.98	3.25	778959.9972	5.89	0.21	5.99	6.35
	PP32-3	0.24	5.46	0.42	5.48	118009331	0.96	8.49	183012271.9	8.26	0.40	8.49	8.93
	PP32-4	0.3	4.54	0.45	9.27	4497342.031	0.94	15.82	7675082.302	6.89	0.33	7.06	7.49
	PP32-5	0.23	5.32	0.42	4.80	199555756	0.96	7.00	290835751.4	8.46	0.09	8.51	8.72

Tab.3 – Input and result obtained using Vona et al., 2011 model.

3.6 Comparison between the models

	Sample	Visc meas (logη Pa*s)		Visc calc (logη Pa*s)	Visc calc vescicle (logη Pa*s)
Arso	PP32-1	8.23	7.94	5.89	6.35
	PP32-3	10.57	9.76	8.26	8.93
	PP32-4	8.14	8.00	6.89	7.49
	PP32-5	10.51	9.72	8.46	8.72
Zaro	PP23-1	9.10	8.50	6.69	7.05
	PP23-3	10.43	9.95	9.75	10.27
	PP23-4	9.02	8.40	7.14	7.43
	PP23-5	10.15	9.79	10.99	11.40

Tab.4 – Viscosity values measured by experimental modelling (reported as interval value) and calculated by numerical modelling with the influence of vesicle component.

In Table 4 the measured viscosity values have been reported as interval, obtained by experimental modelling. The highest and the lowest values are relative to the begin and the end of the steady state viscous behaviour, respectively.

Viscosity values obtain by Vona et al., (2011) model are here reported with the viscosity values which take into account the maximum influence of the vesicle content, which has a greater effect to increase the system viscosity.

Obtained values have been plotted in a diagram together with the 1:1 correlation line, in order to visualize the similitudes between viscosities (Fig. 19).

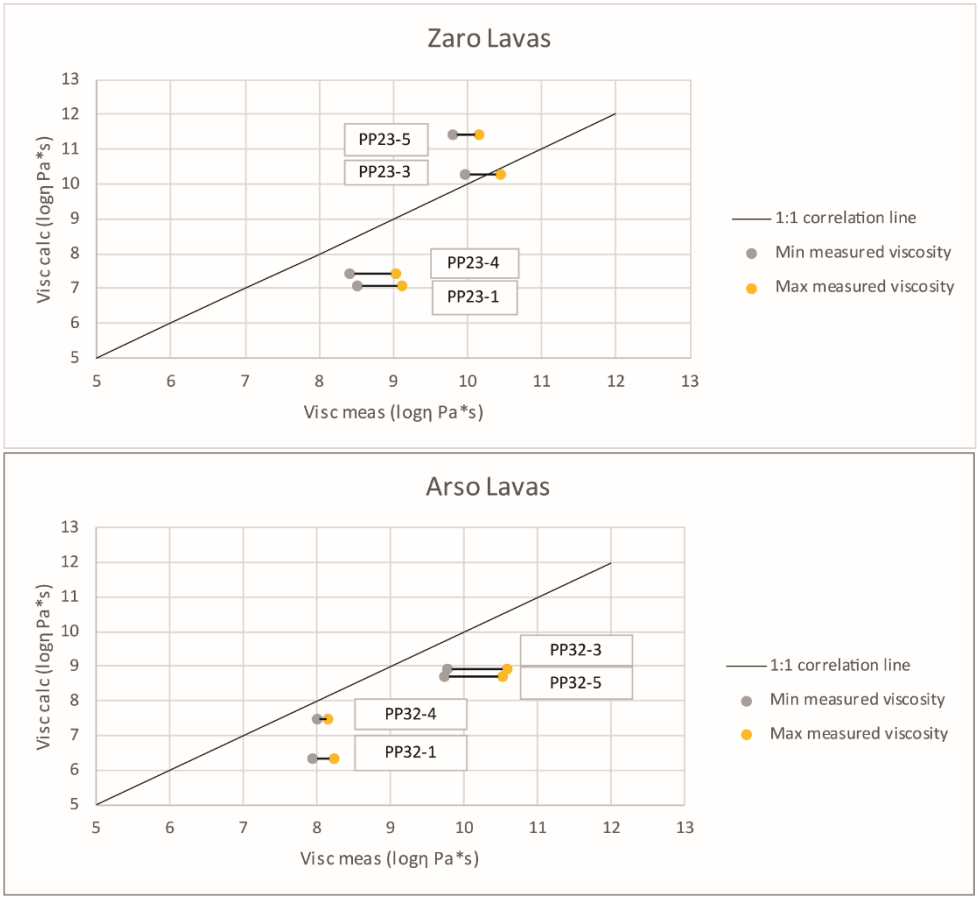

Fig.19 – Measured vs calculated viscosity for Arso e Zaro Lavas. Gray and yellow dots represent the minimum and the maximum measured values, respectively. Calculated values take into account the greater vesicle effect.

For Zaro Lavas the calculated and the measured viscosity values order of magnitude, are roughly the same, especially in the PP23-3 case, where the predicted viscosity is equal to the measured one. Different is the case of Arso Lavas, where the numerical model underestimates the viscosity values in respect to the experimental ones, that are always greater.

4. Discussion

In the last years there has been a great development in lava flow-related modelling. Rheological properties have been calculated taking into account both chemical properties and components content (Moore 1987; Giordano et al., 2008; Cimarelli et al., 2011; Castruccio et al., 2014; Vona et al., 2011, 2013, 2017). We have applied this knowledge of lava flow rheology to a system never studied in detail before and crystal cargo rheological behaviour has been described.
From the fieldwork and textural analysis, it is evident that Zaro Lavas Domes and Flows and Arso Lavas are both characterized by a high total crystal cargo (respectively about 87±12% and 74±4%), values clearly incompatible with lava flows (Cimarelli et al., 2011; Mader et al., 2013) that have moved up to some km. The movement conditions at the emplacement moment have to be restored annihilating the post depositional microlite crystal cargo formed during cooling of lava units. Experimental measurement performed by the high-T uniaxial press, assess the viscosities of lava cylinders with a total crystallinity of 38% and 33% for Zaro Lavas Domes and Flows and Arso Lavas, respectively. These syn-eruptive total crystallinity conditions recreate plausible conditions for the lava flows. Another character that has been described is the brittle/ductile transition observed in the post-run samples with a not pure viscous behaviour. These are manifested in the cores as the fracturing oriented by the σ_1 direction and rearranged by the crystal framework (Cordonnier et al., 2012) and has been observed during the fieldwork, in the outermost portions of the lava flows.

Regarding the rheological modelling, viscosity values obtained with the experimental and numerical ones, are not always the same. The predicted values by the Vona et al., (2011) model, in particular for the Arso Lavas case, tends to underestimate the viscosity up to 1 order of magnitude. This may be due to the particular solid phase composition of Ischia lavas. The labour-intensive analysis done to perform the experimental measurement, in particular the CSD characterization, is therefore justified and allowed to better constrain the rheological behaviour of these lava flows.

These two end-member lava flows are both characterized by a the relatively high viscosity and consequently a very slow magma ascent in the conduit (Cashman & Sparks, 2013). Tremors or other signals may last days or weeks before a similar effusive eruption will occur. This means, in terms of hazard, that the scientific community and authorities could have a long period to understand volcanic dynamics and eventually evacuate the island. On the other hand, the extrusion of a rigid spine and its subsequent collapse, with the emplacement of block and ash flows, has never been registered on the island in the reference period. Furthermore, variations in effusion rate and consequent changes in bulk rheology (Nakada & Motomura, 1999; Watts et al., 2002) were never able to produce a spectrum of lava bodies morphology that includes spines.

4.1 Impact parameters

One of the important targets for this work is to estimate the duration of the eruption starting from the velocity of the lava flows obtained from the characterization of the rheological behaviour. To do this we have applied the Jeffreys' law (Jeffreys, 1925), revisited firstly by Moore, (1987) and then by Castruccio et al., (2014) and Vona et al., (2017) which consider the non-Newtonian component behaviour of the lava. All the data necessary to apply the Jeffreys' equation, relative to the environment and to the area of emplacement, like position, geometry and slope of the channel, have been evaluated by a GIS analysis.
Starting from the known duration of Arso Lavas that is two months, it is possible to verify the travel distance using the velocity obtained by a mean ground slope and the characterized rheological properties.

Fig.20 – Travel distance vs. average slope in the case of Arso Lavas.

Figure 20 illustrates the modelling of the travel distance of the flow as a function of the terrain slope. The best fit viscosity values used has been obtained using the values measured at 1075°C at the beginning of the steady state viscous regime. With this model, in two months of known duration of the eruption, the Arso lava with a 15 m of thickness, on an average slope of 6°, without considering the temperature loss of the system, could travel for 29 km, with an average velocity of $5.7*10^{-3}$ m/s. As the case of Arso Lavas, the viscosity values used for modelling Zaro Lavas are in the same interval at 1075°C and the average flow velocity with the duration on the lava flow, depending to channel slope have been obtained used the occurred travel distance (Fig. 21).

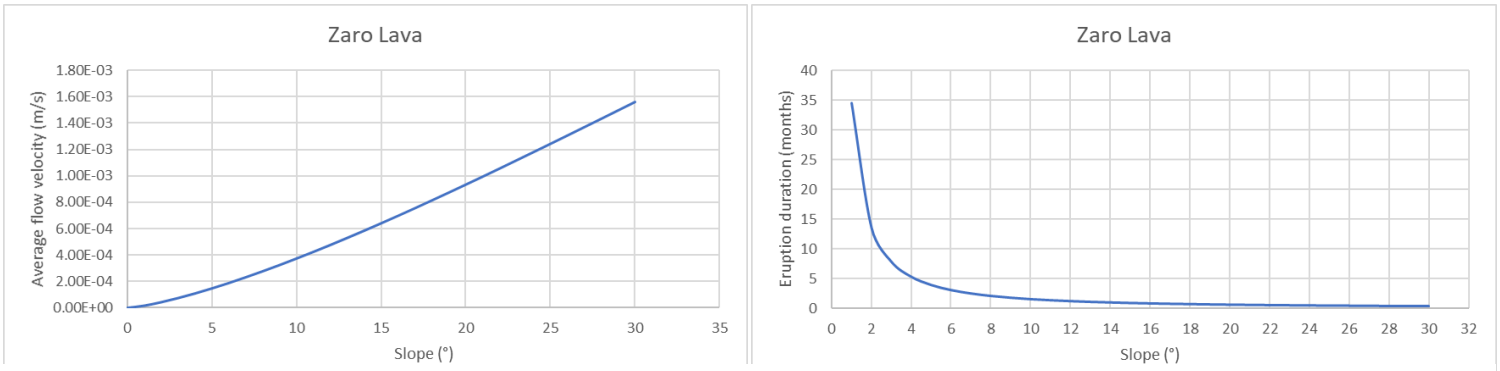

Fig.21 – Zaro Lavas flow velocity and duration vs. slope.

The pre-emplacement channel ground slope has an average of 5°. With a thickness of 30 m, without considering the temperature loss of the system, this flow moved with an average velocity of $1.5*10^{-4}$ m/s and the eruption lasts about 4 months.

The results of the modelling tend to overestimate the travel distance of Arso Lavas of about one order of magnitude, and to underestimate the eruption duration of Zaro Lavas. This can be explained by the fact that this modelling does not consider the cooling rate of the lava flows in the evolution of the eruption. The melt conditions are the same at the vent for all the eruption time, as if the lava moves in a lava tube, without loss of temperature. This fact, allows to estimate the great impact of the extensive groundmass crystallization in the behaviour of a lava flow during the eruption.

5. Conclusions

In this paper, numerical and experimental modelling allowed to parameterize lava flows on Ischia island starting from the known historical chronicles of Arso Lava and extending to the Zaro Lavas case study. A reconstruction of the syneruptive rheology of the lava that can be applied to similar lava domes and flows on Ischia has been presented.

Arso Lavas has been descripted as a “pestilence”. Nowadays, an effusive eruption that could last days or even several months would produce serious troubles. The island will be evacuated for a long period, with secondary effects damage to the community and the economy. To have an idea of what could happen, could help authorities in decision making.

Appendix A

Image acquisition and binarization process are reported for each analysed sample:
Images from top to bottom: Scan, 20x (115 px/mm), 60x (344 px/mm), 240x (1380 px/mm) and 480x (2735 px/mm) magnifications;
Images from left to right: felsic, mafic and vesicle component.

PP01:

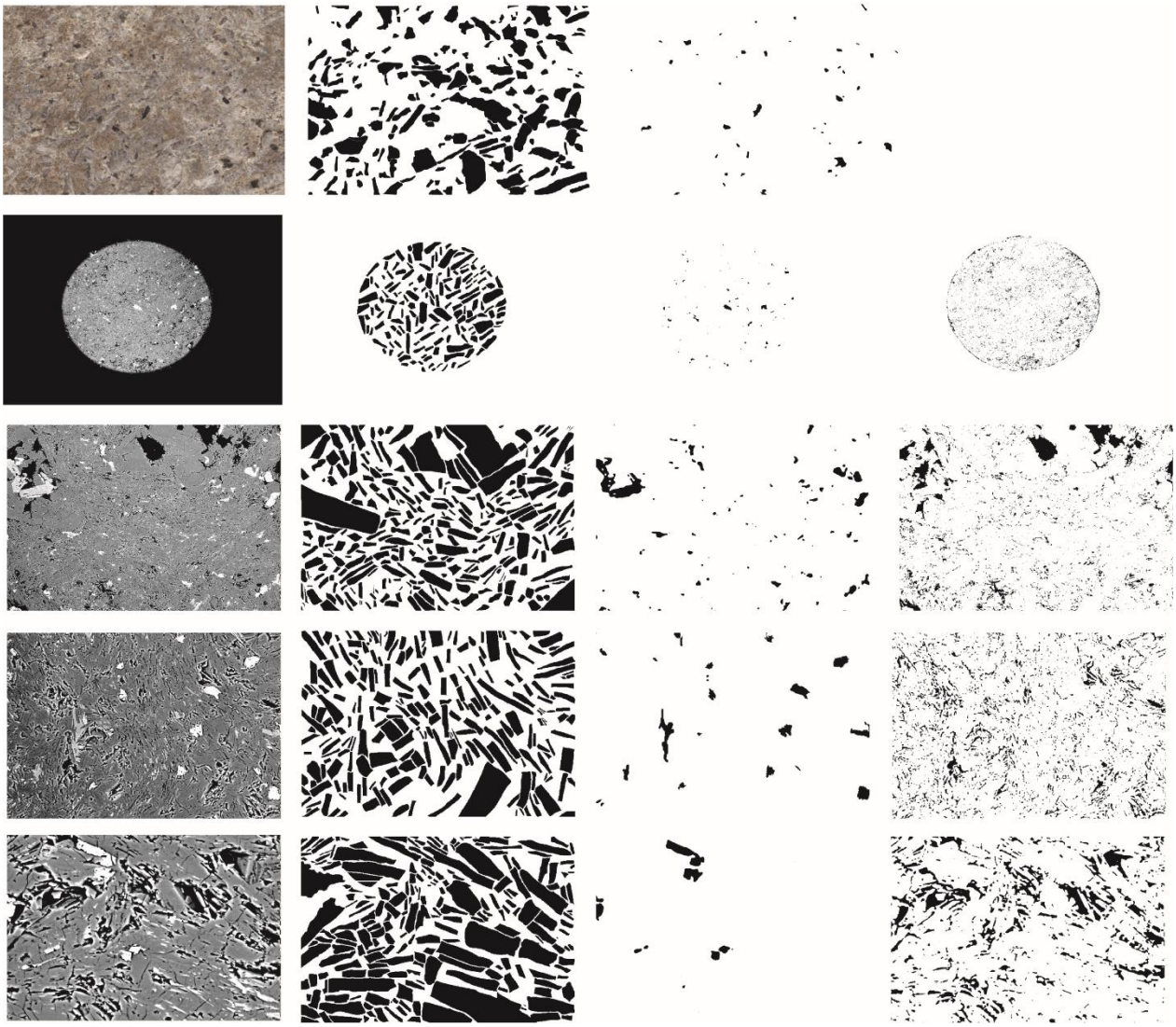

PP02:

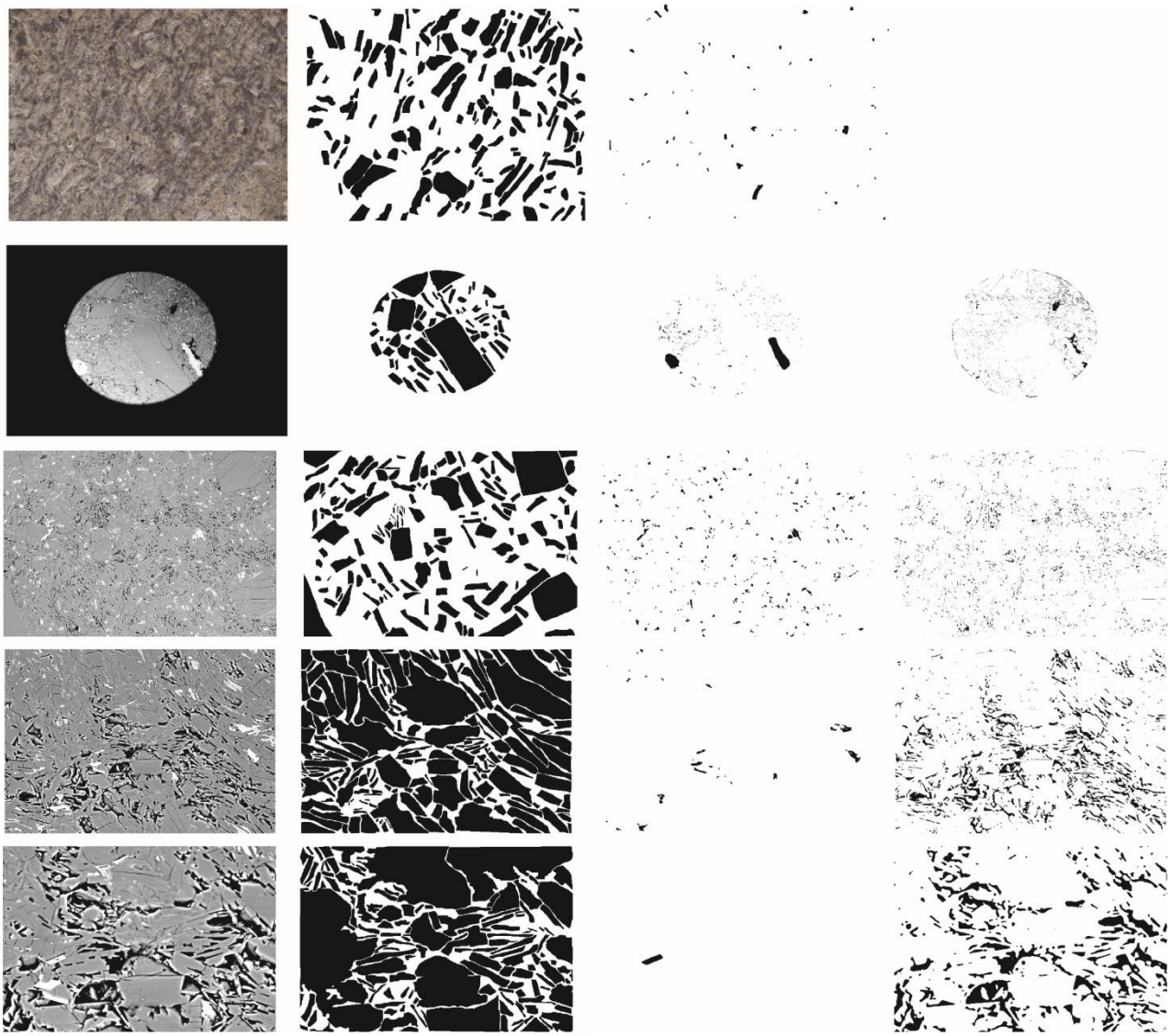

PP03:

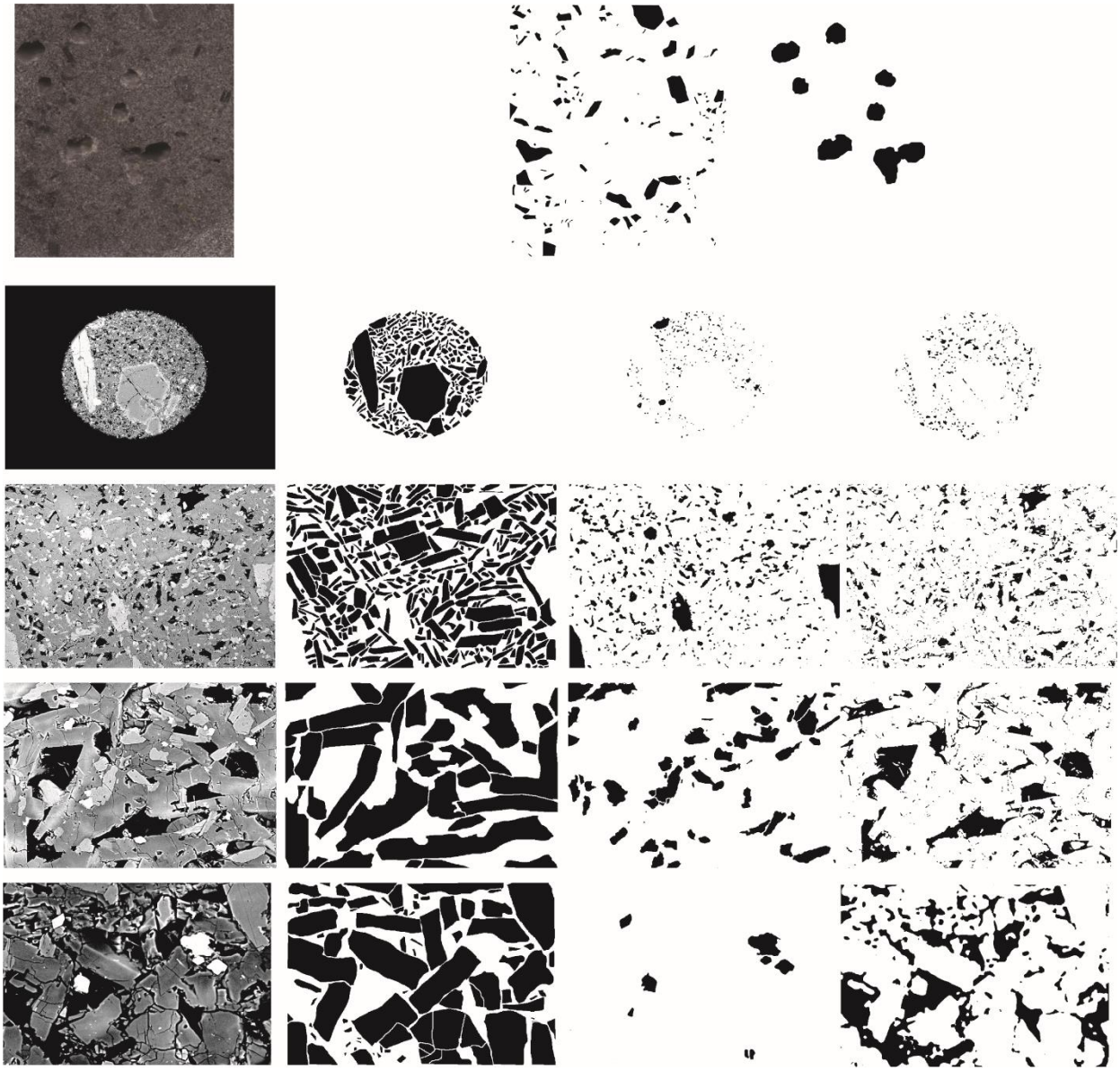

PP04:

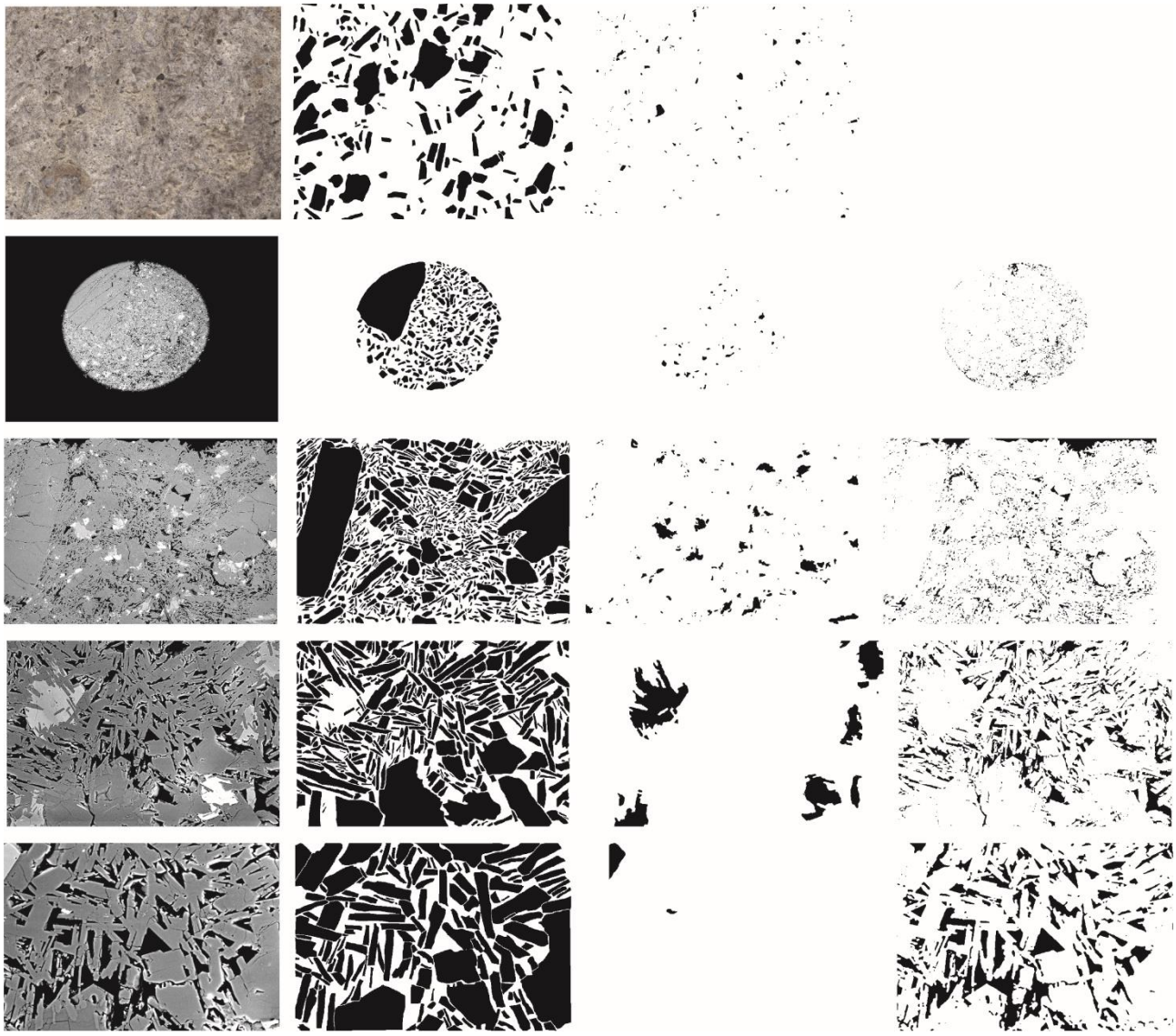

PP21:

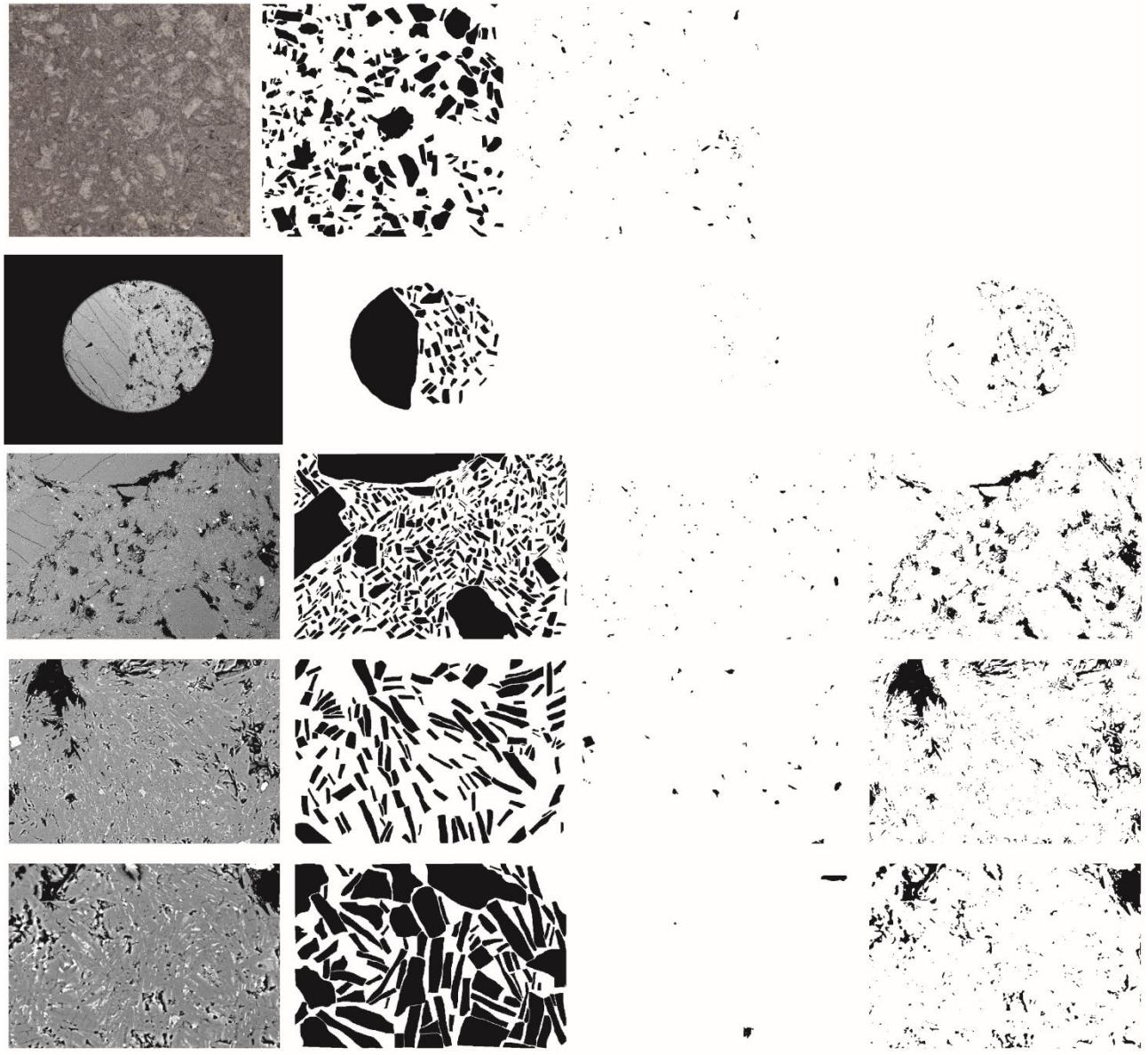

PP22:

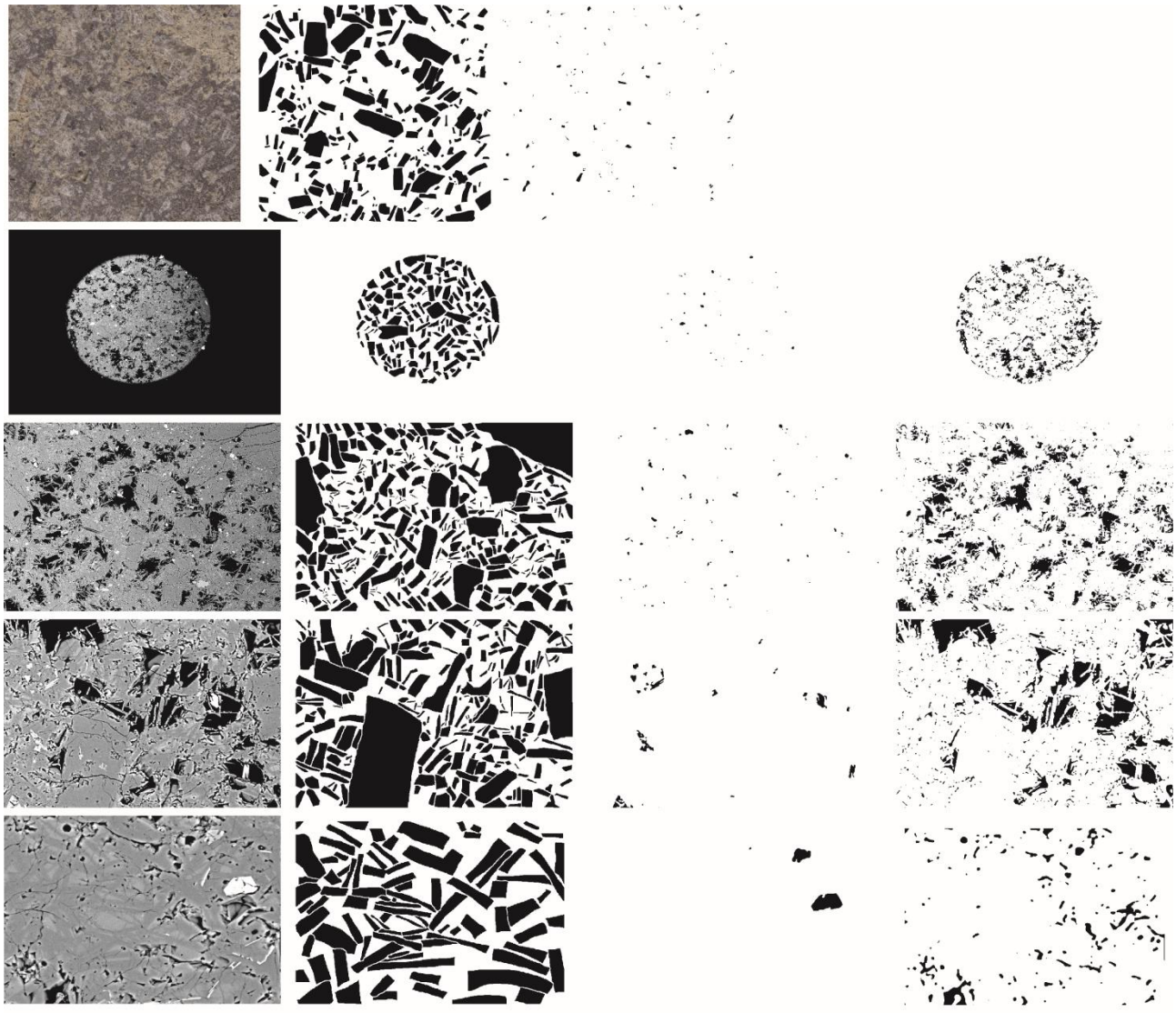

PP61:

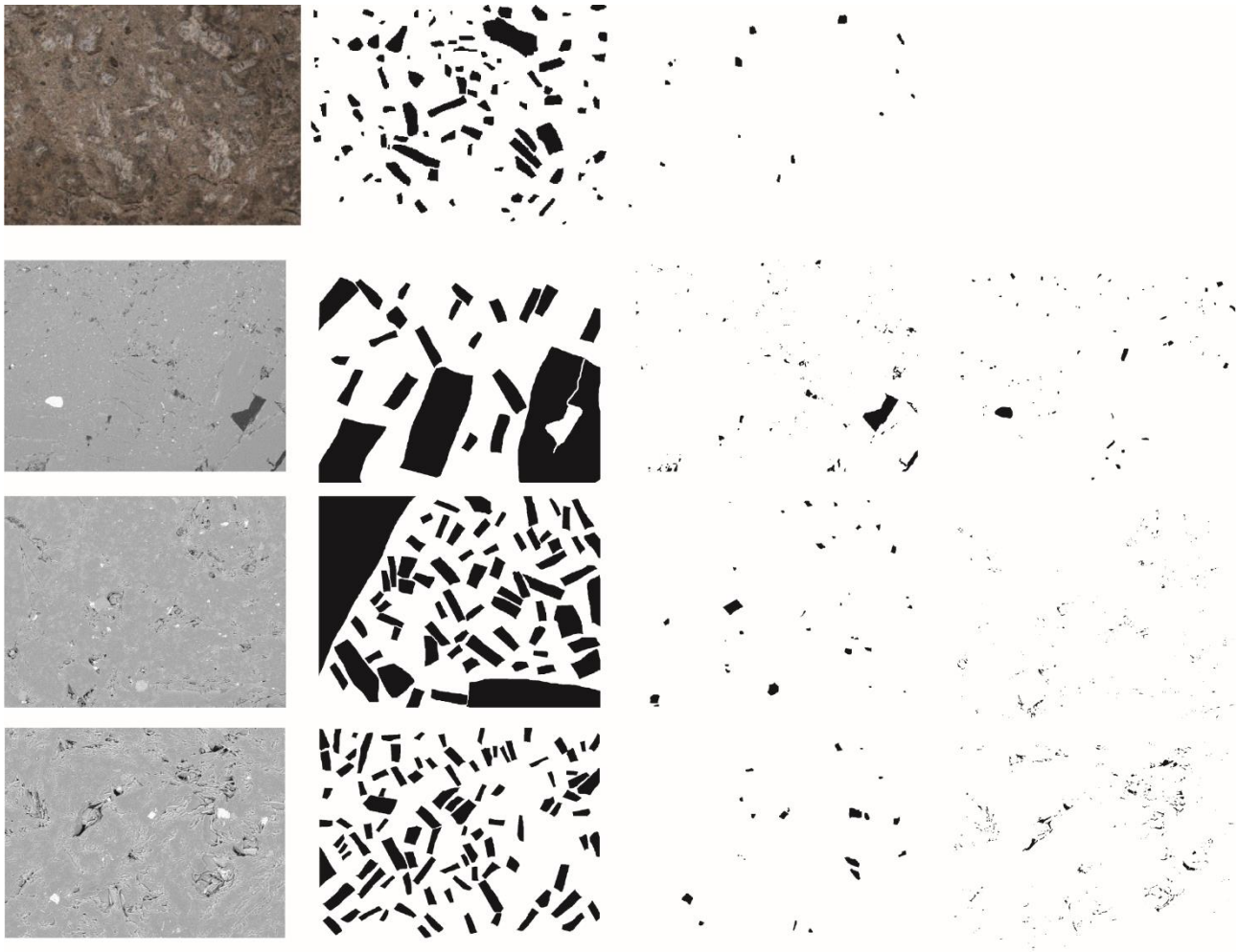

PP19:

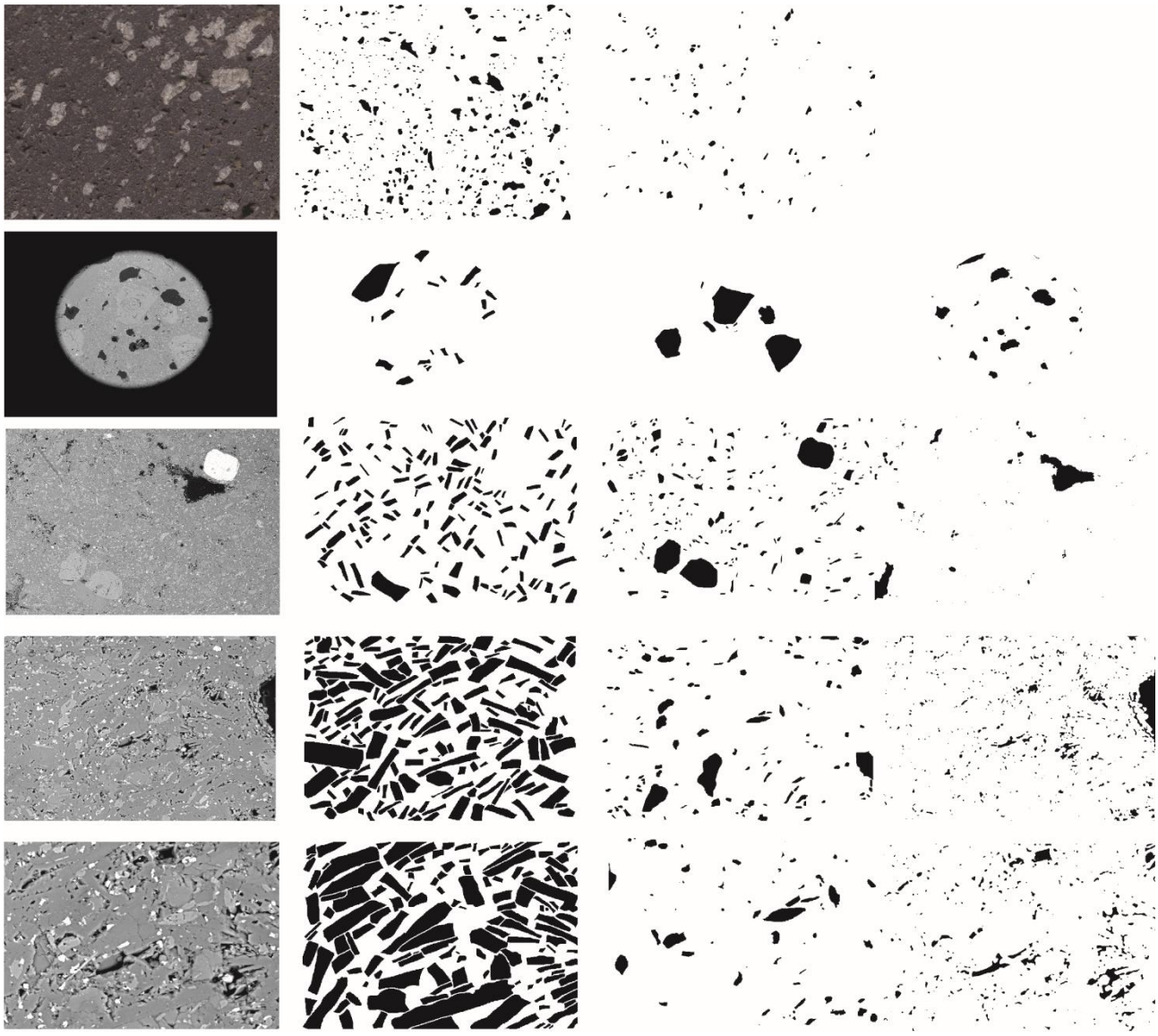

PP42:

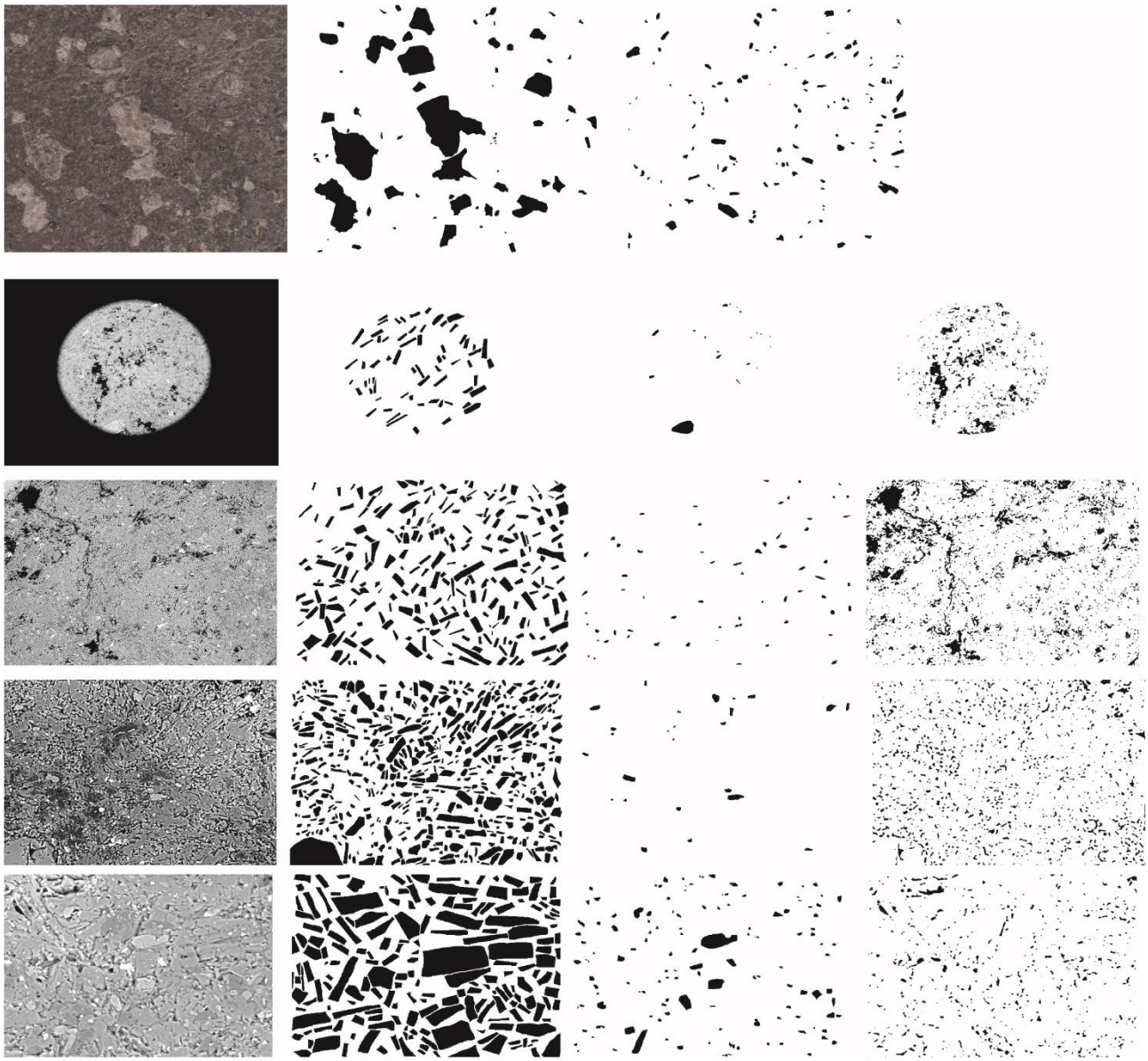

Appendix B

No.	Al2O3	Na2O	K2O	Cl	FeO	SrO	MgO	CaO	SiO2	TiO2	Total	Comment		
Zaro														
41	19.07	4.16	9.85	0.0057	0.1964	0.083	-	0.5902	64.45	0.1418	98.5471	Line 1 zar1		Core
42	19.17	4.23	9.81	-	0.2672	0.0874	0.0263	0.6133	64.13	0.0247	98.3589	Line 2 zar1		
43	19.27	4.19	9.75	-	0.2542	0.0611	0.0263	0.6522	65.06	0.1049	99.3687	Line 3 zar1		
44	19.11	4.19	9.77	-	0.207	0.153	0.0497	0.7398	64.35	0.0062	98.5758	Line 4 zar1		
45	19.32	4.21	9.48	0.0073	0.22	0.2055	0.0083	0.6453	64.36	0.0185	98.475	Line 5 zar1		
46	19.3	4.3	9.58	0.0098	0.2961	0.1181	0.0443	0.6867	64.36	0.0986	98.7937	Line 6 zar1		
47	19.34	4.2	9.47	0.0244	0.1048	0.0547	0.0221	0.751	64	0.1234	98.0904	Line 7 zar1		
48	18.41	4.54	8.92	0.0016	0.1625	0.0591	0.0887	0.7116	62.1	0.1233	95.1169	Line 8 zar1		
49	19.11	4.12	9.8	-	0.1992	0.0699	-	0.5998	64.94	0.074	98.9129	Line 9 zar1		
50	19.45	4.27	9.59	0.0212	0.2594	0.1247	-	0.5536	64.09	-	98.3589	Line 10 zar1		
51	19.2	4.29	9.36	-	0.1573	0.1138	0.0415	0.8566	64.1	0.074	98.1933	Line 11 zar1		
52	19.23	4.21	10.04	0.0016	0.2542	0.1398	0.0442	0.5171	64.57	0.0124	99.0193	Line 12 zar1		
53	19.37	4.22	9.86	0.0073	0.2253	0.2471	-	0.6893	64.18	0.0678	98.8669	Line 13 zar1		
54	19.53	4.29	9.87	0.0114	0.262	0.1861	0.0941	0.7536	64.22	0.074	99.2913	Line 14 zar1		
55	19.1	4.38	9.54	-	0.249	0.1269	0.0194	0.6571	64.11	0.0679	98.2504	Line 15 zar1	Zoned phenocrystal	
56	19.43	4.5	9.3	-	0.2727	0.103	0.0139	0.7627	63.95	0.0185	98.3509	Line 16 zar1		
57	19.55	4.28	9.36	0.0179	0.1652	0.114	-	0.6781	64.09	-	98.2552	Line 17 zar1		
58	19.48	4.31	9.47	0.0179	0.3278	0.0832	0.0153	0.7468	65.27	0.0679	99.7889	Line 18 zar1		
59	19.46	4.19	9.71	0.0138	0.2937	0.1379	0.018	0.6987	64.93	0.105	99.5572	Line 19 zar1		
60	19.37	4.44	9.53	0.0008	0.2256	0.1051	0.0457	0.7034	64.76	0.0309	99.2116	Line 20 zar1		
61	19.47	4.53	9.52	-	0.278	0.0854	0.0624	0.6848	64.32	0.0371	98.9878	Line 21 zar1		
62	19.44	4.47	9.38	0.0122	0.291	0.057	-	0.7993	64.18	0.0309	98.6605	Line 22 zar1		
63	19.37	4.28	9.71	-	0.2285	0.1863	0.0346	0.5688	64.69	-	99.0683	Line 23 zar1		
64	18.57	4.53	8.32	0.0016	0.1678	0.188	0.0111	0.8624	64.03	0.1665	96.8475	Line 24 zar1		
65	19.47	4.61	9.19	0.0073	0.2909	0.2496	0.0527	0.8216	64.71	0.1357	99.5378	Line 25 zar1		
66	19.58	4.38	8.84	0.0147	0.262	0.2411	0.0111	0.881	63.52	0.074	97.804	Line 26 zar1		
67	19.66	4.56	8.41	-	0.3093	0.2194	0.0277	0.9952	64.42	0.0986	98.7002	Line 27 zar1		
68	19.6	4.78	8.72	0.0106	0.2516	0.1295	0.0361	0.89	63.76	0.0802	98.258	Line 28 zar1		
69	19.19	5.05	8.58	0.0196	0.3224	0.1229	0.0682	0.9631	63.92	0.1789	98.4151	Line 29 zar1		
70	20.19	6.5	6.25	0.0025	0.383	0.1458	0.0449	1.72	64.42	0.0801	99.7364	Line 30 zar1		Rim
71	19.75	5.11	8.42	0.0065	0.3147	0.1759	0.0627	1.2315	63.94	0.0555	99.0668	Line 1 zar2		Core
72	19.62	4.41	8.6	0.0098	0.438	0.0769	0.0292	1.0465	62.46	0.037	96.7275	Line 2 zar2		
73	19.91	4.44	8.79	-	0.257	0.1888	0.043	0.87	63.97	0.0988	98.5676	Line 3 zar2		
74	19.83	4.76	9.17	-	0.236	0.149	0.0527	0.9046	65.71	0.1172	100.9295	Line 4 zar2		
75	19.13	4.14	9.25	0.0163	0.3462	0.0614	0.0277	0.7491	63.25	0.0617	97.0324	Line 5 zar2		
76	19.52	4.56	9.34	0.0049	0.2806	0.125	0.0319	0.8062	64.17	0.0988	98.9375	Line 6 zar2		
77	19.63	4.89	9.05	0.0041	0.2675	0.0767	-	0.9205	65.2	0.1481	100.1869	Line 7 zar2		
78	20.02	4.71	8.79	-	0.2282	0.055	0.0125	1.0718	63.36	0.111	98.3586	Line 8 zar2		
79	19.66	4.79	8.81	-	0.3015	0.0878	-	0.9363	64.33	0.0926	99.0083	Line 9 zar2		
80	19.49	4.82	8.8	0.0057	0.4247	0.1381	-	0.9473	65.21	0.1603	99.9962	Line 10 zar2		
81	19.55	4.65	8.69	0.0196	0.2858	0.1206	0.061	0.9841	64.72	0.1789	99.2601	Line 11 zar2		
82	20.12	4.93	8.86	0.0016	0.2857	0.1363	0.0375	1.0118	64.08	0.111	99.574	Line 12 zar2		
83	18.99	4.24	10.36	-	0.299	0.0699	0.0332	0.2347	65.85	0.1419	100.2186	Line 13 zar2	Not zoned phenocrystal	
84	19.87	4.47	8.99	-	0.3907	0.1843	0.0624	0.7507	64.64	0.0801	99.4383	Line 14 zar2		
85	19.7	4.61	9.31	-	0.2387	0.0526	0.0347	0.8569	65.01	-	99.813	Line 15 zar2		
86	19.64	4.67	9.03	0.0033	0.2413	0.0964	0.0069	0.9162	65.15	0.0741	99.8283	Line 16 zar2		
87	19.64	4.89	8.64	0.0073	0.2727	0.0439	0.0291	0.9956	64.71	0.0124	99.2411	Line 17 zar2		
88	19.89	5.19	8.21	0.0122	0.2569	0.1845	-	1.013	64.96	-	99.7167	Line 18 zar2		
89	18.62	4.65	8.2	0.0057	0.236	0.1533	0.0347	1.0135	63.15	0.2098	96.2731	Line 19 zar2		
90	19.75	4.85	9.1	-	0.2462	0.1754	0.0403	0.7866	64.52	0.1972	99.6657	Line 20 zar2		
91	19.69	4.68	8.32	0.0082	0.2543	0.1863	-	1.0591	64.87	0.0062	99.0742	Line 21 zar2		
92	19.59	4.93	8.94	-	0.3171	0.0833	0.0083	0.8533	65.45	0.0371	100.209	Line 22 zar2		
93	19.97	4.82	8.44	0.0188	0.296	0.1933	0.0611	0.8823	64.04	0.1417	98.8633	Line 23 zar2		
94	15.81	4.18	6.74	0.0441	0.2751	0.1315	0.2391	0.7515	53.72	0.0862	81.9775	Line 24 zar2		
95	18.81	5.43	7.84	0.0212	0.7987	0.136	0.1624	0.8301	64.65	0.4799	99.1584	Line 25 zar2		Rim
96	20	5.16	8.36	0.0024	0.2332	-	0.0277	0.9526	66.14	0.1417	101.0175	Line 1 zar3		Core
97	19.66	5.18	8.54	0.0139	0.2488	0.0482	0.025	0.8315	64.49	0.1171	99.1546	Line 2 zar3		
98	18.96	5.71	7.79	0.0229	0.2174	0.1423	0.0335	0.8079	66.12	0.1477	99.9518	Line 3 zar3		
99	19.7	5.34	8.4	-	0.207	0.1009	0.032	0.9625	65.55	0.1171	100.4095	Line 4 zar3		
100	19.72	5.38	8.16	-	0.2857	0.0549	0.0292	0.9713	65.07	0.1417	99.8129	Line 5 zar3		
101	19.76	5.32	8.07	0.0024	0.2255	0.0899	0.0222	1.0285	66.37	0.1417	101.0302	Line 6 zar3		
102	18.65	4.05	7.66	-	0.304	0.1184	0.0208	0.9693	60.94	0.1233	92.8359	Line 7 zar3		
103	20.35	5.4	7.92	-	0.2831	0.0265	0.0683	0.9872	63.16	0.0925	98.2877	Line 8 zar3		
104	19.67	5.42	8.04	0.0163	0.3092	0.1163	-	0.9571	65.55	0.1232	100.202	Line 9 zar3		
105	19.98	5.56	8.26	-	0.2383	0.0856	0.0445	0.9525	65.22	-	100.3408	Line 10 zar3		
106	19.68	5.22	8.32	0.0171	0.2855	0.0834	0.0153	0.7467	64.91	0.0555	99.3336	Line 11 zar3		
107	19.89	5.42	8.15	-	0.2935	0.079	0.0125	0.9483	65.22	0.0493	100.0625	Line 12 zar3		
108	20.19	5.68	7.47	0.0024	0.3668	0.1629	-	1.217	64.93	0.0863	100.1053	Line 13 zar3	Not zoned phenocrystal	
109	19.77	5.69	7.79	-	0.3276	0.1078	-	0.9389	64.62	0.0246	99.269	Line 14 zar3		
110	20.07	5.59	7.53	0.0082	0.2727	0.0968	-	1.0372	65.56	0.0986	100.2635	Line 15 zar3		
111	16.01	6.05	6.05	0.0319	0.2127	0.0591	0.0746	1.0301	60.16	0.1233	89.8018	Line 16 zar3		
112	20.08	5.52	7.37	0.0196	0.2807	0.1123	0.0599	1.0217	65.03	0.0987	99.593	Line 17 zar3		
113	19.9	5.86	7.54	0.0074	0.3227	0.1403	0.0373	1.0415	65.11	0.0371	99.9964	Line 18 zar3		
114	19.9	5.88	7.35	-	0.2414	0.1144	0.0628	0.9254	65.88	0.0124	100.3663	Line 19 zar3		
115	19.99	5.56	7.49	0.0025	0.2676	0.0176	0.0349	0.7926	63.98	0.1604	98.2957	Line 20 zar3		
116	19.62	6.03	7.61	0.0245	0.4066	0.055	0.0336	0.8612	65.68	0.1973	100.5182	Line 21 zar3		
117	19.46	6.07	7.53	-	0.4224	0.022	0.0308	0.7764	65.3	0.1973	99.809	Line 22 zar3		
118	19.25	5.96	7.85	0.0131	0.412	0.1076	-	0.6856	66.33	0.0678	100.676	Line 23 zar3		
119	18.91	5.89	7.48	0.0686	0.3963	0.1253	0.0519	1.67	64.52	0.0679	99.18	Line 24 zar3		Rim
120	20.12	6.51	5.88	0.0057	0.7503	0.179	-	1.73	65.44	0.2279	100.8428	zar4_c	Microphenocrystal	Core
121	20.03	6.18	6.8	0.0115	0.5903	0.1037	0.021	0.94	65.96	0.2648	100.9013	zar4_r		Rim
132	19.42	5.59	7.98	0.0123	0.3385	0.178	0.0056	0.5208	65.63	0.0802	99.7555	zar15_c		Core
133	19.13	6.06	7.77	-	0.8263	0.1298	0.0844	0.5017	65.53	0.2896	100.3217	zar15_r	Microphenocrystal	Rim
134	19.19	5.68	8.1	0.0033	0.4672	0.068	0.0391	0.6147	66.86	0.1357	101.158	zar15_r1		Rim
122	19.66	6.55	6.5	0.0197	0.6534	0.0618	0.107	0.8689	66.08	0.2587	100.7594	zar5	Microcrystal	
123	19.32	6.02	8.23	-	0.9782	0.0572	0.038	0.4217	65.11	0.3265	100.5015	zar6	Microcrystal	
124	19.45	6.59	7.44	0.0294	1.1983	0.0994	0.0439	0.7711	64.03	0.3078	99.96	zar7	Microcrystal	
125	19.27	5.93	7.75	0.0065	0.4489	0.1034	0.0434	0.5802	65.49	0.1665	99.7889	zar8	Microcrystal	
126	19.61	6.19	7.64	0.018	0.3731	0.0573	0.0098	0.6263	66.33	0.2036	101.0581	zar9	Microcrystal	
127	19.72	6.56	6.67	0.0139	0.6515	0.121	-	0.9333	65.13	0.1852	99.985	zar10	Microcrystal	
128	18.91	5.93	8.08	0.0188	0.6091	0.1847	-	0.4383	65.13	0.2529	99.5538	zar11	Microcrystal	
129	19.63	6.67	6.38	0.0057	0.4492	0.1037	0.0535	0.9979	66.63	0.1912	101.1111	zar12	Microcrystal	
130	19.78	6.7	6.6	0.0459	0.5301	0.0838	0.0352	0.938	65.96	0.111	100.7839	zar13	Microcrystal	
131	19.52	6.36	7.24	0.0278	0.648	0.1763	0.031	0.783	65.96	0.2157	100.9617	zar14	Microcrystal	

No.	Al2O3	Na2O	K2O	Cl	FeO	SrO	MgO	CaO	SiO2	TiO2	Total	Comment		
Arso														
135	19.67	4.6	8.67	0.0204	0.1968	0.0835	0.0222	0.8039	63.99	0.1112	98.1681	Line 1 ars1		Core
136	19.2	5.07	8.52	0.0025	0.2807	0.1777	0.064	0.964	64.94	0.1544	99.3734	Line 2 ars1		
137	18.71	4.66	8.94	-	0.168	0.0656	0.0195	0.6939	64.62	0.1481	98.0252	Line 3 ars1		
138	19.48	4.51	9.06	0.0106	0.1416	0.1206	0.043	0.742	63.92	0.105	98.1329	Line 4 ars1		
139	19.61	4.52	9	-	0.1653	0.1995	-	0.9073	64.6	0.0926	99.0947	Line 5 ars1		
140	18.42	4.69	8.06	0.0098	0.1941	0.0832	0.0305	0.989	63.52	0.0309	96.0275	Line 6 ars1		
141	19.84	4.7	8.78	-	0.325	0.1514	0.0194	0.8992	64.38	0.1048	99.1999	Line 7 ars1		
142	18.72	4.52	8.65	-	0.2832	0.1247	0.0679	0.7939	64.25	0.1541	97.5639	Line 8 ars1		
143	19.3	4.5	8.56	0.0147	0.2465	0.0307	0.025	0.9134	63.12	0.0988	96.8092	Line 9 ars1		
144	18.42	4.74	8.68	0.0016	0.2884	0.2273	0.0459	0.8767	64.79	0.0617	98.1317	Line 10 ars1		
145	19.36	4.68	8.66	0.0163	0.1573	0.1009	0.0222	0.8605	63.17	0.1481	97.1754	Line 11 ars1		
146	19.48	4.64	9.17	0.0114	0.2227	0.0219	0.0055	0.801	63.21	0.0493	97.6119	Line 12 ars1		
147	17.9	4.64	8.13	0.018	0.215	0.1457	0.0042	0.8826	68.23	0.1048	100.2702	Line 13 ars1		
148	18.88	4.57	8.43	0.0334	0.2148	0.068	0.0416	0.9514	61.66	0.2219	95.0712	Line 14 ars1		
149	19.86	4.25	8.58	-	0.2463	0.0483	0.0014	1.0684	61.93	0.0986	96.0831	Line 15 ars1	Phenocrystal	
150	19.44	4.63	8.48	0.0049	0.2646	0.046	0.0374	0.9854	63.68	0.1171	97.6855	Line 16 ars1		
151	19.93	4.55	8.69	0.0081	0.2568	0.0746	0.0152	0.9171	63.71	0.1171	98.269	Line 17 ars1		
152	19.23	4.84	8.93	0.009	0.2436	0.1927	0.0069	0.8348	64.13	0.1603	98.5773	Line 18 ars1		
153	19.27	4.75	8.86	0.009	0.2778	0.1512	0.0597	0.9886	63.48	0.1541	98.0005	Line 19 ars1		
154	19.55	4.55	8.41	-	0.2333	0.1475	0.0319	1.0141	59.65	0.0433	93.6301	Line 20 ars1		
155	19.77	4.61	8.89	0.0179	0.2386	0.0659	0.0042	1.0169	63.94	-	98.5536	Line 21 ars1		
156	19.35	3.06	8.35	0.009	0.2621	0.086	0.0027	0.953	55.56	0.0493	87.6822	Line 22 ars1		
157	19.78	4.38	8.61	0.0016	0.2518	0.0681	0.0222	1.0489	63.57	-	97.7327	Line 23 ars1		
158	19.87	4.76	7.89	-	0.2385	0.2024	0.0805	1.6	62.33	0.0802	97.0517	Line 24 ars1		
159	19.07	4.49	9.28	0.0171	0.2728	0.0963	0.0319	0.7215	65.03	0.0864	99.0961	Line 25 ars1		
160	18	4.33	8.49	0.0057	0.2125	0.0831	0.0097	1.0678	62.07	0.0185	94.2874	Line 26 ars1		
161	19.23	3.45	9.14	-	0.1967	0.0417	0.0908	0.7242	61.34	0.0493	94.2628	Line 27 ars1		
162	19.58	4.15	8.96	0.0098	0.2045	0.1251	0.0525	0.6892	62.7	0.0309	96.5021	Line 28 ars1		
163	19.45	4.71	8.97	-	0.299	0.1031	0.057	0.9804	64.21	0.0926	98.8721	Line 29 ars1		Rim
164	23.6	6	3.13	0.0041	0.535	0.2782	0.0858	5.31	59.11	0.1603	98.2135	ars2	Microcrystal	
165	20.92	5.02	6.99	0.0139	0.5271	0.0708	0.0014	2.21	62.07	0.1726	97.9958	ars3	Microcrystal	
166	27.97	4.57	0.8181	0.0081	0.6528	0.2845	0.1048	9.97	54.02	0.1543	98.5527	ars4	Microcrystal	
167	19.37	4.82	7.91	0.0082	1.1375	0.0485	0.122	1.3776	62.13	0.4312	97.3551	ars5	Microcrystal	
168	20.76	5.41	6.26	0.0123	0.7344	0.0909	0.035	2.47	61.61	0.3944	97.7771	ars6	Microcrystal	
169	27.57	4.85	0.7627	0.0033	0.7813	0.362	0.0912	10.08	53.72	0.0246	98.2451	ars7	Microcrystal	Core
170	27.88	4.68	0.819	0.0131	0.7894	0.3208	0.0798	9.83	54.86	0.0432	99.3153	ars8		Rim
171	20.99	5.47	6.62	0.0131	0.59	0.113	0.0742	2.29	62.17	0.3636	98.6939	ars9	Microcrystal	
172	24.68	5.75	2.07	-	0.6348	0.2774	0.1349	6.67	57.48	0.0493	97.7465	ars10	Microcrystal	
193	19.36	4.55	9.19	0.0073	0.2327	0.1026	-	0.8905	65	0.1353	99.4685	Line 1 ars13		Core
194	18.1	4.58	9.21	-	0.2955	0.0741	0.0222	0.7742	63.59	0.1908	96.8369	Line 2 ars13		
195	19.27	4.53	9.12	-	0.2902	0.1072	0.0567	0.822	62.41	0.1661	96.7723	Line 3 ars13		
196	19.43	4.43	9.4	0.0024	0.2588	0.1245	0.0138	0.978	64.17	0.0307	98.8383	Line 4 ars13		
197	19.97	4.44	9.44	0.0016	0.2797	0.1116	0.0069	0.9641	64.21	0.0369	99.4609	Line 5 ars13		
198	19.97	4.32	9.31	-	0.2326	0.1421	0.0703	0.9045	64.7	0.0247	99.6742	Line 6 ars13		
199	19.58	4.41	9.09	0.0057	0.1856	0.1728	0.0414	0.893	63.34	0.0369	97.7555	Line 7 ars13		
200	17.56	4.16	9.47	0.0162	0.1908	0.1004	0.0595	0.823	58.48	0.1477	91.0076	Line 8 ars13		
201	19.42	4.04	9.55	-	0.23	0.1923	0.0579	0.9668	62.7	0.0185	97.1756	Line 9 ars13	Phenocrystal	
202	19.64	4.31	9.34	0.0057	0.1751	0.0196	0.0303	0.9154	64.82	0.166	99.4222	Line 10 ars13		
203	19.02	4.2	9.43	0.0065	0.2639	0.0675	0.0083	0.8516	64.7	0.0861	98.634	Line 11 ars13		
204	19.59	4.37	9.55	0.0122	0.3081	0.2029	0.0594	0.9425	64.22	0.1106	99.3658	Line 12 ars13		
205	19.49	4.36	9.64	0.0146	0.2897	0.133	0.0042	0.6725	64.63	0.1843	99.4184	Line 13 ars13		
206	19.15	3.95	9.71	-	0.235	0.1131	0.0412	0.6043	65.45	0.0861	99.3398	Line 14 ars13		
207	19.84	4.3	9.35	0.0081	0.2089	0.1834	0.0372	1.0728	64.5	0.1907	99.6911	Line 15 ars13		
208	19.54	4.45	9.22	0.0179	0.2899	0.1833	-	0.915	64.65	0.0861	99.3523	Line 16 ars13		
209	20.91	4.96	7.7	0.0106	0.2874	0.2354	0.0568	1.88	62.84	0.2028	99.0831	Line 17 ars13		Rim

Appendix C

XRD analysis results are reported here:

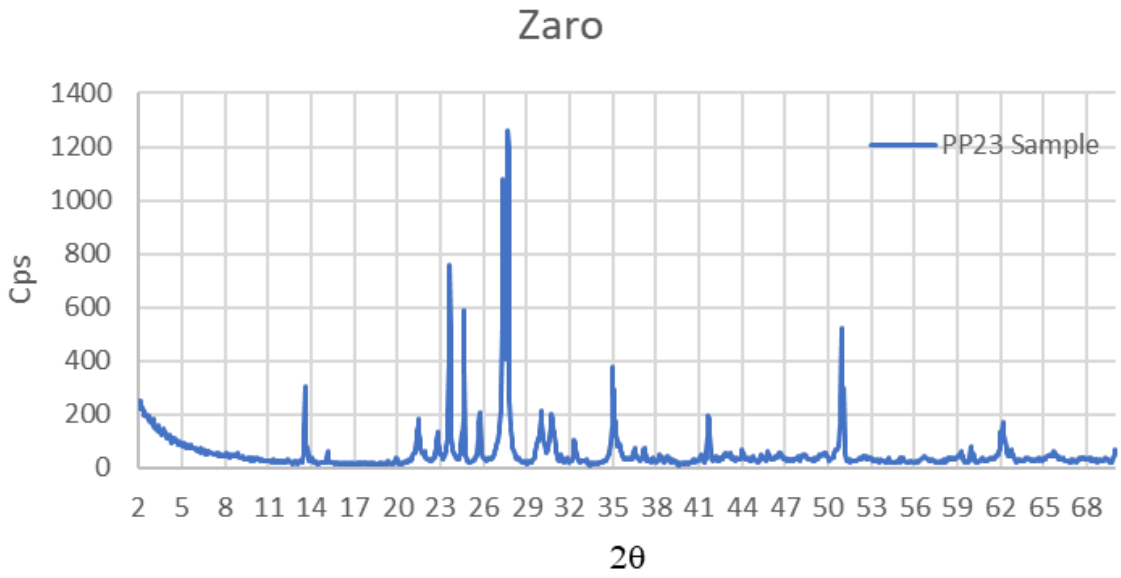

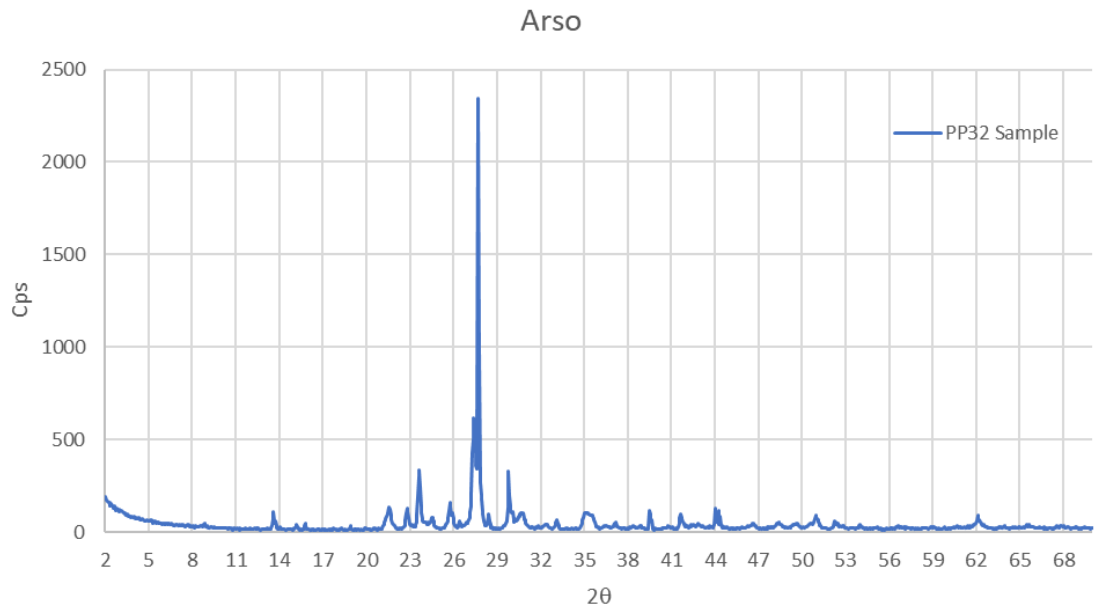

References

Acocella, V. and R. Funiciello (1999). The interaction between regional and local tectonics during resurgent doming: the case of the island of Ischia, Italy. Journal of Volcanology and Geothermal Research 88(1): 109-123.

Andronico, D., Branca, S., Calvari, S., Burton, M., Caltabiano, T., Corsaro, R. A., ... & Murè, F. (2005). A multi-disciplinary study of the 2002–03 Etna eruption: insights into a complex plumbing system. *Bulletin of Volcanology*, *67*(4), 314-330.

Brandelik, A. (2009). CALCMIN–an EXCEL™ Visual Basic application for calculating mineral structural formulae from electron microprobe analyses. *Computers & Geosciences*, *35*(7), 1540-1551.

Brown, R. J., G. Orsi, et al. (2008). "New insights into Late Pleistocene explosive volcanic activity and caldera formation on Ischia (southern Italy)." Bulletin of Volcanology 70(5): 583-603.

Brown, R., L. Civetta, et al. (2014). "Geochemical and isotopic insights into the assembly, evolution and disruption of a magmatic plumbing system before and after a cataclysmic caldera-collapse eruption at Ischia volcano (Italy)." Contributions to Mineralogy and Petrology 168(3): 1035.

Buchner, G. (1986). Eruzioni vulcaniche e fenomeni vulcanotettonici di età preistorica e storica nell'isola d'Ischia. *Tremblements de terre, eruptions volcaniques et vie des hommes dans la Campanie antique*, *7*, 145-188.

Capaldi, G., Civetta, L., & Gasparini, P. (1976). Volcanic history of the island of Ischia (South Italy). Bulletin Volcanologique, 40(1), 11-22.

Caricchi, L., Burlini, L., Ulmer, P., Gerya, T., Vassalli, M., & Papale, P. (2007). Non-Newtonian rheology of crystal-bearing magmas and implications for magma ascent dynamics. *Earth and Planetary Science Letters*, *264*(3-4), 402-419.

Casalini, M., R. Avanzinelli, et al. (2017). "Geochemical and radiogenic isotope probes of Ischia volcano, Southern Italy: Constraints on magma chamber dynamics and residence time." American Mineralogist 102(2): 262-274.

Cashman, K. V., & Sparks, R. S. J. (2013). How volcanoes work: A 25 year perspective. *GSA bulletin*, *125*(5-6), 664-690.

Cashman, K. V., Sparks, R. S. J., & Blundy, J. D. (2017). Vertically extensive and unstable magmatic systems: a unified view of igneous processes. *Science*, *355*(6331), eaag3055.

Castruccio, A., Rust, A. C., & Sparks, R. S. J. (2014). Assessing lava flow evolution from post-eruption field data using Herschel–Bulkley rheology. *Journal of Volcanology and Geothermal Research*, *275*, 71-84.

Chiesa S, P. S., Vezzoli L. (1986). "Studio dell'ultima eruzione storica dell'isola di Ischia." Boll GNV: 153-166.

Cimarelli, C., Costa, A., Mueller, S., & Mader, H. M. (2011). Rheology of magmas with bimodal crystal size and shape distributions: Insights from analog experiments. *Geochemistry, Geophysics, Geosystems*, *12*(7).

Civetta, L., G. Gallo, et al. (1991). "Sr-and Nd-isotope and trace-element constraints on the chemical evolution of the magmatic system of Ischia (Italy) in the last 55 ka." Journal of Volcanology and Geothermal Research 46(3-4): 213-230.

Cordonnier, B., Caricchi, L., Pistone, M., Castro, J., Hess, K. U., Gottschaller, S., ... & Burlini, L. (2012). The viscous-brittle transition of crystal-bearing silicic melt: Direct observation of magma rupture and healing. *Geology*, *40*(7), 611-614.

Della Seta, M., E. Marotta, et al. (2012). "Slope instability induced by volcano-tectonics as an additional source of hazard in active volcanic areas: the case of Ischia island (Italy)." Bulletin of Volcanology 74(1): 79-106.

Della Seta, M., Marmoni, G. M., Martino, S., Paciello, A., Perinelli, C., & Sottili, G. (2015). Geological constraints for a conceptual evolutionary model of the slope deformations affecting Mt. Nuovo at Ischia (Italy). *Italian Journal of Engineering Geology and Environment*, *15*(2), 15-28.

de Vita, S., Sansivero, F., Orsi, G., & Marotta, E. (2006). Cyclical slope instability and volcanism related to volcano-tectonism in resurgent calderas: the Ischia island (Italy) case study. *Engineering Geology*, *86*(2-3), 148-165.

de Vita, S., Sansivero, F., Orsi, G., Marotta, E., & Piochi, M. (2010). Volcanological and structural evolution of the Ischia resurgent caldera (Italy) over the past 10 ky. *Geol. Soc. Am. Spec. Pap*, *464*, 193-239.

Fink, J. H., Malin, M. C., & Anderson, S. W. (1990). Intrusive and extrusive growth of the Mount St Helens lava dome. *Nature*, *348*(6300), 435.

Giordano, D., Romano, C., Papale, P., & Dingwell, D. B. (2004). The viscosity of trachytes, and comparison with basalts, phonolites, and rhyolites. *Chemical Geology*, *213*(1-3), 49-61.

Giordano, D., Russell, J. K., & Dingwell, D. B. (2008). Viscosity of magmatic liquids: a model. *Earth and Planetary Science Letters*, *271*(1-4), 123-134.

Griffiths, R. W., & Fink, J. H. (1993). Effects of surface cooling on the spreading of lava flows and domes. *Journal of Fluid Mechanics*, *252*, 667-702.

Gualda, G. A., & Ghiorso, M. S. (2015). MELTS _ Excel: A Microsoft Excel-based MELTS interface for research and teaching of magma properties and evolution. *Geochemistry, Geophysics, Geosystems*, *16*(1), 315-324.

Higgins, M. D. (2000). Measurement of crystal size distributions. American Mineralogist, 85, 1105–16.

Jeffreys, H. (1925). Lxxxiv. the flow of water in an inclined channel of rectangular section. *The London, Edinburgh, and Dublin Philosophical Magazine and Journal of Science*, *49*(293), 793-807.
Klein, J., Mueller, S. P., Helo, C., Schweitzer, S., Gurioli, L., & Castro, J. M. (2018). An expanded model and application of the combined effect of crystal-size distribution and crystal shape on the relative viscosity of magmas. *Journal of Volcanology and Geothermal Research*, *357*, 128-133.

Landi, P., Francalanci, L., Pompilio, M., Rosi, M., Corsaro, R. A., Petrone, C. M., ... & Miraglia, L. (2006). The December 2002–July 2003 effusive event at Stromboli volcano, Italy: insights into the shallow plumbing system by petrochemical studies. *Journal of Volcanology and Geothermal Research*, *155*(3-4), 263-284.

Latutrie, B., Harris, A., Médard, E., & Gurioli, L. (2017). Eruption and emplacement dynamics of a thick trachytic lava flow of the Sancy volcano (France). *Bulletin of Volcanology*, *79*(1), 4.

Llewellin, E. W., & Manga, M. (2005). Bubble suspension rheology and implications for conduit flow. *Journal of Volcanology and Geothermal Research*, *143*(1-3), 205-217.

MacKenzie, W. S., Donaldson, C. H., & Guilford, C. (1982). *Atlas of igneous rocks and their textures* (Vol. 12). Harlow: Longman.

Mader, H. M., Llewellin, E. W., & Mueller, S. P. (2013). The rheology of two-phase magmas: A review and analysis. *Journal of Volcanology and Geothermal Research*, *257*, 135-158.

Mangan, M. T., & Cashman, K. V. (1996). The structure of basaltic scoria and reticulite and inferences for vesiculation, foam formation, and fragmentation in lava fountains. *Journal of Volcanology and Geothermal Research*, *73*(1-2), 1-18.

Marsh, B. D. (1988). Crystal size distribution (CSD) in rocks and the kinetics and dynamics of crystallization. *Contributions to Mineralogy and Petrology*, *99*(3), 277-291.

Marsh, B. D. (1998). On the interpretation of crystal size distributions in magmatic systems. *Journal of Petrology*, *39*(4), 553-599.

Molin, P., Acocella, V., & Funiciello, R. (2003). Structural, seismic and hydrothermal features at the border of an active intermittent resurgent block: Ischia Island (Italy). *Journal of Volcanology and Geothermal Research*, *121*(1-2), 65-81.

Moore, H. J. (1987). Preliminary estimates of the rheological properties of 1984 Mauna Loa lava. *US Geol Surv Prof Pap*, *1350*(99), 1569-1588.

Morgavi, D., Arzilli, F., Pritchard, C., Perugini, D., Mancini, L., Larson, P., & Dingwell, D. B. (2016). The Grizzly Lake complex (Yellowstone Volcano, USA): Mixing between basalt and rhyolite unraveled by microanalysis and X-ray microtomography. *Lithos*, *260*, 457-474.

Morgan, D. J., & Jerram, D. A. (2006). On estimating crystal shape for crystal size distribution analysis. *Journal of Volcanology and Geothermal Research*, *154*(1-2), 1-7.

Nakada, S., Miyake, Y., Sato, H., Oshima, O., & Fujinawa, A. (1995). Endogenous growth of dacite dome at Unzen volcano (Japan), 1993–1994. *Geology*, *23*(2), 157-160.

Nakada, S., & Motomura, Y. (1999). Petrology of the 1991–1995 eruption at Unzen: effusion pulsation and groundmass crystallization. *Journal of Volcanology and Geothermal Research*, *89*(1-4), 173-196.

Orsi, G., Gallo, G., & Zanchi, A. (1991). Simple-shearing block resurgence in caldera depressions. A model from Pantelleria and Ischia. *Journal of Volcanology and Geothermal Research*, *47*(1-2), 1-11.

Orsi, G., Piochi, M., Campajola, L., D'Onofrio, A., Gialanella, L., & Terrasi, F. (1996). ^{14}C geochronological constraints for the volcanic history of the island of Ischia (Italy) over the last 5000 years. *Journal of Volcanology and Geothermal Research*, *71*(2-4), 249-257.

Orsi, G., D. Patella, et al. (1999). "Magnetic modeling of the Phlegraean Volcanic District with extension to the Ponza archipelago, Italy." Journal of Volcanology and Geothermal Research 91(2-4): 345-360.

Orsi, G., de Vita, S., Di Vito, M., Isaia, R., Nave, R., & Heiken, G. (2003). Facing volcanic and related hazards in the Neapolitan area. *Earth Sciences in Cities*, *56*, 121-170.

Poli, S., S. Chiesa, et al. (1989). "Time dimension in the geochemical approach and hazard estimates of a volcanic area: The isle of Ischia case (Italy)." Journal of Volcanology and Geothermal Research 36(4): 327-335.

Rittmann, A., & Gottini, V. (1980). *L'isola d'Ischia: Geologia*.

Sbrana, A., R. Toccaceli, et al. (2011). "Carta Geologica della Regione Campania, Note Illustrative della Carta Geologica alla scala 1: 10.000, Foglio 464 Isola di Ischia, Regione Campania-Assessorato Difesa del Suolo."

Sbrana, A., P. Marianelli, et al. (2018). "Volcanology of Ischia (Italy)." Journal of Maps 14(2): 494-503.

Selva, J. et al., (2019) Multiple natural hazards at volcanic islands: a review for the Ischia volcano (Italy). Journal of Applied Volcanology.

Shea, T., Houghton, B. F., Gurioli, L., Cashman, K. V., Hammer, J. E., & Hobden, B. J. (2010). Textural studies of vesicles in volcanic rocks: an integrated methodology. *Journal of Volcanology and Geothermal Research*, *190*(3-4), 271-289.

Sparks, R. S. J., Young, S. R., Barclay, J., Calder, E. S., Cole, P., Darroux, B., ... & James, M. (1998). Magma production and growth of the lava dome of the Soufriere Hills Volcano, Montserrat, West Indies: November 1995 to December 1997. *Geophysical Research Letters*, *25*(18), 3421-3424.

Tibaldi, A. and L. Vezzoli (2004). "A new type of volcano flank failure: the resurgent caldera sector collapse, Ischia, Italy." Geophysical Research Letters 31(14).

Vezzoli, L., & Barberi, F. (1988). Progetto finalizzato geodinamica: monografie finali. X: Island of Ischia. *Quaderni de La ricerca scientifica*, (114).

Vezzoli, L., Principe, C., Malfatti, J., Arrighi, S., Tanguy, J. C., & Le Goff, M. (2009). Modes and times of caldera resurgence: the< 10 ka evolution of Ischia Caldera, Italy, from high-precision archaeomagnetic dating. *Journal of Volcanology and Geothermal Research*, *186*(3-4), 305-319.

Vona, A., Romano, C., Dingwell, D.B., and Giordano, D. (2011). The rheology of crystal-bearing basaltic magmas from Stromboli and Etna: Geochimica et Cosmochimica Acta, v. 75, no. 11, p. 3214–3236, doi: 10.1016/j.gca.2011.03.031.

Vona, A., Romano, C., Giordano, D., & Russell, J. K. (2013). The multiphase rheology of magmas from Monte Nuovo (Campi Flegrei, Italy). *Chemical Geology*, *346*, 213-227.

Vona, A., Di Piazza, A., Nicotra, E., Romano, C., Viccaro, M., & Giordano, G. (2017). The complex rheology of megacryst-rich magmas: The case of the mugearitic “cicirara” lavas of Mt. Etna volcano. *Chemical Geology*, *458*, 48-67.

Watts, R. B., Herd, R. A., Sparks, R. S. J., & Young, S. R. (2002). Growth patterns and emplacement of the andesitic lava dome at Soufriere Hills Volcano, Montserrat. Geological Society, London, Memoirs, 21(1), 115-152.

Whittington, A., Richet, P., Linard, Y., & Holtz, F. (2001). The viscosity of hydrous phonolites and trachytes. *Chemical Geology*, *174*(1-3), 209-223.

Williams, H. (1932). The history and character of volcanic domes. University of California Press.

Final remarks

This research project concerns the volcanic risk in Ischia Island in case of renewal of activity, and in particular the calculation of the impact parameters of a set of eruptions identified as the worst potential scenarios for each typology. The problem that the scientific literature about the quantification of the hazard is poor has come to light from the Tavolo di Lavoro – Ischia 2016 which led to the publication of the Selva et al., (2019) paper.

First of all, a work of characterization of the last 10 kyrs in terms of erupted volumes has been performed, in order to understand the role of the last period of quiescence from the last eruption of Arso Lavas in 1302 A.D. (Chiesa et al., 1986). The last 10 kyrs of volcanic activity in Ischia Island has been chosen as a reference period for the analysis because it can be differentiated with respect to the previous period for a series of specific characteristics (Selva et al., 2019). These concern the clear acceleration in the recorded eruptive activity with respect to the previous period, a significant change in the magma chemistry (Civetta et al., 1991; Casalini et al., 2017) and the localization of the eruptive vents in the morphological depression to the east of Monte Epomeo, probably related to the occurrence of the resurgence (Orsi et al. 1991, 1996; Acocella & Funiciello, 1999; de Vita et al. 2006, 2010).

This period is characterized by an emitted total volume of 0,5 km^3 DRE of magma from the intra-caldera monogenetic field, with a clear acceleration in the last 3 kyrs. The cumulative volume through time distribution shows at least 3 changes in the slope with a relative decrease of high magnitude eruptions in the last 3 kyrs.
The characterization of the last phase of activity in Ischia Island, helps us to identify a set of eruptions that could represent the worst potential scenario for each typology of eruption. This set of eruptions has been chosen in the last 3 kyrs, a more suitable subperiod, closer to the last period of quiescence. Both effusive and explosive eruptive scenarios have been analysed in this research project.
Cretaio Tephra has been characterized and treated for the production of the explosive scenario, and Zaro Lava Domes and Flows and Arso Lava have been investigated in order to produce a syneruptive rheology reconstruction to produce an effusive scenario.

The Cretaio Tephra is a violent strombolian to sub-Plinian eruption that has been studied in detail by Orsi et al., (1992) and it is the highest magnitude and intensity event in the chosen reference period. A work of fieldwork, validation of the stratigraphy and numerical modelling allowed us to modelled Cretaio Tephra dispersal, plume height, TGSD, mass distribution, wind profile and diffusion coefficient of the eruptive column using HAZMAP (Macedonio et al., 2005; Pfeiffer et al., 2005) and also estimated the TGSD of Cretaio according to Biass & Bonadonna, (2014). The erupted volume, now is very different from that estimated by Orsi et al. (1992), and in the same way the dispersal axis, now toward S-SE. This represent a new scenario which has so far not been fully considered by the volcanological community and authorities. Recent tephras of Ischia island, in fact, has never been founded or considered in the Campanian or in the central mainland area.

Contextualizing this work in the literature of volcanic islands related hazard, it allows us to improve the awareness about how the sample distribution, used in the modelling of an eruptive column, may change the final results. From this work is evident that for hazard studies, the field time invested on the search of new sampling point in the proximal areas (which in particular for many volcanic islands more or less coincides with the island itself) if these are already conspicuous, will not change or improve significantly the final result. It would be better instead to spend time in adding in the dataset even few distal points in the offshore, even financing new sea core production or interpreting the existent ones.
For the effusive scenario, Arso Lavas (Chiesa et al., 1986) and Zaro Lava Domes and Flows (6 ± 2.2 kyrs, Vezzoli, 1988) have been rheologically characterized. These two effusive eruptions have been chosen because in the selected reference period, represent the compositional and morphological end members in Ischia island. Experimental and numerical modelling have been performed and the results have been compared to each other in order to describe the uncertainties of each model. The rheological reconstruction, useful to calculate the flow duration of lava flows on the island, has been validate using historical chronicles of Arso Lavas, because the duration of the eruption is known and has been used to solve the inverse problem.

This research project has to be considered the first assess in literature to the calculation of the impact parameters of eruptions in Ischia island. Dataset about the volumes calculation, and in particular the explosive eruption volumes values, have to be considered subject to updates. A work like the performed one for Cretaio Tephra has to be necessarily applied to other explosive eruptions in order to characterize the impact parameters of minor eruptions. Through a detailed fieldwork dedicated to each explosive eruption is possible to calculate the volumes by a dispersal model applied with different mechanism from quite purely ballistic depositions (as strombolian eruption such as Fondo d'Oglio Tephra) to fallout or PDC/surge deposits (like Piano Liguori Tephra).
Regarding lava flows and lava domes, the syneruptive rheology reconstruction could be further validated and improved through analogue experiments, aimed to mimic lava flow dynamics, performed on reconstructed paleomorphology by 3D printing.

References

Acocella, V. and R. Funiciello (1999). The interaction between regional and local tectonics during resurgent doming: the case of the island of Ischia, Italy. Journal of Volcanology and Geothermal Research 88(1): 109-123.

Biass, S., Bonadonna, C., 2014, TOTGS: Total grainsize distribution of tephra fallout.

Casalini, M., R. Avanzinelli, et al. (2017). "Geochemical and radiogenic isotope probes of Ischia volcano, Southern Italy: Constraints on magma chamber dynamics and residence time." American Mineralogist 102(2): 262-274.

Chiesa S, P. S., Vezzoli L. (1986). "Studio dell'ultima eruzione storica dell'isola di Ischia." Boll GNV: 153-166.

Civetta, L., G. Gallo, et al. (1991). "Sr-and Nd-isotope and trace-element constraints on the chemical evolution of the magmatic system of Ischia (Italy) in the last 55 ka." Journal of Volcanology and Geothermal Research 46(3-4): 213-230.

de Vita, S., Sansivero, F., Orsi, G., & Marotta, E. (2006). Cyclical slope instability and volcanism related to volcano-tectonism in resurgent calderas: the Ischia island (Italy) case study. *Engineering Geology*, *86*(2-3), 148-165.

de Vita, S., Sansivero, F., Orsi, G., Marotta, E., & Piochi, M. (2010). Volcanological and structural evolution of the Ischia resurgent caldera (Italy) over the past 10 ky. *Geol. Soc. Am. Spec. Pap*, *464*, 193-239.

Macedonio G., Costa A., Longo A. (2005) A computer model for volcanic ash fallout and assessment of subsequent hazard, Comput. Geosci., 31 (7), 837-845.

Orsi, G., Gallo, G., & Zanchi, A. (1991). Simple-shearing block resurgence in caldera depressions. A model from Pantelleria and Ischia. *Journal of Volcanology and Geothermal Research*, *47*(1-2), 1-11.

Orsi, G., G. Gallo, et al. (1992). A comprehensive study of pumice formation and dispersal: the Cretaio Tephra of Ischia (Italy). Journal of Volcanology and Geothermal Research 53(1-4): 329-354.

Orsi, G., Piochi, M., Campajola, L., D'Onofrio, A., Gialanella, L., & Terrasi, F. (1996). ^{14}C geochronological constraints for the volcanic history of the island of Ischia (Italy) over the last 5000 years. *Journal of Volcanology and Geothermal Research*, *71*(2-4), 249-257.

Pfeiffer T., Costa A., Macedonio G. (2005) A model for the numerical simulation of tephra fall deposits, J. Volcanol. Geotherm. Res., 140, 273.

Selva, J. et al., (2019) Multiple natural hazards at volcanic islands: a review for the Ischia volcano (Italy). Journal of Applied Volcanology.

Vezzoli, L., & Barberi, F. (1988). Progetto finalizzato geodinamica: monografie finali. X: Island of Ischia. *Quaderni de La ricerca scientifica*, (114).